ICEFIELD RANGES RESEARCH PROJECT

SCIENTIFIC RESULTS

VOLUME 2

PUBLISHED JOINTLY BY THE
AMERICAN GEOGRAPHICAL SOCIETY
AND THE
ARCTIC INSTITUTE OF NORTH AMERICA

ICEFIELD RANGES RESEARCH PROJECT
ADVISORY COMMITTEE
(1965 – 1968)

Dr. Walter A. Wood, *Chairman*
2561 North Vermont Street
Arlington, Virginia 22207

Dr. Henri Bader
School of Engineering
University of Miami
Miami, Florida 33124

Mr. Robert C. Faylor
Arctic Institute of North America
1619 New Hampshire Avenue, N.W.
Washington, D.C. 20009

Dr. William O. Field
American Geographical Society
Broadway at 156th Street
New York, New York 10032

Dr. G. D. Garland
Department of Physics
University of Toronto
Toronto 5, Ontario, Canada

Dr. Richard P. Goldthwait
Chairman, Department of Geology
The Ohio State University
125 South Oval Drive
Columbus, Ohio 43210

Mr. Trevor A. Harwood
Defense Research Telecommunications Establishment
Shirley Bay
Ottawa 4, Ontario, Canada

Dr. Geoffrey F. Hattersley-Smith
11 Madawaska Drive
Ottawa 1, Ontario, Canada

Dr. Calvin J. Heusser
Department of Biology
New York University
Sterling Forest
P.O. Box 608
Tuxedo, New York 10987

† Dr. Charles B. Hitchcock
American Geographical Society
Broadway at 156th Street
New York, New York 10032

Dr. Mark Meier
General Hydrology Branch
U.S. Geological Survey
1305 Tacoma Avenue, South
Tacoma, Washington 98402

Dr. Svenn Orvig
Department of Meteorology
McGill University
Montreal 2, P.Q., Canada

Dr. George P. Rigsby
411 San Remo Way
San Diego, California 92106

Mr. Graham W. Rowley
245 Sylvan Road
Ottawa 2, Ontario, Canada

Prof. Robert P. Sharp
Department of Geological Sciences
California Institute of Technology
Pasadena, California 91109

† Deceased

551.31
IRRP
Y.Rm.
v.2 c.1

ICEFIELD RANGES RESEARCH PROJECT
SCIENTIFIC RESULTS

Volume 2

ICEFIELD RANGES RESEARCH PROJECT
SCIENTIFIC RESULTS

Volume 2

Edited by

VIVIAN C. BUSHNELL
American Geographical Society

and

RICHARD H. RAGLE
Arctic Institute of North America

Published jointly by

AMERICAN GEOGRAPHICAL SOCIETY, NEW YORK

and

ARCTIC INSTITUTE OF NORTH AMERICA, MONTREAL

1970

This series of volumes is dedicated to

the people of Yukon Territory.

CONTENTS

Editors' Preface

Whereas Volume 1 of this series was concerned entirely with the physical sciences, Volume 2 includes several short papers in the biological sciences as well. The stature of the authors of Volume 2 is similar to that of Volume 1; some authors are students and some are senior researchers. Reports reflect the same multiformity of research and variety of treatment that was evident in Volume 1.

The papers of the present volume report research carried out during 1965–1968. Some articles have been published previously and some have not; those in the latter category have been carefully reviewed by scientifically competent specialists.

The style of previously published articles has been altered very little except for reference lists, which have been made to conform in format throughout the volume. Names of IRRP field stations have been left as the authors used them so as to avoid redrafting of graphs and diagrams. When a station name used by an author does not conform to that appearing on the map inside the back cover of Volume 2, the table facing the map should be consulted.

VIVIAN C. BUSHNELL
RICHARD H. RAGLE

PAPERS IN THE PHYSICAL SCIENCES

Upper-Air Wind Patterns in the St. Elias Mountains Summer 1965*

William Benjey†

ABSTRACT. In the summer of 1965 pilot balloons were used to investigate the upper-air wind patterns over three stations in the heavily glacierized St. Elias Mountains. Observed wind patterns are compared with the streamline directions on 500-mb and 700-mb upper-air charts and with pilot balloon data from the United States and Canadian weather services. Large differences are noted, casting doubt on the accuracy of the charts in such a high mountain region. Topographic influences on winds over each station are examined. Comparison of the results of the study with some models of airflow as affected by mountainous topography (particularly the mountain and valley wind model) reveals that the models fail to account adequately for the winds observed.

Introduction

Mountains have always been noted for complex wind patterns. It is virtually impossible to obtain enough observations to interpret all of the air currents. The greater the topographic relief and the more varied the surfaces, the more difficult the problem becomes. Field studies are often limited to ideal weather conditions and to localities with either a known wind effect or one that is topographically as simple as possible.

There have, however, been attempts to understand the total airflow pattern over a given place in relatively mountainous terrain (Judson, 1965; Jackson, 1965). Among these was the mountain climatology program sponsored by the Icefield Ranges Research Project in the summer of 1965. A network of five stations in the St. Elias Mountains was used. The program included investigation of upper-air winds by pilot balloon soundings above three of the stations during June, July, and August. This paper presents an analysis of upper-air circulation and wind patterns observed.

Study area. The St. Elias Mountains are noted for their great relief and extensive ice cover. Elevations rise from sea level to 6000 m in about 48 km. Each of the three stations utilized for pilot balloon ascents presents a different topographic situation. All are in rugged terrain, located at high elevations, and on glacier surfaces. The stations are Kaskawulsh Station A, Divide Station B, and Seward Station A (Plate 1).[1]

Kaskawulsh Station A (1768 m) is located on the medial moraine formed at the confluence of the central and north arms of the Kaskawulsh Glacier. The glacier flows at a gentle gradient from a high, broad divide, in a steeply walled valley, to about 24 km south of Lake Kluane. The valley and the glacier are about 6 km wide at Kaskawulsh Station. A nunatak rises just west of the station and separates the two arms of the glacier.

Divide Station B (2670 m) is located on the broad hydrologic divide between the Hubbard and Kasakawulsh Glaciers, approximately 20 km west of Kaskawulsh Station A. The Donjek Range to the north rises to elevations in excess of 3000 m; while to the southwest, west, and northwest lie the high barriers of Mts. Logan (6040 m), St. Elias (5490 m), Vancouver (4828 m), Lucania (5226 m), Steele (5010 m), Walsh (4505 m), and Wood (4840 m). To the south the Hubbard and Seward Glaciers afford the easiest avenue for orographic air movement from the Gulf of Alaska.

Seward Station A (1875 m) is located on the eastern end of the upper Seward Glacier in an icefield basin. A ridge to the northeast separates the Seward and the Hubbard Glaciers. The upper Seward Glacier is ringed by the most massive peaks of the St. Elias Mountains (Logan, Vancouver, St. Elias, and Cook). The Seward Glacier empties southward through a narrow outlet to the Malaspina Glacier and the Gulf of Alaska.

Regional weather. The weather patterns in the region of the St. Elias Mountains are caused largely by the position of the mountains, which form a high coastal barrier, blocking westerly air flow in the subpolar low pressure belt. Winter pressure conditions are dominated by two intense, semipermanent pressure systems: the Aleutian Low in the Gulf of Alaska and the Mackenzie

---

*This report is a modified version of an article appearing in Research Paper No. 54, Artic Institute of North America (1969), and is reprinted here with permission.

†Department of Geography, University of Michigan, Ann Arbor

[1]Plate 1 is a map inside the back cover of this volume.

High east of the St. Elias Mountains (Kendrew and Kerr, 1955). Upper-air charts show a warm semipermanent ridge directed northward across Alaska and toward the Pole. Summer conditions show weakened pressure gradients with a ridge along the Alaska–Yukon border on surface charts. The 700-mb and 500-mb pressure charts show "a far weaker gradient in July though they resemble the winter map in shape" (Taylor-Barge, 1969, p. 4).

A climatic profile across the St. Elias Mountains shows that the northeast front of the mountains, as characterized by Whitehorse, has a continental regime; while the coastal or southwest side has a maritime climate typified by Yakutat. Circulation associated with the Aleutian Low dominates throughout the year although maritime tropical air occasionally brings warmer, drier weather during the northward migration of the Hawaiian High (Mitchell, 1958).

The climates of Kaskawulsh, Divide, and Seward Stations fall between the continental and maritime extremes, revealing local orographic adjustments. Taylor-Barge (1969) has located a shifting, synoptic-scale climatic divide between Kaskawulsh and Divide Stations.

Objectives. The purpose of the analysis of summer wind patterns over Kaskawulsh, Divide, and Seward stations is fourfold:

(1) To determine the lowest level of geostrophic flow over each station as an indicator of the vertical extent of the boundary layer
(2) To analyze the local or nongeostrophic wind patterns in relation to topography
(3) To determine to what extent upper-air charts are valid as a means of interpreting wind direction over isolated mountain terrain
(4) To examine the relationship of the observed wind patterns to major airflow models

Methodology. The upper-air wind data were obtained by the use of pilot balloons tracked by a single theodolite. The balloons were helium-filled, 10-gm, ceiling balloons designed for an assumed rate of ascent of 140 m/min. Ascents were made twice a day at 0600 and 1800 GMT (0900 and 2100 Yukon Standard Time), cloud cover permitting. These are the times at which permanent synoptic weather stations, including Yakutat, Alaska, and Whitehorse, Yukon, take comparable pilot balloon ("PIBAL") soundings. Table 1 indicates the periods of record for PIBAL ascents at each mountain station. Surface wind data were taken from Icefield Ranges Research Project weather observations as reported by Marcus, Rens, and Taylor (1966). The University of Michigan IBM 360 computer was used to reduce the PIBAL data.

TABLE 1. Dates of Pilot Balloon Ascents, Summer 1965

Station	Dates
Kaskawulsh	June 24 – July 25
Divide	June 24 – July 5 July 17 – August 9
Seward	July 10 – July 25

Boundary layer limits were determined by comparing the PIBAL velocity values at the 500-mb and 700-mb levels with those over Yakutat and Whitehorse. Directions from pilot balloon observations were compared to protractor measurements of the streamline nearest the mountain stations on 500-mb and 700-mb upper-air charts. Any deviations from geostrophic flow should indicate the upper limit of the boundary layer, if the upper-air charts are accurate. The comparisons were also used to provide measurements in determining the validity of geostrophic flow as presented on upper-air charts.

Each ascent was graphed for speed and altitude. Wind arrows along the right side of each graph indicate direction (Fig. 1). The points plotted are at intervals of 140 m or one minute of ascent time. These graphs were used in determining local wind patterns and trends and as another means of finding the lower limits of geostrophic flow. Wind direction roses and speed frequency tables were computed to assist in analysis (Appendixes I and II).

TABLE 2. Presence of Pressure Cells at the 500-mb Level.

Type of cell	Percent of total observation period
Low	81.7
High	6.4
Indeterminate	11.9

Observational constraints. The main source of error lies in the use of the single-theodolite tracking method, which assumes a constant rate of balloon ascent. Updrafts and downdrafts related to turbulence in mountainous topography may drastically vary the rate of ascent. A further problem is the bias toward fair weather observations. Cloud cover, especially at higher altitudes, limits many observations. In addition, this study necessarily focuses on low-pressure situations since they prevailed for 81.7% of the study period at the 500-mb level (Table 2). High-pressure situations at 500 mb were few and scattered in time.

Lower Limits of Geostrophic Winds

The extent of the effect of mountainous topography upon airflow is indicated by the lower limit of the geostrophic winds[2], since that limit defines the upper level of the boundary layer. Two methods were used to determine this limit over Kaskawulsh, Divide, and Seward Stations. The first method was the identification of specific instances during pilot balloon ascents when the lower level

[2]Gradient wind would perhaps be a more appropriate term, but geostrophic wind is used here to provide continuity with terminology of other studies in the area and to avoid confusion with references to downglacier winds caused by localized pressure gradients.

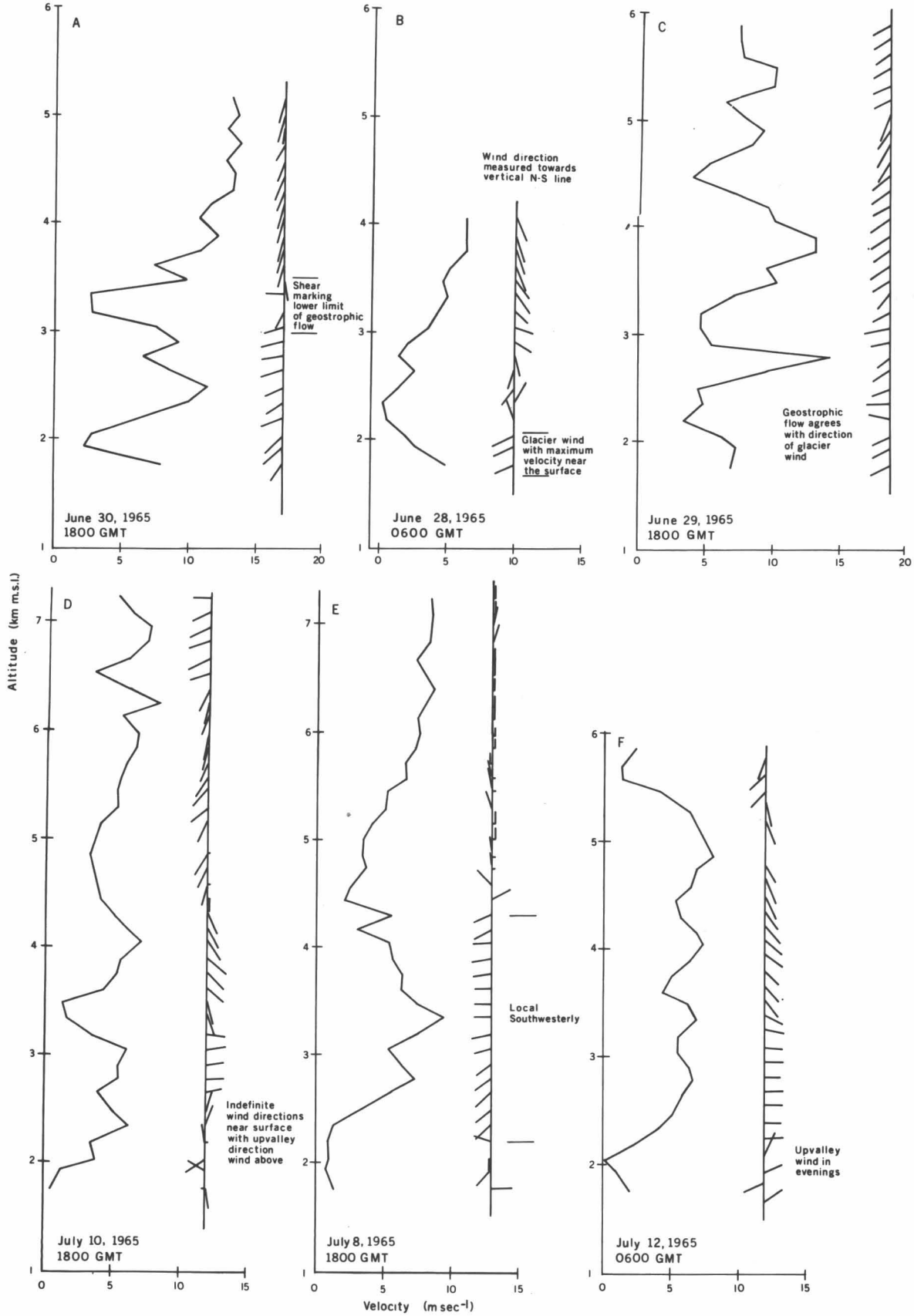

Fig. 1. Wind velocity and direction, Kaskawulsh Station.

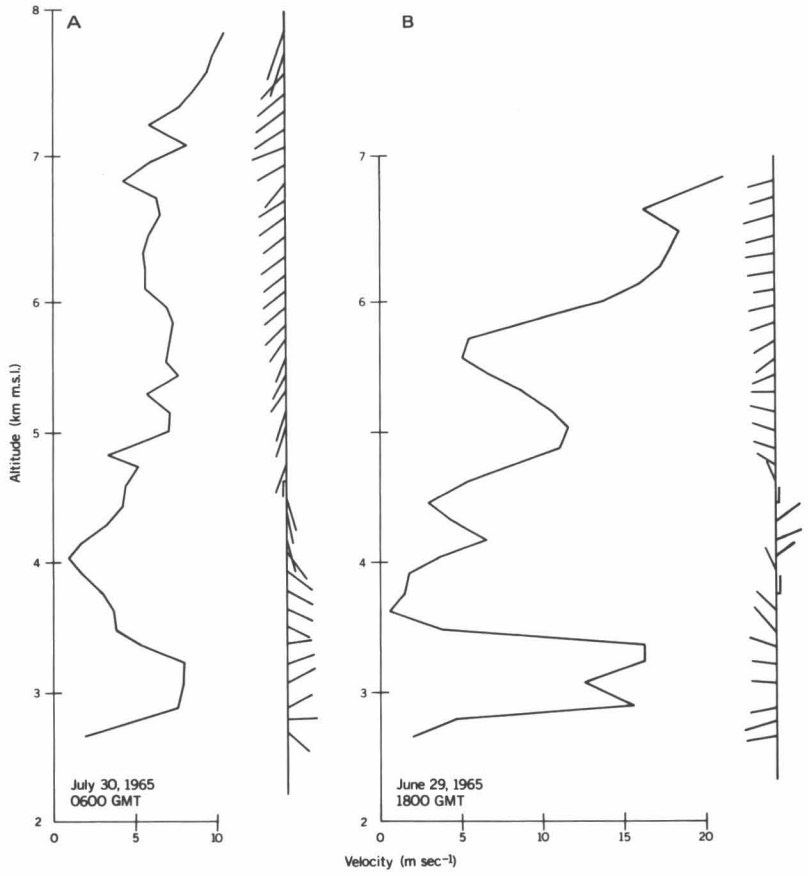

Fig. 2. Wind velocity and direction, Divide Station.

of geostrophic flow was apparent over the mountain stations. The second method is the comparison of geostrophic winds at the 500-mb and 700-mb levels between stations in the St. Elias Mountains with stations at the base of the windward and leeward sides. This analysis also tests the validity of the wind directions shown on the constant-pressure charts over the mountains.

Method I: Specific observations of geostrophic winds. Observations of individual pilot balloon ascents provide examples from which patterns of airflow may be selected. The advantage of this method for finding the lower limits of geostrophic flow is that it allows examination of the total air column over a given station at a given time. The sum of many such observations gives an altitude range of the lower limit of geostrophic flow for varying synoptic situations. The vertical zone of lower geostrophic flow is depicted by means of wind roses (Appendix I). The blurring of a marked pattern of local airflow direction with increasing altitude indicates increasing prevalence of geostrophic flow.

If individual pilot balloon ascents are studied in connection with pressure charts it becomes apparent that a good many ascents do reach into the geostrophic winds. This is indicated by the persistence and constancy of direction of the uppermost winds in longer ascents, and the fact that the directions consistently shift in agreement with the movements of the pressure systems.

Interpretation of data from pilot balloon ascents suggests the following:

(1) The greater the intensity of a given pressure system, the lower will be the level of effective geostrophic winds over the mountain stations.
(2) Geostrophic circulation may enhance, hinder, or overcome local mountain and valley winds, depending upon the intensity of the pressure system and the relation between topography and geostrophic wind direction.
(3) The break between local winds and geostrophic flow is usually marked by a decrease in velocity and a change of direction (Fig. 1A).
(4) The level of geostrophic winds at the Kaskawulsh Station is generally between 3000 m and 4000 m although the shear has been observed as high as 5500 m. Rose diagrams for Kaskawulsh Station A (Appendix I) illustrate this point. This low a level is possible because the terrain within 30 km of Kaskawulsh Station rarely exceeds 3650 m in elevation while 2750 m is more usual.
(5) The geostrophic flow over Divide Station begins on an average at 3250 m to 4000 m.[3] The lower level of geostrophic flow is actually quite variable, ranging from the surface to 3330 m above the station. The following situations were observed at Divide Station. (a) Intense winds from the south and southeast tend to be channeled parallel to the Seward and Hubbard Glacier systems. These

[3]The winds noted over Divide may be only apparently geostrophic. Pilot balloon observations indicate that some winds to 8000 m may be channeled to the southwest around the larger peaks. No observations are available above 8000 m.

are the geostrophic winds which come closest to the surface. (b) Geostrophic winds from the southwest are either not intense enough to overcome a local easterly wind which extends up to about 4000 m, or their flow is coming over the peaks to the southwest at an extremely high level with the surface easterly at Divide being the reverse component of a rotor in a lee wave (Fig. 2A). (c) One case was observed in which a pressure system was in a position to provide geostrophic winds from the north, toward Divide. In that case the lower geostrophic wind limit fluctuated between 3000 m and 6000 m.
(6) The sparse observations available from the Seward Station indicate that the lower level of geostrophic flow there varies between 4000 m and 5000 m.

These conclusions were arrived at primarily by analyzing wind directions. The speeds appear to follow no predictable pattern in relation to the lower geostrophic wind limits, other than a decrease in wind speeds at the shear between wind layers.

Method II: Comparison and analysis of upper-air data. Method II, though less effective for determining lower levels of geostrophic flow, provides insights into the nature and accuracy of upper-air charts.

Comparisons of geostrophic winds over different stations were made for three types of pressure systems: (1) well-defined high-pressure cells, (2) well-defined low-pressure cells, and (3) periods of negligible cell development. The duration of each type of pressure situation over the mountains was also determined from the 500-mb charts. The reason for using the 500-mb level was that the identification of a pressure system type should be as unaffected as possible by surface friction.

Wind speeds over the mountain stations taken from pilot balloon observations were compared with pilot balloon data from Yakutat and Whitehorse, and wind directions were compared with geostrophic wind directions from 500-mb and 700-mb constant-pressure charts. These levels were chosen because charts below the 700-mb level are actually below the station elevations, and very few pilot balloon observations are available for comparison with charts above the 500-mb level. Average altitudes in meters above mean sea level were computed for the 500-mb and 700-mb levels; and the pilot balloon observation levels nearest these were used for comparison.

The wind direction differences between the pilot balloon observations and the nearest chart streamline at each of the two levels over each mountain station were then measured. These differences were averaged within the periods during which each of the three selected pressure system types prevailed. This was also done for Whitehorse and Yakutat. Accuracy of measurement was to the nearest 10° of azimuth. Theoretically, any differences in actual direction would indicate that flow was not geostrophic at that pressure level.

Similarly, wind speed comparisons were accomplished by taking the difference between the observed and standard speeds for each mountain station, each ascent, and for both 500-mb and 700-mb levels. Accuracy was to the nearest tenth of a meter per second. The standard in each case was the speed at the 500-mb or 700-mb level at Yakutat or Whitehorse as determined by their pilot balloon data. Yakutat was used whenever the data were available since it is on the windward side of the mountains and should be relatively free of many topographic wind effects.

Several factors limit the accuracy of the comparisons. First is the fact that only two levels could be compared. Secondly, the use of average altitudes for the 500-mb and 700-mb levels introduces an error; the altitudes of the two varied about 400 m during the study. An extra variability of $\pm$ 70 m is introduced because of the difference in altitude of pilot balloon observations. Some of the errors are compensating, however. Perhaps the most serious weakness in the study is the fact that the upper-air charts are six hours out of phase with the pilot balloon observations. Nevertheless, the comparisons do yield useful generalized data. Findings are most significant for low-pressure situations, which were dominant during 81.7% of the study period. Results are given in Tables 3, 4, and 5.

It is difficult to attach any definite meaning to the average deviations of wind velocity from geostrophic flow, since the small differences may reflect only errors in measurement, or at most small perturbations in velocity across hundreds of miles. The average directional differences of observed winds from streamlines are, however, more marked in magnitude. These differences vary from 0° to 180° and seem to follow no particular pattern. Kaskawulsh and Divide wind directions vary from the charts by about the same average difference at the 700-mb level—56.4° and 56.6° respectively. The variation over Divide at the 500-mb level (41.6°) is much greater than it is over Kaskawulsh (27.1°). The similarity in average directional differences at 700 mb is probably due to the fact that at this level the winds are usually oriented east or west for both stations because of topographic influences (for example, the 3000-m Kaskawulsh and Divide wind rose, Appendix I). Figure 3 illustrates the differences between chart and observed wind directions. Streamline directions from upper-air constant-pressure charts over Whitehorse and Yakutat also depart appreciably from pilot balloon observations taken over those stations.

A rough comparison of averages leads to three possibilities: (1) the streamlines over the St. Elias Mountains are inaccurate, (2) the flow over the mountains is not geostrophic at either the 500-mb or 700-mb levels, or (3) probably a combination of (1) and (2). The first possibility is supported by the wide spacing between stations used to plot the upper-air charts. The second possibility is suggested by the size and elevation of the mountains.

Local Winds

The St. Elias Mountains area is subject to a great variety of local winds, as a result of extreme relief, the great extent of the mountain range, and great thermal contrasts due to a differential heating of slopes and the presence of vast glaciers. In such a situation the local factors may cancel out the geostrophic winds near the surface. Near the surface, Coriolis force is ineffective and winds flow

along local pressure gradients producing "antitriptic winds" (Defant, 1951, p. 655). This is not meant to imply that geostrophic flow has no effect on local winds. The local currents do vary, or are at least altered, by changes in the flow aloft. The following paragraphs discuss the local winds at the three stations in the St. Elias Mountains as determined by pilot balloon observations.

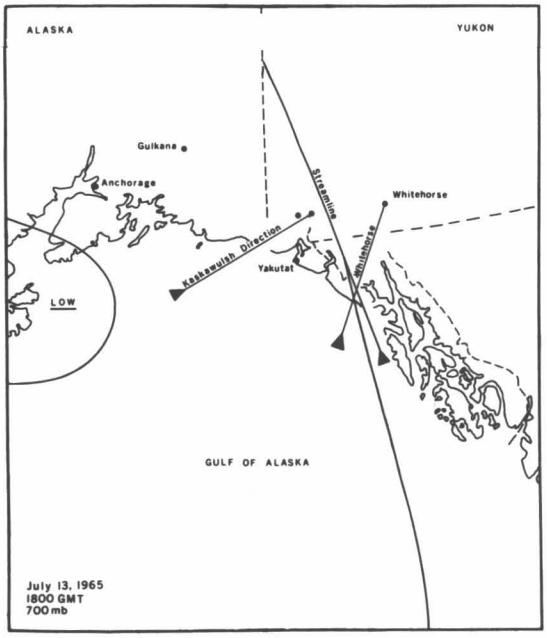

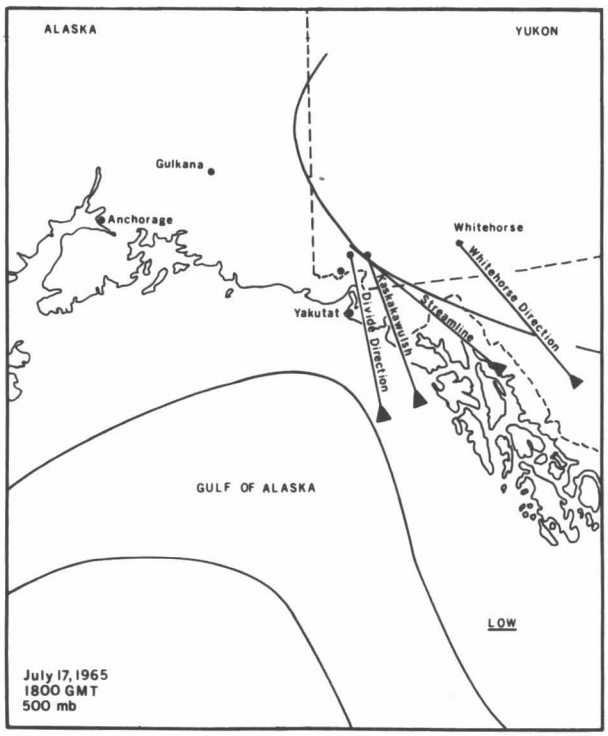

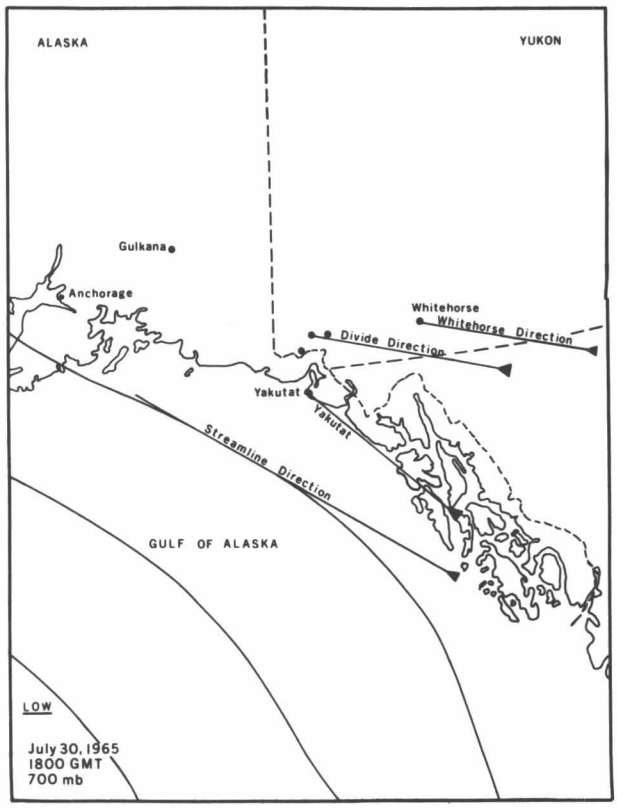

Fig. 3. Examples of differences between observed and streamline wind directions.

Kaskawulsh Station. The most notable local wind observed at Kaskawulsh Station is a glacier wind which flows from 240° of azimuth, down the central arm of the Kaskawulsh Glacier about 70% of the time. It shows no relation to diurnal fluctuations. A glacier wind is caused by radiative cooling of the air immediately above the glacier, which increases the density of the air, causing it to flow downslope. The Kaskawulsh Glacier valley provides a fine channel for the dense air. The glacier wind at Kaskawulsh Station is characterized by a maximum velocity which usually is greater than the velocity of the wind layer just above. The maximum glacier-wind speed varies between 8 and 12 m/sec and occurs from near the surface to a height of more than 200 m above the station (Fig. 1B). When the maximum speed is near the surface, the glacier wind is shallow. The maximum is then not detected by the pilot balloon observations, because the first reading in an ascent is more than 70 m above the surface.

There is evidence of a diurnal velocity fluctuation which is not shown by the balloon ascents. Surface data show that wind velocity increase is more than twofold during the daylight hours (Table 6). This increase is due to an intensified ice-to-air thermal gradient. The thickness of the glacier wind at Kaskawulsh varies from less than 50 m to almost 500 m and depends largely upon the direction of the geostrophic wind.

TABLE 3. Results of Comparisons of Wind Speeds and Directions During Low-pressure Periods

Station	500-mb level				700-mb level			
	Direction*	No. of comparisons	Speed†	No. of comparisons	Direction*	No. of comparisons	Speed†	No. of comparisons
Kaskawulsh	27.1°	15	+0.96	9	56.4°	22	-1.73	18
Divide	41.6	18	+1.51	7	56.6	33	-0.22	30
Seward	33.3	3	+1.3	1	55.0	2	-1.70	1
Whitehorse	48.2	18	–	–	42.6	46	–	–
Yakutat	16.0	5	–	–	14.0	10	–	–

*Average differences between PIBAL data and data from pressure charts
†Average differences between PIBAL data from IRRP stations and PIBAL data from Yakutat and Whitehorse

TABLE 4. Results of Comparisons of Wind Speeds and Directions During High-pressure Periods

Station	500-mb level				700-mb level			
	Direction*	No. of comparisons	Speed†	No. of comparisons	Direction*	No. of comparisons	Speed†	No. of comparisons
Kaskawulsh	10°	1	–	–	97.1°	7	+0.82	6
Divide	150	1	-1.3	1	83.3	6	-1.3	4
Seward	–	–	–	–	–	–	–	–
Whitehorse	150	1	–	–	52.5	8	–	–
Yakutat	15	2	–	–	58	5	–	–

*Average differences between PIBAL data and data from pressure charts
†Average differences between PIBAL data from IRRP stations and PIBAL data from Yakutat and Whitehorse

TABLE 5. Results of Comparisons of Wind Speeds and Directions During Indeterminate Pressure Periods

Station	500-mb level				700-mb level			
	Direction*	No. of comparisons	Speed†	No. of comparisons	Direction*	No. of comparisons	Speed†	No. of comparisons
Kaskawulsh	52.5°	4	–	–	74.6°	13	+1.4	12
Divide	20	2	+4.7	1	44.4	9	+1.23	9
Seward	–	–	–	–	78	5	+0.48	5
Whitehorse	120	1	–	–	83	13	–	–
Yakutat	–	–	–	–	–	–	–	–

*Average differences between PIBAL data and data from pressure charts
†Average differences between PIBAL data from IRRP stations and PIBAL data from Yakutat and Whitehorse

TABLE 6. Average Surface Wind Speed at Kaskawulsh Station, June 24 to July 25, 1965

Time (YST)	Wind speed (m/sec)
03	2.6
06	2.0
09	4.0
12	5.4
15	6.5
18	7.7
21	4.1
24	2.6

The following generalizations can be drawn:

(1) The glacier wind has greatest depth when a strong geostrophic wind flows parallel to it, aiding its movement (Fig. 1C).

(2) Low-level upvalley winds replace the glacier wind 12% of the time in conjunction with geostrophic flow from the south, east or north, and occasionally with a weak geostrophic wind in the downglacier direction. Weak and variable winds at the surface accompany the upvalley wind 10% of the time (Fig. 1D).

There are three local winds over Kaskawulsh Station in addition to the glacier winds. They are definable by altitude and direction as (1) local southwesterly, (2) easterly, and (3) high elevation westerly. The upper and lower levels of all three may be marked by a sharp shear in wind direction, although the change is not always abrupt. None of these winds has any correlation with the glacier wind, diurnal thermal variations, or each other. Any combination of these winds may occur at a given time. They may be related to (1) local thermal conditions aloft, for which no data are available, (2) mountain waves, (3) a combination of (1) and (2), or (4) a thermally induced diurnal mountain and valley wind system masked by other effects and therefore very irregular.

A southwesterly wind is sometimes found just above and flowing parallel to the glacier wind, although the glacier wind need not be present at the same time. Its depth ranges from 200 m to more than 2000 m and its upper level may attain an altitude of 4500 m (2732 m above station level—Fig. 1E).

An easterly wind, 200 m to 1500 m thick, is noted at levels ranging to 4500 m above the surface. This easterly cannot be defined as a valley wind in a strict sense as it extends well above the walls of the Kaskawulsh Glacier valley. It does flow between the highest peaks on either side (north and south) of the valley, however, and may oppose the glacier wind on occasion. In the classical valley-wind scheme, an upvalley wind is a relatively warm, thermally induced phenomenon. Such a wind should consistently rise over the denser glacier wind. The observed winds do not fit this pattern. The tops of the ridges at the lower or east end of the Kaskawulsh Glacier are at about the Kaskawulsh Station elevation. This would allow a nonvalley, perhaps geostrophic, easterly wind access to the station.

Occasionally an unexplained westerly wind with a depth of 200 to 500 m appears at about 5000 m (3232 m above station level).

It is hypothesized that these three local winds, especially the first two, may be caused by a large-scale boundary layer separation ("air-mass separation") from geostrophic flow, ascribed to regions of high mountains (Scorer, 1955). Passive airflow around an obstacle rather than changes in local thermal gradients between mountains and plains would then be the cause. It is not known what triggers shifts from east to west and vice versa in the lower winds.

An overall pattern appears in wind rose diagrams for different levels over the Kaskawulsh Station (Appendix I). The surface and 2000-m (232 m above the station) diagrams illustrate a strong southwesterly flow due to the glacier wind, with a smaller opposite component representing the upvalley flow. The northwesterly component probably represents drainage winds from the north arm of the Kaskawulsh Glacier. At 2250 m (482 m above the station) the pattern is dissipating, yet still has a strong southwesterly component, probably marking the average upper limit of the glacier wind. Levels 2500 m (732 m above the station) and 2750 m (982 m above the station) also illustrate a strong southwesterly component due to the local southwesterly wind; again there is a less prevalent flow in the opposite direction.

The 3000-m level (1232 m above the station) still shows two opposite components but a dispersal of the pattern is apparent. This reflects the increasing presence of the geostrophic winds. The dispersal continues up to about 4000 m (2232 m above the station). There a dominant southerly to southwesterly component is noted, which may be observed forming at lower levels. This reflects the fact that most low-pressure systems come from the Gulf of Alaska.

The velocity-frequency table (Appendix II) for low-pressure systems over the Kaskawulsh Station shows a scattered range of velocities rather than the steady increase with altitude characteristic of geostrophic winds, indicating the presence of local winds. The surface level wind speeds appear to be bimodal. One peak is between 0 and 2 m/sec, and the other between 4 and 8 m/sec. The lower speeds show the presence of upvalley winds; the greater speeds are typical of the glacier wind.

Divide Station. The local winds at Divide Station are not as complex as those at Kaskawulsh, but neither is the topography. The surface winds at Divide Station are almost always from the east or west; occasionally from the south-southeast. Surface westerlies are often, but not always, found in conjunction with westerly or southwesterly geostrophic flow. The upper limit of surface westerly winds is at least 4000 m (1330 m above the station) and possibly higher. They vary in thickness from less than 100 m to more than 1000 m and possess a higher speed than the airflow just above them (Fig. 2B). The westerlies appear to be caused by air channeled inland parallel to the Hubbard and Seward Glaciers; or possibly the surface westerly winds may sometimes reach Divide by way of the valleys of the Logan and Walsh Glaciers west of the station.

There is a less frequent surface wind from the east with the same thickness and velocity characteristics as the westerly. The easterly may occur during a westerly, southwest-

erly, or an easterly geostrophic flow. There are three possible explanations for the surface easterly. First, during an easterly geostrophic wind the easterly surface wind is probably caused by a lowering of the influence of the geostrophic wind; the topographic barriers to the east of Divide are much less than those to the west. Second, the easterly may sometimes be an extension of the upvalley wind noted at Kaskawulsh, although the evidence for this is weak; the two winds usually do not coincide in time. Finally, there is a small possibility that the surface easterly at Divide could be the reverse component of a rotor in a streaming lee wave (see Fig. 4) of westerly or southwesterly geostrophic flow over the summits of Mt. Logan and Mt. St. Elias. There are examples of the surface easterly flowing in an opposite direction to the geostrophic winds just above it (Fig. 2A). But the upper levels of pilot balloon observations usually indicate flow parallel to the Hubbard and Seward Glaciers.

It is further possible that relatively strong surface westerly winds may at times impede the boundary layer separation which allows a rotor to form. Cooling or speeding up of surface wind with respect to the wind above is theoretically capable of doing this (Scorer, 1955).

When the geostrophic wind is from the south or south-southeast, winds varying in direction by only a few degrees (no more than 20°) from the geostrophic direction sometimes appear. These winds probably result from the deflection of the lower winds around the mountains and large nunataks separating the ice field from an arm of the Hubbard Glacier.

The wind rose diagrams (Appendix I) for periods when low-pressure systems prevail show an overall wind direction pattern for each level. The surface (2670 m) through 3000 m (330 m above station) diagrams show the strong surface westerly, less prevalent easterly, and south-southeasterly surface components. Above 3000 m each level up through the 3750 m (1080 m above station) illustrates the dispersal of the surface pattern as geostrophic winds begin to appear. At 4000 m (1330 m above station) a southerly component shows the winds from the Gulf of Alaska. A persistent southwest tendency appears with altitude above 6000 m.

The velocity–frequency table (Appendix II) shows the increased speed of the winds at the 2750 and 3000 m levels (80 m and 330 m above station), with a maximum of 4–8 m/sec. A general tendency appears for greater speed with greater altitude above the surface, as is characteristic of geostrophic winds.

Seward Station. The dominant wind characteristics noted at Seward Station are related to the fact that the Seward Glacier lies in a basin-shaped wind and cloud trap. Speeds are very low (generally less than 2 m/sec) and directions variable (Appendixes I and II). During slightly more than half the time the surface winds come from the west. Though there is a relatively narrow downslope opening to the southwest where the Seward Glacier flows into the Malaspina Glacier, any southerly flow probably passes over the Seward Station at levels above the outlet opening of the glacier. Pilot balloon data at Seward are too sparse to be definite on this point.

Relation to Other Studies

Most investigations of upper-air wind patterns in mountainous areas have attempted to study a particular facet of the problem. The two main airflow models are (1) diurnal thermally induced mountain and valley winds (Buettner and Thyer, 1965), and (2) the passive effects due to airflow over mountains (Corby, 1954). Field investigations have usually been initiated to determine and/or test airflow models. Thus field studies have generally simplified the situation as much as possible by selecting idealized sites and investigating during only short periods of time in fair weather conditions. The intent of this study was to describe and interpret wind patterns in an actual complex mountainous terrain.

Divide and Seward Stations are not topographically suited to application of the mountain and valley wind model, but because of the prominent trough shape of the Kaskawulsh Glacier valley, the model would be expected to have application at Kaskawulsh Station. This did not prove to be the case, however. The ideal sequence of mountain and valley winds is missing over the Kaskawulsh Glacier. The model is directly opposed by downvalley winds in daylight hours (Figs. 1A and 1C) and upvalley winds during night hours (Fig. 1F). Even the glacier wind does not agree with the model. It is much thicker and has a maximum speed of up to three times the 3 m/sec stated by Geiger (1966).

The main difference between the Kaskawulsh Glacier valley and other valleys studied is the presence of a large expanse of snow and ice cover which undoubtedly upsets the thermal contrasts found in alpine valleys without such cover. The mountain and valley wind model may be invalid in heavily glacierized alpine areas. Although other factors are known to cause variations from the model, they are probably minor compared to the effect of snow and ice cover on local thermal conditions which in turn effect the winds.

Passive local winds result from air flowing around an obstacle, in contrast to dynamic local winds which are initiated by causes such as uneven heating. Passive wind effects are large-area phenomena usually studied from synoptic station reports. Queney and Scorer (Corby, 1954) applied perturbation theory to derive a theory of mountain waves, or undulating flow above or on the leeward side of a barrier. The main weakness in their work is the assumption of steady laminar flow over mountains.

Four types of mountain-wave flow have been identified, depending on the wind speed, wind shear, and height of mountain (Forchtgott, cited in Corby, 1954, pp. 515–516). The types are (see Fig. 4):

(1) Undisturbed streaming, which is found when light winds are present.
(2) Standing stream eddy, which is found with a stronger wind, and with the surface streamline having separated and formed one standing lee eddy with flow uphill. The crest of the lee wave is over the eddy.
(3) Wave streaming which occurs when yet stronger winds form a series of lee waves with a rotor (vortex) system under each wave.
(4) Rotor streaming which occurs with very strong winds in a layer thin relative to mountain height. The rotors

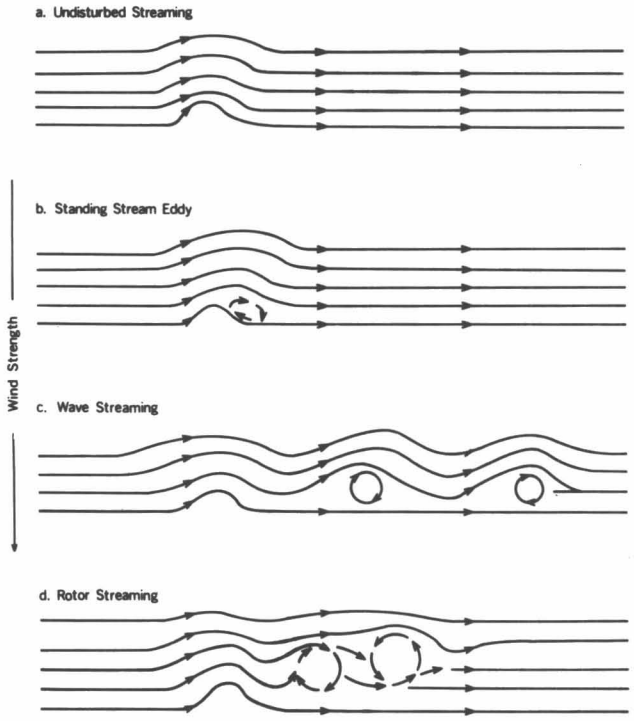

Fig. 4. Types of airflow in the lee of a mountain (after Forchtgott, in Corby, 1954).

intensify and move closer together while the streamlines above flatten.

There are two possible cases for which the results of this study may be explained by passive mountain airflow: (1) the surface easterly observed at Divide Station, which may be a reverse component of a rotor under a lee wave; and (2) the local winds, other than the glacier wind, at Kaskawulsh Station, which may be caused by air-mass boundary layer separation.

One of the persistent problems evident in the analysis of the data is the ever-changing and overlapping scales of reference. The mountain and valley wind model is usually thought to cover an area intermediate in size, while mountain wave phenomena cover a much greater area. Although the explanations of the observations are fairly speculative, there appears reason to suspect that the large-area passive airflow phenomenon has extended to surface winds and into a valley. It may be that the topographic features of the St. Elias Mountains, such as the Kaskawulsh Glacier valley, are large enough to come under the influence of synoptic scale factors.

The most pertinent findings of this study may be summarized as follows:

(1) Wind directions as presented on constant-pressure upper-air charts are not reliable over the St. Elias Mountains area, mainly because of an insufficient number of upper-air stations, and the wide spacing between them.
(2) The mountain and valley wind model is not valid in a highly glacierized alpine situation. Results from Kaskawulsh Station indicate that extensive snow and ice cover may overcome the thermal contrasts present without this cover. This suggests that a different model is needed for such areas.

References

Buettner, K. J. K., and Thyer, N. (1965) Valley winds in the Mt. Rainier area, *Archiv. Meteorol., Geophys., Bioklimatol.,* 14, 9–148.

Corby, G. A. (1954) The airflow over mountains; a review of the state of current knowledge, *Quart. J. Roy. Meteorol. Soc.,* 80, 491–518.

Defant, F. (1951) Local winds, in *Compendium of Meteorology,* edited by T. F. Malone, pp. 655–672, Am. Meteorol. Soc., Boston.

Geiger, R. (1966) *The Climate Near the Ground,* Harvard Univ. Press, Cambridge, Mass., 611 pp.

Jackson, G. I. (1965) The vertical profile of wind at Lake Hazen, Northwest Territories, *Arctic,* 18, 21–35.

Judson, A. (1965) The weather and climate of a high mountain pass in the Colorado Rockies, *Res. Paper RM-16,* Fort Collins, Colorado, U. S. Forest Serv., 28 pp.

Kendrew, W. G., and Kerr, D. (1955) *The Climate of British Columbia and the Yukon Territory,* Queen's Printer, Ottawa, 222 pp.

Marcus, M. G., Rens, F., and Taylor, B. E. (1966) Icefield Ranges Climatology Program: 1965 data presentation and programing analysis *Res. Paper No. 33,* Arctic Inst. North Am., 111 pp.

Mitchell, J. M. (1958) The weather and climate of Alaska, *Weatherwise,* 11, 151–160.

Scorer, C. I. (1955) Theory of airflow over mountains: IV—separation of flow from the surface, *Quart J. Roy. Meteorol. Soc.,* 81, 340–350.

Taylor-Barge, B. (1969) The summer climate of the St. Elias Mountains region, *Res. Paper No. 53,* Arctic Inst. North Am., 160 pp.

APPENDIXES

The appendixes are limited to data taken during low-pressure conditions since other pressure situations prevailed relatively infrequently and the data are too few to be significant. The total observational period is used, however, when computing percentages.

The percentages of time when lows prevailed during the study period are: Kaskawulsh Station, 80.9%; Divide Station, 82.8%; Seward Station, 80.6%.

I

WIND DIRECTION ROSES FOR LOW-PRESSURE PERIODS

Since balloon ascents were not all tracked to the same altitude, the number of observations at each level varies. The percentage of observations missing at each level, relative to the number at the surface, is given below each diagram.

Seward Station

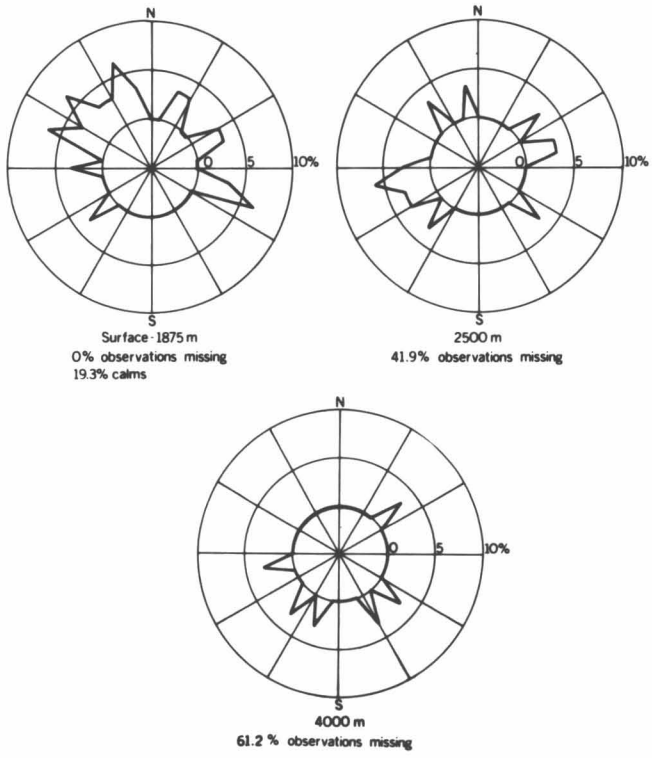

Kaskawulsh Station

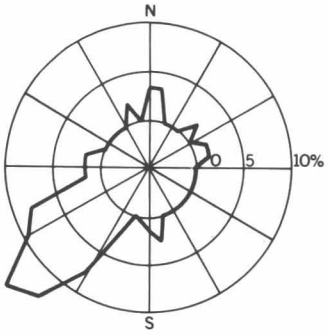

Surface - 1768 m
0% observations missing
4.76 calms

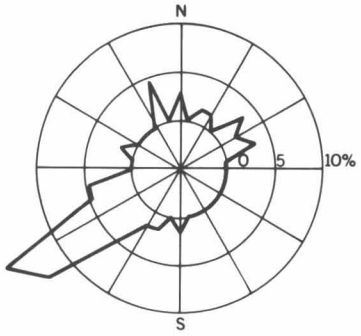

2000 m
12.7% observations missing

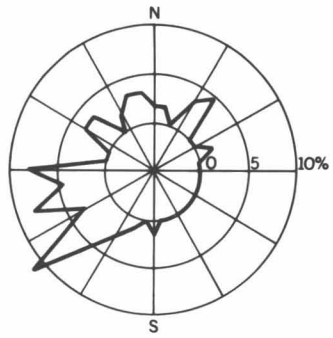

2250 m
12.7% observations missing

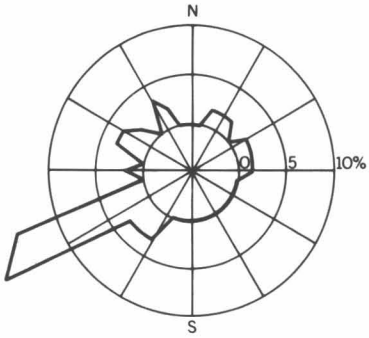

2500 m
14.2% observations missing

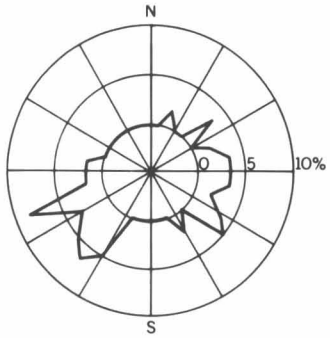

3000 m
20.6% observations missing

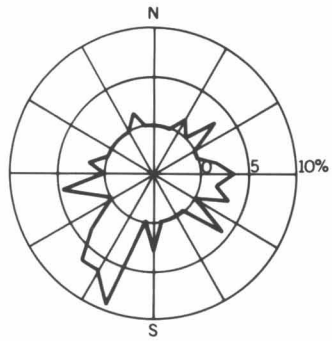

3250 m
20.6% observations missing

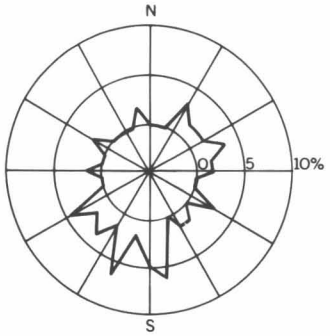

3500 m
25.3% observations missing

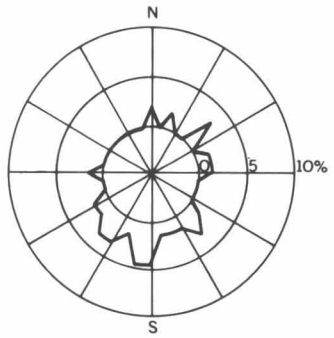

4000 m
34.9% observations missing

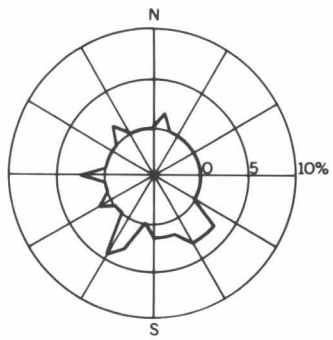

5000 m
50.8% observations missing

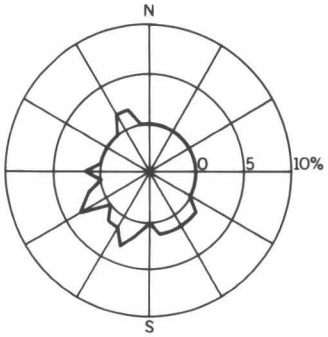

5559 m, 500 mb
55.5% observations missing

Divide Station

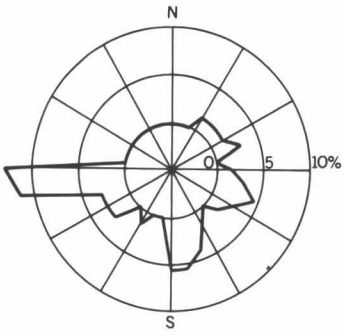

Surface - 2670 m
0% observations missing
10.3% calms

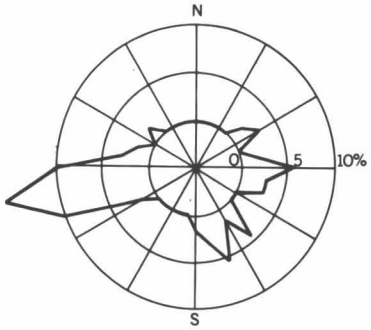

2750 m
7.14% observations missing

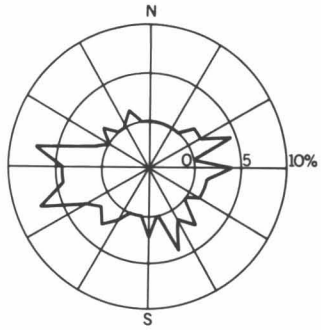

3000 m
21.4% observations missing

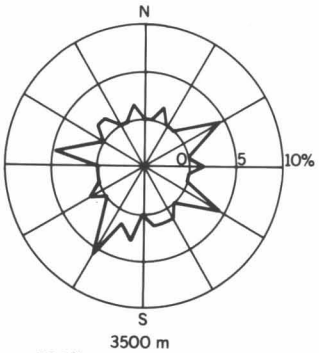

3500 m
38.5% observations missing

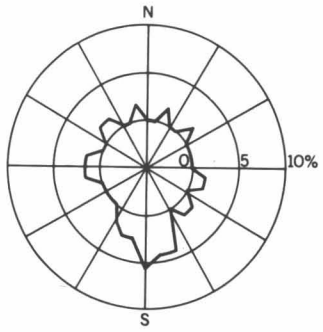

4000 m
44.2% observations missing

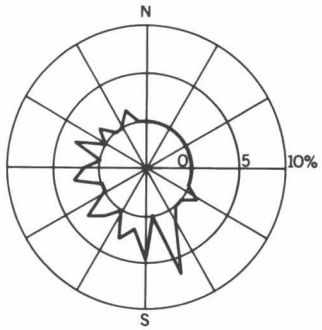

4750 m
50% observations missing

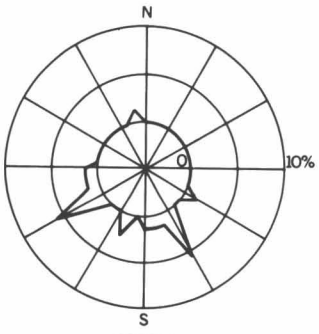

6000 m
54.2% observations missing

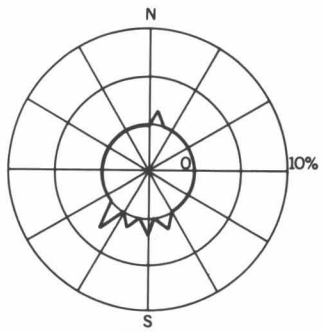

8000 m
74.2% observations missing

II

WIND SPEED FREQUENCIES DURING LOW-PRESSURE PERIODS

Altitude (meters above sea level)	Frequency (% of total study period)												
	0 -2	2.1 -4	4.1 -6	6.1 -8	8.1 -10	10.1 -12	12.1 -14	14.1 -16	16.1 -18	18.1 -20	20.1 -22	22.1 -24	Wind speed (m/sec)
Kaskawulsh Station*													
7000	–	1.60	1.60	3.17	1.60	–	–	–	–	–	–	–	
6000	–	3.17	6.34	4.76	1.60	1.60	3.17	–	–	–	–	–	
5559	1.60	3.17	11.10	4.76	–	1.60	1.60	–	–	–	–	–	
5000	–	12.70	6.34	4.76	3.17	1.60	1.60	–	–	–	–	–	
4500	7.93	9.52	6.34	4.76	7.93	1.60	–	–	–	–	–	–	
4000	3.17	19.04	4.76	7.93	3.17	4.76	–	–	–	–	–	–	
3750	7.93	4.76	20.60	3.17	3.17	4.76	1.60	3.17	–	–	–	–	
3500	11.10	11.10	14.20	11.10	4.76	4.76	–	–	–	–	–	–	
3250	11.10	15.80	19.04	3.17	6.34	3.17	–	–	–	–	–	–	
3000	11.10	14.20	17.40	11.10	3.17	1.60	–	–	–	–	–	–	
2750	15.80	17.40	12.70	6.34	1.60	1.60	3.17	1.60	–	–	–	1.60	
2500	17.40	19.04	20.60	3.17	–	3.17	–	3.17	–	–	–	–	
2250	14.20	25.30	12.70	4.76	6.34	–	–	1.60	1.60	–	–	–	
2000	11.10	23.80	9.52	7.93	6.34	3.17	1.60	3.17	–	–	–	1.60	
Surface (1768)	20.60	11.10	17.40	15.80	11.10	3.17	–	–	–	–	–	–	
Divide Station†													
8000	–	2.85	2.85	–	–	2.85	–	–	–	–	–	–	
7000	–	2.85	4.20	2.85	1.42	1.42	2.85	1.42	–	1.42	1.42	–	
6000	–	1.42	7.14	1.42	5.70	7.40	4.30	–	–	–	–	–	
5500	1.42	2.85	2.85	7.14	8.60	2.85	2.85	–	–	–	–	–	
5000	1.42	2.85	5.70	10.00	7.14	5.70	–	–	–	–	–	–	
4750	–	7.14	8.60	8.60	4.30	4.30	–	–	–	–	–	–	
4500	1.42	10.00	11.40	8.60	1.42	1.42	–	–	–	–	–	–	
4250	5.70	5.70	10.00	8.60	4.30	–	2.85	–	–	–	–	–	
4000	5.70	10.00	7.14	8.60	4.30	2.85	–	–	–	–	–	–	
3750	5.70	10.00	7.14	11.40	2.85	1.42	–	1.42	–	–	–	–	
3500	4.30	14.20	11.40	7.14	2.85	4.30	1.42	–	–	–	–	–	
3000	7.14	10.00	17.10	11.40	8.60	4.30	–	1.42	–	–	–	–	
2750	11.40	17.10	15.70	18.50	7.14	4.30	–	–	1.42	–	–	–	
Surface (2670)	39.49	24.20	15.70	7.14	2.85	–	1.42	–	–	–	–	–	
Seward Station††													
6000	3.20	6.40	3.20	–	–	–	–	–	–	–	–	–	
5650	–	9.67	3.20	–	–	–	–	–	–	–	–	–	
5000	3.20	6.40	6.40	–	–	–	–	–	–	–	–	–	
4500	3.20	–	9.67	3.20	–	–	–	–	–	–	–	–	
4000	9.67	6.40	3.20	–	–	–	–	–	–	–	–	–	
3500	12.90	6.40	–	–	–	–	–	–	–	–	–	–	
3000	9.67	12.90	–	–	–	–	–	–	–	–	–	–	
2500	32.20	6.40	–	–	–	–	–	–	–	–	–	–	
2000	35.40	9.67	–	–	–	–	–	–	–	–	–	–	
Surface (1875)	74.50	6.40	–	–	–	–	–	–	–	–	–	–	

*Total at any one level never exceeds 80.9%, the portion of the total study period during which low-pressure systems occurred at Kaskawulsh Station.

†Total at any one level never exceeds 82.8%, the portion of the total study period during which low-pressure systems occurred at Divide Station.

††Total at any one level never exceeds 80.6%, the portion of the total study period during which low-pressure systems occurred at Seward Station.

Microclimatological Studies Over the Seward Glacier Snowpack*

Ray Lougeay†

ABSTRACT. Microclimatic observations for a ten-day period in the summer of 1965 on the upper Seward Glacier show that wind profiles closely approximate log-linear curves, as would be expected under the stable conditions characteristic of the period. Temperature profiles have a distinct double inversion pattern during daytime hours. Net radiation is the dominant heat source during each day of the period, whereas sensible and latent heat fluxes were almost insignificant due to low wind speeds and limited temperature ranges, with temperatures generally close to 0°C.

Introduction

This study isolated and monitored heat sources on the Seward Glacier for ten days during 1965, in an attempt to determine the relative importance of each component of the total energy balance at the air–snow interface. A comparison of these findings with those of similar studies may provide a greater understanding of microclimatic phenomena under various environmental and meteorological conditions.

Site. The St. Elias range trends northwest through southwestern Yukon and into eastern Alaska, attaining a maximum elevation of 6040 m with eight peaks over 5000 m. The vast accumulation basin of the Seward Glacier is pocketed between the Mt. St. Elias (5490 m), Mt. Logan (6040 m), and Mt. Vancouver (4828 m) massifs, approximately 75 km from the Gulf of Alaska (Plate 1).[1]

Maritime air, which dominates the climate of this area, is funneled up the Malaspina and Seward Glaciers from the Gulf of Alaska. This marine influence produces high annual snowfall and numerous overcast days (Taylor-Barge, 1969). The observation site was located in the eastern portion of the Seward catchment basin, 4 km west of the base of Mt. Vancouver, at an elevation of 1700 m (134°54′ W, 60°23′ N). The surface of the micrometeorological observation site was a relatively level stretch of snow, 0.75 km northeast of the nearest small nunatak, on which the camp and general meteorological instruments were situated (Seward Station A, Plate 1).

Methods. Observations were conducted continuously for ten days during the summer of 1965–from 2100 Yukon Standard Time (YST), 15 July, to 1000 YST 25 July. Individual observations were taken every fifteen minutes. Varied weather conditions prevailed during the study period (Fig. 1). The following data were collected: (1) ambient air temperature at 20, 40, 80, and 160 cm above the snow surface; (2) wind velocity at 20, 40, 80, and 160 cm; (3) incoming and reflected short-wave radiation; and (4) incoming and net all-wave radiation. In addition to these data, psychrometric readings were taken every half hour at approximately 50 cm and 160 cm. Regular synoptic meteorologic observations were obtained at three-hour intervals at Seward Station A. Ablation measurements were made daily at 0600, 1200, 1800, and 2400 YST, at five ablation stakes near the site. Snow pits–to obtain snow density and compaction data–were dug at the beginning and termination of the microclimatology program.

Instrumentation. Two Eppley pyrheliometers, sensitive from 0.3 to 4.5 μ, were used to measure short-wave radiation, one oriented upwards and the other oriented perpendicular to the snow surface, which was practically level. All-wave radiation was measured by two Beckman and Whitley thermal radiometers, one for all-wave incoming radiation and the other for all-wave net radiation.

Wind velocity was recorded with a Thornthwaite Wind Profile Register, a sensitive totalizing anemometer system developed for use in microclimatic observations. When this anemometer system ceased to operate on the third day of observations, four Fuess totalizing anemometers were attached to the mast at the same levels.

All radiation, wind, and temperature instrument lead wires were fed into a small tent where the observer could record the data using a twelve-channel master switch and potentiometer, calibrated to an ice bath.

Weather Conditions. During the period, nine of the ten days were characterized by a mean cloud cover of over six-tenths; fog was present 20% of the time. Often the fog was associated with snowfall, which was also present 20% of the total period. Light rain fell for one 18-hour period on 19 July and 20 July, representing 7% of the total period of observation. Weather was clear only on 16 July. Overcast conditions moderated temperature ranges during most of the study period. Temperatures at the 160-cm level ranged from a high of 5.5°C to a low of -6.8°C with an overall mean of -0.1°C. Wind speeds at 160 cm were in general quite low, usually less

---

*This report is a modified version of an article appearing in *Research Paper No. 54,* Arctic Institute of North America (1969), and is reprinted here with permission.

†Department of Geography, University of Michigan, Ann Arbor

[1] Plate 1 is a map inside the back cover of this volume.

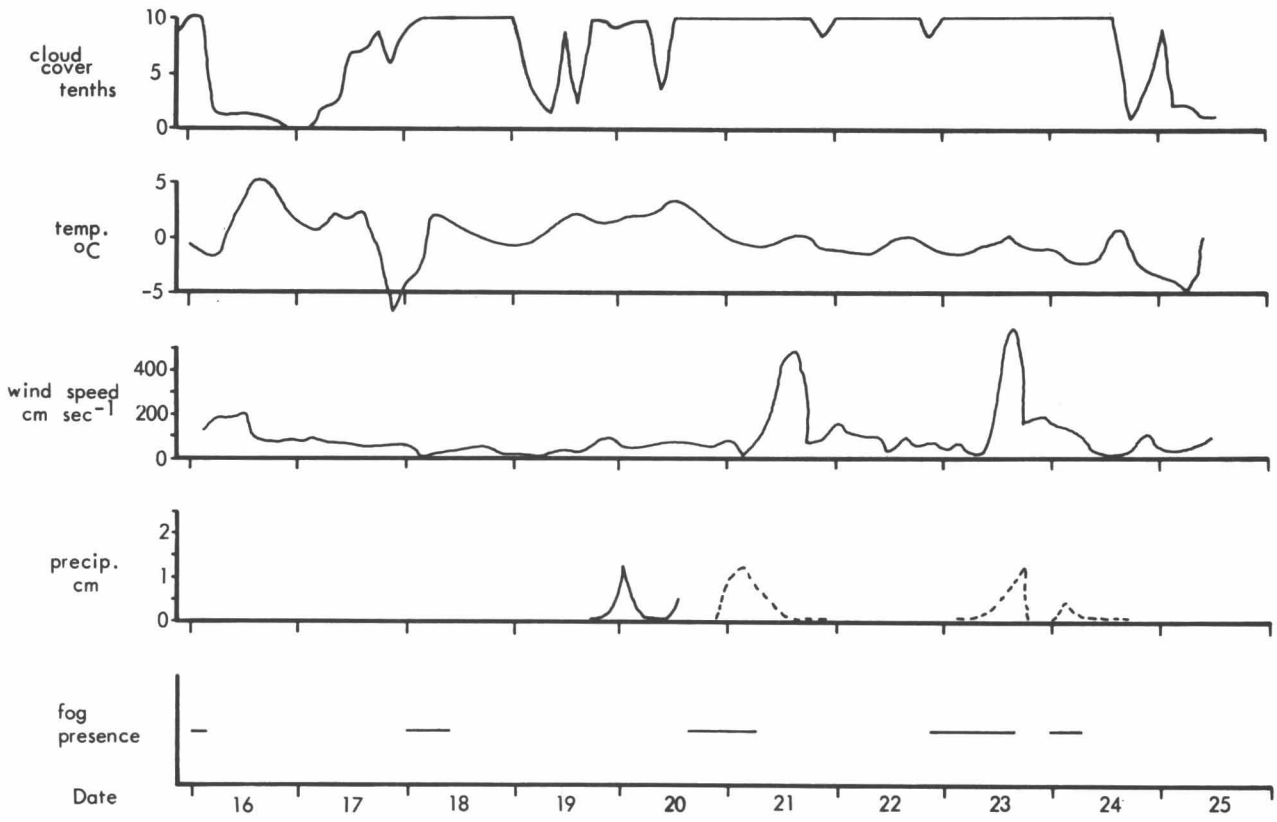

Fig. 1. Meteorological conditions on the upper Seward Glacier, July 15–25, 1965

than 100 cm sec^{-1}. The 10-day mean was 93 cm sec^{-1}, rising above 200 cm sec^{-1} on only two occasions.

Microclimatic Observations

Radiation. The net radiation budget, R, across the air–snow interface may be expressed by:

$$R = S_i - S_o + L_i - L_o \qquad (1)$$

where

S_i = incoming short-wave radiation
S_o = outgoing short-wave radiation
L_i = incoming long-wave radiation
L_o = outgoing long-wave radiation

All terms of equation 1 were measured except L_o, which was computed.

Positive radiation budgets characterized 81% of the study period. Negative radiation budgets occurred only at night under relatively clear skies or conditions of mixed light rain and snowfall. Figure 2 shows the trends of various components of the radiation budget as well as cloud cover during the period. The mean net radiation value for the entire period was +0.14 ly min^{-1} (5.86 kJ m^{-2} min^{-1}), with a maximum of +0.58 ly min^{-1} (24.28 kJ m^{-2} min^{-1}) on the late morning of 16 July and a minimum of -0.06 ly min^{-1} (-2.51 kJ m^{-2} min^{-1}) on the early morning of 17 July.[2]

[2]The above radiation values—and all other data presented in the text—represent the means of three-hour aggregates unless otherwise noted.

Incoming radiation was mainly short wave during the daytime, especially during periods of little cloud cover (Fig. 2, Table 1), and at night long-wave radiation was dominant. Long-wave radiation under overcast conditions represented a greater portion of the radiation budget (Tables 1, 2). Dominance of long-wave radiation in the budget was accentuated when fresh snowfall accompanied the overcast conditions, since the new snow increased the albedo to approximately 85–95%.

The mean daytime albedo for the entire period of observation was 75.4%, a value slightly higher than those obtained in some other studies over snow surfaces (Hubley, 1955; Lister and Taylor, 1961; Keeler, 1964; Brazel, 1968). Although the albedo of a snow surface varies inversely with the solar elevation, in this study the lowest albedo values usually were recorded just after local sunrise and just before twilight. The observed albedo values do seem, however, to represent actual conditions. In the early morning Mt. Vancouver to the east obscured direct low-angle solar radiation, and Mt. Logan to the northwest obscured direct low-angle solar radiation in the evening. Thus the lower albedo values observed in the morning and evening are due to the difference between direct solar radiation and the diffuse global radiation experienced as the shadow of the adjacent mountains passed over the study site.

Maximum albedo values of 91.4% were observed in the early afternoon of 24 July with fresh snow on the glacier surface and a low, stratus cloud-layer overhead. All relatively high albedo values were associated with fresh snow

TABLE 1. Mean Radiation Rates, Day and Night

Date (July 1965)	Si (ly min^{-1})	So (ly min^{-1})	Albedo %	Ai (ly min^{-1})	Ao (ly min^{-1})	R (ly min^{-1})	Cloud cover (tenths)
15 n				0.416	0.485	-0.069	8
16 d	0.919	0.679	73.1	1.411	1.023	0.388	1
n				0.395	0.445	-0.050	0
17 d	0.926	0.643	69.9	1.456	1.065	0.391	5
n				0.438	0.435	0.003	8
18 d	0.623	0.510	82.0	1.198	0.815	0.383	10
n				0.492	0.467	0.025	8
19 d	0.699	0.561	75.7	1.279	0.929	0.350	5
n				0.404	0.448	-0.044	10
20 d	0.619	0.469	74.3	1.232	0.932	0.300	9
n				0.433	0.466	-0.033	10
21 d	0.596	0.541	68.7	1.102	0.943	0.159	10
n				0.508	0.471	0.037	9
22 d	0.761	0.579	71.5	1.337	0.983	0.354	10
n				0.486	0.463	0.023	7
23 d	0.384	0.314	78.3	0.909	0.789	0.120	10
n				0.471	0.458	0.013	10
24 d	0.641	0.614	90.4	1.195	0.949	0.246	8
n				0.414	0.434	-0.020	5
25 d	0.595	0.464	70.2	1.112	0.958	0.154	1
Mean	0.676	0.537	75.4	1.223	0.508	0.285	7

d = day = 0600 to 2100 YST
n = night = 2100 to 0600 YST

Si = short-wave incoming radiation
So = short-wave outgoing radiation
Ai = all-wave incoming radiation
Ao = all-wave outgoing radiation
R = all-wave net radiation

TABLE 2. Daily Radiation Totals

Date[1] (July 1965)	R (ly)	Ai (ly)	Ao (ly)	Li (ly)	Lo (ly)	Si (ly)	So (ly)
16	281	1437	1156	687	602	750	554
17	284	1410	1126	660	644	750	482
18	328	1241	913	734	521	507	392
19	283	1320	1037	770	603	550	434
20	210	1244	1034	760	667	484	367
21	120	1179	1059	676	618	503	441
22	306	1372	1066	778	614	594	452
23	91	1033	942	744	707	289	235
24	198	1247	1049	752	582	495	467
25 (10 hr)	68	683	615	405	386	278	229
Total	2709	12166	9997	6966	5944	5200	4053

[1]day = 2100–2100 YST
R = all-wave net radiation
Ai = all-wave incoming radiation
Ao = all-wave outgoing radiation

Li = long-wave incoming radiation
Lo = long-wave outgoing radiation
Si = short-wave incoming radiation
So = short-wave outgoing radiation

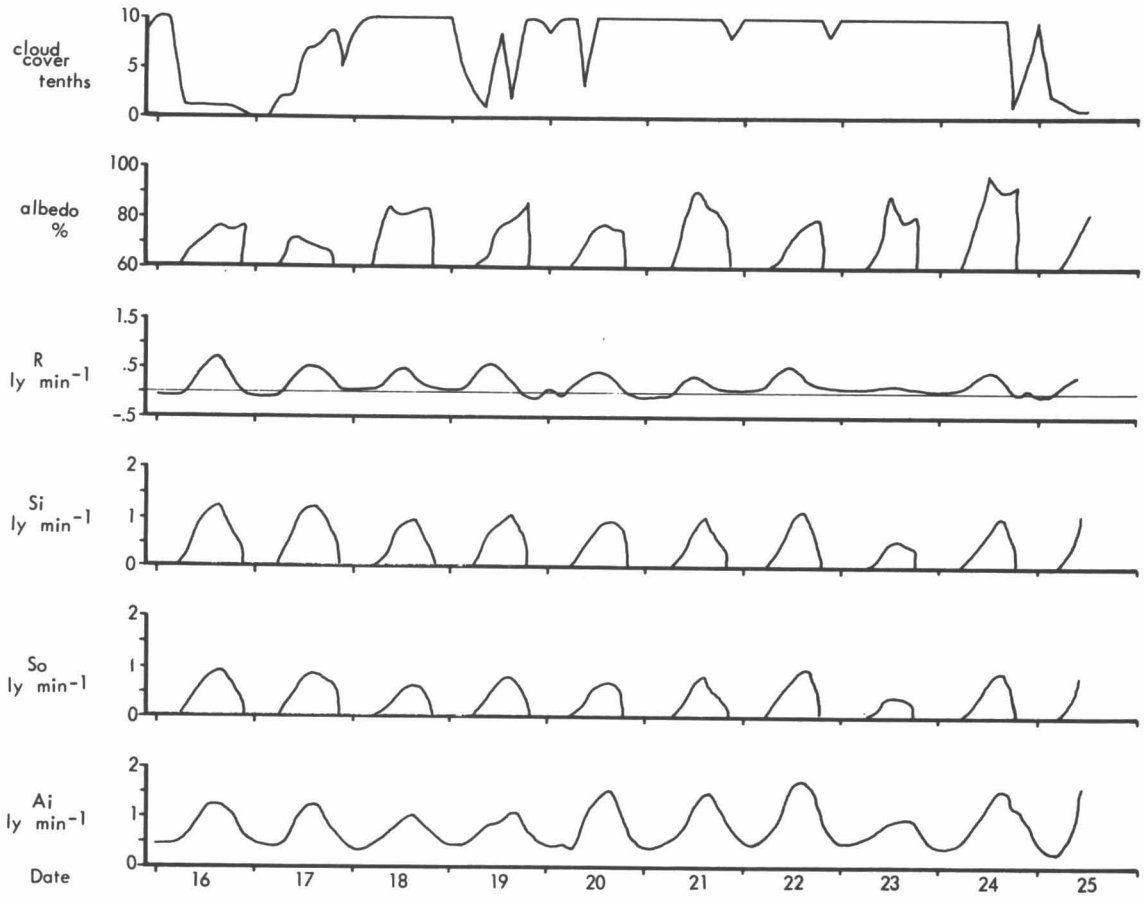

Fig. 2. Solar radiation recorded on the upper Seward Glacier, July 15–25, 1965

conditions, whereas lower values usually were associated with older, granular, saturated, and sun-cupped snow. The differences in observed albedo and their association with changing cloud cover, precipitation, and surface conditions are given in Figure 2, and Table 1. Greater detail is given in Lougeay, 1969, Appendix II.

Temperature. Temperatures were recorded from four thermocouples positioned at 20, 40, 80, and 160 cm above the snow surface. These thermocouples were shielded from direct and reflected solar radiation by two horizontal metal plates. These temperature sensors produced highly accurate temperature data, capable of showing even slight temperature gradients.

Table 3 shows the general temperature regime for the entire period. The 160-cm level is approximately the height of the standard Stevenson screen, and therefore the data from this level are most comparable with data from studies using instruments mounted in such shelters.

The overall mean temperature for the period at the 160-cm level was -0.1°C with a minimum of -6.75°C on the evening of 17 July and a maximum of 5.46°C the afternoon of 16 July (Fig. 1).

Temperature profiles (Figs. 3, 4) indicate that stable conditions prevailed over the snow surface throughout the period. The nighttime temperature profiles (Fig. 3;

TABLE 3. Temperature Regime for Study Period*

Height (cm)	Mean max (°C)	Mean min (°C)	Mean range (°C)
20	3.16	-2.42	5.66
40	1.57	-2.03	3.90
60	4.96	-2.09	7.08
160	2.01	-1.85	3.85

*Compiled from 3-hr aggregate data

Table 4) are quite close to log-linear profiles above 20 cm, which is expected under such conditions (McVehil, 1964). Periods of nighttime isothermal temperature gradients above 20 cm for 15, 20, 22, and 23 July were associated with advective fog and thick, cold-air ponding on the glacier surface (Fig. 1, 3). It is assumed that during periods of positive radiation budget, when the snow surface is known to have been saturating and melting, the surface temperature was 0°C. The resultant nighttime temperature profiles often indicate that the minimum temperature occurs at some level above the surface, a phenomenon observed by others under negative radiation budget conditions. This has never been fully understood. Lettau *et al.* (1967)

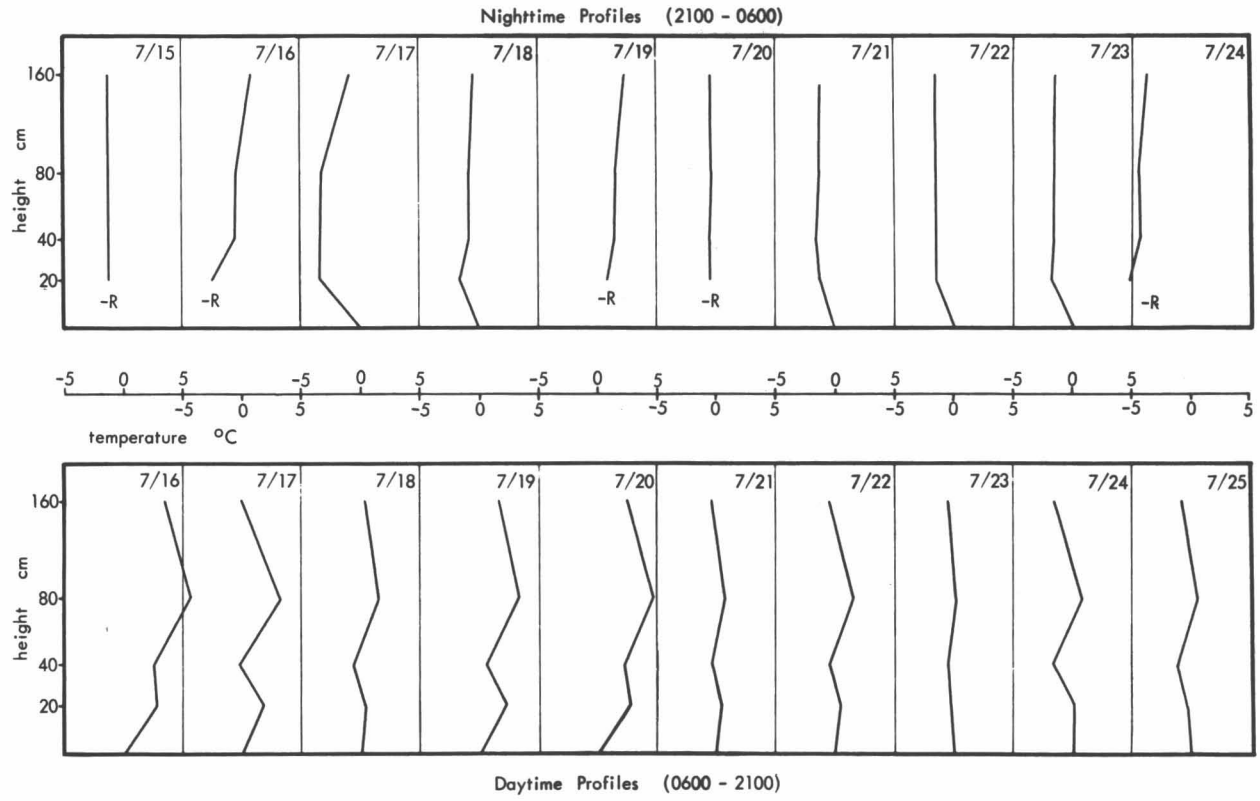

Fig. 3. Mean daily temperature profiles, upper Seward Glacier, July 15–25, 1965

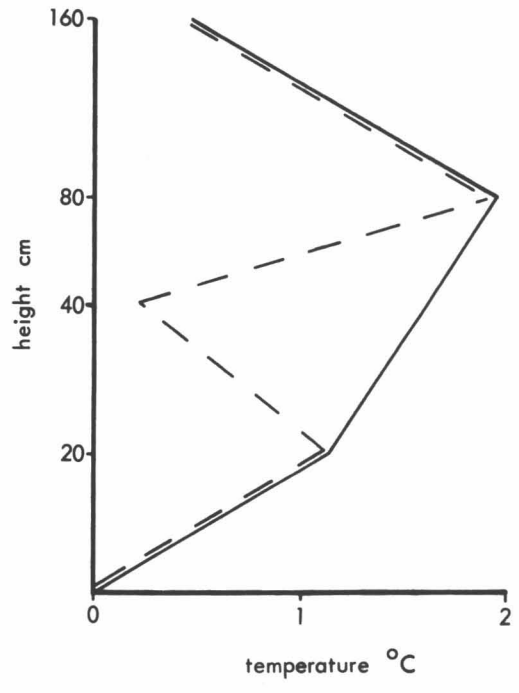

Fig. 4. Mean daytime temperature profile for period July 15–25, 1965, shown with and without 40-cm level data

TABLE 4. Mean Temperatures, Day and Night

Date (July 1965)	20 cm	40 cm	80 cm	160 cm
15				
n	-1.02	-1.07	-1.11	-1.18
16 d	2.84	2.48	5.70	3.34
n	-2.58	-0.61	-0.49	0.88
17 d	1.77	-0.33	3.05	-0.17
n	-3.32	-3.23	-3.21	-1.00
18 d	0.32	-0.61	1.30	0.21
n	-1.62	-0.90	-0.92	-0.58
19 d	2.13	1.54	3.14	1.61
n	0.92	1.40	1.60	2.07
20 d	2.72	2.19	4.67	2.27
n	-0.40	-0.44	-0.42	-0.49
21 d	0.26	-0.21	0.71	-0.40
n	-1.18	-1.45	-1.25	-1.23
22 d	0.52	-0.52	1.54	-0.49
n	-1.49	-1.57	-1.55	-1.54
23 d	-0.22	-0.51	0.03	-0.47
n	-1.96	-1.69	-1.71	-1.59
24 d	0.04	-1.55	0.86	-1.46
n	-5.17	-4.46	-4.50	-3.98
25 d (4 hr.)	-0.29	-1.09	0.41	-0.91

d = day = 0600–2100 YST
n = night = 2100 to 0600 YST

present a summary of similar observations and a short discussion of the possible origin of this "temperature anomaly." They support Lütze's (1960) theory that the anomaly depends on relatively low subsurface heat-flux values. During this study period, however, the phenomenon of the "elevated minimum" occurs at times of positive radiation budgets and overcast skies. The temperature profile below 20 cm was not estimated during periods of negative radiation balance when the surface temperature was below 0°C.

The daytime temperature profiles (Fig. 3; Table 4) are more complex. Two distinct inversion layers over the snow surface were present in 87% of the daytime observations. Those observations which departed from this pattern were usually made in the early morning or early evening—the transition between nighttime and daytime conditions. Every effort was made in the field to minimize instrumental error. All connections, thermocouples, and lead wires were thoroughly checked and recalibrated with an ice bath after it was found that this strong daytime temperature profile persisted.

The mean daytime temperature profiles for 21 and 22 July exhibit only one weak inversion at the 80-cm level. Temperatures were colder during these periods and the 20-cm level was below 0°C—the assumed temperature of the snow surface. These two periods, when the double inversion pattern was ameliorated, were also periods of relatively high wind speeds. No satisfactory explanation has been found to explain this double-inversion phenomenon which appears so regularly in this study, yet seems

TABLE 5. Mean Wind Velocities, Day and Night

Date (July 1965)	20 cm	40 cm	80 cm	160 cm
15				
n	112.6	122.9	138.3	153.3
16 d	90.9	100.4	107.3	124.2
n	59.5	65.4	74.7	85.3
17 d	49.6	54.3	74.7	71.1
n	21.6	19.8	27.6	29.9
18 d	19.0	27.9	44.0	36.8
n	0.0	0.5	14.6	6.4
19 d	12.0	30.0	49.4	48.4
n	21.4	34.9	54.5	51.7
20 d	37.4	55.3	74.7	74.7
n		94.9	32.3	50.6
21 d	185.8	187.7	250.6	257.7
n	64.0	102.2	113.5	123.1
22 d	84.8	69.3	85.8	68.1
n	25.0	37.5	50.6	46.2
23 d	168.7	202.2	226.1	238.2
n	93.0	121.0	130.3	138.3
24 d	18.7	46.9	44.2	40.5
n	14.1	29.9	42.6	37.9
25 d (4 hr.)	29.9	53.3	91.7	79.5

d = day = 0600–2100 YST
n = night = 2100 to 0600 YST

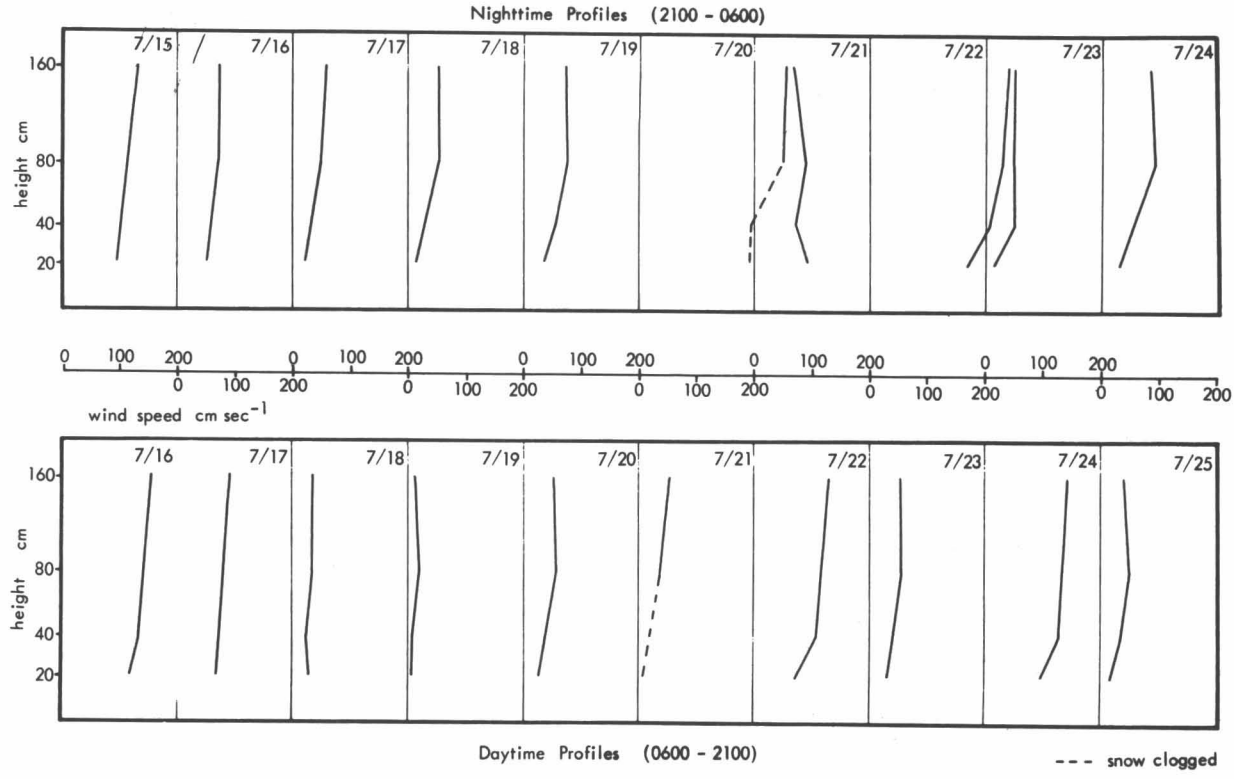

Fig. 5. Mean daily wind profiles, upper Seward Glacier, July 15–25, 1965

anomalous in terms of other studies (for example, Lister and Taylor, 1961: Keeler, 1964; Orvig, 1951, 1954; Lettau *et al.*, 1967.) The 40-cm data are the most anomalous when compared with observations from similar environments. Figure 4 presents mean daytime temperature profiles for the entire period, both including and excluding the 40-cm-level data. The profile which excludes the 40-cm data (solid line on Fig. 4) might reasonably be expected considering the environment of the study site, with its moderate daytime temperatures and snow surface.

Wind. Wind speeds were measured at the 20-, 40-, 80-, and 160-cm levels. The mean wind speed at the 160-cm level for the total period was 93.3 cm sec^{-1}, and the maximum wind speed was 605.7 cm sec^{-1}, occurring in the early afternoon of 23 July. During 74% of the entire period, winds were less than 100 cm sec^{-1}. From these data and those presented in Table 5 it can be seen that wind speeds associated with this microclimatic study are very slight indeed. It is perhaps of interest to mention that only a few hours after the observations were terminated, the micrometeorological station was almost destroyed by winds over 3000 cm sec^{-1}.

Grainger and Lister (1966) give a summary of wind profiles associated with various stability conditions. Theoretically, wind speed when plotted against the log of height should produce a curve which is convex downward under stable conditions, and wind profiles for this period (Fig. 5) bear out this expectation. Conditions were almost always quite stable and both the night- and daytime wind profiles produce this type of curve.

Sensible and latent heat fluxes. The sensible and latent heat fluxes across the air–snow interface were computed for each day (2100–2100) of the study period (Table 6). The procedures for these calculations follow the outlines presented in Lister and Taylor (1961) and Keeler (1964).

The data presented in Table 6 represent sensible and latent heat-flux values calculated between the surface and 20-cm level. Surface wind speed is assumed to be zero; the temperature of the surface is 0°C. A mean roughness parameter value of 0.41 cm was used in the calculation of all heat flux values.[3] This value is comparable to those found by other investigators under similar environmental conditions (Deacon, 1949; Lister and Taylor, 1961; Keeler, 1964).

[3]The roughness parameter was calculated from data obtained with the Thornthwaite Wind Profile Register. It was felt that these data were more accurate than the wind data from the Fuess anemometer. Only a slight error in the measurement of wind velocity would change the roughness parameter greatly.

TABLE 6. Daily Heat Balance Terms

Date[1] (July 1965)	R (ly)	S (ly)	E (ly)	P (ly)	M (ly)	Melt = M/80 (cm H_2O)
16	281	21.60	-18.0	–	285	3.6
17	284	1.21	- 7.8	–	277	3.5
18	328	- 3.28	- 3.6	–	321	4.0
19	283	0.86	- 1.2	–	283	3.5
20	210	10.36	43.2	0.05	264	3.3
21	120	0.60	1.8	–	122	1.5
22	306	- 1.47	0.2	–	304	3.8
23	91	-12.61	-30.0	–	48	0.6
24	198	- 3.54	- 5.4	–	189	2.4
25 (2400-1000)	68	-10.45	- 2.4	–	55	0.6
Totals (10 days)	2169	3.28	-23.6	0.05	2149	26.8

[1]day = 2100–2100 YST

Positive values represent energy flux into the snowpack; negative values are outgoing flux.

R = net radiation budget
S = sensible heat flux
E = latent heat flux
P = energy transferred by precipitation
M = energy used in the melting of the snowpack

It is assumed in the computation of the sensible and latent heat fluxes that logarithmic wind and temperature profiles and neutral stability conditions prevail, thus a source of error was introduced since these conditions were not the norm during this period. The assumption that the air temperature immediately above the surface would equal the snow surface temperature is also questionable (Lister and Taylor, 1961).

Energy Balance of the Snow Surface

The total heat balance of the snow surface is expressed by the following equation.

$$\pm R \pm S \pm E \pm I + P - M = 0 \qquad (2)$$

where

R = the all-wave net-radiation budget
S = heat energy transferred by convection (sensible heat flux)
E = latent heat transferred by evaporation or condensation (latent heat flux)
I = energy used in conductive heating of the snowpack
P = energy transferred by precipitation (direct, not latent)
M = energy used in the melting of the snowpack

P, the energy transferred to, or from, the snow surface by precipitation is that heating or cooling of the snow surface caused by the temperature difference between the snow surface and the precipitation. P may be computed by use of the following equation:

$$P = C_w (T_p - T_s) P_r \qquad (3)$$

TABLE 7. Percentage Comparisons of the Energy Balance Components at Diverse Locations

Location	Lat. (N)	Elev. (m)	*R*	*S*	*E*	Surface type	Investigator	Investigation year	Publication year
Seward Glacier	60°	1770	99.8	0.2	- 1.1	snow	Lougeay	1965	1969
Ellesmere Ice Shelf	82°	50	96	4	4	ice	Lister	1960	1962
Fairbanks	65°	144	86	14	-24	snow	Wendler	1966	1967
Greenland	-	-	78	22	- 8	ice	Ambach	1960	1960
Salmon Glacier	56°	1700	75	15	10	ice	Adkins	1957	1958
Britannia Glacier	77°	470	75	20	5	ice	Lister & Taylor	1953	1961
Ottawa, Canada	-	-	74	26	-74	snow	Gold & Williams	1961	1961
Blue Glacier	48°	2000	69	25	6	snow	LaChapelle	1958	1959
Alps (Kesselwandferner)	-	-	68	32	- 2	snow	Ambach & Hoinke	1963	1963
Barnes Ice Cap	70°	865	68	32	32	snow/ice	Orvig	1950	1951
Penny Ice Cap	67°	2050	61	9	30	snow	Orvig	1953	1954
Worthington Glacier	61°	850	51	29	20	ice	Streten & Wendler	1967	1968
Sverdrup Glacier	76°	300	51	34	15	ice	Keeler	1963	1964
Karsa Glacier	68°	1100	32	44	24	snow	Wallen	1942	1948
Britannia Glacier	77°	620	67	32	1	snow/ice	Lister & Taylor	1953	

where

C_w = specific heat of water
T_p = temperature of precipitation
T_s = temperature of the surface (0°C)
P_r = amount of precipitation (gm cm^{-2})

Latent heat is considered in the E term and is not treated in the calculation of P. P values were calculated for each day of the study period (Table 6); in the computations it was assumed that the temperature of the precipitation, T_p, was equal to the 160-cm-level temperature. It can be seen that the amount of energy transferred by precipitation is small.

Table 6 presents the values of all the terms of the energy balance equation as computed for each day of the period. It should be remembered that the snowpack was assumed to be isothermal and therefore the I term (energy conducted into the snowpack) would be zero. Values of M—energy used in melting of the snowpack—were found by use of equation 2.

Ablation

Marcus and Ragle (1970) have computed that the snowpack lost 12.7 cm of water equivalent during the study period. This is approximately half the theoretical melt value of the energy balance (Table 6). The discrepancy between measured ablation values and those computed with the energy balance formula is not surprising when one considers the assumptions which were made in computing the various terms of the energy balance equation. Also, the "measured ablation" figures, calculated from snow density data measured in snow pits dug at the beginning and end of the study period, do not account for meltwater which had percolated below the upper layers of firn.

Conclusions

During the study period the net radiation budget was dominant in the energy balance of the snow surface. Radiation accounted for over 99% of the total energy source (Tables 6, 7). This dominance of radiation and the insignificance of sensible and latent heat fluxes are due to the low wind velocities and limited temperature ranges—temperatures were generally close to 0°C—characteristic of this study period. Table 7 presents a comparison of relative energy balance data from this study with data from similar studies of other glaciers. Radiation is usually dominant in the energy balance of all the studies, but seldom are sensible and latent heat values as insignificant as those observed during this study.

The extremely low sensible and latent heat-flux values for Seward can be explained, however, in light of the assumptions made in the calculations of these values and the prevailing meteorological conditions during the period. Low wind speeds and stable atmospheric conditions prevented large energy exchange by turbulent transfer. The absence of warm, wet storms, which usually contribute greatly to the glacial ablation in this region (Hubley, 1957), explains lower latent heat-flux values than would be expected. Assumptions made about the wind, temperature, and stability conditions were possibly erroneous during parts of the study period. Therefore it is probable that the sensible and latent heat-flux values are in error. In reality, S and E may have represented a greater percentage of the total energy balance then the calculated figures indicate.

The relative magnitude of the terms of the energy-balance equation, as obtained in this study, are probably not representative of those values for the whole ablation season. The observations of this study are, however, indicative of microclimatic conditions under meteorological situations similar to those at Seward during this period.

Acknowledgments

I would like to thank Karen Ewing, Robert Farrell, Melvin Marcus, Bea Taylor-Barge, and Christopher Warntz for their help in recording the data. Also, I would like to acknowledge the help received from Dr. Melvin G. Marcus and Dr. Thomas R. Detwyler, and the logistical support provided by the staff of the Icefield Ranges Research Project.

References

Adkins, C. J. (1958) The summer climate in the accumulation zone of Salmon Glacier, *J. Glaciol.*, 3, 195–206.

Ambach, W. (1960) Investigations of the heat balance in the area of ablation in the Greenland Ice Cap, *Archiv. Meteorol. Geophys. Bioklimatol.*, Ser. B, 10, 279–288.

Ambach, W., and Hoinkes, H. C. (1963) The heat balance of an Alpine snowfield, *Assoc. Intern. Hydrol. Sci., Gentbrugge, Publ. 61,* pp. 24–36.

Brazel, A. J. (1968) Icefield Ranges Climatology Program, St. Elias Mountains, 1964, Pt. 2: Presentation and analysis of radiation data, *Res. Paper No. 31-B,* Artic Inst. North Am., pp. 1–31.

Deacon, E. L (1949) Vertical diffusion in the lower layers of the atmosphere, *Quart. J. Roy. Meteorol. Soc.,* 75, 89–103.

Gold, L. W., and Williams, G. P. (1961) Energy balance during the snow melt period at an Ottawa site, *Assoc. Intern. Hydrol. Sci.,* pp. 288–294.

Grainger, M. E., and Lister, H. (1966) Wind speed, stability and eddy viscosity over melting ice surfaces, *J. Glaciol.,* 6, 101–127.

Hubley, R. C. (1955) Measurements of diurnal variation in snow albedo on Lemon Creek Glacier, Alaska, *J. Glaciol.,* 2, 560–563.

Hubley, R. C. (1957) An analysis of surface energy during the ablation season on Lemon Creek Glacier, Alaska, *Trans. Am. Geophys. Union,* 38, 68–84.

Keeler, C. M. (1964) Relationship between climate, ablation, and run-off on the Sverdrup Glacier, 1963, Devon Island, N.W.T., *Res. Paper No. 27,* Arctic Inst. North Am., 125 pp.

LaChapelle, E. (1959) Annual mass and energy exchange on the Blue Glacier, *J. Geophys. Res.,* 64, 443–449.

Lettau, H. H., Wolleston, S. H., and Dalrymple, P. G. (1967) Little America micrometeorology program, data analysis, *Tech. Rept. 67–46–ES,* U. S. Army Natick Labs.

Lister, H. (1962) Heat and mass balance at the surface of the Word Hunt Ice Shelf, Ellesmere Island, *Res. Paper No. 19,* Arctic Inst. North Am.

Lister, H., and Taylor, P. F. (1961) Heat balance and ablation on an Arctic glacier, *Medd. Grøn., 158,* 1–54.

Lougeay, R. (1969) Microclimatological studies over the Seward Glacier snowpack, *Res. Paper No. 54,* Arctic Inst. North Am., pp. 51–102.

Lütz̈ke, R. (1960) Unter welchen Bedingungen hebt sich des nächtlichen Temperatur Minimum von der Bodenoberfläche ab ?, *Angew. Meteorol.,* 4, 1–10.

Marcus, M. G., and Ragle, R. (1970) Snow accumulation in the Icefield Ranges, St. Elias Mountains, Yukon, *Arctic and Alpine Research,* Vol. 2, No. 4 (in press).

McVehil, G. E. (1964) Wind and temperature profiles near the ground in stable stratification, *Quart. J. Roy. Meteorol. Soc.,* 90, 136–146.

Orvig, S. (1951) The climate of the ablation period on the Barnes Ice Cap in 1950, *Geogr. Ann.,* 33, 166.

Orvig, S. (1954) Glacial-meteorological observations on ice caps in Baffin Island, *Geogr. Ann.,* 36, 193–318.

Streten, N. A., and Wendler, G. (1968) Midsummer heat balance of an Alaskan maritime glacier, *J. Glaciol.,* 7, 431–440.

Taylor-Barge, B. (1969) The summer climate of the St. Elias Mountains region, *Res. Paper No. 53,* Arctic Inst. North Am., 265 pp.

Wallen, C. C. (1948) Glacial meteorological investigations on the Karsa Glacier in Swedish Lappland: 1942–48, *Geogr. Ann.,* 30, 451–672.

Wendler, G. (1967) The heat balance at the snow surface during the melting period (March–April 1966) near Fairbanks, Alaska, *Gerlands Beitr. Geophys.,* 76, 453–460.

Morphology and Ablation Processes on Glacier Ice*

Stuart R. Loomis†

ABSTRACT. Differential ablation on debris-laden glacier ice has long been recognized for its importance in producing ice-cored topographical features. A study of ablation rates on a medial moraine of the Kaskawulsh Glacier is used in conjunction with ice-flow data and an equilibrium hypothesis of mass movement in the debris mantle to explain the morphological form that the moraine assumes.

Ice ablation and surficial topographic form on glaciers have long been related causually in glaciological literature. Where a glacier carries a surficial debris load, the relationship between ablation and topography is particularly obvious. Descriptive accounts of ablation features and debris-laden ice have appeared since before the turn of the century (Chamberlin, 1895, p. 212; Russell, 1897, p. 89). More recent accounts include Sharp (1949), and Clayton (1964). Glacial surficial features produced by differential ablation are currently designated as ice-cored topography. In the last decade a few investigators (for example, Østrem, 1959 and 1964; McKenzie, 1969) have contributed quantitative measurements to the qualitative observations reported in the earlier literature. This paper presents the results of a further study into the relationships of ablation to morphology on debris-covered ice on Kaskawulsh Glacier. Associated consideration of moraine structure and lithology are reported elsewhere (Loomis, 1970).

Data were collected on the Kaskawulsh Glacier medial moraine at the confluence of the north and central arms (60° 44′N, 139°10′W). The confluence is located at 1740 m elevation between the two east-flowing glacier tributaries; at the confluence the north arm is 3 km wide and the central arm is 3.5 km wide. Ice depths, determined by seismic measurement (Dewart, 1968, pp. 154–155), have a maximum thickness of 800 m for the north arm and 1000 m for the central arm. Ice-flow rates reach a maximum of 215 m/yr for the north arm and 152 m/yr for the central arm (Anderton, 1967, p. 8).

The medial moraine is nearly 1 km wide in the zone where the two contributing lateral moraines first merge. The debris band rapidly narrows to about 60 m at a point 0.75 km downglacier. This 60-m width remains fairly constant for several kilometers downglacier. The debris load is largely supraglacial with relatively clear ice lying below the sharp ice–debris interface. That is, by volume it is estimated less than ten percent of the rock debris of the medial moraine is englacial in nature. The till layer is predominantly coarse, angular limestone with smaller linear concentrations of basalt and shale.

There is a definite trend to moraine relief measured longitudinally from the confluence. At the head of the moraine, the relief is low (less than 2 m). Downglacier the relief increases until it reaches a maximum of 20 m at a distance of 1.4 km. The relief subsequently decreases to a height of 7 m at 5 km below the confluence. The moraine then maintains this relief magnitude for several kilometers toward the terminus.

Ablation and Moraine Cover

To examine the role of ice melting in relief development, an ablation transect was established at a point 0.5 km downglacier from the confluence and transverse to the moraine (Fig. 1). The moraine here is 300 m wide; its central ridge is 13 m high. The ablation transect consisted of 31 stakes drilled through the till cover into the ice core at approximately 15 m intervals. Stakes at the ends of the transect extended onto the debris-free ice of the central and north arms. Stake measurements were taken daily from 14 July to 7 August 1966.

Figure 2 presents some of the findings of this study in graph form. The trends of the two values plotted—mean daily ablation rate and moraine cover thickness—are apparent. Near the central ridge of the moraine, till thickness increases as mean daily ablation decreases. Calculation of the degree of correlation in this relationship, using $\log_{10}$ of mean daily ablation and the value of till thickness, yields a correlation coefficient of -0.91 (Fig. 3). The correlation is significant at the 95 percent confidence level.[1] The standard error of the estimate is 1.3 cm/day.

The Kaskawulsh findings are in agreement with the results of an experiment conducted by Østrem (1959, p. 228)

---

*This report is a modified version of an article appearing in the *Proceedings of the Association of American Geographers,* Volume 2 (1969), and is reprinted here with permission.

†Department of Geography, University of Michigan, Ann Arbor

[1] Fisher's Z transformation statistic, as used in standard statistical texts such as Downie and Heath (1965), gives a population correlation coefficient value ranging from -0.82 to -0.96.

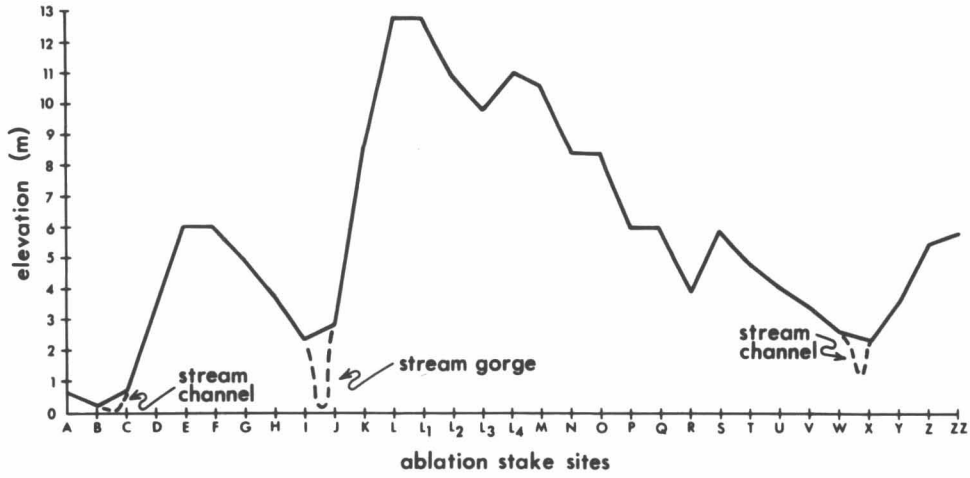

Fig. 1. Relative elevation of ablation points on or near the ablation transect across the medial moraine. Points A and B lie on the debris-free central arm of the Kaskawulsh Glacier; points Y, Z and ZZ lie on the debris-free north arm. (Note: zero datum is the stream on the central arm flowing along the moraine–ice contact; vertical relief exaggeration is approximately 13 times).

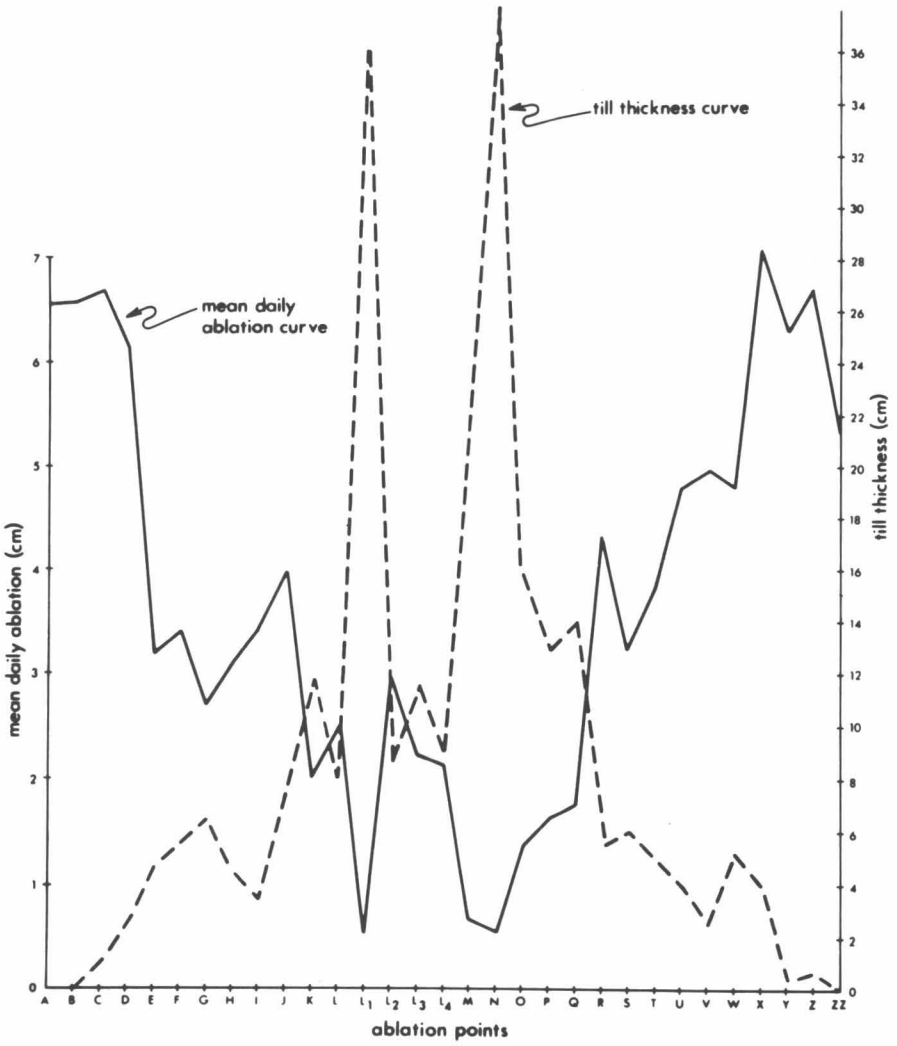

Fig. 2. Mean daily ablation and till cover thickness for ablation points on or adjacent to the ablation transect across the medial moraine of the Kaskawulsh Glacier. Point A is located on the central arm debris-free ice; point ZZ on the north arm debris-free ice.

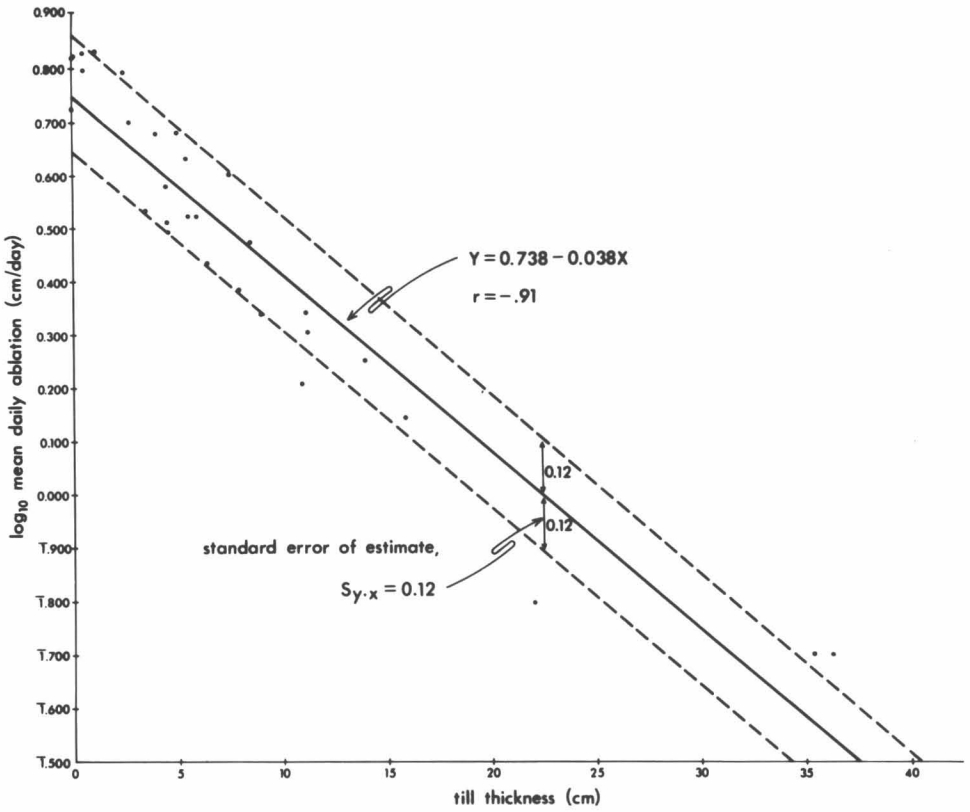

Fig. 3. Scatter diagram relating $\log_{10}$ mean daily ablation and thickness of till cover. Correlation coefficient of sample is -0.91.

in 1956 on Isfallsgläciären, Sweden. Figure 4 compares the data from the two areas. Østrem's experiment utilized thin layers of sand and gravel placed on clean glacier ice in small test fields. During his experimental period (15 July to 8 August), when the mean air temperature was 5.4°C, uncovered ice was observed to ablate at a mean rate of 4.5 cm/day. On Kaskawulsh Glacier, during a similar observation period, a mean air temperature of 5.0°C was recorded and point ZZ, located on debris-free ice, ablated at a mean rate of 5.4 cm/day. With a debris cover greater than 0.5 cm thick, Østrem found that the ice ablation rate was retarded. Similar retardation was observed on the Kaskawulsh Glacier; the thickness of debris cover required for retardation, however, was closer to 1 cm. Østrem notes that a cover 20 cm thick slowed the mean ablation rate to about 1 cm/day. On Kaskawulsh Glacier a mean ablation rate of 0.6 cm/day was determined at point M where ice is buried 22 cm under till. For thin debris layers (up to 0.5 cm thick) Østrem states that the ablation rate was accelerated. This occurs because thin layers of debris, rather than insulating the ice, succeed only in darkening the ice surface, lowering its albedo, and increasing the radiant energy absorbed by the ice. The Kaskawulsh ablation data show similar accelerated melting (for example, Fig. 2, ablation points B, C, and Z) immediately adjacent to the moraine where a thin scattered layer of silt and small particles, less than 1 cm thick, darkened the ice surface.

While there is a high correlation between rate of ice ablation and thickness of the overlying till, the correlation is not perfect. Variables other than till thickness affect ablation rates. These include particle size, which affects internal air exchange and heat transfer processes, the color of the debris, which affects radiant energy exchange, and local topography. Of these three variables, topography appears to be the most important on the Kaskawulsh moraine; that is, degree of slope and slope orientation of a site markedly increase or decrease the rate of ablation. Ablation Stake J (Fig. 4), for example, shows a mean daily ablation rate considerably greater than would be expected for the till thickness present. This stake, however, is situated on a south-facing, 30° slope (Fig. 5). Since a slope of this steepness and southerly exposure has a high receipt of solar radiation, the discrepancy is explained. Conversely, point P (Fig. 4) has an ablation value somewhat less than expected for the till cover present; but ablation point P is located on a northerly facing slope (Fig. 5) which is effectively shielded from direct solar energy input.

Development of Moraine Morphology

Ablation characteristics help to explain the relief trends observed on the medial moraine. At the broad head of the moraine, topographic relief under the thin moraine cover is low. In a downglacier direction, the relief increases along the moraine as the debris band narrows under the effects of

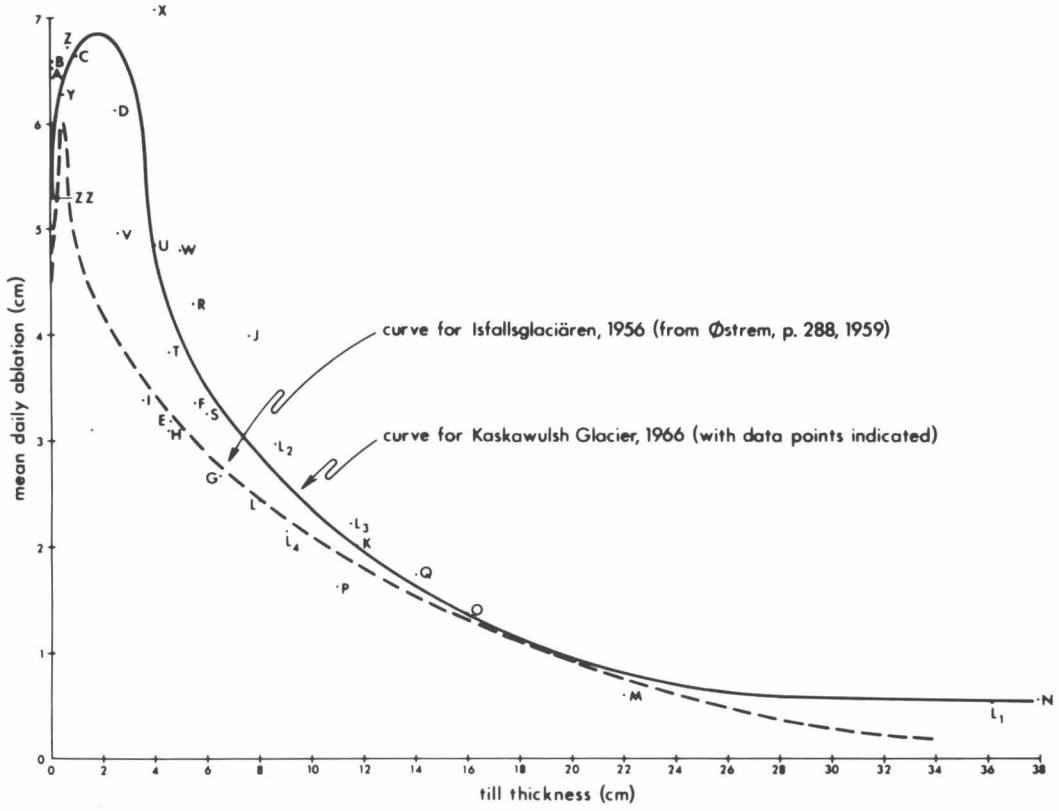

Fig. 4. Relation of mean daily ablation to till cover thickness on Isfallsglaciären (1956) and Kaskawulsh Glacier (1966).

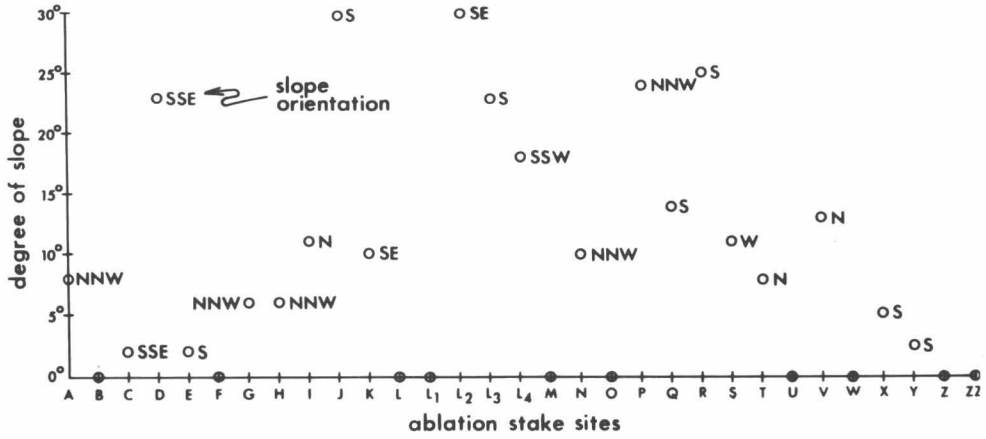

Fig. 5. Slope degree and slope orientation of sites along the ablation transect.

lateral compression of ice along the juncture of the two ice arms (Anderton, 1967, p. 24). At the same time the till layer thickens and ablation rates decrease. After a few summer-melt seasons, the differential ablation occurring between the ice of the ice core below the moraine's debris mantle and the clean ice of the adjacent glacier arms creates a prominent ice-cored moraine ridge standing above the surrounding glacier surface. Eventually the slopes of the ice-cored ridge become steepened beyond the angle of repose of the particles composing the debris mantle. Particles then begin to slide from the ice-cored slopes in quantity. On the Kaskawulsh moraine this phase is found some 1.5 km downglacier from the confluence. Here the relief on the central ridge reaches 20 m where slopes have segments with maximum angles of 39° to 43°. These are the steepest slopes known in the study area that are capable of maintaining continuous (although mass moving) debris cover.

As this process of debris instability is developing on the steepening ice-cored slopes, another process affecting mantle thickness is occurring. The ice on which the medial moraine rests undergoes extending flow associated with accelerating ice velocity (Anderton, 1967, p. 17). The combination of slope steepening and ice-flow extension results in thinning of the debris veneer, particularly along the central ridge of the moraine. This effect is most active about 1.5 km downglacier. Below that position, the moraine relief lowers as the till becomes thinner and less effective as an insulator, and ablation rates increase.

At a distance of approximately 5 km downglacier the moraine mantle has shifted to create a uniformly thinner layer, but one still sufficiently thick to retard moraine ice-core ablation rates relative to uncovered ice on the adjacent glacier arms. Thus, because of the equilibrium state now established, moraine relief remains constant above the nearby clean ice surfaces for some number of kilometers further downglacier. Evidence of stability in the moraine mantle is indicated by large patches of mossy vegetation. On this section of the moraine, where maximum slopes are less than 18°, some of the vegetation formed continuous patches up to 3 m across. No vegetative masses of significant size were found on the rugged upglacier ice-cored slopes, where the mantle is increasingly unstable.

The aspects of the Kaskawulsh moraine study considered in this paper have been restricted to an examination of the significant role that ablation plays in determining ice-cored moraine morphology. There is, of course, marked modification in detail of the gross morphology described above caused by factors not discussed, such as the effect of meltwater stream action on the surface of the moraine and the influence of transverse crevassing in breaking up the continuity of the moraine's central ridge crest. These and other factors are incorporated in an ongoing investigation of the origin, structure, thermal characteristics, and morphology of ice-cored glacial topography.

Acknowledgments

The study on which this paper is based was made possible with the financial and logistical assistance of the Icefield Ranges Research Project. I also wish to express my appreciation for field assistance and consultation to K. Ewing, R. Lougeay, and M. Marcus, Department of Geography, the University of Michigan.

References

*Anderton, P. W. (1967) Structural glaciology of a glacier confluence, Kaskawulsh Glacier, Yukon Territory, Canada, University Microfilms, Ann Arbor, 192 pp.

Chamberlin, T. C. (1895) Recent glacial studies in Greenland, *Bull. Geol. Soc. Am.,* 6, 199–220.

Clayton, L. (1964) Karst topography on stagnant glaciers, *J. Glaciol.,* 5, 101–112.

*Dewart, G. (1968) Seismic investigation of ice properties and bedrock topography at the confluence of two glaciers, Kaskawulsh Glacier, Yukon Territory, Canada, *Rept. No. 27,* Inst. Polar Studies, The Ohio State University, Columbus, 207 pp.

Downie, N. M., and Heath, R. W. (1965) *Basic Statistical Methods,* Harper and Row, New York, 325 pp.

Loomis, S. R. (1970) Morphology and structure of an ice-cored medial moraine, Kaskawulsh Glacier, Yukon, *in* Studies of morphology and stream action on ablating ice, by S. R. Loomis, J. Dozier, and K. J. Ewing, pp. 1–56, *Res. Paper No. 57,* Arctic Inst. North Am.

McKenzie, G. D. (1969) Observations on a collapsing kame terrace in Glacier Bay National Monument, South-eastern Alaska, *J. Glaciol.,* 8, 413–425.

Østrem, G. (1959) Ice melting under a thin layer of moraine, and the existence of ice cores in moraine ridges, *Geogr. Ann.,* 41, 228–230.

Østrem, G. (1964) Ice-cored moraines in Scandinavia, *Geogr. Ann.,* 46, 282–337.

Russell, I. C. (1897) *Glaciers of North America,* Ginn, Boston.

Sharp, R. P. (1949) Studies of superglacial debris on valley glaciers, *Am. J. Sci.,* 247, 289–315.

*Modified versions of these reports appear in the present volume.

Snow Accumulation on Mount Logan*

C. M. Keeler†

ABSTRACT. Measurement of snow accumulation for the year from summer 1967 to summer 1968 on Mt. Logan, St. Elias Mountains indicates that annual precipitation is approximately 0.65 meters yr^{-1} for elevations between 3350 and 5400 meters. This is less by a factor of 5 than annual precipitation at sea level on the Gulf of Alaska. On a regional basis precipitation decreases inland from the Pacific Ocean at a rate of approximately 2×10^{-5} meters km^{-1}. Precipitation decreases on the windward and increases on the leeward sides of the St. Elias Mountains with respect to elevation.

Introduction

Space and time variations of precipitation in mountainous areas present a major problem in solving the water-balance equation for many watersheds. In areas of perennial snow and ice, changes in storage due to changes in the mass balances of glaciers also produce significant uncertainties. A lack of field data and the unusual hydrologic processes involved when precipitation falls as snow have contributed to this problem (Meier, 1967).

Fortunately, however, in areas of perennial snow and ice any single location acts as a storage precipitation gage (with many of the attendant errors of a standard gage), and precipitation for almost any time interval can be measured at any time. This, of course, assumes negligible evaporation, which is probably a reasonable assumption for all but the most continental mountain ranges.

This paper briefly describes measurements of snow accumulation made on a high mountain and relates them to regional trends in precipitation.

Geographic Setting

Mt. Logan, which is about 6100 meters above MSL, is the highest peak of the St. Elias Mountains. It is approximately 90 km inland from the Gulf of Alaska (Figure 1). The meteorology of this area is typified by cyclonic storms associated with low pressures in the Gulf of Alaska. The predominant storm tracks are from the WSW. Despite the fact that Mt. Logan is somewhat protected by a barrier range of peaks up to 5500 meters in height (Mt. St. Elias), it receives most of its precipitation from these maritime storms. Mt. Logan is one of the major units in the topographic barrier between the marine environment of the Gulf of Alaska and the dry continental interior. The rain shadow created by Mt. Logan and the many lesser peaks of the St. Elias Mountains is obvious from the climatic records of Yakutat, which for the past seven years (1960–1967), received a mean annual precipitation of 3.86 meters, and Whitehorse, which received an average of 0.26 meter yr^{-1} during the same period.

Field Methods

Field sampling of the previous year's snow accumulation was made at 300-meter intervals between 3350 meters and 5400 meters on Mt. Logan during June 1968. The determination of annual accumulation was made by examining the stratigraphy, density, and temperature of snow revealed in a hand-dug pit. The principal difficulty lies in ascertaining the horizon marking the previous summer. The pit at 3350 meters contained ice layers and other evidences of melt attributable to summer conditions. All other pits were above the zone of summer melt, and the criterion used to determine the summer

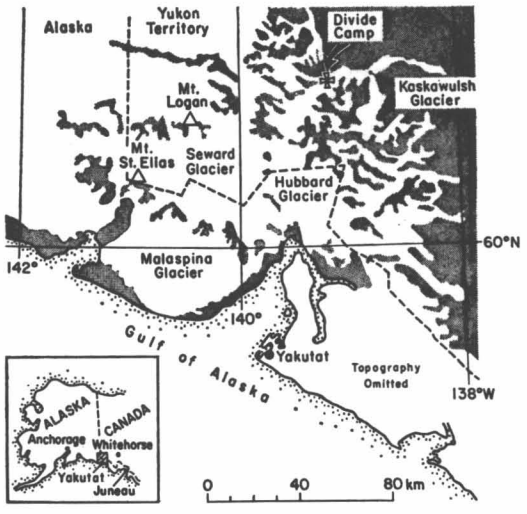

Fig. 1. Index map of the St. Elias Mountains.

*This report has previously appeared in *Water Resources Research,* Vol. 5, pp. 719–723 (1969), and is reprinted here with permission.

†United States Army Cold Regions Research and Engineering Laboratory, Hanover, New Hampshire

surface was a slightly iced, coarse-grained layer. This was chosen because it was thought to be the product of relatively warm conditions with intense insolation. In other areas with perennially dry snow, grain size enlargement is associated with warming conditions (Koerner, 1964), and, if there is sufficient accumulation during all seasons, the coarse-grained snow should be summer accumulation. At 5400 meters this layer was absolutely dated by its content of refuse left by a research team during July and August of 1967.

At 5400 meters on the summit plateau of Mt. Logan three pits were dug, and a 12-meter core was taken at the bottom of one of the pits. At all other locations the data are from a single pit but are supported by additional tests with a ram penetrometer, an instrument that measures resistance to penetration and can be used to map the lateral extent of subsurface stratigraphy. These data are admittedly from a small sample of an infinite population. While all sites were chosen to be as free as possible of such local effects as wind drift, it would be naive to believe that a perfect catch was obtained.

Results

Annual accumulation data for 1967–1968 are summarized in Table 1. North and south slope designations are included to differentiate between essentially leeward (north) and windward (south) settings. The accumulation figures for the lower elevations (3400 to 4150 meters) differ by from 5% to 40% from similar data collected by Alford (1967) for the accumulation year 1965–1966. It is impossible to apportion the amount of this variation among differences in interpretation, local differences caused by wind drift, and differences in annual accumulation between the two years.

The 12-meter core taken at 5400 meters permitted the estimation of annual accumulation of 0.82 meter, 0.69 meter, and 0.58 meter for the years 1966–1967, 1965–1966, 1964–1965, respectively. These figures were determined by visual inspection of the core stratigraphy. Below approximately eleven meters in depth no stratigraphic variation was visible to the naked eye. Accepting the inherent limitations in generalizing from a single sample, the relatively low accumulation of 1964–1965 is consistent with a similarly low figure reported for the Arctic Institute of North America's Divide Station (2900 meters, see Figure 1) for that same period (Marcus, 1965).

Based on the single-core record, the mean annual accumulation for the period 1966–1968 is 0.70 meter of water, suggesting that, for this very limited period of record, the year 1967–1968 at 5400 meters can be considered normal. This is substantiated somewhat by data from Yakutat, where the 1967–1968 precipitation was 3.36 meters as compared with the long-term (1921–1968) average of 3.41 meters.

The principal value of the 12-meter core was the depth-density profile it yielded, which can be used as an 'order of magnitude' check on the accumulation figures determined by stratigraphic means. Figure 2 shows the depth-density profile (both actual data and smoothed curve) for Mt. Logan and similar profiles for the South Pole and Site 2, Greenland (Gow, 1968).

TABLE 1. Thickness, Depth, Water Equivalent, and Mean Density of the 1967–1968 Snow Accumulation at Several Sites on Mt. Logan

Pit elevation, meters	Thickness, meters	Water equivalent, meters	Mean density, kg meter^{-3}
5400 N*	2.50	0.73	290
5400	2.00	0.60	333
5400	2.54	0.84	302
5400 S*	2.07	0.63	328
4900	1.80	0.54	333
4600	1.92	0.64	300
4150	2.10	0.71	295
3800	1.76	0.55	320
3350	0.96	0.32	293

*N and S are north and south slope, respectively.

The densification of dry snow is largely a creep process and, as such, the densification rate is proportional to temperature and time. Temperature, taken as the mean annual temperature, can be approximated by the snow temperature at that depth at which annual temperature fluctuations are fully damped. In the case of dry cold snow, this is at a depth of approximately 10 meters. In the Logan core hole the temperature between 10 and 15 meters was almost constant at -24.5°C. This is in close

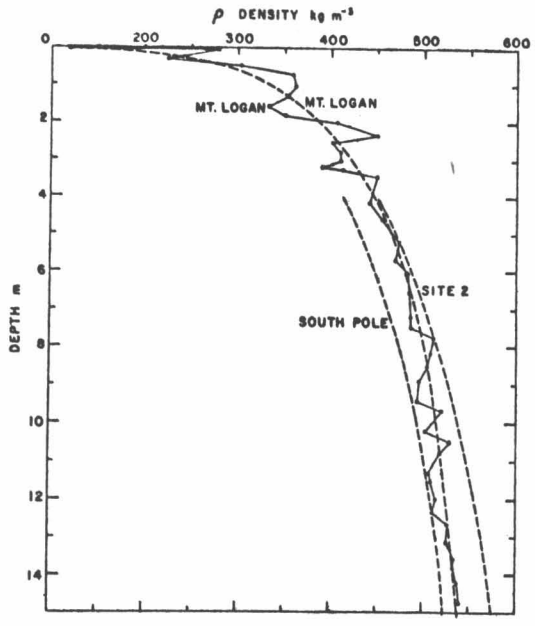

Fig. 2. Depth–density profile for Mt. Logan at 5400 meters.

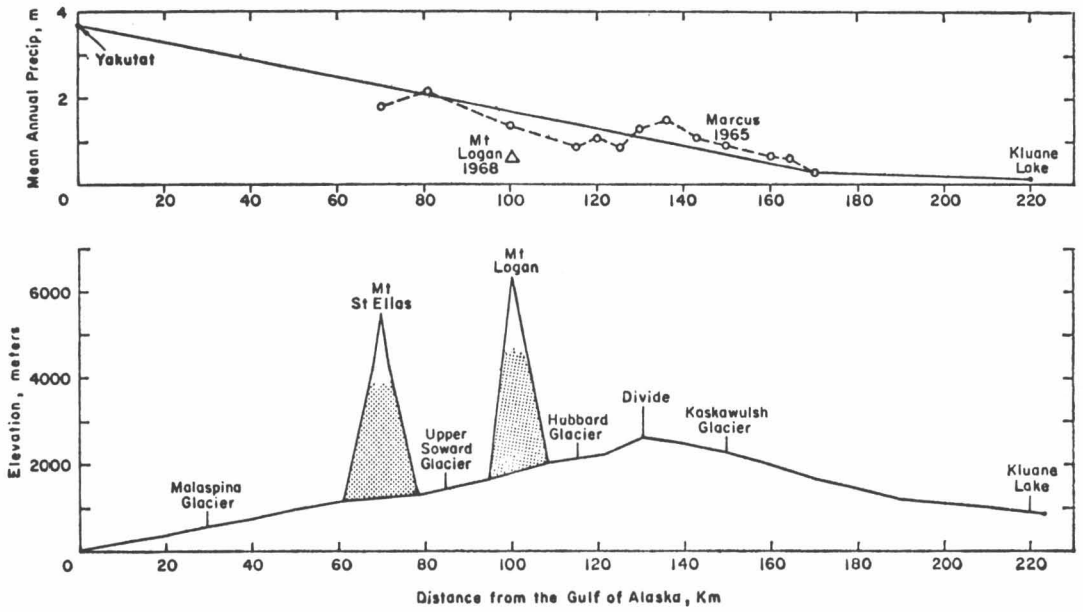

Fig. 3. Terrain profile and precipitation pattern from Yakutat, Alaska, to Kluane Lake, Y. T.

agreement with the 500-mb radiosonde temperatures above both Yakutat and Whitehorse and with the temperature predicted using the dry adiabatic lapse rate from Divide Station, which has a mean annual temperature of approximately -0.5°C (Wood, 1963). Time can be approximated by the accumulation rate. A high accumulation rate results in lower densities at any given depth.

As a rule of thumb, Gow (1968) found that, to maintain the same depth–density profile, doubling the accumulation rate would require a temperature increase of 4°C. Comparing the Mt. Logan profile with profiles for which both mean annual temperature and accumulation rate are known (South Pole: -51°C, 0.07 meter yr^{-1}; Site 2: -24°C, 0.40 meter yr^{-1}) places limits on the accumulation required to produce the Logan profile. If the Logan profile and Site 2 profile were the same, then one would expect the accumulation rate on Logan to be identical to that at Site 2, as they have similar mean annual temperatures. The fact that the Logan profile is displaced to the low-density side suggests that the accumulation rate is considerably higher than at Site 2. By the same token, if the Logan and South Pole profiles were the same, then the accumulation rate on Logan would have to be 64 times that of the South Pole, or 4.48 meters yr^{-1} to make up for the considerably higher temperatures. While this comparison provides no absolute value for the accumulation rate on Mt. Logan, it suggests that a figure on the order of one meter yr^{-1}, as determined by stratigraphy, is by no means unreasonable.

Discussion

Of greatest interest from a hydrologic standpoint is the relation between these data and regional precipitation patterns. Figure 3 shows both the terrain profile and distribution of precipitation along a traverse line from the Malaspina Glacier, up the Seward and Hubbard Glacier, and down the Kaskawulsh Glacier to Kluane Lake, which lies about 20 km NE of the Kaskawulsh Glacier terminus. The precipitation data are taken from Marcus (1965), the U. S. Weather Bureau records for Yakutat, Alaska, and this study. It should be noted that these data are not entirely compatible, and quantitative conclusions are therefore estimates. For example, the data of Marcus are for the snow accumulation of 1964–1965, which may have been a year of less than normal precipitation. These data also do not include summer precipitation, which, judging from 30 years of record (1921–1950), at Yakutat, is normally 17% of the annual precipitation. Errors are likely to be greatest at elevations below 2500 meters, where both summer rain and melt of some of the previous winter's snow accumulation may occur. The precipitation gradient from Yakutat to 1615 meters on the Kaskawulsh Glacier is -2×10^{-5} meters km^{-1}, where distance is generally synonymous with distance from the coast and downwind from the source of moisture. Allowing for the errors just discussed, the gradient is still probably not less than 1×10^{-5} meters km^{-1}.

In Figure 4 the effect of elevation alone is shown. At elevations between 1000 and 2500 meters a gradient of 0.65 meter km^{-1} of elevation exists on both windward and leeward slopes. Above 2500 meters elevation appears to exert little control on precipitation amounts. The reason for this may be that precipitation here is associated primarily with frontal, as opposed to purely orographic, processes. Site-to-site differences in precipitation on Mt. Logan itself reflect local processes, such as redistribution by the wind, rather than elevational control.

From these data there is no evidence that precipitation increases with elevation to a maximum before declining,

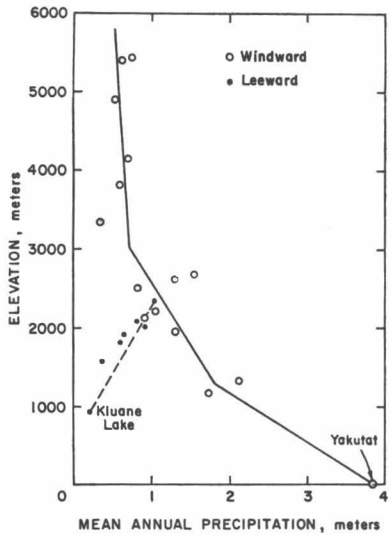

Fig. 4. Distribution of precipitation with elevation from Yakutat to Kluane Lake.

owing to a depletion in moisture supply. Previous studies (Marcus, 1965) suggested that maximum precipitation might be found at 1700 meters on the Seward Glacier, and Murphy and Schamach (1966) found a threefold increase in precipitation from sea level to 1500 meters in the mountains directly east of Juneau, Alaska. Unfortunately, data are lacking for the lower Malaspina Glacier in this critical range of elevation.

On a regional basis it is interesting to note that annual snow accumulation at 4300 meters on Mount Wrangell, Alaska, 250 km northwest of Mt. Logan and 200 km inland from the Gulf of Alaska, is on the order of one meter (Benson, 1968), not greatly different from the accumulation on Mt. Logan at a similar elevation.

Owing to a lack of sufficient data on ice ablation and stream discharge from these glacierized basins, it is impossible at present to assess storage changes. In 1949 it appeared that there was considerable loss from storage in the Seward–Malaspina Glacier system (Sharp, 1951); however, recent glacier fluctuations along the North Pacific Coast have been rather ambiguous (Meier and Post, 1962). It is quite apparent that the great bulk of ice contained in the St. Elias Mountains would necessitate studies at a number of locations with varying exposures and elevations.

References

*Alford, D. L. (1967) Density variations in alpine snow, *J. Glaciol.*, 6, 495.

Benson, C. S. (1968) Glaciological studies on Mt. Wrangell, Alaska, 1961, *Trans. Am. Geophys. Union*, 49, 167 (abstr.).

Gow, A. J. (1968) Deep core studies of the accumulation and densification of snow at Byrd Station and Little America V, Antarctica *Res. Rept. 197*, U. S. Army Cold Regions Res. Engin. Lab., 45 pp.

Koerner, R. M. (1964) Firn stratigraphy studies on the Byrd-Whitmore Mountains traverse, 1963–1964, in *Antarctic Snow and Ice Studies*, edited by M. Mellor, p. 219, *Antarctic Res. Ser.* (Vol. 2), Am. Geophys. Union, Washington.

Marcus, M. G. (1965) A hydrologic traverse of glaciers in the Icefield Ranges, St. Elias Mountains, Alaska–Yukon Territory, p. 317, *Intern. Assoc. Quatern Res., VII Congr. Boulder, Abstr.*

Meier, M. F. (1967) Why study glaciers?, *Trans. Am. Geophys. Union*, 48, 798.

Meier, M. F., and Post, A. S. (1962) Recent variations in mass net budgets of glaciers in western North America, in *Intern. Assoc. Sci. Hydrol., Sympos. Obergurgl*, Publ. 58, pp. 63–77.

Murphy, T. D., and Schamach, S. (1966) Mountain versus sea level rainfall measurements during storms at Juneau, Alaska, *J. Hydrol.*, 4, 12.

Sharp, R. P. (1951) Accumulation and ablation on the Seward-Malaspina Glacier system, Canada–Alaska, *Bull. Geol. Soc. Am.*, 62, 725–744.

Wood, W. A. (1963) The Icefield Ranges Research Project, *Geogr. Rev.*, 53, 163.

*This article is reprinted in the present volume.

Stratigraphic Studies of the Winter Snow Layer Mount Logan, Saint Elias Range*

Donald Alford† and Charles Keeler ‡

ABSTRACT. Results of a traverse study of near-surface snow properties in the King Trench area of Mount Logan, St. Elias Range, are presented. Based upon the assumption that these snow properties are related to thermodynamic processes operating during the depositional period, a climatological model of the King Trench is presented which relates the observed variations in snow properties along the traverse line to localized topographic obstruction or enhancement of katabatic air drainage. It is suggested that the near-surface climate of snow-covered slopes generally may be inferred partially from the interaction between local topography and katabatic wind flow.

Introduction

Stratigraphic studies of snow and firn on the Greenland Ice Sheet are a useful approach to understanding the climate there (Benson 1959, 1962). These studies were made by correlating stratigraphic units from the edge of the ice sheet to the high interior by digging a series of pits. Variations in the layering of the snow produced by annual, seasonal and individual storm cycles may be correlated with variations in wind speed, air temperature and rate of accumulation. Thus the annual snow layer is equivalent to an infinite set of automatically recording climatological stations. The primary difficulty lies in learning to read the records correctly.

In order to apply these techniques to other areas, it is necessary to assume that extensive melting did not occur and that weather, snow sedimentation and post-depositional changes are sufficiently interrelated so that stratigraphy provides a climatic record. If this assumption is valid, it should be possible to study the regional climate of any geographical area which possesses a significant snow cover during all or most of the year. One such environment, of which at present we have only the most limited knowledge, is that found in the earth's major mountain ranges. Similarities between ice caps and mountain ranges indicate that techniques devised for use in one could be applied to studies in the other. The primary differences between the two are the greater significance of topography and local relief in mountain ranges and the relatively small surface area of mountain ranges when compared to that of the Greenland ice sheet.

The greatest difficulty in applying traverse snow study techniques to the study of the climate of a large mountain range is that of movement from place to place. At present, the only generally practical means of conducting a traverse study in the mountains is on foot. This is much less efficient than mechanized transport and reduces the time available for the study and the amount of scientific and support equipment which can be used.

To ascertain if the techniques of stratigraphic analysis could be successfully applied to studies of the alpine climate, the U. S. Army Cold Regions Research and Engineering Laboratory of Hanover, New Hampshire, in June 1965, sent a reconnaissance expedition to the west flank of Mount Logan (6,050 m) in the St. Elias Range on the Alaska-Yukon border. The objectives of this expedition were:

(1) To determine if systematic variations in snow properties could be detected using the simple tools and techniques which back-packing necessitates
(2) To attempt to establish the relative influence of topography and elevation on any variations which were observed

This paper presents the preliminary results and conclusions of this expedition.

Geographical Description of the Study Area

Mount Logan is approximately 20 miles north of the Alaska-Yukon border near the centre of the extensively glacierized St. Elias Range. On the north, south and east, near-vertical walls with a relief approaching 3,000 m separate the summit snowfields from the surrounding glaciers. It is only on the western flank that a breach exists. This is the King Trench, which rises from Upper Ogilvie Glacier at an elevation of 2,300 m to King Col at 4,500 m. From King Col, access to the summit plateau of the mountain is relatively straightforward. Fig. 1 is a sketch map of the King Trench showing the route, location and elevation of the pit sites. Fig. 2 is a cross-section of the traverse route. It can be seen that the central portion of the Trench is relatively flat-lying with fairly steep ice falls above and

*This report has previously appeared in *Arctic,* Vol. 21, pp. 245–254 (1969), and is reprinted here with permission.
†Montana State University, Bozeman, at time of writing; present address, Institute of Arctic and Alpine Research, University of Colorado, Boulder.
‡United States Army Cold Regions Research and Engineering Laboratory, Hanover, New Hampshire

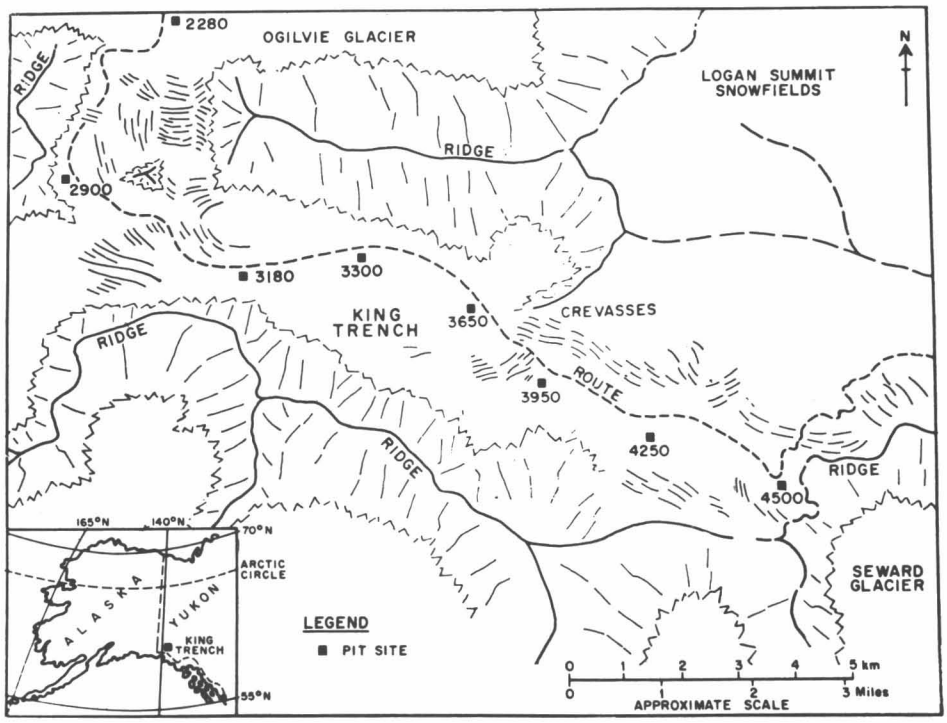

Fig. 1. The King Trench on the west flank of Mt. Logan, St. Elias Range, showing the traverse line and pit locations. Numerical value adjacent to pit sites indicates approximate elevation in meters above sea level.

below. The slopes above the upper icefall, while still quite gentle, are somewhat steeper than those found in the central portion of the Trench. The total elevation range covered by the traverse was approximately 2,200 m in a horizontal distance of 16 km (Fig. 2).

Study Techniques

Only a brief summary of the techniques of snow stratigraphy is given here. Details are given by Benson (1962).

Eight pits were excavated through the annual layer at approximately 300 m vertical intervals between the upper Ogilvie Glacier and King Col. Table 1 summarizes the elevations and locations of the individual camps and pit sites.

Following excavation of each pit, one wall was smoothed and brushed with a whisk broom to bring out discontinuities in snow cohesion. A steel tape, graduated in centimeters, was suspended from a board lying on the surface of the snow pack and was used as a reference for all measurements. Weston dial thermometers, graduated in degrees C were inserted into the pack at 10 cm intervals to measure the existing temperature gradient between the surface and the bottom of the pit. Stainless steel tubes with an internal volume of 500 cm^3 were placed in the pit wall at 5 to 10 cm intervals, then cut out, trimmed, capped and weighed to measure vertical variations. The individual density measurements were also averaged over the depth interval of the pit to obtain the average density for the snow at that point. Density measurements were considered accurate to within 0.005 gm/cm^3, temperature measurements to within 1.0°C.

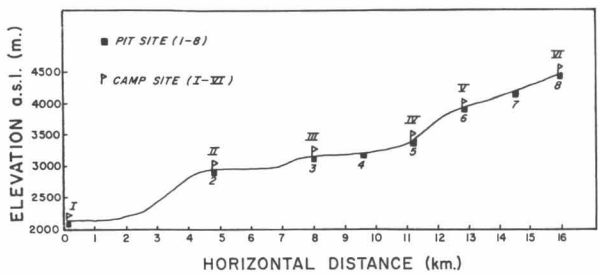

Fig. 2. Longitudinal profile of King Trench showing camp and pit sites.

Observations and Discussion

(1) The 1964-65 winter accumulation layer varied from 23 cm water-equivalent at base camp on the Ogilvie Glacier to over 1 m at King Col (Fig. 3). On the Ogilvie Glacier, this snow layer was underlain by glacier ice, indicating that at that elevation, none of the winter accumulation of 1963 had persisted through the summer melt season of 1964. At Camp I (Pit 2), the depth of this layer had increased only 4 cm, to 60 cm, but at this elevation it was underlain by very coarse, well-cemented firn rather than solid ice. At Camp II (Pit 3), there was no clear break between the 1964-65 accumulation and that of the preceding year. At this elevation, a series of interbedded ice layers and coarse-grained, poorly bonded snow

TABLE 1. Elevations and Locations

Camp	Location	Pit	Approx. Elev.	Dist. from Base Camp	Date
Base	Ogilvie Glacier	1	2280 m.	—	6/2/65
I	Lower King Trench	2	2900 m.	5.0 km.	6/6/65
II	Lower King Trench	3	3180 m.	8.0 km.	6/9/65
	Middle King Trench	4	3300 m.	9.5 km.	6/12/65
III	Middle King Trench	5	3650 m.	11.5 km.	6/19/65
IV	Upper King Trench	6	3950 m.	12.5 km.	6/15/65
	Upper King Trench	7	4250 m.	14.5 km.	6/18/65
V	King Col	8	4500 m.	16.0 km.	6/17/65
VI	Summit Plateau	-	5150 m.	18.5 km.	
				21.5 km.	to summit

Note: Vertical and horizontal distances between camps have been taken from the St. Elias 1:250,000 sheet, Canada Department of Mines and Technical Surveys. Conversion to meters and kilometers is approximate. While the absolute values may be greatly in error, it is felt that relative elevations are accurate to within ± 50 m.

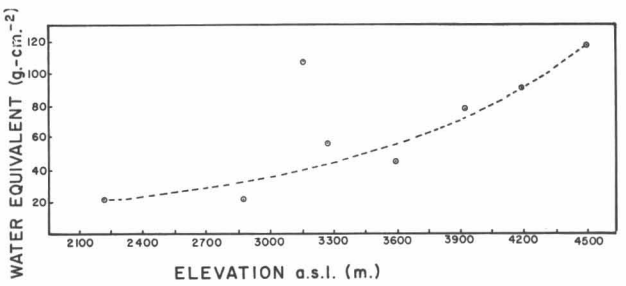

Fig. 3. The water-equivalent of the 1964-65 winter snow layer in the King Trench as a function of elevation.

was interpreted as the transition between 1963-64 and the 1964-65 accumulation. At King Col, it is not believed that the pit penetrated the entire thickness of the 1964-65 winter accumulation. However, measurements of the thickness of individual ice bands (assumed to represent the mean annual accumulation) in crevasse walls in the upper icefall indicate that 1 m of water-equivalent may closely approximate the annual accumulation in the vicinity of King Col.

These observations indicate that the firn line was below 3,000 m during the summer of 1964. Since most of the surface area of the King Trench lies above this elevation, it seems reasonable to infer that the Trench is an area of net annual accumulation. On the other hand, the Ogilvie Glacier, lying mainly below this elevation, would appear to have a negative annual budget in terms of seasonal snowfall and is probably nourished primarily by the avalanches which fall onto it constantly from the summit plateau of Mount Logan and the other surrounding peaks.

The low water-equivalent value measured at 2,200 m on the upper Ogilvie Glacier is somewhat surprising as, at an equivalent elevation on the divide between the Hubbard and Kaskawulsh Glaciers, 40 km to the northeast, the 1964-65 accumulation exceeded 1 m, which was over four times as much (Marcus 1965; unpublished data).

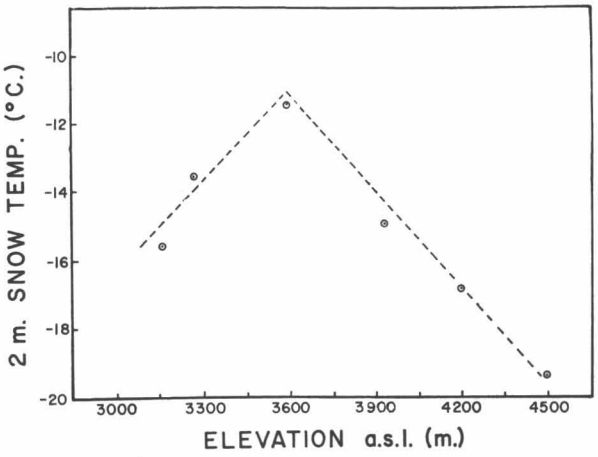

Fig. 4. Snow temperatures at a depth of two meters along the traverse line.

Since the temperature gradient in the snow at the Ogilvie Glacier pit site was not yet isothermal at 0°C, it is unlikely that any significant mass loss due to melt had occurred. This would suggest that the northwest flank of Mount Logan is a desert in terms of annual precipitation. If this is so, it is probably because the bulk of Mount Logan is in the path of the prevailing storms from the Gulf of Alaska. If these storms follow the *path of least resistance* through the range, the Hubbard, Seward and Kaskawulsh Glacier systems should receive a disproportionately larger amount of the precipitation falling on the range as a whole than would the Logan or Walsh Glacier systems. To some extent, this is borne out by the available aerial photography of the range, which shows far more bare rock and morainal material to the northwest of Mount Logan than to the northeast, in the direction of the Hubbard and Kaskawulsh Glaciers.

(2) Before melt starts, temperatures in the annual snow layer are related to the near-surface air temperature regime.

Fig. 4 shows the snow temperatures measured at a depth of 2 m for all the pits excavated to that depth plotted against their respective elevation.

It is assumed that the trend exhibited by the 2 m snow temperatures is in some way related to the lateral air temperature gradients existing in the King Trench. It can be seen that this temperature distribution consists of two inflected segments, the upper being very close to the dry adiabatic lapse rate of 1°C/100 m and the lower being an inverted lapse rate with a variation of approximately 1.3°C/100 m.

(3) Because of its low resistance to wind erosion, the snow surface gives some indication of the relative wind speed at any point along the slope. The existence of sastrugi, hard slab or the exposed edges of individual depositional laminae, is interpreted as being indicative of intensive surface-wind scour, whereas a soft, smooth snow surface is assumed to indicate relatively calm conditions. Evidence of surface-wind scour was best developed

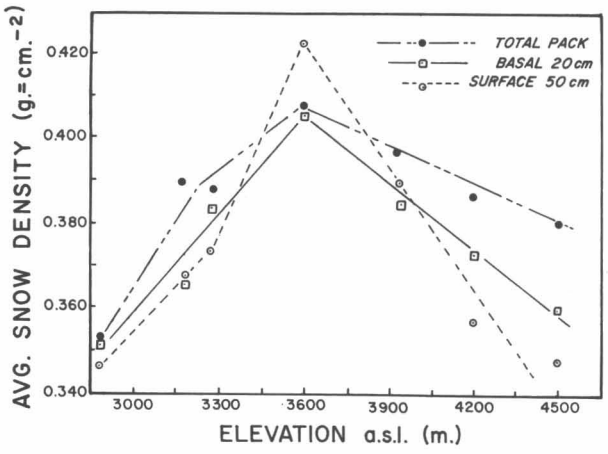

Fig. 5. Average snow density values for selected snow thicknesses in the 1964-65 winter accumulation layer as a function of pit elevation.

on, and immediately below, the two icefalls in the Trench. Below the upper icefall, in the relatively flat, central portion of the Trench, evidence of surface wind scour died out rapidly down the slope, virtually disappearing within less than 100 vertical meters. The zone of most intense surface-wind scour was in the immediate vicinity of Camp IV (Pit 5) suggesting that the highest, near-surface wind speeds occurred at that point.

(4) The variation in average snow density along the traverse route is shown in Fig. 5. While snow density fluctuations may result from the interaction of a complex of environmental influences, it has been suggested (Schytt, 1958) that perhaps the most important of these in terms of values measured in the near-surface layers are wind speed and air temperature. Wind may be expected to increase densification by mechanically breaking up the original snow crystals into forms which are more susceptible to close packing. Temperature increases will increase the instability of the initial crystal forms, promoting the formation of a grain with fewer crystallographic faces and greatly decreased area per unit mass (Bader *et al.* 1939; Bader 1962; de Quervain 1945). The third major factor contributing to dry metamorphism is plastic deformation under the load of overlying layers, but this is assumed to occur only at depths greater than 10 m (Benson 1962), so should not affect the values obtained in this study.

In addition to the average density of the total annual layer, values for a basal layer 20 cm thick and the upper 50 cm of the pack at each pit site on the traverse route are also shown in Fig. 5. It is assumed that this basal zone represents some time period at the beginning of the 1964-65 accumulation while the surface 50 cm represent an event, or events, much closer in time to the study period.

The relationship between average snow density and elevation shown in Fig. 5 has several implications. These may be summarized:

(a) The trend of density with elevation has not been determined by a single event during the period of deposition but appears to be the result of processes which influence the snowpack more or less continuously during accumulation.

(b) Maximum densities were measured in that part of the King Trench which showed evidence of greatest wind scour and where the warmest 2-m temperatures were obtained. This lends some credence, however indirect, to the hypothesis relating dry metamorphism of the surface layers to variations in the influence of wind and temperature.

(c) Snow deposited at or near the beginning of the 1964-65 accumulation season exhibits essentially the same trend as that deposited immediately before the study period, some 8 or 9 months later. This implies that the geographical distribution of the factors influencing snow densification in the King Trench is reasonably constant with time. It should be noted that this latter point requires a much more thorough understanding of the efficiency of the energy transfer process below the level of the surface layers before it can be accepted or rejected.

(5) No pits were dug above 4,500 m. The following were noted between this elevation and 6,000 m during a reconnaissance of the upper portion of the mountain:

(a) Snow accumulation fell off rapidly above 5,000 m and on the summit plateau, new snow of any appreciable depth was observed only in sheltered areas. The remaining areas were hard-packed and wind-sculptured.

(b) The snow plume blowing from the summit ridge of Mount Logan streamed away to the north, indicating that the prevailing winds at an elevation of 6,000 m were from the south.

(c) No evidence of riming was seen below 4,500 m. At this elevation it was observed as small "frost feathers" on the tent guy ropes. On the summit ridge, large "mushroom" formations of snow were seen and ascribed to the combined action of rime deposition and wind erosion.

The writers are indebted to P. Lev for the latter observations.

Conclusions

The primary difficulty in using the annual snow layer as a recording climatological station is our present inability to relate absolutely a single climatic element to a specific snow property. In all probability, this will never be possible on an absolute basis because any one property is affected by several climatic elements. In the case of the Mount Logan data, however, it is believed possible to construct a simple climatological model which will successfully account for the observed variations in stratigraphic parameters.

Snow-covered surfaces are particularly conducive to the formation of strong "inversions" i.e., temperature increasing with height above the surface (Wexler 1936). These are caused by the fact that the snow surface radiates approximately like a black body for all wavelengths in the absence of short-wave solar radiation. The atmosphere radiates with black-body intensity only in certain bands of the spectrum, which are mainly due to water vapor. Also, the air loses energy both upward and

downward but the snow surface radiates upward only. As a result of these conditions, the snow surface will be in equilibrium with the air above when its temperature is lower than that of the air. In the high latitudes, it can be expected that this process will be effective even in summer because the sun never rises high above the horizon and much of its short-wave energy is reflected by the snow surface. While snow acts nearly as a black body for terrestrial long wave radiation, it has a high albedo for solar radiation.

The existence of an inversion will develop a very stable stratification of the air in contact with the snow surface which will inhibit vertical mixing because the higher density air layers are closest to the surface. If the slope on which the inversion is forming is sufficiently steep, these denser bottom layers will eventually flow downhill. This will give rise to the katabatic winds which are a common feature of snow-covered slopes (Benson 1962; Geiger 1965). In areas where this katabatic air drainage is impeded by a topographic barrier, the inversion layer will be much more persistent. As the katabatic winds flow down the slope, they will warm at approximately the dry adiabatic rate of 1°C/100 m. Because katabatic winds are flowing primarily in response to gravitational attraction, it can be expected that, in the absence of topographic *funneling,* they will reach their greatest speed on the steepest slopes. Evidence of wind scouring should be most apparent on slopes under the influence of the katabatic air flow and should be largely absent where this movement is absent or greatly restricted, assuming that the slopes are protected from the prevailing winds related to the more general regional circulation.

In the King Trench, all of the stratigraphic observations suggest that the climate on the slopes between 3,500 and 4,500 m is strongly influenced by persistent katabatic winds. The close agreement of the measured snow-temperature lapse rate to the dry-adiabatic rate, the evidence of surface-wind scour in the lower portion of this region and, indirectly, the gradual decrease in average snow density with increasing elevation all point to katabatic winds as the primary climatological control. Between 3,500 and 3,000 m, on the other hand, the snow temperature lapse rate was inverted, there was little evidence of surface wind erosion and average snow density decreased with decreasing elevation. This is interpreted as indicating that the inversion layer which forms in this region of the Trench is prevented from flowing downhill, and that a semi-stable inversion develops which controls the climate in the central portion of the Trench. Geiger (1965) refers to the high viscosity of the near-surface air layer and it is assumed that it is this viscosity, together with the virtually level floor of the glacier, that contributes to the formation of an inversion layer at this point. Below 3,000 m, the slope again becomes quite steep, the snowcover of much of the lower icefall is hard-packed and windblown and the limited temperature data indicate that a nearly dry adiabatic lapse rate exists at this elevation. On the basis of these observations, it seems justifiable initially to divide the King Trench region of Mount Logan into three climatological sections, the highest and lowest of which are largely the result of normal katabatic wind flow while the intermediate section is characterized by a semi-stable inversion layer resulting from the obstruction of this katabatic drainage; very likely this obstruction is the result of topographic control.

The limited geographical extent of these data does not warrant extensive conclusions concerning the near-surface climate which may be found in other large mountain ranges or even in other parts of the St. Elias Range. However, they do suggest directions for future study of the alpine climate. These are presented here in the form of a tentative hypothesis.

> Topography is perhaps the most important control in determining the area distribution of near-surface climatic elements in the mountains. While the climate of any mountain range is largely determined by factors related to general atmospheric circulation and geographic location, local variations may be much more accurately inferred from pronounced inflections in slope angle.
>
> Extrapolation of climatological parameters such as wind speed and air temperature to mountain slopes from nearby valley climatological stations or free-air soundings, as is commonly done, is not a valid approach. This is due to the strong control which is felt to be exerted by the compositon and geometry of the surface on the near-surface climate. While the end result is undoubtedly conditioned by free air values, these will be primarily significant in determining the general climatological characteristics of the area in question, which will then be modified to a greater or lesser extent by local surficial properties.
>
> While much work remains to be done, this study suggests that an analysis of the pertinent stratigraphic parameters of the alpine snow pack, such as density and temperature, may be a useful approach to the study of local mountain climates.

Acknowledgments

The authors would like to express their appreciation to Peter Lev and George Denton, co-workers on Mount Logan. This study was financed by USA-Cold Regions Research and Engineering Laboratory out of the Director's in-house fund. Logistic support was provided in part by the Icefield Ranges Research Project of the Arctic Institute of North America. Special thanks are due to Dr. Walter Wood, President, American Geographical Society; Mr. Richard Ragle, Scientific Director of IRRP; and Messrs. Philip Upton and Jack Wilson who made a total of 10 landings with ski-equipped aircraft on and near Mount Logan in support of the expedition. The authors would like to thank Drs. Arlin Super and Valter Schytt for their useful criticisms of the paper. The writers are, of course, solely responsible for the final form the paper has taken.

References

Bader, H. (1962) The physics and mechanics of snow as a material, *Cold Regions Sci. Engin. Ser.,* Pt. 2: Phys. Sci. Sect. B, U. S. Army Cold Regions Res. Engin. Lab., pp. 1–16.

Bader, H., and others (1939) Der Schnee und seine Metamorphose, *Beitr. Geol. Schweiz, Geotech, Ser., Hydrol.,* Lief. 3, Bern, U. S. Army Snow, Ice, Permafrost Res. Establish., Tr. 14, 1954, 313 pp.

Benson, C. (1959) Physical investigations of the snow and firn of northwest Greenland, 1951, 1953, and 1954, *Res. Rept. 26,* U. S. Army Snow, Ice, Permafrost Res. Establish., 62 pp.

Benson, C. (1962) Stratigraphic studies in the snow and firn of the Greenland Ice Sheet, *Res. Rept. 70,* U. S. Army Snow, Ice, Permafrost Res. Establish., 93 pp.

De Quervain, M. (] 945) Schnee als Kristallines Aggregat, *Experimentia,* Vol. 1, U. S. Army Snow, Ice Permafrost Res. Establish., Tr. 21, 7 pp.

Geiger, R. (1965) *The Climate Near the Ground,* Harvard University Press, Cambridge, Mass., 611 pp.

Marcus, M. (1965) A hydrological traverse of the glaciers in the Icefield Ranges, St. Elias Mountains, Alaska–Yukon Territory, p. 317, *Intern. Assoc. Quatern. Res., VII Congr., Boulder, Abstr.*

Marcus, M. (1965) Preliminary data: Pit locations and densities, Icefield Ranges (May-June, 1965), presented at Intern. Assoc. Quatern. Res., VII Congr., Boulder (unpublished).

Schytt, V. (1958) Glaciological investigations in the Thule Ramp area, *Res. Rept. 28,* U. S. Army Snow, Ice, Permafrost Res. Establish., 88 pp.

Wexler, H. (1936) Cooling in the lower atmosphere and the structure of Polar Continental air, *Monthly Weather Rev.,* 64, 122 – 136.

Optical Measurements on Snow*

Malcolm Mellor†

ABSTRACT. Spectral extinction measurements for the visual range were made on homogeneous snow samples prepared under controlled conditions, with snow density and grain size as variables. Comparative measurements were made on coarse-grained natural snow. Extinction coefficient ν was in the range 0.8 to 1.7 cm^{-1} for fine-grained dense snow, and 0.16 to 0.37 cm^{-1} for the coarse-grained snow. In the fine-grained snow, where scattering is thought to be the dominant attenuating process, there is a general decline in ν as wavelength λ increases from 0.4 to 0.7 microns. In the coarse-grained snow, where absorption becomes significant, spectral selection was slight, with a weak minimum in the region 0.5 to 0.6 microns. When ν is related to density it must have a maximum value; limited data for fine-grained snow show this maximum in the density range 0.45 to 0.60 g/cm^3, and the density for maximum extinction is inversely related to wavelength. For a given density ν decreases as grain size increases, the rate of change varying with wavelength. Spectral reflectance measurements on natural snow are reported, and attenuation data are interpreted to give surface reflectivity for fine-grained snow. Diffuse reflection from fine-grained snow is believed to have little spectral dependence in the visual range, but with coarse-grained snow reflectance is expected to become inversely dependent on wavelength. It is suggested that optical principles might be applied in the measurement of snow structure, and also for remote sensing of snow-covered terrain.

Introduction

The optical properties of snow profoundly influence metamorphism and ablation which, in turn, determine mechanical properties and stability of a snow cover. Since optical properties vary with the structure and condition of snow, they offer a means for the investigation of snow types, both in large masses and in small samples.

Apart from gross albedo measurements, there have been few experimental studies of optical effects in snow, and a compilation of available data produces a picture which is not entirely clear (Mellor, 1964). To check on some of the puzzling features reported in the literature, simple measurements were made using available equipment. These measurements were incidental to another project, so that the study was in no way comprehensive.

Homogeneous samples of fine-grained snow were prepared in the USA CRREL cold rooms and extinction measurements were made as a function of wavelength in the visible spectrum. Grain size and density were varied separately, and comparative measurements were made on natural spring snow. Extinction measurements were made on wet snow during the Icefield Ranges Research Project, together with spectral reflectance measurements on various snow surfaces and under different lighting conditions.

---

*This report has previously appeared as *Cold Regions Research and Engineering Laboratory Research Report 169* (1965), and is reprinted here with permission.

†United States Army Cold Regions Research and Engineering Laboratory, Hanover, New Hampshire

Absorption and Scattering

Light entering a mass of very clear ice is absorbed; disregarding scattering from minute inclusions and imperfections, there is no reflection from beneath the surface in a deep mass of completely clear ice. Absorption is selective with respect to wavelength, being stronger at the red end of the visible spectrum than at the blue end (see University of Minnesota, 1951). Hence a thick layer of clear ice appears blue by transmitted (white) light, and blue also by reflected light when underlain at moderate depth by a white reflecting surface. When ice contains air bubbles, entrant light is scattered; attenuation of transmitted light is greater than in clear ice, and subsurface reflection (back-scattering) contributes to the gross reflectance. Spectral selection, however, is still likely to be governed by absorption rather than scattering. In polar glacier ice, bubble size is large compared to light wavelength and is also about an order of magnitude smaller than bubble spacing; under these conditions theory of independent single scattering may be applied for thin layers (van de Hulst, 1957) and, as shown by cloud and fog studies, no marked spectral selection by scattering is to be expected.

In snow the particles and cavities are closely packed, and single scattering theory is no longer applicable. Postulating a theoretical model for reflectance and transmittance of snow, Dunkle and Bevans (1956) consider that spectral selection is controlled by absorption, while scattering is taken to be independent of wavelength. Applying this model to analysis of field data, Ambach and Habicht (1962) show the absorption coefficient increasing with wavelength while the scattering coefficient remains constant. However, since cold, wind-blown snow

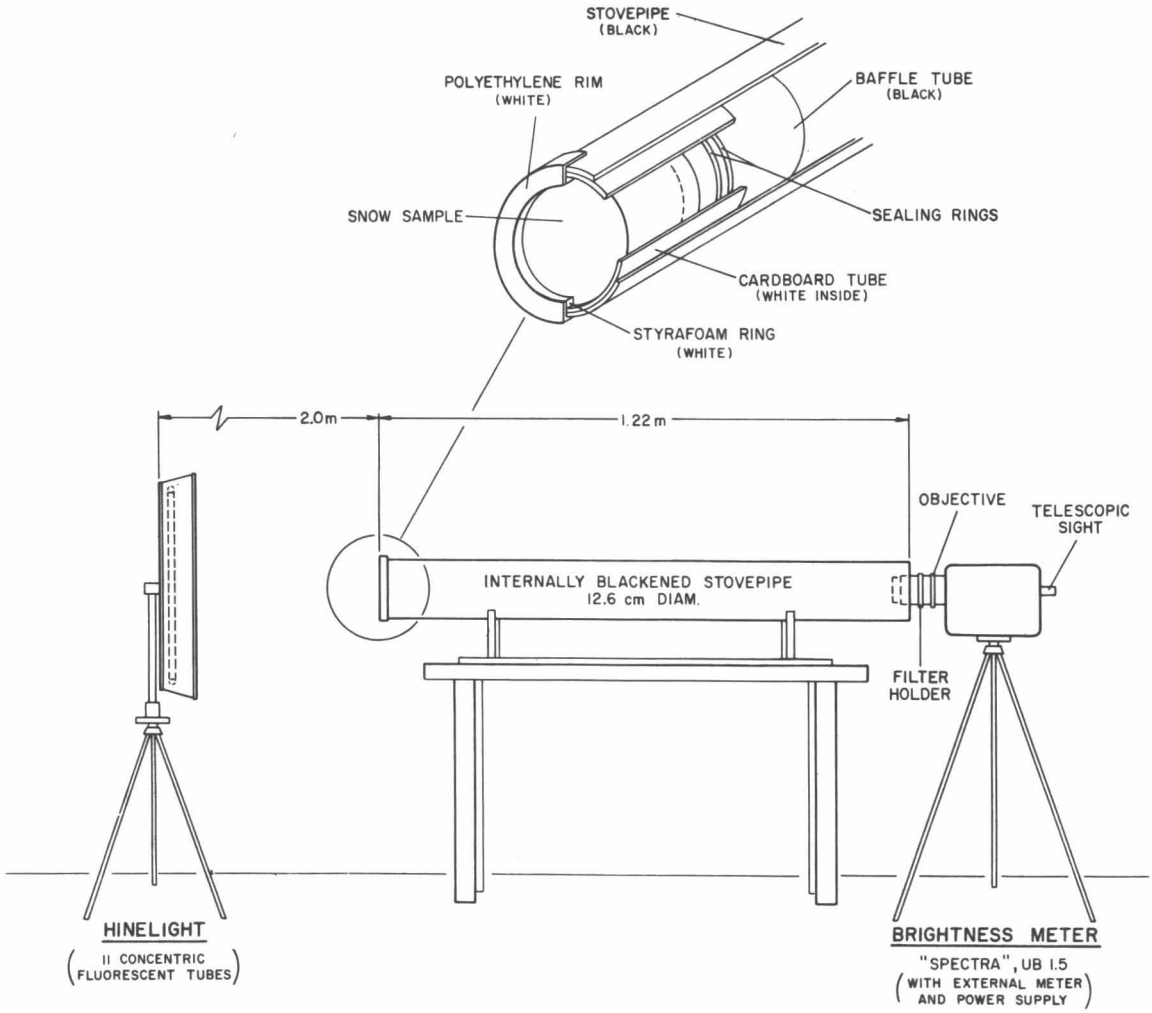

Fig. 1. Experimental arrangement for cold room attenuation measurements.

is a finely powdered dielectric it is not clear why absorption should be considered of prime importance; at first sight it seems more likely that scattering might dominate extinction and reflection processes.

Extinction as a Function of Wavelength

Attenuation was measured by a modified slab method using the arrangement shown in Figure 1. Light passing through a snow sample to a black-body receiver was measured by a filtered detector, and transmitted intensity was plotted logarithmically against slab thickness to give the extinction coefficient for exponential attenuation.

Samples of varying grain size were prepared by grinding and sieving natural snow at -10°C and compacting the sieved aggregate to a controlled degree in 11.1-cm diameter cardboard tubes. The samples were sintered at -10°C for 3 weeks, and tests were made at -10°C. The snow cylinders were trimmed to the required length on a band saw, and the finely powdered residue left by the saw was carefully brushed from the faces. After early difficulties a system of light baffles was arranged on the sample holder as shown in the detail of Figure 1.

Samples were diffusely illuminated by a cold white fluorescent lamp consisting of eleven concentric tubes. A central hole in the lamp permitted detector sightings from behind.

The detector used was an ultra-sensitive brightness meter (Spectra, Model UB 1½) in which an optical system accepts light from a 1½° angle and focuses it on a phototube. The output from the phototube is amplified electronically and indicates on a large scale of an external meter. The indicating meter has 100 scale divisions, and the instrument has five sensitivity ranges (100, 10, 1.0, 0.1, 0.01). A x100 neutral density filter extends the range for high intensities. Regulated stable voltage is provided by a special power supply. The instrument is calibrated in foot-lamberts for use with a filter which

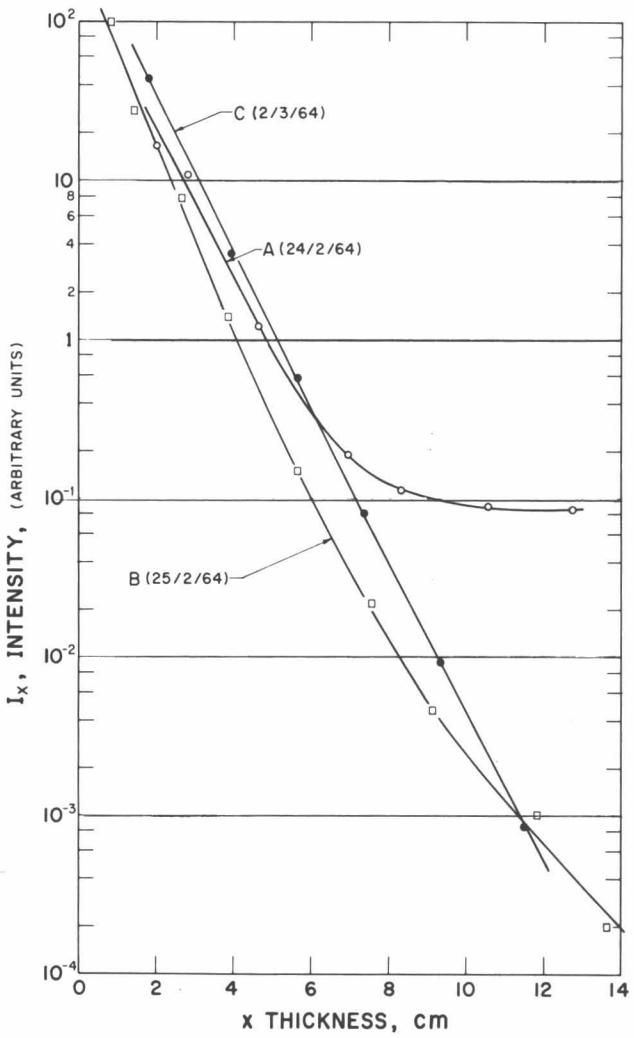

Fig. 2. Attenuation curves before and after elimination of light leaks. Line A was obtained with the original arrangement, line B after baffles were fitted to the sample holder, and line C after additional light leaks in the detector were eliminated. The three curves do not refer to exactly the same type of snow.

simulates the spectral response of the human eye, but since external filters were used directly with the S-4 phototube in the present work, the readings taken were in arbitrary units.

The filters used were narrow band pass interference filters which isolate 10 uniformly spaced bands in the visible spectrum (Spectracoat "Monopass" filters by Optics Technology, Inc.). The filters, which are individually calibrated, have no secondary transmission peaks in the wings.

To make a set of measurements a sample was trimmed to length L_1 and placed in the holder, while lamp and detector were turned on and left to warm up for 15 minutes. All room lights other than the test source were turned out, and the entire detector end of the "black-body" tube was shrouded with a black cloth. With the detector trained on the center of the sample's dark surface, readings of transmitted intensity were made using each filter in turn. The procedure was repeated with the sample trimmed successively to lengths L_2, L_3, etc.

The precautions to exclude stray light were found by experience to be necessary. Light baffles around the sample were not used at first, as it fitted snugly into the holder, but with large slab thicknesses light leaking around the sample gave a spurious reading for transmitted intensity (Fig. 2, A). It was also found that the detector had two leaks which permitted stray light to reach the phototube: the light cut-off shutter was not completely effective, and the sighting eyepiece allowed light to enter.[1] Before the necessary corrections were made, plots of log intensity against thickness showed curvature, implying that extinction coefficient decreased with increasing depth. When stray light was excluded the effect disappeared (Fig. 2, C). A decrease of extinction coefficient with increasing depth has been predicted and reported previously (Giddings and LaChapelle, 1961).

A specimen plot of extinction data is shown in Figure 3.[2] It provides adequate justification for representing the attenuation in this experiment by a Bouguer-Lambert type of law:

$$I_x = I_o \, e^{-\nu x}$$

where I_x is the intensity of radiation transmitted through a thickness x to the black body, I_o is the net radiation entering the snow in the x-direction, and ν is the extinction coefficient for the wavelength under consideration. The values of ν obtained from plots like Figure 3 are summarized in Figure 4.

In all cases for fine-grained snow the extinction coefficient decreased with increasing wavelength. Since this trend is contrary to that which might be expected if absorption controlled the attenuation, the implication is that spectral selection in extinction for cold, fine-grained snow is due primarily to scattering effects.

Previous reports show an opposite trend; an increase of extinction coefficient with increasing wavelength was found in field tests by Liljequist (1956), Thomas (1963) and, with some qualification, Ambach and Habicht (1962). This might be expected in coarse-grained snow, as is argued later, but Liljequist's strong selection was measured in dry polar snow. There may be a possibility that Liljequist's results, obtained by inserting sensors into the wall of a snow pit, were influenced by the cavity (Holraum) effect. A cavity in snow often looks blue, presumably because of selection by multiple reflection. The color is not due to selective transmission, as is commonly believed; white light transmitted through snow to the receiver tube in the experiment had no definable color when viewed by eye.

[1] These instrument faults were serious in open daylight, and much reflectance data taken before their discovery had to be discarded.
[2] Editor's note: Complete data tabulations are given in the appendix of the original report.

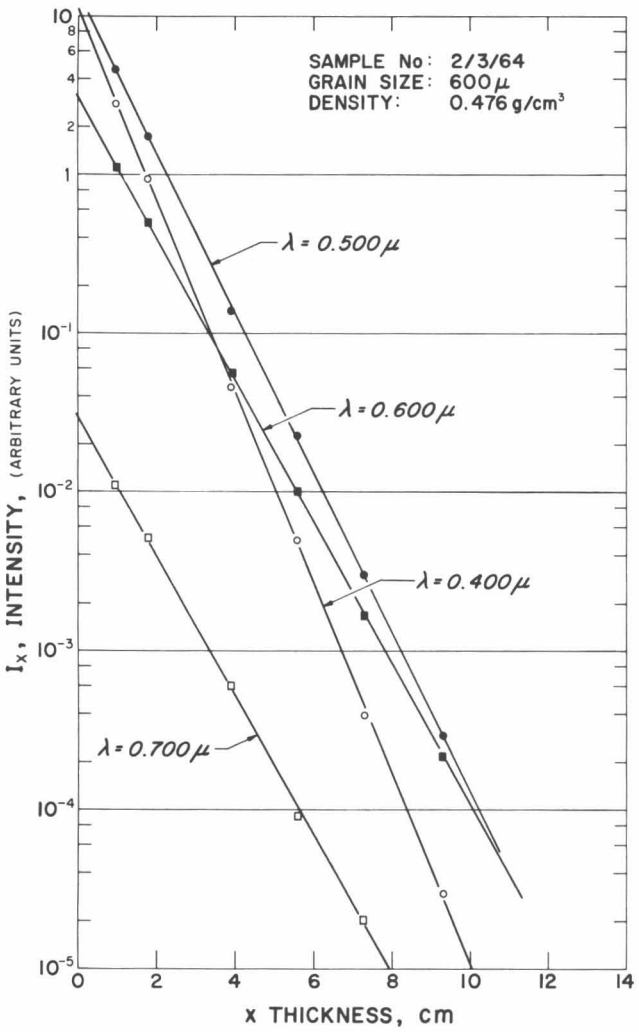

Fig. 3. Specimen plot of log intensity against sample thickness for different wavelengths.

Snow particles are very large compared with light wavelengths (the Mie parameter $2\pi a/\lambda$, where a is particle radius, is in the range 1 to 5 x 10^3 for the prepared snows), and in a dispersed cloud such particles would not be expected to show much selective scattering. However, the refractive index of ice is about 1.4% higher at λ = 0.4 μ than at λ = 0.7 μ, so that the reflectivity for direct incidence is about 6.8% greater at 0.4 μ than at 0.7 μ, and under conditions of dense packing this may significantly affect the characteristics of multiple scattering.

Measurements on refrozen spring snow did not show the same continuous decrease of extinction coefficient with increasing wavelength. The test snow was extracted from a natural snow cover by a special Plexiglass sampling tube, and after refreezing of the free water the experiment was run at -10°C. The extinction coefficient decreased as wavelength increased from 0.400 μ to 0.566 μ, and thereafter gradually increased again as wavelength increased to 0.700 μ (Fig. 4). In the absence of further information it was tentatively assumed that this was caused by a combination of scattering and absorption effects.

The apparatus shown in Figure 1 was unsuitable for testing wet snow, and so a slab experiment was made in the field. A fluorescent lamp consisting of three concentric tubes (maximum diameter 46 cm) was placed in a white box and covered by a sheet of frosted glass. A slab of wet snow, 63 x 63 x 15 cm thick, was set on top of the frosted glass, and the brightness meter was sighted vertically down onto the center of the slab. After each set of readings the thickness of the slab was reduced by trimming in place with a handsaw. The experiment was performed at night inside a dark tent. Minimum extinction coefficients were found at wavelengths 0.466 μ, 0.500 μ and 0.533 μ (Fig. 4). There was an increase as wavelength dropped from 0.466 μ to 0.400 μ, and also a steady increase as wavelength increased from 0.533 μ to 0.700 μ.

Although limited, the results suggest that as transparency increases because of grain growth and smoothing of angularities, especially by melting, absorption tends to become more important than scattering, so that spectral selection is gradually reversed.

Extinction as a Function of Snow Density

Ambach and Habicht (1962) show extinction coefficient decreasing linearly with increasing snow density, and results by Thomas (1963) also plot linearly in the same sense (Mellor, 1964). It is obvious that such a relation cannot be valid for low densities, as extinction coefficient must tend to zero as density tends to zero.

In the present experiment density was varied independently of grain size, but the range of densities was insufficient to define a general relation. In most cases extinction coefficient increased with increasing density, as can be seen from inspection of Figure 4, but there was an intriguing exception.

When extinction coefficient was plotted against density with wavelength as parameter, the results for snow having a mean grain diameter of 200 μ showed an interesting trend (Fig. 5). Since both air and ice are more transparent than snow, the curve relating extinction coefficient and density must have a maximum; it appears from the limited data in Figure 5 that the density at which this maximum occurs is dependent on wavelength. In this fine-grained snow the density for maximum extinction decreases with increasing wavelength, from about 0.63 g/cm^3 at 0.400 μ to about 0.485 g/cm^3 at 0.700 μ. Figure 5 further implies that the degree of spectral selection in extinction changes with density; at 0.44 g/cm^3 the ratio of extreme values (λ = 0.400 μ, λ = 0.700 μ) is 1:20, while at 0.62 g/cm^3 the same ratio is 1:53.

Judging from Figure 5, the general curve relating extinction and density may have one or more inflections in the low density range, for there cannot be an intercept

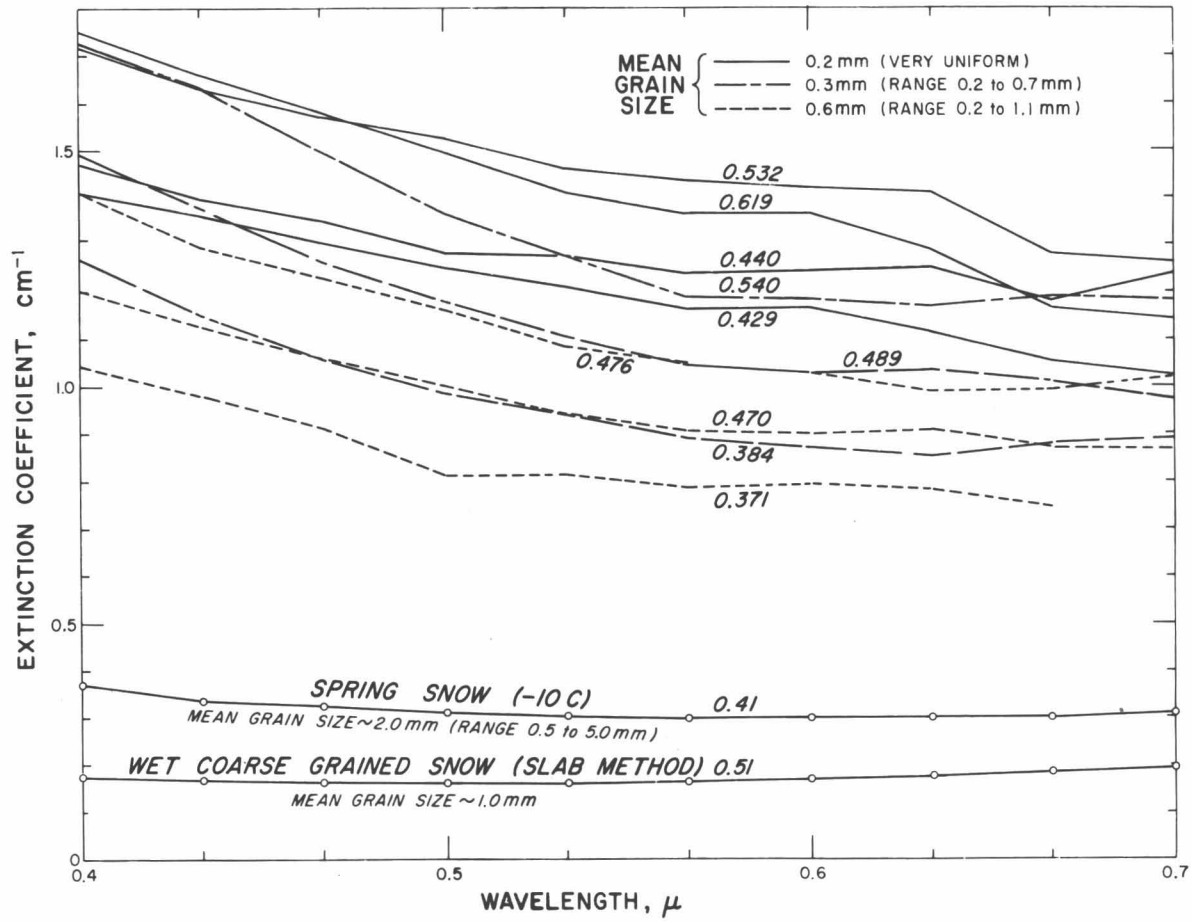

Fig. 4. Summary of results for the attenuation experiment.

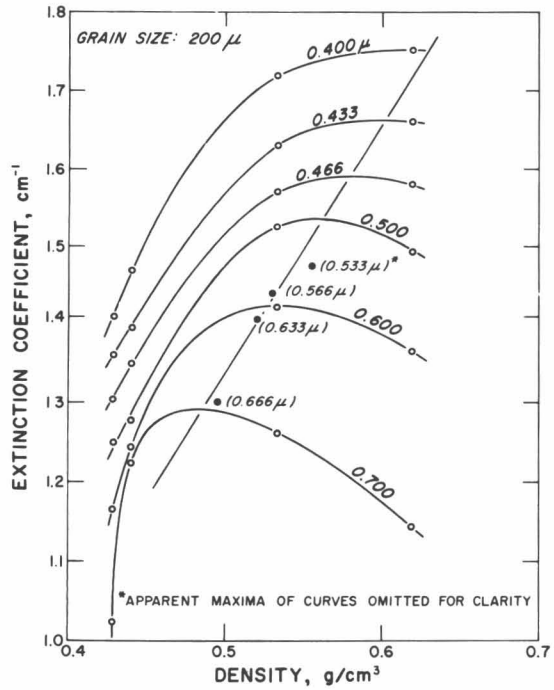

Fig. 5. Extinction coefficient as a function of density for fine-grained snow. The parameter is wavelength in microns.

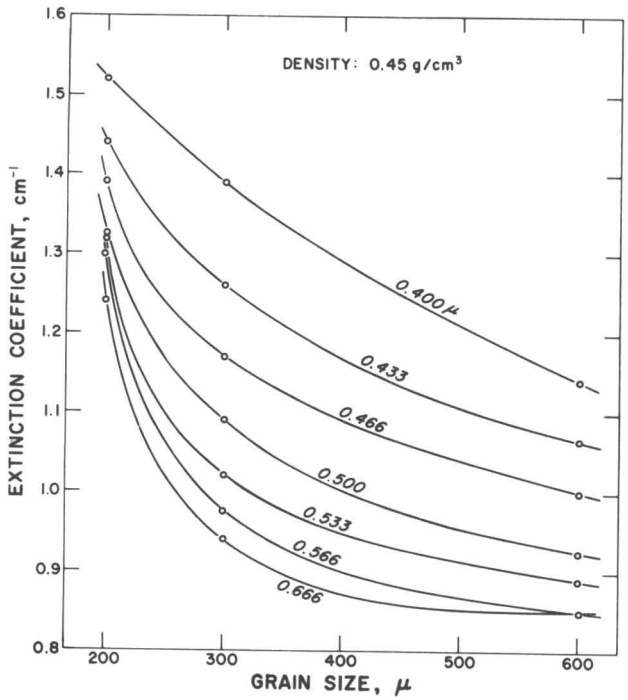

Fig. 6. Extinction coefficient as a function of grain size for snow of density 0.45 g/cm^3. Numbers on the curves give wavelength in microns.

on the density axis. Attempts to explore the low density region by measuring transmission through blowing snow during the hours of darkness were foiled by lack of suitable weather conditions.

Extinction as a Function of Grain Size

A plot of extinction coefficient against grain size was prepared (Fig. 6) by reading values for density 0.45 g/cm^3 from the graphs of extinction coefficient versus density. Extinction coefficient is inversely related to grain size, and the relationship is influenced by wavelength. The curves in Figure 6 appear to converge as grain size both increases and decreases from the range studied; the indication of convergence for increasing grain size is supported when the data for refrozen spring snow (density 0.41 g/cm^3, grain size 2 mm) are added to the plot (Fig. 7). Some data for longer wavelengths are omitted from Figures 6 and 7 for clarity; when plotted on expanded scales these curves intersect between grain sizes of 600 μ and 2 mm, since ν for the spring snow was a minimum at $\lambda = 0.566\ \mu$.

Although inadequate, the data indicate that extinction coefficient increases sharply as grain size falls below 200 μ; they also suggest that spectral selection may disappear for very small particle sizes. Attempts to prepare very finely ground aggregates failed because of spontaneous bonding between grains, presumably as a result of high surface energy and perhaps electrical effects. As grain size increases, absorption must assume the dominant role in extinction, and the absorption coefficients for ice can probably be taken as limiting values for extinction as grain size tends to infinity.

Reflectance as a Function of Wavelength

On simple reasoning, both preferred back-scattering of blue light and preferred absorption of red should tend to make reflectance decrease with increasing wavelength, but published data do not always show this effect. In fact, some investigators show a pronounced increase of reflectance with increasing wavelength.

To complement the extinction measurements, reflectance measurements on the same samples were planned, but they could not conveniently be made because of space limitations, and field observations were substituted instead. Data obtained in Hanover proved unreliable owing to the instrument problem mentioned earlier, but dependable readings were made on a flat snowfield (elevation 8500 ft) at the head of the Kaskawulsh and Hubbard glacier systems in the St. Elias Mountains. The brightness meter already described was mounted on a gantry frame and directed vertically downward toward undisturbed snow, while accessories (power supply, indicating meter, filter box) were placed in a case at some distance from the test plot. The normal component of reflected radiation was measured at each filter wavelength by taking alternate readings on the snow and on a freshly scraped magnesium oxide block set flush with the snow surface. At first three pairs of readings were made at each wavelength, but the number was later increased to six pairs.

Results are given in Figure 8. In all cases the lowest reflectance was found at 0.700 μ (the limit of the range studied), but the trend of spectral selection differed according to the lighting conditions. With diffuse light from

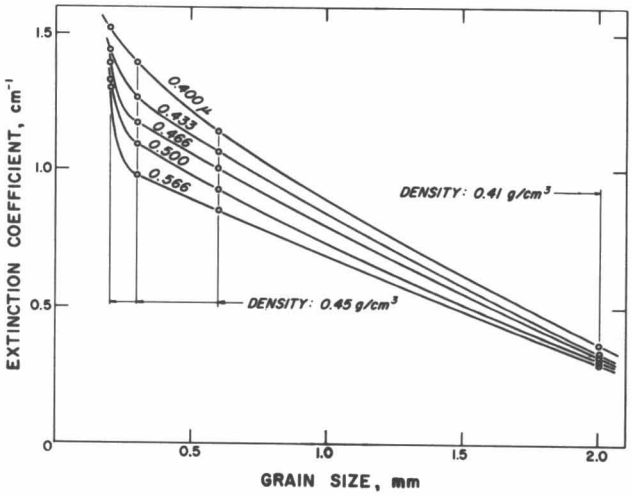

Fig. 7. Extinction coefficient as a function of grain size.

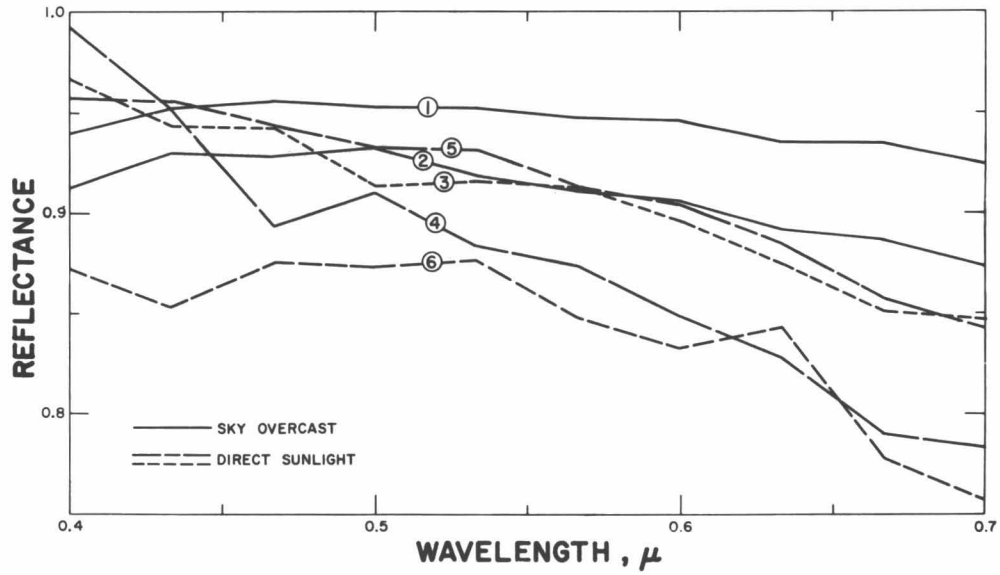

Fig. 8. Summary of results from field measurements of reflectance.
(1) Fresh snow (dry), 0.28 g/cm^3, O°C.
(2) 1–2 cm fresh snow (0.1 g/cm^3) on older snow (0.4 g/cm^3), O°C.
(3) Metamorphosed snow, 0.43 g/cm^3, O°C.
(4) Slightly metamorphosed new snow, 0.2 g/cm^3, O°C.
(5) Wet snow, 2 days old, 0.4 g/cm^3, melting during test.
(6) Same as (5) after 5 hours more melting.

a uniform overcast,[3] spectral selection was not very strong, and there was a weak maximum at about 0.466 μ - 0.500 μ. With direct sunlight from a cloudless sky there was a distinct decrease of reflectance with increasing wavelength, although it should be noted that the method used was ill-suited for measurement under direct lighting conditions, since specular effects are involved. It might be mentioned in passing that the data of Figure 8 for direct sunlight are in good agreement with the theoretical predictions of Dunkle and Bevans, who assumed that absorption controlled spectral selection.

To supplement the field data, results of the extinction experiment were reexamined. If the intercept for $x = 0$ on graphs like Figure 3 is regarded as the intensity of entrant light I_o, the reflectivity of the snow surface can be calculated when the incident intensity I_i is known, since the reflected intensity I_r is $(I_i - I_o)$. Incident intensity for each filter was measured by replacing the extinction sample with a magnesium oxide disk of known spectral characteristics and observing the normal reflection with the brightness meter through a hole in the center of the fluorescent lamp. The resulting values for surface reflectivity are shown in Figure 9. They give no significant evidence of spectral selection in reflection from the first surface; this first reflection accounts for about 40-80% of the total reflected intensity, and it seems to be inversely related to grain size (Table 1).

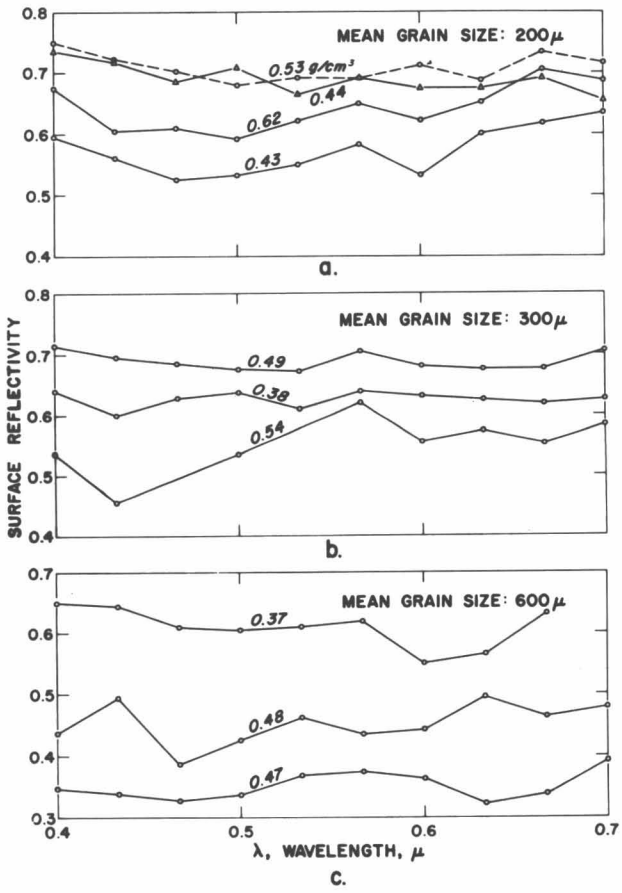

Fig. 9. Surface reflectivity of cold room samples calculated from the intercept of the attenuation curves.

[3]Infrequency of occurrence of uniformly dense overcasts or completely clear skies at the test site limited the opportunities for study.

TABLE 1. Mean surface reflectivity (0.400 μ – 0.700 μ) deduced from extinction data.

Snow density (g/cm^3)	Mean grain size (μ)	Mean surface reflectivity
0.43	200	0.573
0.44	200	0.690
0.53	200	0.709
0.62	200	0.642
0.38	300	0.625
0.49	300	0.688
0.54	300	0.551
0.37	600	0.610
0.47	600	0.351
0.48	600	0.452

Broadly following Dunkle and Bevans, the surface reflectivity may be translated to a scattering coefficient by dividing it by the particle radius, although such a coefficient certainly cannot represent scattering behavior in subsurface layers. The range of values thus found from the data of Figure 9 is 10 to 75 cm^{-1} and, since these values are 3 to 5 orders of magnitude greater than Sauberer's values for ice absorption coefficient (see University of Minnesota, 1951), a simplification of the Dunkle and Bevans expression for extinction coefficient seems justifiable if the coefficients for subsurface multiple scattering are of comparable magnitude to the surface coefficients. Thus

$$v = \sqrt{k^2 + 2kr} \cong \sqrt{2kr}$$

where k is absorption coefficient and r is the scattering coefficient.

The crude results of Figure 9 suggest that diffuse reflection from the surface, or single back-scatter, is nonselective with respect to wavelength. If this surface reflectivity is high, as in the case with fine grains, reflectance will show little dependence on wavelength. When surface reflectivity is low, as with coarse grains, subsurface scattering and absorption significantly affect the reflectance and a selection favoring blue light might be expected. Spectral selection by subsurface back-scattering can be simply demonstrated by sticking a metal pipe into the snow to eliminate the surface reflection; when an observer peers down the pipe the light seen is blue.

Conclusions

Extinction in snow depends on scattering and absorption. In fine-grained snow, such as cold wind-packed snow, scattering is dominant and extinction coefficient diminishes as wavelength increases. Extinction coefficient is inversely related to grain size; it increases sharply as grain size decreases below 300 μ, the rate of increase being directly related to wavelength. In low density snow extinction increases with increasing density, eventually reaching a maximum and thereafter declining as density tends to the ice limit. The density for maximum extinction varies with wavelength and probably also with grain size. In coarse-grained snow typical of a melting snow cover absorption becomes important. As grain size increases and angularities are subdued, spectral selection in extinction tends to reverse, so that extinction gradually becomes directly related to wavelength.

The reflectance of fine-grained snow is not greatly dependent on wavelength, since surface reflectivity is high and single back-scatter from the first layer of grains is apparently not very selective with respect to wavelength. As grain size increases, the reflectance and the surface reflectivity are expected to decrease; a relatively large proportion of the reflected light is back-scattered from beneath the surface, so that reflectance becomes inversely dependent on wavelength.

Extinction coefficient is more heavily dependent on grain type than on density for the kinds of snow usually encountered in surface deposits, so that extinction coefficient may be a useful descriptive parameter in snow studies. Construction of an inexpensive extinction meter for field use would be quite feasible.

Since the magnitude and wavelength dependence of reflectance vary with snow type, remote sensing of snow covers may have some useful application. Under suitable lighting conditions the author has air-photographed wind-drift patterns in color on the Greenland Ice Cap with an ordinary 35 mm camera; with special equipment it might be possible to detect more subtle differences of snow type.

Studies need to be extended into the infrared range, and toward this end simple comparisons of visible and infrared extinction have been initiated.

References

Ambach, W., and Habicht, J. L. (1962) Untersuchungen der Extinktions-eigenschaften des Gletschereises und Schnees, *Archiv Meteorol., Geophys. Bioklimatol.*, Ser. B, Bd. 11, pp. 512–532.

Dunkle, R. V., and Bevans, J. T. (1965) An approximate analysis of the solar reflectance and transmittance of a snow cover, *J. Meteorol.*, 13, 212–216.

Giddings, J. C., and LaChapelle, E. (1961) Diffusion theory applied to radiant energy distribution and albedo of snow, *J. Geophys. Res.*, 66, 181–189.

Liljequist, G. H. (1956) Energy exchange of an Antarctic snowfield, *Sci. Res., Norwegian-Brit.-Swedish Ant. Exped.*, Norsk Polarinst., Oslo, 298 pp.

Mellor, M. (1964) Properties of snow, *Cold Regions Science and Engineering*, (edited by F. J. Sanger) U. S. Army Cold Regions Res. Engin. Lab. monogr., Pt. III, sect. A1, 105 pp.

Thomas, C. W. (1963) On the transfer of visible radiation through sea ice and snow, *J. Glaciol.*, 4, 481–484.

University of Minnesota (1951) Review of the properties of snow and ice, *Res. Rept. 4*, U. S. Army Snow, Ice, Permafrost Res. Establish., 106 pp.

Van de Hulst, H. C. (1957) *Light Scattering by Small Particles*, John Wiley/Chapman and Hall, New York and London, 470 pp.

Density Variations in Alpine Snow*

Donald Alford†

ABSTRACT. Stratigraphic studies of the annual snow layer in the Beartooth Mountains of south-western Montana and on Mount Logan in the St. Elias Range have disclosed a similiar distribution of at least one physical property of the snow pack in the two areas. The average density of the pack, obtained by integrating a series of measurements taken at 5–10 cm vertical intervals over the total thickness of the annual layer, reaches a maximum value near a midpoint of the total elevation covered by each traverse and decreases linearly toward the elevation extremes. A preliminary hypothesis, relating the distribution of average snow-density values along slopes to a semi-stable zonation of near-surface air temperatures, is presented.

Introduction

Processes controlling the densification of snow have been the subject of a considerable research effort in the past. This is in part a reflection of the importance of density in determining the reaction of the snow to external and internal stresses and gradients, and the close relationship which exists between snow density and the environment in which it develops. Sorge (1938) proposed that snow density could be considered an environmental indicator and in recent years this property has been related to virtually every environmental parameter with varying degrees of success. Schytt (1958) has discussed wind and temperature as being the two most important factors. Sorge (Bader, 1954) and later Benson (1962) suggested that, in the absence of melt, overburden pressure became the dominant process. Langway (1961) correlated average snow density in northern Greenland with elevation, accumulation and temperature, while Taylor (1965) has empirically related this property to latitude in the vicinity of the South Pole.

The above has been interpreted to indicate that the average values of certain index properties of the snow pack may be related to the average intensity of those environmental factors capable of modifying the process of snow metamorphism. In view of the largely irreversible nature of many of the metamorphic processes operating in the snow pack, it is suggested that the effect of those processes will be evident in accumulation increments ranging from that deposited from several storms during a single season through a number of annual layers. This increment will be determined by the depth to which any given environmental influence can penetrate into the pack and its significance as a metamorphic process.

There have been two approaches to the study of snow metamorphism in response to environmental factors as a field problem in the past. One has been to analyze the stratigraphy of the snow pack along a traverse line using pits dug at selected intervals and to relate the measured variations in snow properties from pit to pit to actual or assumed changes in environmental factors along the same line. The best example of this approach is found in Benson (1962). Another approach has been to conduct snow studies at a single site and to measure temporal variations in the various properties. Studies such as those by Bader and others (1939) are a good example of this method. Due to obvious logistic considerations, the traverse technique has been used most successfully on the Greenland and Antarctic Ice Sheets, while the site study has been applied to the study of alpine snow where terrain complicates movement from one site to another. The studies discussed in the present paper are the outgrowth of an attempt by the author and others at the U.S. Army Cold Regions Research and Engineering Laboratory to adapt the traverse technique to a study of alpine snow.

It is the purpose of this paper to present one aspect of the results obtained from two traverses in alpine areas and to discuss the assumed significance of the systematic changes of average snow density with elevation which were found to exist along both traverse lines. The data are presented primarily in graphical form and only the most obvious conclusions are drawn. It is felt that the primary need of research into facets of the alpine environment at the present time is direction in the form of a preliminary hypothesis and the development of practical research approaches. It is to these ends that this paper is specifically directed.

Location and Nature of the Research Sites

Beartooth Mountains. This range lies in south-western Montana between 45°00′ and 45°30′ N, and 109° and 110° W. A traverse of 12 km was made on the south flank of the range between Cooke City, Montana (2,350 m), and Star Lake (2,890 m). The location of the traverse line and pit locations are shown in Figure 1. A detailed description of the general area has been given by Alford and

*This report has previously appeared in the *Journal of Glaciology*, Vol. 6, pp. 495–503 (1969), and is reprinted here with the permission of the Glaciological Society.

†Department of Geology, University of British Columbia, Vancouver, Canada at time of writing; present address, Institute of Arctic and Alpine Research, University of Colorado, Boulder

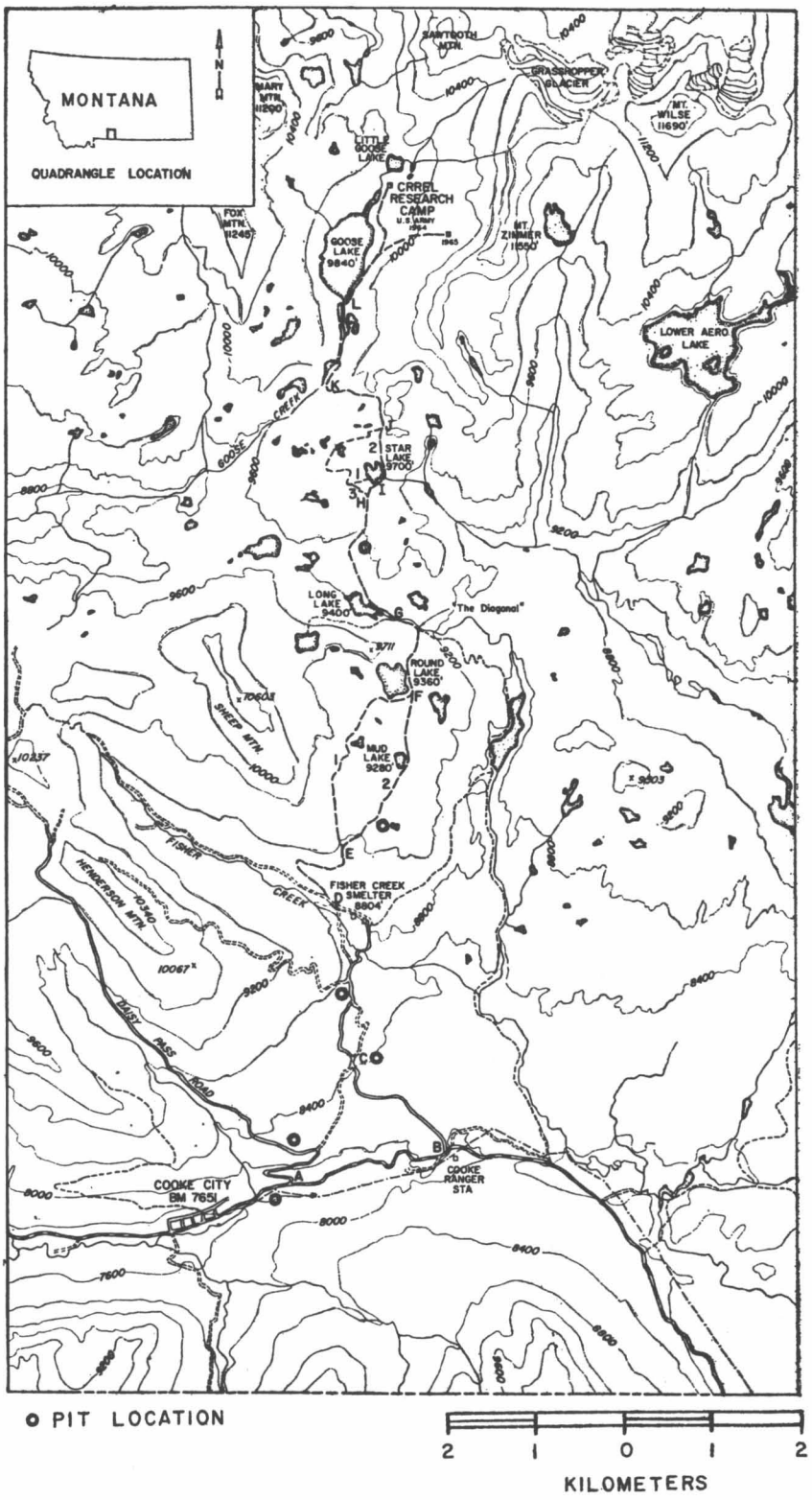

Fig. 1. A map of part of the southern flank of the Beartooth Mountains, southwestern Montana, showing the location of the traverse line and pit flank locations.

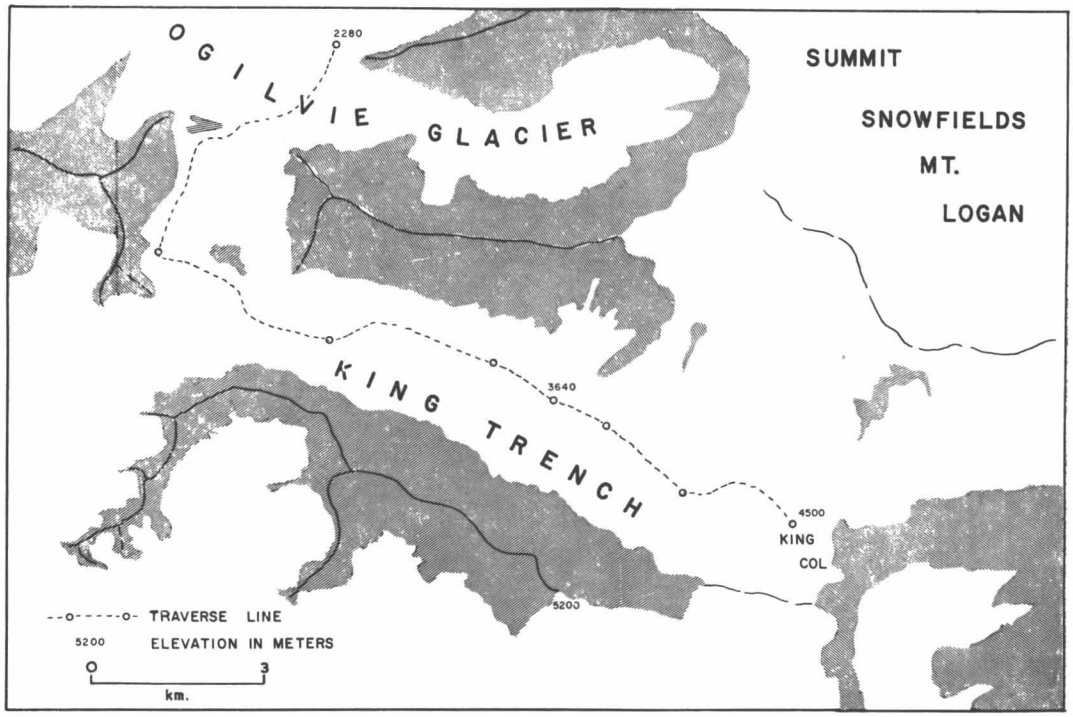

Fig. 2. The King Trench on the west flank of Mt. Logan in Canada's St. Elias Range, showing the traverse line and pit locations.

Weeks (1965). The terrain along the line of the traverse consists of a gently rolling glaciated upland, timbered to an elevation of approximately 2,500 m, above which trees exist in scattered groups to the timber line at approximately 2,850 m. Experience during the springs of 1964 and 1965 indicates that, while the prevailing wind at the surface during the day is from the south at an elevation of 2,980 m, major storms invariably move into the range from the north, making the slope on which the traverse line was located a lee slope in terms of accumulation. Pronounced development of sastrugi was noted at Goose Lake (2,980 m) and Long Lake (2,840 m) during the 1964 and 1965 field seasons but the remainder of the traverse line appeared to be unaffected by surface wind.

Mount Logan, St. Elias Range. This range lies between 60° and 61° N, and 138° and 142° W on the Yukon-Alaska boundary. A 16 km traverse was made on the west flank of Mount Logan (6,050 m) from 2,280 m on the upper Ogilvie Glacier to 4,500 m at King Col (Fig. 2). All of the pits but one were dug in the snow and firn of the King Trench which, with the exception of one small ice fall at between 3,600 and 3,900 m, possesses an extremely uniform gradient of from 5° to 10° throughout its entire length. During June 1965 the near-surface wind direction was continuously down-glacier. Features associated with marked surface-wind scour were most pronounced immediately below the ice fall mentioned above, at an elevation of approximately 3,600 m. These died out above and below that point to become completely nonexistent within a vertical distance of 400 m.

Research Techniques

The density values discussed in this paper were obtained with the standard SIPRE snow-density kit, which consists of twelve 500 cm^3 stainless-steel tubes with rubber caps, a spring balance graduated in grams and two trimming plates. Individual density values were measured at 5–10 cm intervals down each pit wall as measured with a steel tape hung from a board resting on the surface of the snow pack. Bader (1962) has stated that with care an accuracy of 0.005 g/cm^3 can easily be obtained by this method. The average density values were obtained by integrating the individual measurements at each site over the depth of the pit and these values are assumed to have a relative accuracy of 0.005 g/cm^3.

On the Beartooth Mountains traverse, pits were dug at vertical intervals of approximately 120 m. Pit locations were determined by triangulation with a Brunton pocket transit and elevations were taken from the U. S. Geological Survey Cooke City, Montana–Wyoming quadrangle map (1:62,500) with a contour interval of 80 ft (24.4 m).

On Mount Logan, pits were dug at vertical intervals of approximately 300 m. Pit locations were estimated from vertical aerial photographs (approximate scale of 1:63,000) and the Mount St. Elias sheet of the Canadian Department of Mines and Technical Surveys (1:250,000). Elevations were taken from this same map and, while absolute accuracy is undoubtedly low, relative

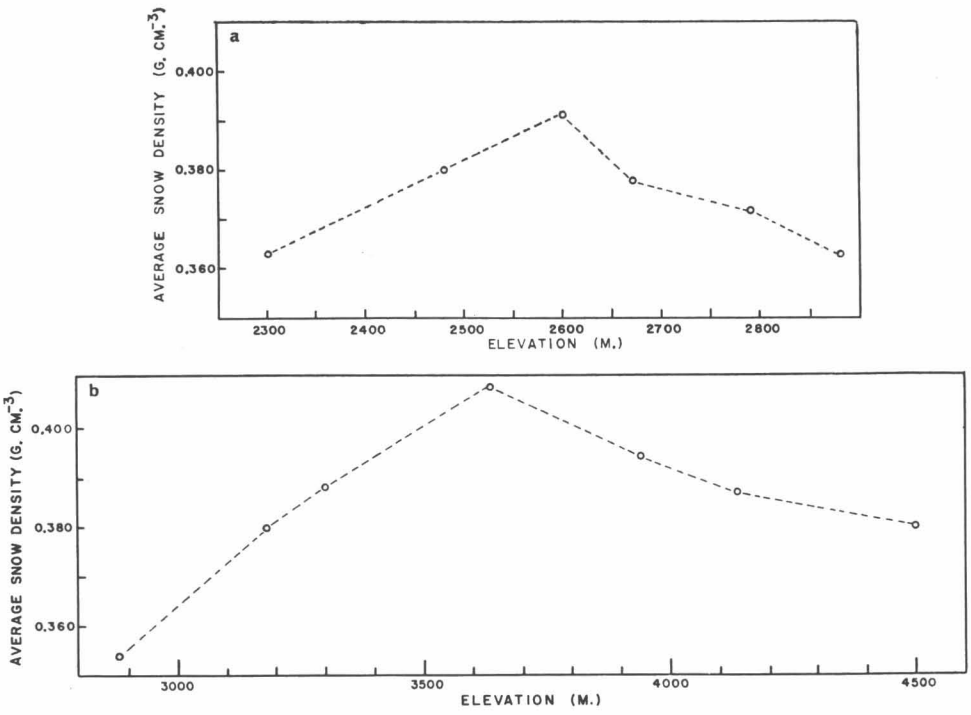

Fig. 3. a. Average snow density vs. elevation along the Beartooth Mountains traverse line; April 1965. b. Average snow density vs. elevation along the Mt. Logan traverse line; June 1965.

accuracy is felt to be within 30 m. Aircraft landings were made at the sites of pits 1, 2 and 3, affording an opportunity to check the altimeter of the aircraft against the estimates made from the map. In all cases, the agreement was within the above value.

Results

The distribution of average snow density along each traverse line as function of elevation is shown in Figure 3a and b. It can be seen that the distribution in each area is similiar, with the highest value measured near the elevational midpoint of each traverse line and decreasing in both directions from that point to minimum values at the elevation extremes of the traverse.

Total accumulation obtained from the density measurements and expressed in g/cm^2 is shown plotted against elevation in Figure 4a and b. In both areas, the general trend of the accumulation is towards increasing values at higher elevations. The secondary maximum on the Mount Logan curve is believed to be the product of drifting from the zone of intense wind scour at 3,600–3,900 m.

Snow temperatures measured at a depth of 1.50 m on the Mount Logan traverse and at 1 m on the Beartooth Mountains traverse are plotted against elevation in Figure 5a and b. In the case of the Mount Logan data, a depth of 1.50 m was selected as this was the depth of the shallowest pit. While temperatures this close to the surface cannot be compared with the mean annual temperature, it is felt that they can be used to provide some insight into the air-temperature lapse-rate prevailing along the slope during the period of investigation. Temperatures are not given for the lowest pits on the traverse line due to the initiation of spring melt at their elevations. The temperatures shown for the Beartooth Mountains traverse are those measured in the coldest part of the snow pack. Because this snow cover is seasonal, temperatures at its base will be modified by heat introduced from the underlying ground. It will therefore be less strongly affected by variations in air temperature. Unpublished data from a site study of the Beartooth Mountains snow pack obtained at the Goose Lake research station immediately prior to the traverse indicate that diurnal air-temperature variations were largely damped out at a depth of 1.00 to 1.50 m, at which depth the coldest temperatures of the snow pack were measured. These temperatures were measured on the assumptions that they were primarily the product of an atmospheric heat source and that they were sufficiently stable to allow pit to pit correlations during the time required to complete the traverse (approximately one week).

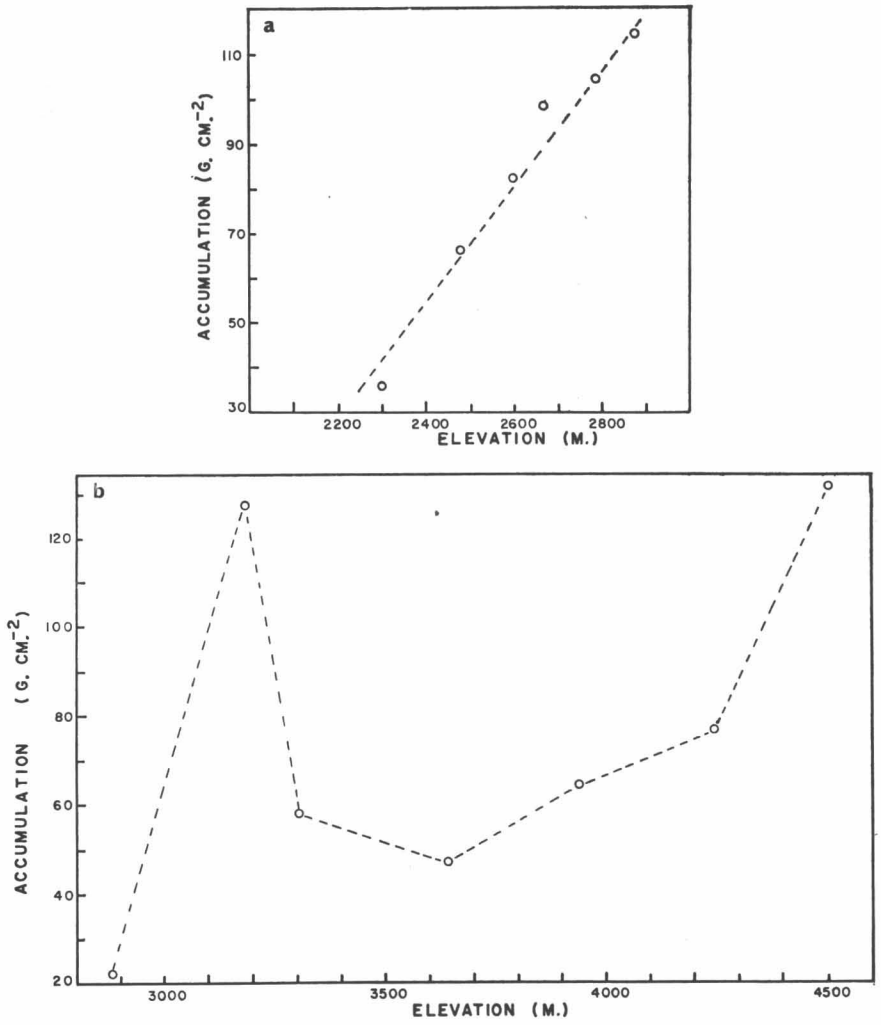

Fig. 4. a. Accumulation vs. elevation; Beartooth Mountains traverse line; April 1965.
b. Accumulation vs. elevation; Mt. Logan traverse line; June 1965.

In the case of the Beartooth Mountains traverse also, temperatures from the two lowest pits are not included, as both had been modified by percolating melt water.

Discussion of Results and Conclusions

From a purely mechanical standpoint, processes of densification fall into three categories based on temperature, wind speed and overburden pressure. Models relating metamorphism to latitude, longitude, elevation, age, etc., must, in the final analysis, be reducible to one of those three. In view of the interrelated nature of temperature and accumulation, and the influence of wind on both of these, it is difficult to discuss the effect of one independently of the others on the basis of evidence provided by field data. In the analysis of the data presented above, a number of arbitrary assumptions were made. It was assumed that the variations in the average density of the annual snow layer were produced principally by a single process and that the intensity of this process varies along the traverse line in the same fashion as the density values. While the average density value at any given pit is undoubtedly the result of an interaction between wind, temperature and accumulation, it is unreasonable to assume that the three will maintain a constant relationship at all points on any traverse line. The only one of the three processes which appears to have a distribution similar to that of the average density values on both traverse lines is temperature. On the basis of the Mount Logan data alone, it can reasonably be argued that the density values are related to both wind and accumulation as well, inasmuch as the maximum density was measured in a zone of intense wind action and at a point of inflexion on the accumulation curve. Combining the data from the two traverses, however, indicates that only the density and temperature curves remain directly related. More

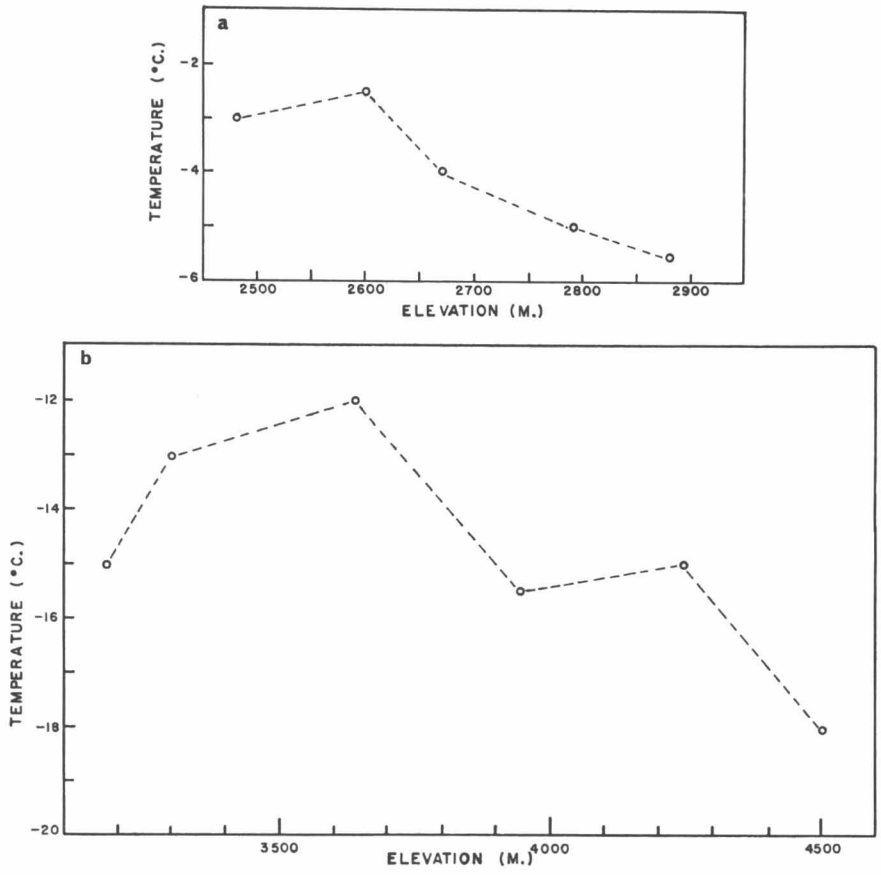

Fig. 5. a. Snow temperatures measured at a depth of 1.50 m vs. elevation; Mt. Logan traverse; June 1965; b. Snow temperatures of the coldest part of the snow pack vs. elevation; Beartooth Mountains traverse line; April 1965.

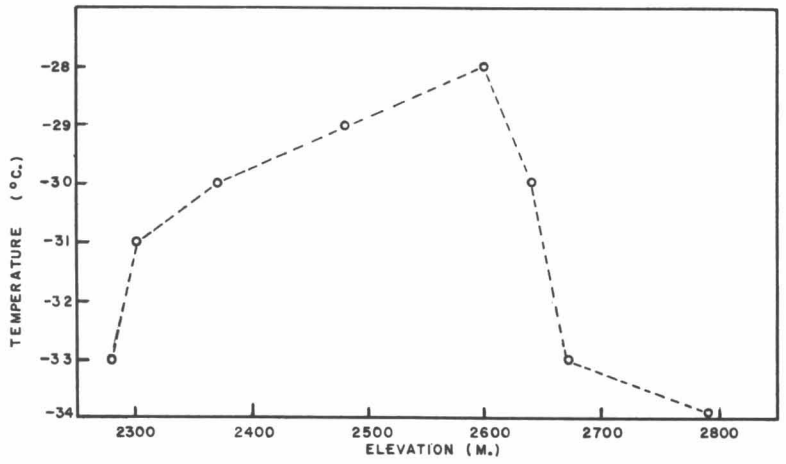

Fig. 6. Average minimum diurnal air temperatures measured at a height of 1.50 m above the snow surface vs. elevation; Beartooth Mountains traverse line; 14–17 February 1966.

recent work by the author which is the subject of a separate communication has shown that a zonation of near-surface minimum air temperatures parallels the distribution of average snow-pack densities along the Beartooth Mountains traverse line. This temperature distribution is shown in Figure 6. While this cannot be considered conclusive evidence for the relationship proposed above, it does indicate that the near-surface temperature zonation over mountain slopes discussed by Geiger (1965, p. 367–467) is a factor in the winter alpine environment.

By relating the density variations directly to temperature, it is possible to explain their distribution in terms of a simple model. Wexler (1936) has suggested that inversions of the normal air-temperature lapse-rate are a common feature over snow-covered surfaces, particularly in polar-continental air masses. These inversions tend to be quite stable and persistent. Geiger (1965, p. 367–467) has shown that an inversion of the normal air-temperature lapse-rate is a semi-stable phenomenon immediately above alpine slopes which lack a snow cover. From this, it is reasonable to assume that snow-covered slopes also exhibit this inverted lapse-rate. On this basis, the point of inflexion on the average snow density–elevation curves can be interpreted as the elevation of the mean winter depth of the inversion layer above and below which air temperatures decrease, and the amount of heat available to promote densification of the pack becomes less. The depth of this inversion will be controlled primarily by topography. It is quite probable that more complex topography than that encountered on the two traverses discussed here will result in more complex density–elevation curves. Long undulating slopes may develop a series of density maxima in response to a series of "stacked" inversions along the slope due to impeded cold-air drainage. The subparallelism of the measured snow- and air-temperature lapse-rates above the point of inflexion to the dry adiabatic rate of 1°C/100 m suggests that these rates may result in part from a warming of katabatic air drainage along the slope.

This paper is the result of a pilot study designed to determine the value of snow stratigraphy analyses as an approach to a better understanding of the alpine environment. Due primarily to problems of accessibility, little is known about the winter environment which exists in large mountain ranges and yet the influence of this environment will become an increasingly significant problem as man's activities in the mountains increase. A complete understanding of glacial hydrology cannot be gained until the depositional environment of the annual snow layer is studied in more detail than is presently the case. It is felt that the results obtained in the present case present the possibility that the annual snow layer may be used as an environmental indicator and that a refinement of these studies will allow valid correlations concerning variations in this environment to be drawn, not only within a single mountain range but between separate mountain ranges.

Acknowledgments

These studies were made while the author was employed by the U. S. Army Cold Regions Research and Engineering Laboratory, Hanover, New Hampshire, U.S.A. A preliminary draft of this paper was read by Dr. Carl Benson, Geophysical Institute, University of Alaska, and Dr. Chester Langway, U. S. Army Cold Regions Research and Engineering Laboratory, and the author is indebted to them for their constructive comments. The opinions expressed here, however, are the sole responsibility of the author.

The air-temperature studies along the Beartooth Mountains traverse line were made possible by funds provided by Dr. W. H. Mathews, Department of Geology, University of British Columbia, Vancouver, Canada. Steve Toth, Charlie Keeler, Peter Lev and George Denton, the author's co-workers during various periods of this investigation, deserve particular thanks.

References

Alford, D. L., and Weeks, W. F. (1965) Accessibility, logistics and field techniques, Goose Lake, Montana, *Spec. Rept. 77,* U. S. Army Cold Regions Res. Engin. Lab.

Bader, H. (1954) Sorge's law of densification of snow on high polar glaciers, *J. Glaciol.,* 2, 319–323.

Bader, H. (1962) The physics and mechanics of snow as a material, *Cold Regions Sci. Engin. Ser.,* Pt. 2, Phys. Sci., Sect. B, U. S. Army Cold Regions Res. Engin. Lab., pp. 1–16.

Bader, H., and others (1939) Der Schnee und seine Metamorphose, *Beitr. Geol. Schweiz, Geotech Ser., Hydrol.,* Lief. 3, Bern. U. S. Army Snow, Ice, Permafrost Res. Establ., Tr. 14, 1954. 313 pp.

Benson, C. S. (1962) Stratigraphic studies in the snow and firn of the Greenland Ice Sheet, *Res. Rept. 70,* U. S. Army Cold Regions Res. Engin. Lab., 93 pp.

Geiger, R. (1965) *The Climate Near the Ground,* Harvard Univ. Press, Cambridge, Mass., 611 pp.

Langway, C. C., Jr. (1961) Accumulation and temperature on the inland ice of north Greenland, 1959, *J. Glaciol.,* 3, 1017–1044.

Schytt, V. (1958) Glaciological investigations in the Thule ramp area, *Res. Rept. 28,* U. S. Army Snow, Ice, Permafrost Res. Establish.

Sorge, E. (1938) Die Firnschrumpfung in den obersten Schichten des grönländischen Inlandeises, *Assoc. Intern. Hydrol. Sci., Bull. 23,* pp. 725–731.

Taylor, L. D. (1965) Glaciological studies on the South Pole traverse, 1962–1963, *Rept. No. 17,* Inst. Polar Studies, The Ohio State Univ., Columbus, 13 pp.

Wexler, H. (1936) Cooling in the lower atmosphere and the structure of polar continental air, *Monthly Weather Rev.,* 64, 122–136.

Deformation of Surface Ice at a Glacier Confluence, Kaskawulsh Glacier*

Peter W. Anderton†

ABSTRACT. Measurements of surface velocity at the confluence of the north and central arms of the Kaskawulsh Glacier show a progressive change from independent profiles across each arm towards a unified profile across the combined glacier. Strain-rate determinations near the point of confluence show that the surface ice flows through a changing stress field equivalent to simple shear with an increasing component of transverse compression. The stress field across the median line is characterized by dominant transverse compression and concomitant longitudinal extension.

Surface structures such as fractures, folds, foliation, and lineation are related to the stress field at the confluence. Changes in optic-axis fabrics of the ice are also correlated with changes in the stress field near the point of confluence. Fabric symmetry probably reflects the symmetry of small-scale movements in the ice, particularly in fabrics where the optic-axis and noncrystallographic subfabrics are closely related in symmetry.

INTRODUCTION

The object of this study was to investigate the deformation of the surface ice at a glacier confluence, with emphasis on the structures produced by confluent flow. A study of the optic-axis fabrics developed in the ice under the changing stress conditions at a glacier confluence promised to be particularly interesting. While previous studies have discussed, in passing, certain aspects of confluent flow in glaciers (Allen *et al.*, 1960, p. 619; Grove, 1960, p. 81; Lliboutry, 1965, p. 609; Meier, 1960, p. 27), this is the first specific study of a glacier confluence.

AREA OF STUDY

The confluence of the north and central arms of the Kaskawulsh Glacier was selected for study (Fig. 1). The point of confluence lies at an altitude of about 1760 m, and the north and central arms are, respectively, 3 km and 3.5 km wide as they enter the confluence. This confluence has an apparently stable, and fairly symmetrical flow pattern; the ice surface is relatively flat, and free from large crevasses.

Field camps were maintained at the head of the medial moraine from June 28 to August 22, 1964, and from May 17 to August 17, 1965. Because of the large size of the confluence area, most of the study was concentrated close to the point of confluence. Measurements of surface movement and strain rates were made in order to determine the general mechanics of confluent flow, and core samples of surface ice were collected for petrographic and petrofabric study. Surface structures were mapped from ground observations and analysis of aerial photographs.

SURFACE MOVEMENT

Surface movement was measured across both arms of the glacier, and more detailed measurements were made near the head of the medial moraine. Positions of the bamboo markers were determined by intersection from theodolite stations situated on bedrock. The survey data were processed by computer to determine marker positions, surface motion, and surface velocities (Brecher, 1966, pp. 25–26). All positions are referred to an arbitrary coordinate system in which the x and y axes are horizontal, and roughly parallel and perpendicular to the flow, and the z axis is vertical. Only the horizontal component of surface motion was analyzed.

Cross-Glacier Survey

Sixty markers were set out in three transverse lines, one upglacier and two downglacier from the point of confluence (Fig. 1). Motion of the uppermost line was recorded during the 1964 summer, and a resurvey at the start of the 1965 season provided annual values for all three lines. Velocities computed for the uppermost line show a smooth, parabolic profile across the north arm, where the maximum annual velocity recorded is about 215 m/yr. The central arm, on the other hand, shows little differential flow across the middle of the glacier, and a maximum annual velocity of only 152 m/yr was recorded.

Surface velocities computed for the central line of stakes yield a profile with a marked velocity minimum across the medial moraine, where the marginal ice of the two confluent arms is still accelerating towards the central

*This report is a modified version of *Report No. 26,* Institute of Polar Studies (1970), and is reprinted here with permission.

†Institute of Polar Studies, The Ohio State University, Columbus, at time of writing; present address, 22 Redwood Lane, Lees, Oldham, Lancashire, England

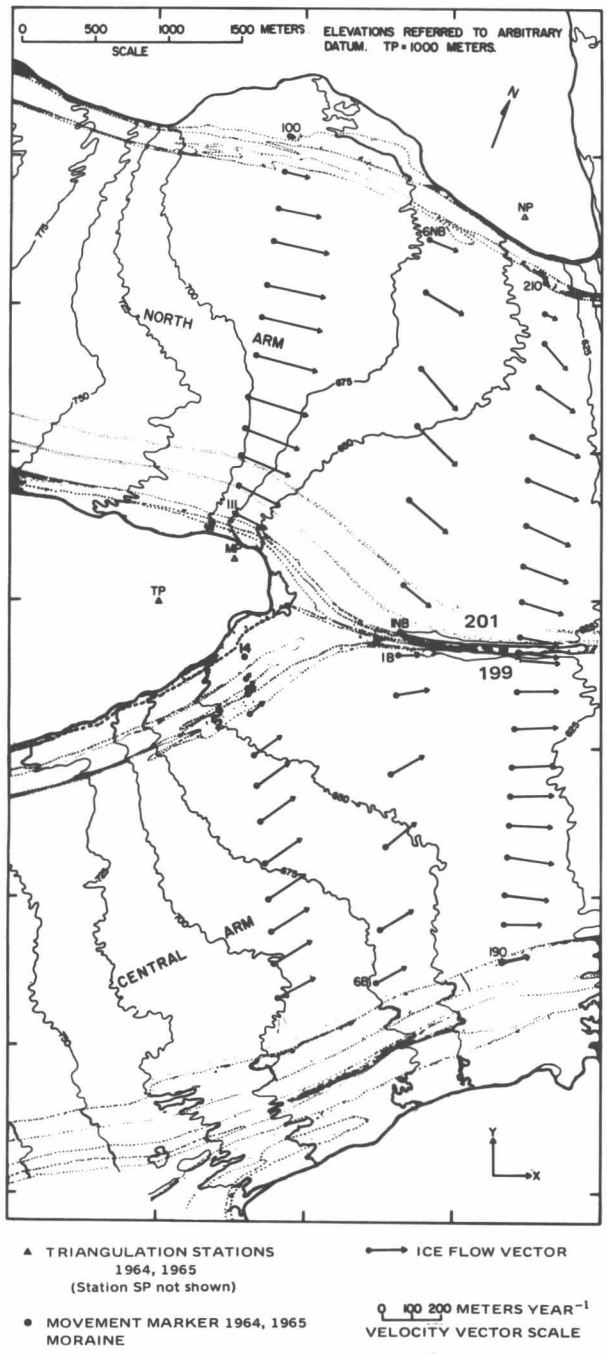

Fig. 1. Surface ice-flow vectors at the confluence of the north and central arms of the Kaskawulsh Glacier.

velocities of the combined glacier. Flow directions show a strong convergence which is apparently correlated with changes in surface slope.

Across the lowest line of stakes, the velocity profile shows a less pronounced minimum across the medial moraine, and it seems likely that a unified profile is established across the entire glacier within a kilometer or so downglacier from this cross section.

Detailed Survey

Detailed measurements of surface movement were made over a small area of about 1.5 km^2 near the head of the medial moraine. The velocity data summarized in Figures 2A and 2B are based on an initial survey of the motion of 29 markers during the 1964 summer, and a later survey of 43 additional markers during the 1965 summer. Both sets of data show good correlation, and have therefore been combined.

Flow appears to be continuous across the area, since there is no indication of discrete shear across the median line between the two arms of the glacier. The marginal ice of the north arm is probably slipping past bedrock upglacier from the confluence, however, in contrast to the almost stagnant ice at the margin of the central arm, where thick, dry moraine intervenes between ice and bedrock. Transverse profiles of velocity all show a marked velocity minimum across the medial moraine.

Flow directions appear to follow the traces of the superficial moraines quite closely, and longitudinal profiles of velocity were computed for several representative flow lines. These profiles show that the marginal ice entering the confluence undergoes an initial decrease in velocity before being accelerated downglacier. Ice at the head of the medial moraine is almost stagnant, so the velocity profile along the median line shows a continuous increase in velocity downglacier.

SURFACE STRAIN RATES

The surface strain-rate tensor was determined at selected localities across both arms of the glacier, and near the head of the medial moraine. Values and orientations of the principal compressive ($\dot{\epsilon}_2$) and extending ($\dot{\epsilon}_1$) strain rates were determined from measurements of stake arrays at the locations of each of the movement markers across the central cross-glacier line, and from velocity data in the area near the point of confluence.

Stake Array Measurements

Strain rates were derived from measurements of the deformation of square stake-patterns (diamonds) with 50-m diagonals, each centered on one of the movement markers 6B to 6NB (Fig. 3). The method of measurement is described by Nye (1959). During summer 1964 the movements of the stakes were small in relation to errors in their measurement, and strain rates were calculated only for the localities of greatest deformation. Two of the diamonds, 1B and 1NB, were lost in a meltwater lake at the start of the 1965 summer, but the remaining 11 diamonds were remeasured at that time. The validity of strain rate values based on measurements taken a year apart is uncertain, but in cases where these strain rates can be compared with those computed for the previous summer, the orientations and relative values are in fair agreement.

In general, the values of the principal strain rates are less than 10^{-4}/day across the central part of each arm,

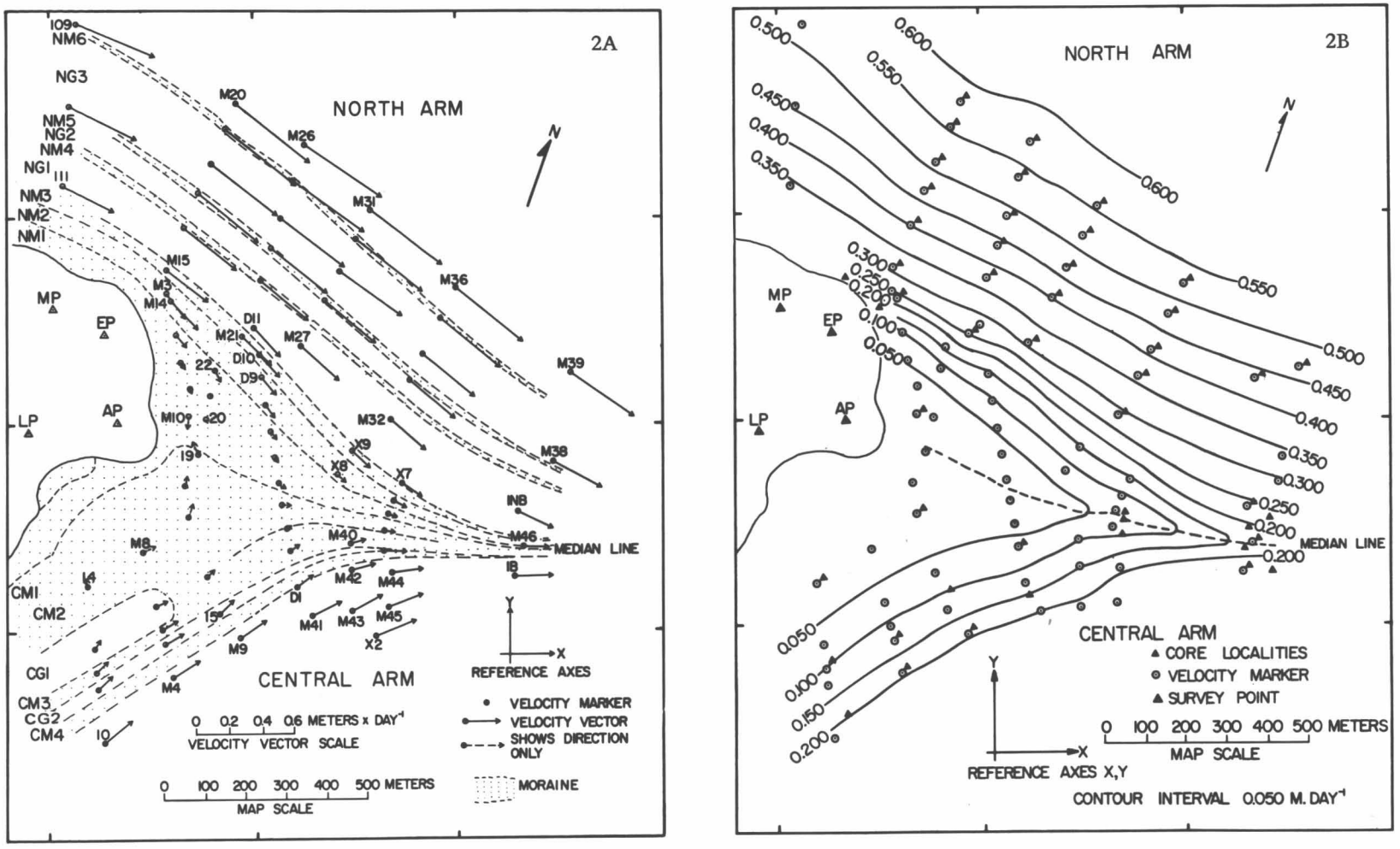

Fig. 2. Surface ice-flow near the point of confluence: (A) vectors; (B) contours. Moraines and ice streams are numbered.

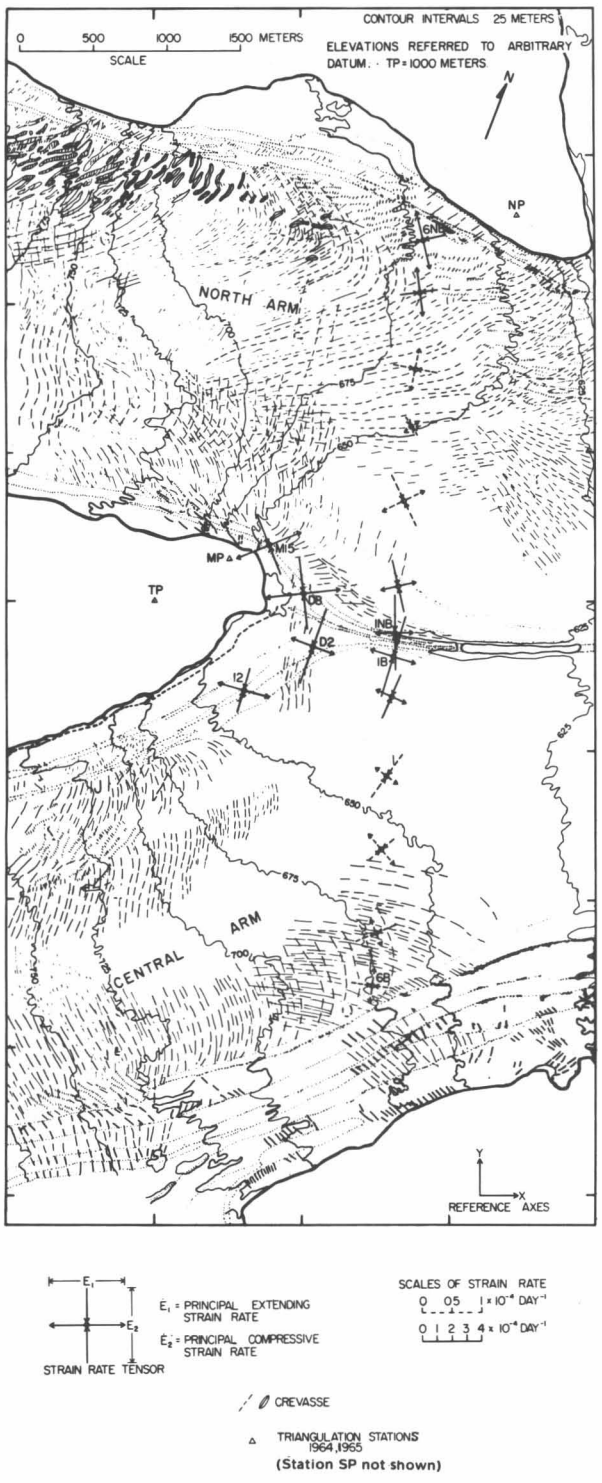

Fig. 3. Crevasse patterns and principal strain rates in the north and central arms of the Kaskawulsh Glacier, at their confluence.

but are greater than 10^{-4}/day close to the glacier margins and the medial moraine. In the central zone of each arm, the principal compressive strain rate lies parallel, and the principal extending strain rate lies transverse to, the direction of flow. Toward the glacier margins, both axes gradually rotate to an orientation about 45° from the flow direction, while toward the median line the axes rotate until the principal compressive strain rate is transverse, and the principal extending strain rate is parallel, to the flow. The magnitude of the principal compressive strain rate exceeds that of the principal extending strain rate close to the median line.

Velocity Gradient Measurements

Strain rates were determined graphically from detailed velocity data using the procedure suggested by Meier (1960, p. 32). Contours of V_x and V_y, the components of surface velocity parallel to the x and y axes of the survey coordinate system, were drawn and velocity gradients derived from these contours were used at selected localities to compute the strain-rate tensor at the surface. At two localities (markers 1B and 1NB) where the principal strain rates were determined both by this method and from measurement of strain diamonds, the agreement between the two methods is good.

The principal strain-rate field at the head of the medial moraine is summarized in Figures 4A and 4B. Upglacier from the confluence the trajectories of the principal strain rates lie at about 45° to the flow direction, but downglacier the compressive axis becomes transverse and the extending axis parallel to the flow. Marginal ice approaching the confluence from both arms moves from a stress field in which deformation is by simple shear to one in which an increasing component of transverse compression is superimposed on the shear deformation. Close to the median line the stress field shows dominant transverse compression and concomitant longitudinal extension.

SURFACE STRUCTURES

Only the surface structures near the head of the medial moraine are considered here.

Moraines

The moraines at the confluence (Fig. 2A) are superficial, and the underlying ice can be seen in fractures, moulins, and meltwater channels. Moraine debris increases in thickness towards the median line between the glacier arms, but does not exceed 60 cm except in moraine CM1, where the dry, weathered debris is at least 1 m thick. Beneath all moraines except CM1, a sharp transition from debris to glacier ice was observed, although the ice still contained sufficient debris to hinder core sampling.

Fractures

Crevasses, which are here defined as fractures open to a measurable degree, occur perpendicular to the direction of flow near the head of the medial moraine (Fig. 5). The trends of these transverse crevasses are roughly perpendicular to the direction of the principal extending strain rate. At the head of the medial moraine, most of the transverse crevasses greater than 30 cm in width are found in the central arm. They are not so well developed in the adjacent ice of the north arm.

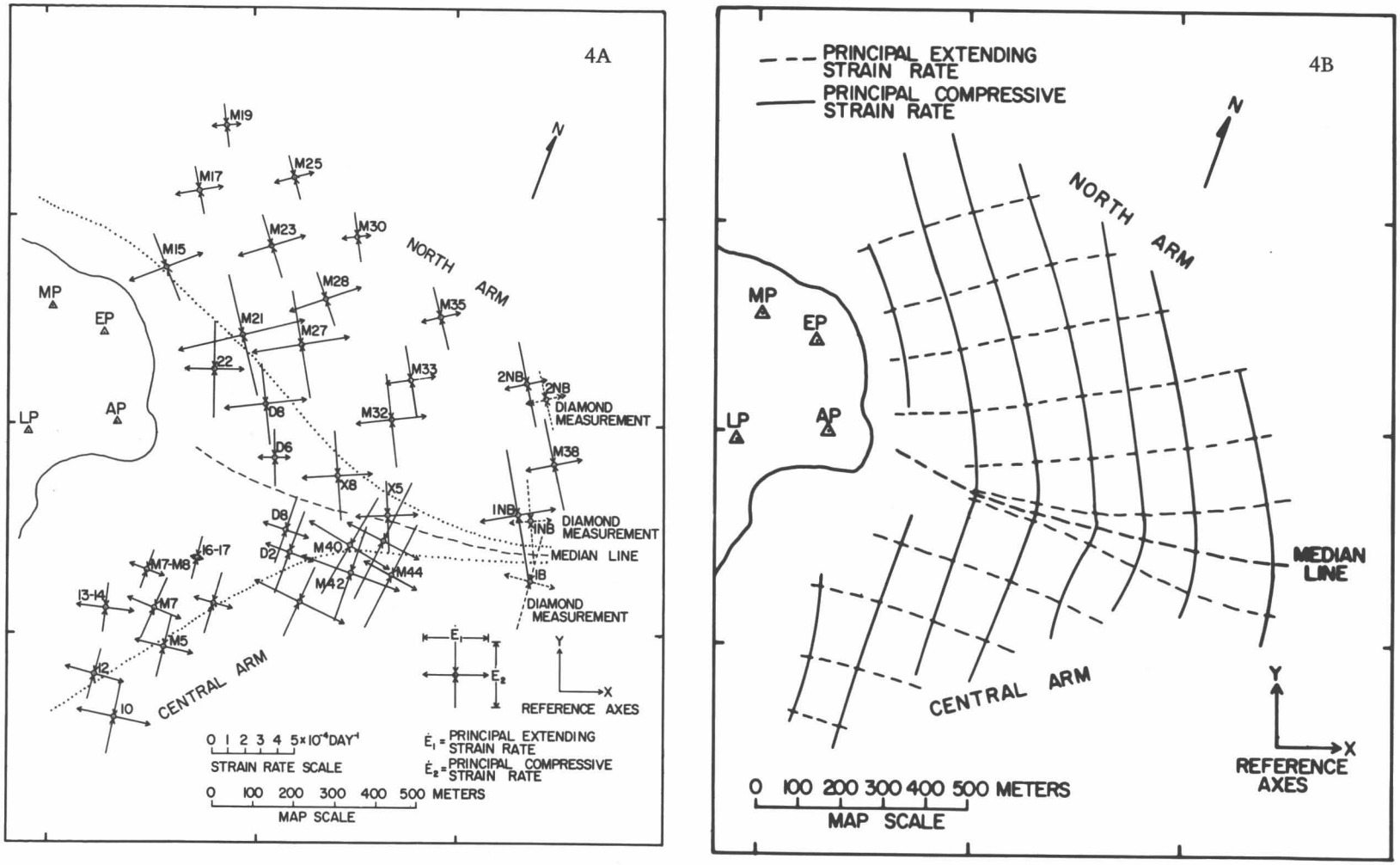

Fig. 4. Principal strain rates near the point of confluence; (A) vectors; (B) trajectories.

Downglacier, transverse crevasses are confined to the width of the medial moraine, and, when viewed from the air, the moraine appears to be broken into boudin-like segments separated by crevasses. The local stress field is similar to that postulated for the formation of boudinage structures in rocks. The difference in mechanical behavior between the moraine ice and the adjacent ice can probably be attributed to the higher debris content of the moraine ice, and the fact that, being protected from ablation by the debris cover, it forms a ridge standing some 7 m above the surrounding ice.

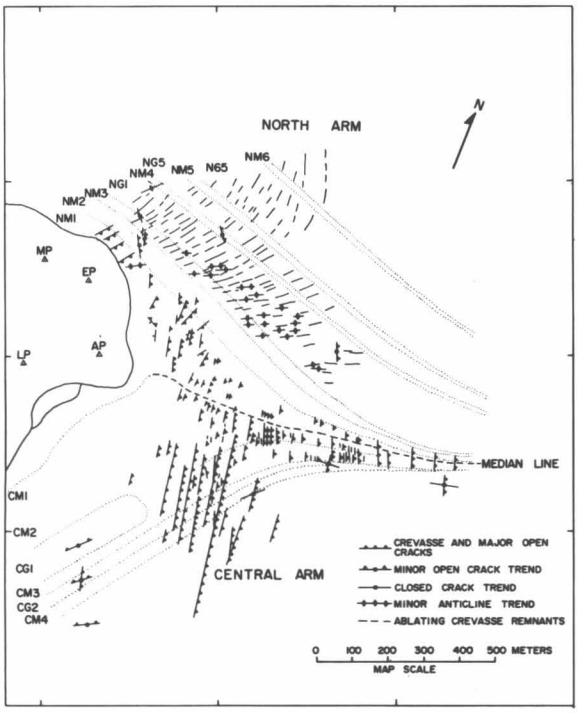

Fig. 5. Trends of fractures and minor fold axes near the point of the confluence of the north and central arms, Kaskawulsh Glacier.

Most of the fractures near the head of the medial moraine are cracks, either closed or open less than 30 cm. One set of cracks is parallel to the major transverse crevasses, and is well developed in the ice of the central arm. Also, longitudinal cracks occur subparallel to flow in the central arm. Upglacier from the confluence, these cracks appear to be slightly open, but downglacier they are closed.

Folds

A number of small, superficial anticlinal folds are present in the ice of the north arm (Fig. 5). These folds are oriented with their axes perpendicular to the principal compressive strain rate, and are cut by transverse, steeply dipping fractures.

An unusual fold structure, composed of hummocked slabs of ice, was observed adjacent to the medial moraine at the start of the 1965 summer (Fig. 6). This structure followed the course of a melt channel active during the previous summer. The stream had apparently frozen during the winter to form an ice cover about 30 cm thick, which was then folded and fractured by the transverse compression and longitudinal extension at the median line.

Bubble Foliation

Foliation defined by alternating layers of bubbly and relatively bubble-free ice is present near the point of confluence. The clear, bubble-free layers of the foliation are visible at the glacier surface as faint bluish bands, and are usually thinner than the intervening bubbly layers. Beneath the outermost moraines of the central arm, where the glacier is almost stagnant, the ice is relatively free from bubbles and shows no true foliation.

Over much of the area it is not possible to observe the true attitude of the foliation, and only surface trends, mostly subparallel to the flow, could be mapped. In the north-arm ice, close to the medial moraine, the trend of the longitudinal foliation is parallel to the flow direction, but farther away from the moraine the foliation shows a marked splaying trend. A broad zone of central-arm ice adjacent to the medial moraine shows regular foliation parallel to the flow.

Where observations were made in crevasses, channels, or moulins, the longitudinal foliation generally appeared to be vertical or steeply dipping. In the medial moraine ridge the longitudinal foliation has a fan-like structure with vertical orientation near the center, and steep inward dips at each side.

Foliation in the north arm is generally developed on a finer scale than in the central arm, and shows far more fold structures. The complexity of folding varies from simple intrafolial and shear folds to complicated structures similar to the "confluent" structures described by Taylor (1963, pp. 744–746).

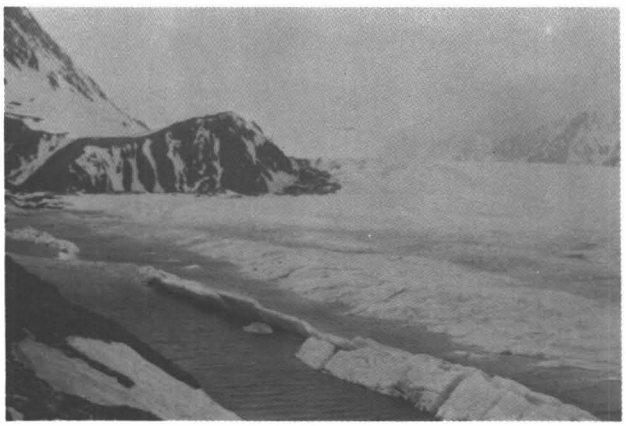

Fig. 6. Hummocked slabs of ice from a former melt channel, projecting above the surface of a meltwater lake adjacent to the medial moraine, north arm of Kaskawulsh Glacier.

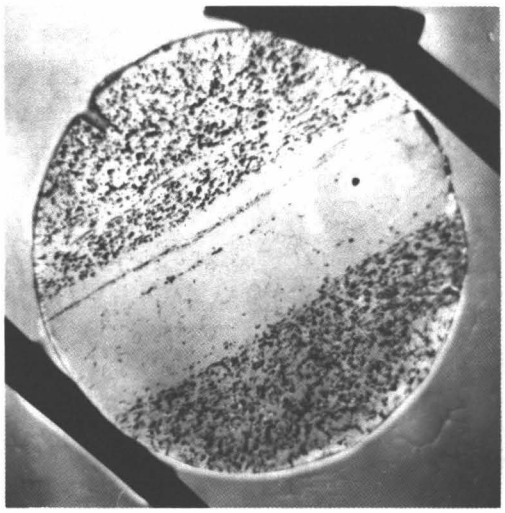

7A

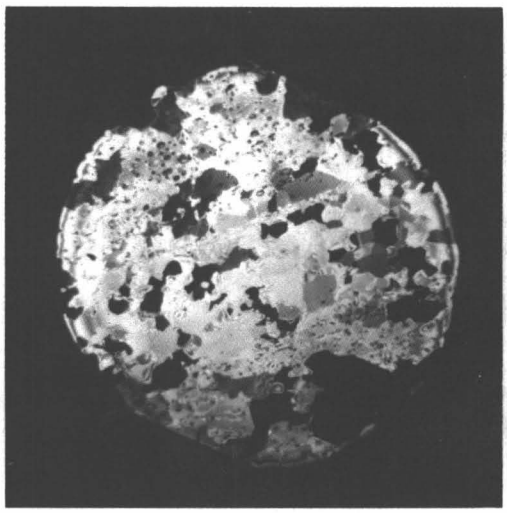

7B

Fig. 7. Horizontal section of ice with bubble layering parallel to the flow. (A) Bubbles are crowded and show increased flattening toward the margins of the clear layer. A bubbly septum is present in the clear layer. (B) Section seen through crossed polaroids. The clear layer is marked by fine-grained ice, and the bubbly septum by a zone of very small crystals (core 65-21A, X 0.8).

Many well-spaced clear layers which cut across the longitudinal foliation have a characteristic columnar crystal texture, visible on weathering. These ice veins probably mark the sites of former open fractures which have been healed by refreezing of meltwater trapped within them. Although such veins often truncate or offset the longitudinal foliation, several were observed to be folded relative to the foliation, indicating that differential movement had occurred parallel to the foliation layering.

PETROGRAPHY OF ICE CORES

Only those core samples collected from the area near the head of the medial moraine (Fig. 2B), and downglacier across the moraine between stakes 199 and 201 (Fig. 1), are considered here. A total of 51 cores of 7.5-cm diameter were obtained from depths of 1 to 2 m using a CRREL auger. Sections were cut by handsaw to about 1-cm thickness, and thinned by melting to a thickness of 2 to 3 mm for examination between crossed polaroids.

Definitions

The term "foliation" is used here to describe all planar surfaces (*S*) defined by metamorphic structures in the ice (Turner and Weiss, 1963, p. 97; Ragan, 1967). Planar surfaces may be defined by layering, which in ice can comprise layers of varying grain size, varying bubble content, or varying debris content. Such surfaces may also be defined by preferred dimensional orientation of components of the glacier ice, such as flattened grains, flattened bubbles, or tabular debris fragments, or by surfaces of discontinuity, such as fractures, slip zones, or cataclastic zones.

The term "lineation" is used to describe all linear metamorphic structures in the ice, such as preferred orientation of elongated bubbles or debris fragments.

Bubble Texture

Most of the north-arm ice contains more bubbles than the ice of the central arm, and the weathered surface of the north arm appears whiter in comparison. The cores contained abundant small bubbles, usually less than 0.3 cm in maximum dimension. Beneath the moraines closest to the margin of the north arm, however, the ice contains fewer, but larger, bubbles up to 1 cm in size. Similar bubbles are found in the ice from the central arm although there are very few bubbles in the ice beneath the outermost moraines. Ice from the medial moraine ridge appears to be less bubbly than adjacent ice, but contains the largest bubbles, up to 3 cm in size, recorded in this area.

Clear layers are generally well defined in the north-arm ice (Fig. 7A), but more diffuse in the central-arm ice. Toward the margin of the central arm, the cores showed minor bubble-rich zones scattered through dominantly clear ice.

In north-arm cores from above the confluence, the bubbles are not noticeably flattened except close to the margin of the glacier. Downglacier and towards the median line, there is a general increase in the degree of flattening of bubbles. The planes of flattening are sometimes parallel to, but are often at an angle to, the foliation layering. Most of the bubbles in the central-arm ice are flattened parallel to the foliation layers. The most highly compressed bubbles were observed in ice along the median

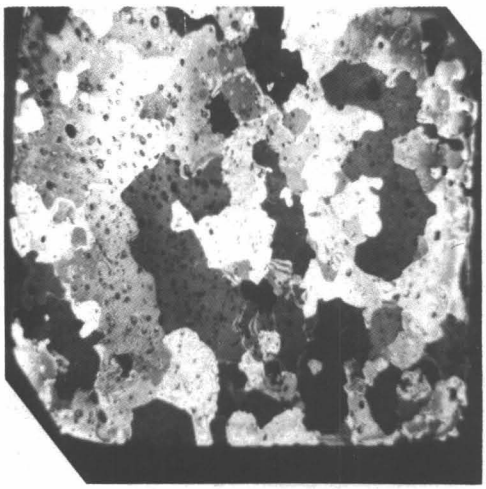

Fig. 8. Vertical section of bubbly ice viewed between crossed polaroids, showing characteristic irregular interlocking texture (stake 201, X 0.8).

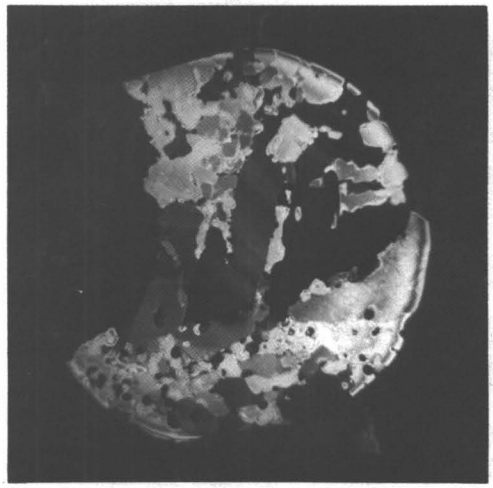

Fig. 9. Horizontal section across an ice vein, viewed between crossed polaroids. Large crystals show peripheral granulation and lamellar substructures (stake 5NB, X 0.8).

line. These bubbles are flattened in nearly vertical planes oriented parallel to the flow, and tend to be concentrated in narrow zones, forming a cleavage-like structure. In places the bubbles have a skeletal form suggesting that they are distorted remnants of flattened bubbles. Cores from the medial moraine downglacier near marker 200 showed not only extremely flattened and skeletal bubbles, but also bubbles that had apparently been drawn out into filaments parallel to the flow.

Very few clear layers in the cores were completely free from bubbles. Flattened bubbles were often observed, usually flattened in the plane of the foliation layers. Sometimes increased flattening or concentration of bubbles occurred at the margins of clear layers, but generally the boundaries of the layers simply truncated the normal bubbly texture. Thin layers or septa of minute bubbles were present in the clear layers from several cores (Fig. 7A).

Debris Content

Debris fragments up to 3.5 cm in maximum dimension were encountered in some cores, but most fragments were less than 1 cm in size. Close to the median line between the arms, platy rock fragments are often oriented in the plane of the bubble foliation with their long dimension parallel to the flow direction. The distribution of debris within the cores themselves is usually irregular, but beneath the north arm moraine NM1 (Fig. 2A) some weak segregation of debris occurs both above the confluence and adjacent to the median line. Vertical debris-rich layers are oriented parallel to the flow and the plane of bubble flattening. Streaks of fine debris may also occur parallel to the flow.

Crystal Texture

The characteristic crystal texture of the surface ice as observed in thin section consists of an interlocking aggregate of irregularly shaped grains, which are often deeply embayed (Fig. 8). All sections, when examined between crossed polaroids, contained groups of grains showing identical crystallographic orientation, and undergoing simultaneous extinction during rotation of the section. Each group probably represents a number of cross sections through different branches of a single complex crystal. The presence of complicated, branching crystals in temperate glacier ice has been observed in the Malaspina Glacier (Bader, 1951, p. 526) and the Blue Glacier (Rigsby, 1968). Therefore, the apparent grain size of the ice seen in thin section may not have any relationship to the actual dimensions of the individual crystals.

Bubbly ice is coarse grained throughout the confluence area, and grains generally show maximum dimensions of 0.5 to 4 cm in section. There does not appear to be any definite relationship between the apparent grain size of a sample and its position in the confluence. The north-arm ice generally shows more irregular crystal shapes than the ice of the central arm, although simpler textures were observed in cores close to the margin. Many sections showed crystals flattened slightly in the plane of the bubble foliation.

No differences in apparent grain size were noted between most of the clear layers and the adjacent bubbly layers. Cores from seven localities on the north arm, however, showed smaller crystals in the clear layers, although the difference was significant in only two of the cores. On the other hand, ten cores representing both arms of the glacier showed clear layers with somewhat larger crystals than the adjacent bubbly ice.

Sharp changes in crystal texture across the boundaries of contiguous clear layers are unusual. Individual crystals normally overlap the margins and often cut completely across clear layers. Occasionally, the edges of

clear layers are marked by sharp textural breaks or discontinuities. Where differences in grain shape exist between bubbly and clear ice, crystals in the clear ice seem to be simpler in form. The dominantly clear ice close to the glacier margins and in the medial moraine ridge also shows simpler grain shapes.

In a number of clear foliation layers, particularly in ice from the north arm, thin bubbly septa appeared to mark discontinuities in crystal texture, parallel to the plane of the foliation. In section these discontinuities appear as linear alignments of grain boundaries or sharp fractures sometimes showing evidence of slip. Some of the fractures were associated with finer grain size, while a few seemed to mark zones of cataclasis characterized by very fine crystals less than 0.1 cm in size (Fig. 7B).

Glacier ice throughout the confluence area showed no evidence of substructures, which indicate stress in the grains. In a sample of congelation ice collected near the medial moraine from a deformed slab over a melt channel, however, the crystals showed both undulatory extinction and kink bands. In another sample of congelation ice from an ice vein undergoing deformation, the crystals showed well developed kink bands and peripheral granulation or recrystallization of the larger grains (Fig. 9). The lack of such stress phenomena in the normal glacier ice must be attributed to recrystallization during long-continued flow.

ICE FABRICS

In this study "ice fabric" refers primarily to the preferred orientation of crystallographic fabric elements (optic axes) in the core samples, but also includes the preferred orientation of noncrystallographic elements such as bubbles.

The orientations of the optic axes of grains in thin sections from 32 oriented cores were measured in the field by means of a Rigsby universal stage. Approximately one hundred grains were measured from each core, only one measurement being recorded from each group of crystals showing simultaneous extinction. About twelve sections per core were required, the sections being cut at intervals of about ten centimeters to minimize the risk of measuring the same crystal twice.

The measured optic-axis orientations have been plotted on equal area stereographic diagrams. The resulting point diagrams were contoured by computer at standard intervals using a 1% counting area. Because of the small number of measurements per diagram, the statistical validity of the recorded patterns is uncertain, but it has been assumed that the best criterion of validity is the consistency of the patterns.

The characteristics of the measured optic-axis fabrics are summarized in Table 1. Only the gross features and symmetry of the patterns have been used in the interpretation of the diagrams. Strong, discrete maxima ($> 10\%$) are assumed to be real, especially where they define recurring symmetrical patterns. Orientation measurements from individual sections of a core were separately identified in each fabric diagram and the degree of consistency of the orientations among the sections was estimated qualitatively.

Where the fabric consistency is poor, the maxima are probably the result of inadequate sampling. Fabrics of three cores from the same locality (65-21 A and B, 64-9), for instance, show the same broad concentration of optic axes, but differing minor maxima within the overall pattern. Minor maxima of this type probably have no significance, as demonstrated by Stanley (1965, pp. 125, 169) in ice fabrics from the Athabasca Glacier. It has been noticed in previous studies that the maxima in ice-fabric diagrams are often stronger in diagrams representing fewer measurements. While this effect may well reflect bias in the smaller samples, the patterns in such samples may also indicate short-range ordering of the fabric, especially if individual patterns show good consistency.

The fabrics showing poor consistency have been contoured by computer using a method suggested by Kamb (1959, pp. 1908-1909) in order to determine their statistical significance. The results of this contouring support the interpretation of some of the weaker patterns as single maxima or girdles.

The symmetry of the optic-axis fabrics is described in terms of symmetry planes, m, and axes of symmetry, ∞-fold and 2-fold (Turner and Weiss, 1963, pp. 44, 64-67). These fabrics are classified as axial if they show a single ∞-fold symmetry axis, orthorhombic if they show three mutually perpendicular planes of symmetry, monoclinic if they show a single symmetry plane, and triclinic if no symmetry planes are present. Most are technically triclinic if the details of the fabric pattern are considered, but also show a gross symmetry. Noncrystallographic subfabrics are described using mutually perpendicular geometric axes, a, b, and c (Turner and Weiss, 1963, pp. 86-90). Where a planar structure, S, is present, S defines the ab plane and c is the pole to S. Where a lineation occurs it defines b (Fig. 10).

In the fabric diagrams, the optic-axis and noncrystallographic fabric symmetries are indicated, as are the orientations of the measured principal strain rates and the flow direction. Diagrams have been rotated so that the plane of projection coincides with that of a planar foliation structure at the core locality. An explanation of symbols used in the fabric diagrams is presented in Figure 11.

Fabric Patterns

The cores selected to illustrate the variation of ice fabrics in the confluence area represent mainly bubbly ice samples except at localities where clear ice was dominant. In the following discussion, the directions of the principal compressive and extending strain rates are identified, as $\dot{\epsilon}_c$ and $\dot{\epsilon}_t$, respectively; the direction of theoretical maximum shearing strain rate, at 45° to the principal axes, is identified as $\dot{\epsilon}_s$. The locations of core

TABLE 1. Optic-axis Fabric Data

Core number	Bubble Content[1]	Number of optic-axis measurements	Core locality[2]	Ice stream identification[3]	Fabric consistency[4]
64-2	B	95	1B	CA	G
64-3	B	118	2B	CA	M
64-4	B	126	3B	CA	G
64-5	B	119	4B	CA	M
64-6	B	109	5B	CA	P
64-7	B	110	6B	CA	M
64-8	CB	111	near 1B	MM(C)	M
64-9	B/C	119	1NB	NG1	P
64-10	B	87	2NB	NA	M
65-1	BC	137	12	CM3	M
65-2	CB	151	near 15	CM3	P
65-3	BC	148	D2	CM3	P
65-4	BC	133	X4	CM3	M
65-5*	C	81	14	CM2	None
65-6	CB	110	17	CM2	P
65-7	CB	157	D4	CM2	M
65-8	BC	129	near X5	CM2	M
65-9	BC	106	X5	NM1	P
65-10	B	115	near M14	NM1	G
65-11	BC	104	near 111	NM1	M
65-14	B/C	128	near 111	NG1	M
65-15*	CB	78	near M14	NM1	None
65-16	BC	129	M10	NM1	P
65-17	CB	135	19	CM2	P
65-19	B	104	5NB	NA	M
65-20A	C	84	near 10	CA	M
65-20B	B	101	near 10	CA	M
65-21A	B/C	108	1NB	NG1	P
65-21B	B/C	105	1NB	NG1	P
65-22	CB	128	M46	MM(N)	P
65-23	C	98	1B	CA	P
65-24	CB	111	200	MM(C)	P

[1] Symbols are defined in Figure 11.
[2] Locations are shown in Figure 12.
[3] Locations of stream lines (CM, NM, NG) are shown in Figure 5; CA = central arm, NA = north arm; MM(C), MM(N) = medial moraine ridge, central portion and north portion, respectively.
[4] G = good; M = moderate; P = poor.

* Fabrics unreliable because of poor core orientation.

samples near the head of the medial moraine are shown in Figure 12, together with the corresponding fabric diagrams. Core samples were also taken across the glacier at the sites of the strain diamonds (Fig. 3).

Fabrics Near the Median Line

Central-arm fabrics. All cores except 65-2 and 65-5 contained flattened, elongated bubbles defining an orthorhombic fabric. The optic-axis diagrams have been rotated so that the plane of projection is parallel to S of the local bubble foliation.

The optic-axis fabrics (Fig. 13A) of the cores collected farthest upglacier show poorly developed girdles. The planes of the girdles are perpendicular to S and dip upglacier at an angle of 10°–15°. A tendency for greater concentrations of optic axes to lie near c, which is roughly coincident with $\dot{\epsilon}_s$ here, is apparent in three of the fabrics but not in 65-6.

A second group of fabrics (Fig. 13B) from cores taken below the point of confluence shows broad concentrations of optic axes centered approximately on $\dot{\epsilon}_s$ rather than on c. In two of these fabrics, 64-2 and 65-7, the center of the pattern is displaced toward $\dot{\epsilon}_c$. The fabrics 64-2 and 65-4 both show four discrete maxima with orthorhombic symmetry, while fabric 65-7 seems to include the same pattern minus one of the maxima. Fabric 64-9 (Fig. 12), which was measured at a locality close to that of 64-2, shows no discrete maxima although the overall distribution of the optic axes is very similar in both. Fabric 65-3 is also diffuse.

A third group of fabrics (Fig. 13C) from cores collected very close to the median line shows a single broad

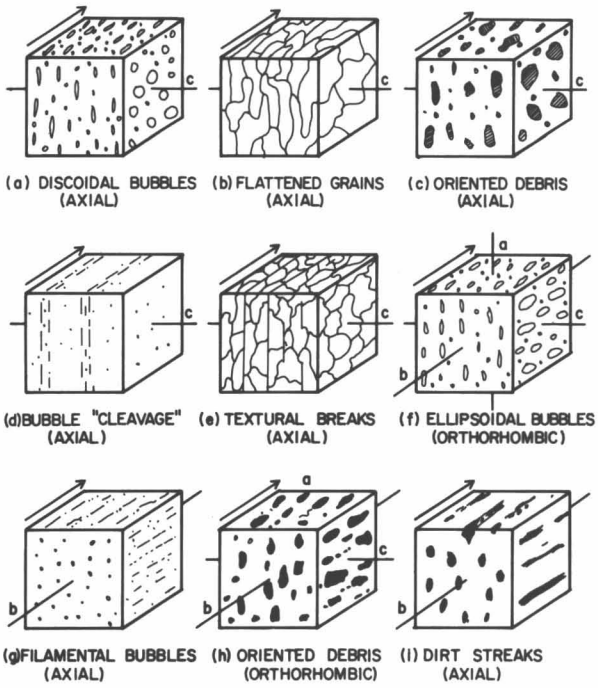

Fig. 10. Planar and linear structures in glacier ice. Directions of flow and geometric symmetry axes (*a, b, c*) are marked.

concentration of optic axes centered roughly on *c*, which coincides approximately with $\dot{\epsilon}_c$.

Fabric 64-3 (Fig. 14) shows a pattern of four maxima centered on $\dot{\epsilon}_c$ and not on *c*. This fabric does not fit the pattern established for the other samples from this area.

Apart from fabric 64-3, the fabrics near the head of the medial moraine seem to be related to the flow. Girdle fabrics upglacier from the confluence appear to change to partial girdles or patterns of multiple maxima downglacier, and to broad single maxima close to the median line. Major concentrations of optic axes tend to be centered approximately perpendicular to the measured flow direction. The optic-axis concentrations are centered on $\dot{\epsilon}_s$ upglacier from the confluence and show a rotation towards $\dot{\epsilon}_c$ as the median line is approached. These changes reflect the changing orientation of the principal strain rates with respect to the flow direction, and the increasing component of transverse compression.

North-arm fabrics. All cores except 65-15 showed bubble layering or flattened, elongated bubbles defining an *S*-plane. The plane of projection of the optic-axis diagrams is parallel to *S*.

The cores collected farthest upglacier, together with core 64-10, yielded optic-axis fabrics (Fig. 15A) with discrete maxima. Fabric patterns 65-11 and 65-14, although differing in number of maxima, are both centered at a high angle to the measured flow direction, and show a single symmetry plane dipping upglacier at about 10°. No strain-rate measurements were made near the sample locations, but the patterns are probably centered

EXPLANATION OF DIAGRAM

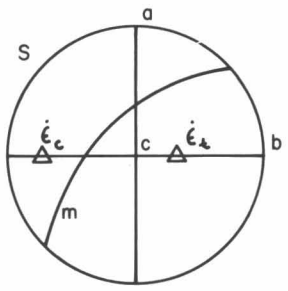

a, b, c Symmetry axes of dimensional fabric

S Plane of planar structure in the ice (*ab* plane)

m Symmetry plane of optic axis fabric

△ Direction of principal compressive ($\dot{\epsilon}_c$) or tensile ($\dot{\epsilon}_t$) strain rate

→ Measured flow direction

Contours: 1 – 3 – 6 – 9 – 12 – 15 – 18%

EXPLANATION OF CAPTION

65-1 = core number

NA (M14) = north arm, Stake M14

CA 12 = central arm, Stake 12

137 BC = number of measurements and bubble content (B = bubbly; BC = bubbly with clear zones; CB = clear with bubbly zones; C = clear; B/C = distinct clear and bubbly zones)

Fig. 11. Explanation of ice-fabric diagrams shown in Figures 12–16.

close to $\dot{\epsilon}_s$. A pattern of four maxima in fabric 65-10 is centered not on *c*, but close to the local direction of $\dot{\epsilon}_s$. Fabric 64-10 shows a similar pattern with one of the maxima much reduced, and also centered on $\dot{\epsilon}_s$.

A second group of cores (Fig. 15B) was collected close to the median line. Fabric 65-16 shows two bubble foliation structures: S_1, defined by flattened bubbles, and S_2, defined by bubble layering which truncates and is apparently younger than S_1. The optic axes form a rough girdle within which the main concentrations show roughly the same relationship to S_1 as does the fabric pattern of core 65-10 to its local *S*-surface. Fabric 65-16 may therefore be a relict pattern from upglacier. A partial girdle present in fabric 65-9 farther downglacier shows major concentrations centered close to $\dot{\epsilon}_s$ but displaced towards $\dot{\epsilon}_c$, and dips upglacier at a low angle. Broad concentrations of optic axes, interpreted here as single maxima, are seen in fabrics 65-21 AB and 65-22.

Fabric 65-22 was measured in ice from the medial moraine ridge and is centered on c of the steeply dipping foliation, which strikes perpendicular to $\dot{\epsilon}_c$. The other three fabrics, measured adjacent to the moraine, are also centered on c, close to $\dot{\epsilon}_c$.

Fabrics with discrete multiple maxima were recorded away from the median line, while poorly defined girdle fabrics were found in the uppermost ice closest to the head of the medial moraine, and broad single maxima were measured farther downglacier. Optic-axis concentrations in cores upglacier from the confluence seem to be roughly centered on $\dot{\epsilon}_s$, but downglacier and towards the median line the concentrations shift towards $\dot{\epsilon}_c$.

Comparison of central- and north-arm fabrics. The optic-axis fabrics from the central arm seem to show more correspondence with the changing deformation than the optic-axis fabrics from the north arm, possibly because the flow of the marginal ice of the central arm

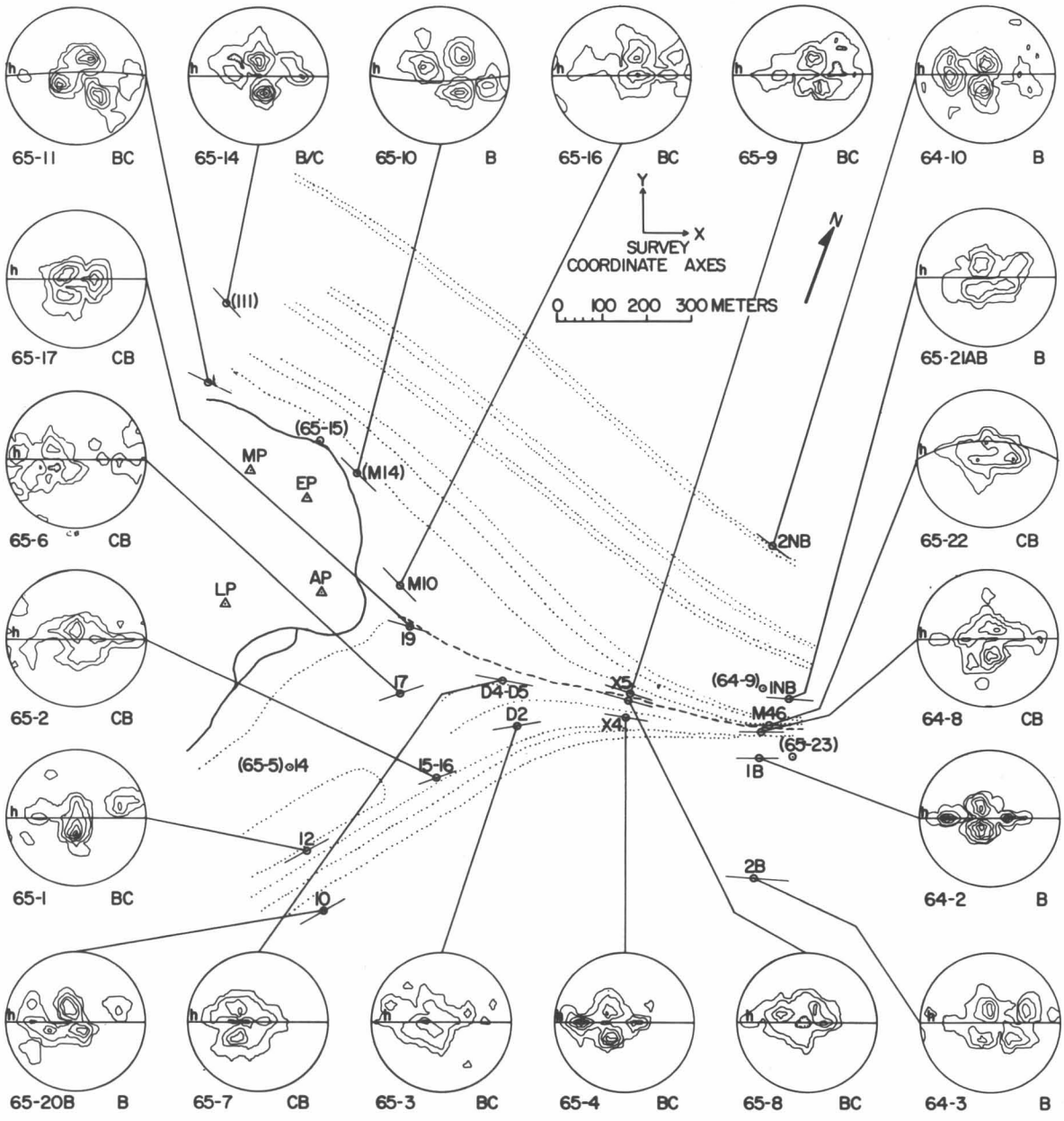

Note: 64-9 same pattern as 65-22; 65-23 similar to 64-2; 65-5 and 65-15 fabric unreliable.

Fig. 12. Ice-fabric diagrams from the area near the point of confluence of the north and south arms, Kaskawulsh Glacier (see Fig. 11 for explanation). Locations of the sites where the core samples were obtained and orientations of the vertical or nearly vertical planes of projection of the diagrams are shown on a map of the area.

is less disturbed by the confluence. Above the confluence the north-arm ice, which is slipping past the bedrock, possesses fabrics with discrete maxima, whereas the central-arm ice, which is stagnant at the glacier edge, possesses girdle fabrics. The north-arm ice, where it joins the central arm at the head of the medial moraine, also appears to show girdle fabrics. Both types of fabric are essentially similar, however, as they both share a plane of symmetry, and have their major optic-axis concentrations centered close to $\dot{\epsilon}_s$.

Downglacier, fabric patterns become more closely centered on $\dot{\epsilon}_c$, and a broad single maximum seems to be characteristic of the ice along the median line, where the transverse compression is dominant. North-arm fabrics appear to change more slowly, perhaps in part because the initial fabrics are stronger.

Fabric patterns on either side of the medial moraine reflect the change in the sense of shear across the interface between the two arms. Across the line between markers 1B and 1NB, seven fabrics illustrate this change in orientation. Fabrics 64-8 and 65-22 from the medial moraine show patterns centered on $\dot{\epsilon}_c$, while fabrics 64-2 and 65-23 from the central arm show patterns still centered close to $\dot{\epsilon}_c$, but displaced towards $\dot{\epsilon}_s$. North-arm fabrics 65-21 AB, and 64-9 also show patterns closely centered on $\dot{\epsilon}_c$, but these are displaced towards $\dot{\epsilon}_s$ in

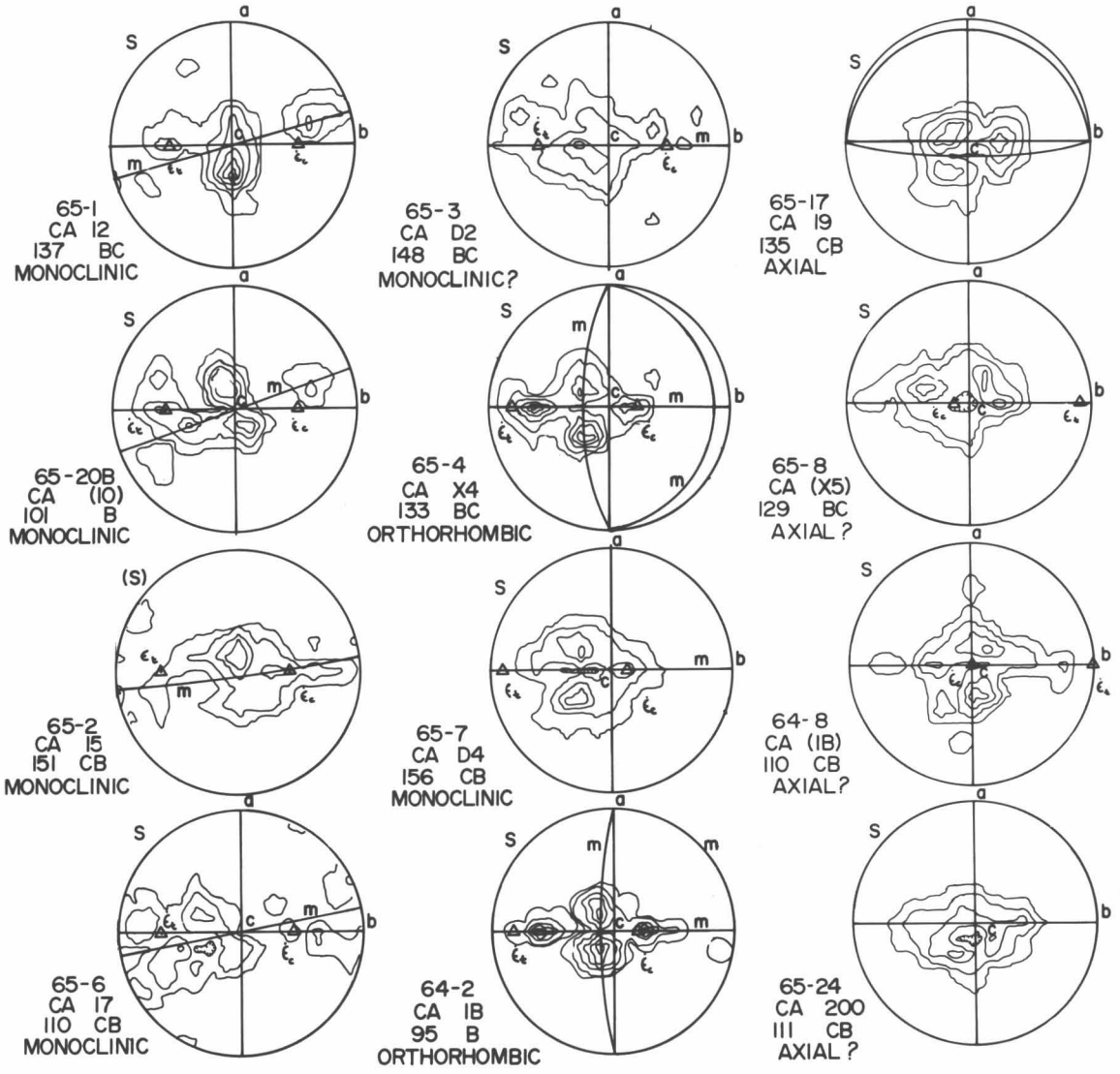

Fig. 13. Ice-fabric diagrams, central arm, Kaskawulsh Glacier.

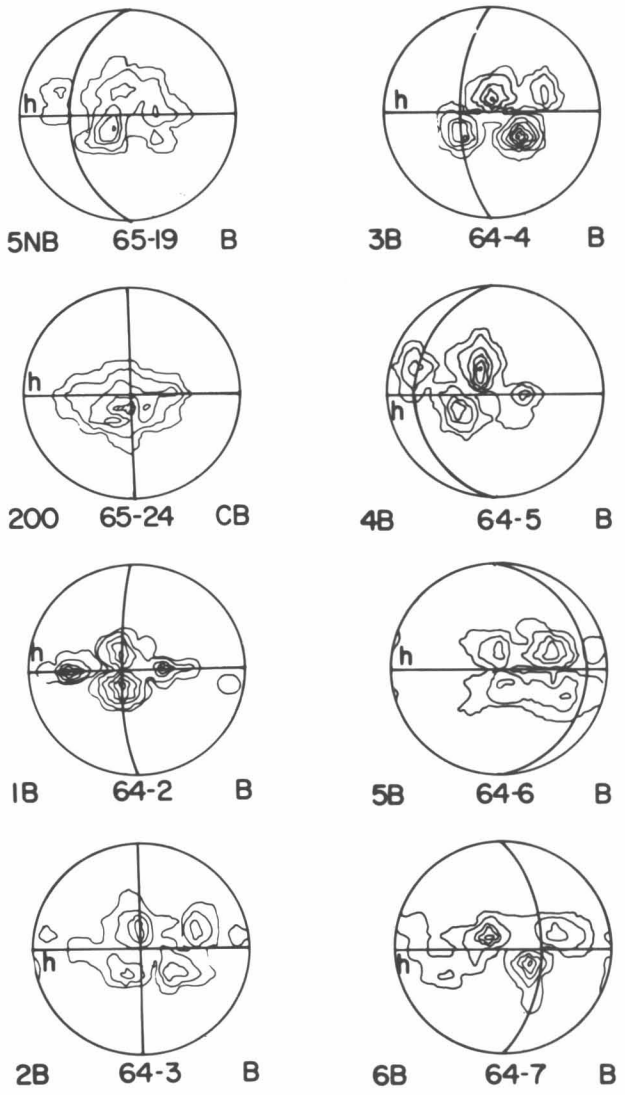

Fig. 14. Ice-fabric diagrams, north and central arms, Kaskawulsh Glacier.

the opposite sense. A similar change in orientation of the fabric patterns across the median line is shown by fabrics 65-4, 65-8, and 65-9.

All fabrics seem to show optic-axis concentrations or patterns centered at a high angle to the flow direction, although no consistent relationship was observed. The fabric patterns also show no consistent symmetry relationship to the foliation. Fabric patterns can, however, be correlated with the changes in orientation of the principal strain-rate field.

In none of the fabrics are the symmetries of the crystallographic and noncrystallographic subfabrics identical. The fabrics can therefore be termed heterotactic. The subfabrics, however, may share specific symmetry planes or axes. For instance, in fabrics 64-8 and 65-22, the ∞-fold symmetry axis of the optic-axis fabric pattern coincides with c of the bubble fabric. Symmetry planes or axes of the optic-axis fabric that do not coincide with elements of the bubble fabric are simply related to the bubble fabric by small rotations about the bubble fabric axes. This can be seen in fabric 65-4, where the three 2-fold symmetry axes of the orthorhombic optic-axis fabric can be brought into coincidence with the geometric axes of the bubble fabric by a small rotation about a.

Fabric 64-10, from the north arm, may be a relict pattern inherited from upglacier. It resembles patterns recorded farther upglacier, and the local deformation conditions are not greatly different from those upglacier. Across the other side of the medial moraine at a comparable distance, fabric 64-3 is probably also relict, being related to other fabrics from the middle of the central arm rather than those from near the median line.

Fabrics of clear and bubbly ice. At two localities on the central arm, a pair of cores were obtained in order to compare the fabrics of clear and bubbly ice in adjacent foliation layers (64-2, 65-23; 65-20A and B). Both of the clear layers that were sampled showed somewhat coarser grain size and simpler grain shapes than the bubbly layers. Apart from variation of individual maxima, however, the overall fabrics were virtually identical in each case (Fig. 16).

Clear and bubbly ice fabrics were measured in four cores from the north arm. Cores 65-21A and B intersected the same thin, clear layer, which was finer grained than the bubbly ice, and showed evidence of cataclasis. Again, no difference in fabric between the clear and bubbly ice was observed (Fig. 16). Likewise, no significant fabric differences were recorded from samples 64-9 and 65-14 (not shown).

Fabrics at Cross-Glacier Sites

Fabrics (Fig. 14) were measured in cores taken within each of the strain diamonds across the central arm (Fig.3). Strong patterns of four maxima, centered approximately on $\dot{\epsilon}_c$, were recorded at three of these localities (64-3 to 64-5). These fabrics are possibly inherited from upglacier because local deformation rates across the middle of the glacier are low. There is no simple relationship between the symmetries of the optic-axis and bubble fabrics, as observed in the fabrics near the head of the medial moraine.

Fabric 64-6 is rather diffuse, while fabric 64-7 shows a girdle pattern comparable to the fabrics from the edge of the central arm just above the confluence.

A single sample (65-19), collected near the margin of the north arm at diamond 5NB (Fig. 13), shows a broad optic-axis concentration centered on $\dot{\epsilon}_s$, and c of the local longitudinal foliation.

DISCUSSION

In this study, the orientations and relative magnitudes of the principal strain-rates measured at the glacier surface are assumed to represent the surface stress field. Ice entering the confluence from both arms is subjected to a

changing stress field equivalent to simple shear with an increasing component of transverse compression superimposed on the shear deformation. The stress field along the median line is characterized by dominant transverse compression and concomitant longitudinal extension. Many surface structures in the ice, such as fractures, folds, foliation, and lineation, are directly related to the stress field at the confluence. Changes in optic-axis fabric of the ice are also correlated with changes in orientation of the stress field.

Development of Foliation

Longitudinal foliation with a roughly vertical dip, as observed at the Kaskawulsh confluence, often occurs at the interface between confluent glaciers, and may be very strongly developed (Allen *et al.*, 1960, p. 609; Meier, 1960, p. 54; Taylor, 1963, pp. 738-739; Untersteiner, 1955). Such foliation appears to be active in the deformation at a confluence, and may be carried passively downglacier. Confluence foliation often includes layers of differing grain size as well as the type of bubble layering observed at the Kaskawulsh confluence.

There has been controversy about the origin of glacier foliation; some think that the foliation forms parallel to the planes of maximum shearing stress, and others that it forms perpendicular to the axis of principal compressive stress (Sharp, 1954, p. 826; Lliboutry, 1965, p. 612). In specific instances, however, foliation may form with either of these orientations. The longitudinal foliation at the Kaskawulsh confluence is more or less parallel to the flow direction and shows no consistent orientation with respect to the stress field. Upglacier the foliation

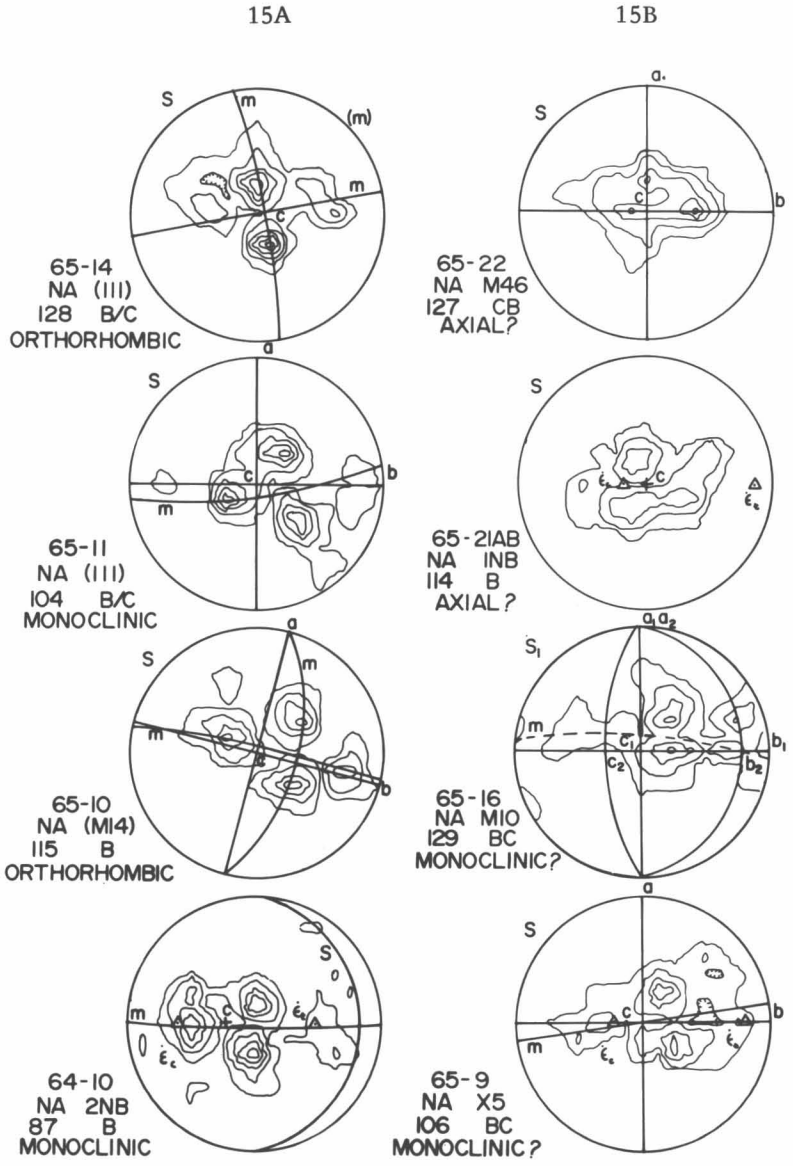

Fig. 15. Ice-fabric diagrams, north arm, Kaskawulsh Glacier.

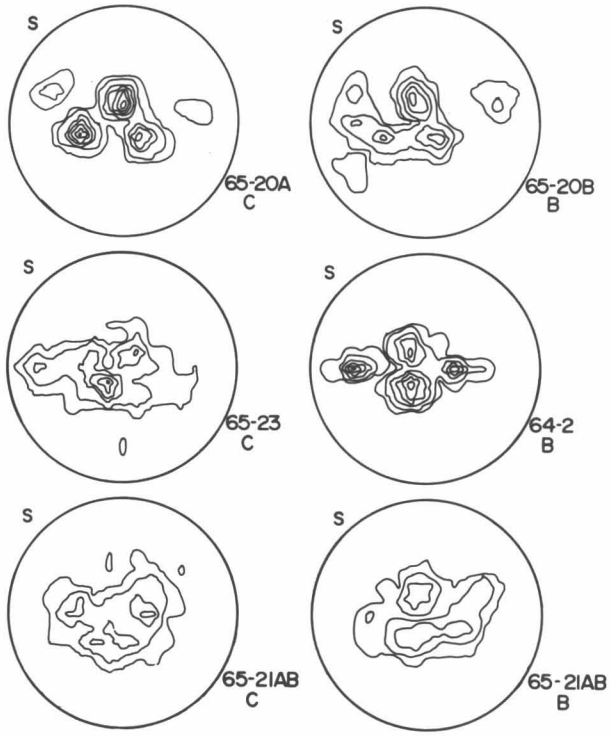

Fig. 16. Ice-fabric diagrams of clear and bubbly ice.

is parallel to the planes of maximum shearing stress, and downglacier it becomes oriented perpendicular to the principal compressive stress. Apparently the foliation marks planes of concentrated shearing strain, the orientation of which is controlled by differential flow near the ice–bedrock interface, and across the interface between the two glaciers.

Clear layers, as observed in the Kaskawulsh ice, have been produced experimentally by deformation of bubbly ice near the melting point (Kamb, 1964, p. 363), but their origin is uncertain, because the precise mechanism or mechanisms of segregation or removal of the bubbles is not known. Redistribution of bubble foliation layers during flow can occur in absence of internal melting of the ice, as shown by Merrill (1960, pp. 73-74). Meier (1960, p. 60) suggests that initial anisotropy of the glacier ice may cause some parts to strain more rapidly than others, forming "soft" zones that propagate in planar directions, expelling air bubbles into the adjacent, less strained layers. Such a process involves redistribution of the bubble content of the ice, and might be expected to give rise to an increased concentration of bubbles at the margins of clear layers. In addition the locally accelerated plastic flow might be expected to produce distinctive crystal textures and optic-axis fabrics in the clear layers. In the Kaskawulsh samples, however, there was little difference in texture or fabric between clear and bubbly ice layers.

Development of foliation by a friction regelation process was suggested by Phillip (1920, pp. 520-521). This hypothesis assumes that ice flow can take place by movement along closely spaced fracture or fault zones. The frictional heat generated by slip along these zones results in melting of the ice close to the fault plane, and escape of the bubbles. This process may be partly responsible for the formation of some of the Kaskawulsh clear layers, which included fractures and cataclastic zones.

Many of the Kaskawulsh clear layers show no distinctive textural features, however, and may not be active in the deformation. The action of percolating meltwater in dissolving bubbles and promoting recrystallization may also rapidly modify the structure of clear layers. In the uppermost 15 m of a temperate glacier, the ice is permeable to meltwater, and clear layers are apparently far more permeable than the bubbly layers (Lliboutry, 1964, pp. 112-113). Possibly the clear layers, once formed, tend to persist or even to enlarge because of increased local percolation of meltwater, particularly if the layers are sites of fracturing.

Development of Optic-Axis Fabrics

Optic-axis fabrics showing strong multiple maxima appear to be characteristic of coarse-grained glacier ice. A pattern commonly encountered is a roughly orthorhombic arrangement of four maxima, as observed in some of the Kaskawulsh fabrics. Fabrics of this type have been recorded in active and stagnant ice from several temperate glaciers (Bader, 1951, p. 532; Kamb, 1959, pp. 1900-1902; Rigsby, 1960, p. 594).

Fabrics recorded from some glaciers show diffuse patterns of girdles and small-circle girdles with multiple maxima varying in orientation (Allen *et al.*, 1960, pp. 614-617; Hashimoto *et al.*, 1966; Stanley, 1965, pp. 99-100; Taylor, 1963, p. 742). Many of the Kaskawulsh fabrics seem to show similar patterns, and the median-line fabrics may well be poorly developed small-circle girdles rather than broad single maxima.

Foliation often seems to control the orientation of optic-axis fabrics in glacier ice. Patterns, especially those showing axial symmetry, are frequently centered on c, the pole of the foliation. Most of such fabrics, however, were measured in ice subject to relatively constant flow conditions. At the Kaskawulsh confluence, where flow conditions change rapidly, the fabric patterns are not consistently centered on c, the pole of the foliation.

Little is known about the relationships between optic-axis fabrics and stress in temperate glacier-ice. In ice from the edge of the Blue Glacier, fabrics show optic-axis concentrations centered about the pole to the plane of expected maximum shearing stress (Kamb, 1959, p. 1904). Small-circle girdles from the Antler Glacier (Hashimoto *et al.*, 1966) and the Athabasca Glacier (Stanley, 1965, p. 75) were found to be centered about the axis of principal

compressive stress. The Kaskawulsh fabrics are probably controlled in part by the type and orientation of the stress field, because they show changes in character and orientation related to changes in the stress field. This control may not be direct, however, because the change in fabric orientation is also broadly correlated with the change in flow direction.

Stanley (1965, p. 160) has suggested that fabrics in ice from the Athabasca Glacier are controlled by local planes of movement which are not directly related to the stress field and may diverge from the overall flow direction. The Kaskawulsh fabrics may similarly reflect small-scale movement within the ice. Where deformation rates are small, the fabrics may be relict or modified by recrystallization, and need not be related to local flow conditions.

In samples of ice deformed by uniaxial compression, small-circle girdle fabrics have been observed, centered on the compression axis (Stanley, 1965, p. 151; Steinemann, 1958, Fig. 62-64). Various multiple-maxima fabrics have been produced in ice under torsional simple shear (Kamb, 1964, pp. 363-364, 1966; Steinemann, 1958, Fig. 60). Kamb has reported that when ice near the melting point is deformed by torsional shear and a gradually increasing uniaxial stress is superimposed, the two-maxima shear-fabric changes to a small-circle girdle pattern. Fabric changes similar to these were observed in ice from the Kaskawulsh confluence subject to similar changes in stress.

The dominant process of flow in glacier ice is believed to be plastic flow by basal glide in individual crystals. Long-continued flow is made possible by the growth of less-stressed crystals through syntectonic recrystallization. Such recrystallization under stress is responsible for the characteristic interlocking crystal texture of temperate glacier ice, as has been demonstrated experimentally (Kamb, 1964, p. 356; Steinemann, 1954, p. 454). In ice deformed experimentally by basal glide accompanied by recrystallization, the crystals show stress phenomena such as undulatory extinction and kink bands, whereas crystals of temperate-glacier ice are generally free from such substructures unless deformation is extremely intense. Clear crystals, such as those observed at the Kaskawulsh confluence, have probably been produced by long-continued flow with gradual removal of lattice defects and formation of a fabric oriented most favorably for flow.

Control of the orientation of deformation fabrics in ice may be by mechanical control of basal glide, by thermodynamic control of recrystallization, or by a combination of both processes. Many fabrics have been interpreted in terms of basal glide, because this is the only mechanism of flow that has been demonstrated experimentally in ice. In plastic deformation the basal planes of ice crystals tend to become aligned parallel to the planes of maximum shearing stress, and deformation fabrics might be expected to show concentrations of optic axes close to the pole of the shear planes. However, while some strong single-maximum fabrics may be directly related to active shear planes, multiple maxima in ice fabrics should not be regarded individually as poles to sets of shear planes.

Kaskawulsh fabrics in this study have been interpreted in terms of symmetry relationships, as proposed by Sander (1930). Fabric symmetry is assumed to represent the movement picture (or plan), which is the pattern of small-scale movements resulting in the observed gross deformation (Turner and Weiss, 1963, p. 370). Thus a four-maxima fabric might represent a movement plan involving four preferred orientations of glide, and might equally well represent an entirely different movement plan based on solid diffusion. The fabric patterns alone do not reveal the mode of deformation, only the symmetry. Fabrics actively related to deformation in the Kaskawulsh confluence area seem to be those in which the various subfabrics are very closely related in symmetry, and those in which the subfabrics are widely different are probably relict.

Acknowledgments

The guidance of Prof. C. Bull of the Ohio State University is gratefully acknowledged. Special thanks must also go to Dr. G. Dewart, who carried out a concurrent seismic study of the confluence, and Mr. J. P. Freeman for their assistance in the field. The assistance of members of the Icefield Ranges Research Project who contributed in many ways to the study is greatly appreciated.

Logistic support was provided by the Icefield Ranges Research Project, and financial assistance came from the Institute of Polar Studies and the Department of Geology at the Ohio State University, and the Arctic Institute of North America.

References

Allen, C. R., Kamb, W. B., Meier, M. F., and Sharp, R. P. (1960), Structure of the lower Blue Glacier, Washington, *J. Geol.*, 68, 601–625.

Bader, H. (1951) Introduction to ice petrofabrics, *J. Geol.*, 59, 519–536.

*Brecher, H. H. (1966) Surface velocity measurements on the Kaskawulsh Glacier, Yukon Territory, Canada, *Rept. No. 21,* Inst. Polar Studies, The Ohio State Univ., Columbus, 73 pp.

Grove, J. M. (1960) A study of Veslgjuv-breen, in *Norwegian Cirque Glaciers,* edited by W. V. Lewis, pp. 69–82, Res. Ser., No. 4, Roy. Geogr. Soc., London.

Hashimoto, S., Shimizu, H., and Nakamura, K. (1966) Glaciological studies of the Antler Glacier, Alaska, *J. Faculty Sci., Ser. 4, Geol. Mineral.,* Vol. 13, pp. 237–256, Hokkaido Univ.

Kamb, W. B. (1959) Ice petrofabric observations from the Blue Glacier, Washington, in relation to theory and experiment, *J. Geophys. Res.,* 64, 1891–1910.

Kamb, W. B. (1964) Glacier geophysics, *Science,* 146, 353–365.

Kamb, W. B. (1966) Experimental recrystallization of ice under deformation (Abstr.) *Trans. Am. Geophys. Union,* 47, 187–188.

Lliboutry, L. (1964) *Traite de Glaciologie,* Masson, Paris, Vol. 1, pp. 1–428.
Lliboutry, L. (1965) *Traite de Glaciologie,* Masson, Paris, Vol. 2, pp. 429–1040.
Meier, M. F. (1960) Mode of flow of the Saskatchewan Glacier, Alberta, Canada, *Prof. Paper 351,* U.S. Geol. Surv., 70 pp.
Merrill, W. M. (1960) Structures in glacier ice, North Ice Cap, northwest Greenland, *Intern. Geol. Congr.,* 21st Sess., Norden, Pt. 21, pp. 68–80.
Nye, J. F. (1959) A method of determining the strain-rate tensor at the surface of a glacier, *J. Glaciol.,* 3, 409–419.
Philipp, H. (1920) Geologische Untersuchungen über den Mechanismus der Gletscherbewegung und die Entstehung der Gletschertextur, *Neues Jahrb. Mineral., Geol., Palaeontol.,* 43, 439–556.
Ragan, D. M. (1967) Planar and layered structures in glacial ice, *J. Glaciol.,* 6, 565–567.
Rigsby, G. P. (1960) Crystal orientation in glacier and experimentally deformed ice, *J. Glaciol.,* 3, 589–606.
Rigsby, G. P. (1968) The complexities of the three-dimensional shape of individual crystals in glacier ice, *J. Glaciol.,* 7, 233–251.
Sander, B. (1930) *Gefügekunde der Gesteine,* Springer, Berlin, 352 pp.
Sharp, R. P. (1954) Glacier flow; a review, *Bull. Geol. Soc. Am.,* 65, 821–838.
Stanley, A. D. (1965) Relation between secondary structures in the Athabasca Glacier and laboratory deformed ice, *Ph. D. dissertation,* Univ. Brit. Columbia.
Steinemann, S. (1954) Flow and recrystallization of ice, *Intern. Union Geod. Geophys., Int. Assoc. Sci. Hydrol., Symposium of Rome,* Vol. 4, pp. 449–462.
Steinemann, S. (1958) Experimentelle Untersuchungen zur Plastizität von Eis, *Beitr. Geol. Schweiz, Hydrol. No. 10,* pp. 46–50.
Taylor, L. D. (1963) Structure and fabric on the Burroughs Glacier, south-east Alaska, *J. Glaciol.,* 4, 731–752.
Turner, F. J., and Weiss, L. E. (1963) *Structural Analysis of Metamorphic Tectonites,* McGraw-Hill, New York, 545 pp.
Untersteiner, N. (1955) Some observations on the banding of glacier ice, *J. Glaciol.,* 2, 502–506.

---

*A modified version of this report appeared in Icefield Ranges Research Project, Scientific Results, Vol. 1 (1969).

Seismic Investigation of Ice Properties and Bedrock Topography at the Confluence of the North and Central Arms of the Kaskawulsh Glacier*

Gilbert Dewart†

ABSTRACT. The purpose of the study is twofold: (1) to investigate seismic velocity inhomogeneity and anisotropy in strongly deformed glacier ice; and (2) to determine the form and dimensions of that part of a subglacial valley where two large temperate glaciers merge. The field investigations were carried out during the summers of 1964 and 1965 at the confluence of the north and central arms of the Kaskawulsh Glacier in the St. Elias Mountains.

Continuous seismic noise, attributable chiefly to wind, interfered with the measurements. Individual pulses of noise were also recorded; they are apparently associated with the process of ice deformation and changes in air temperatures.

According to the results of wide-angle seismic reflection measurements the mean vertical *P*-wave velocity in the glacier is 3.70 km/sec. At depths of 10–100 m the mean *P*-wave velocity is 3.63 km/sec, *S*-wave velocity is 1.74 km/sec and Poisson's ratio is 0.350. From 10-m depth to the surface the velocities of *P* and *S* waves decrease markedly to approximately 3.0 km/sec and 1.5 km/sec, respectively.

It appears that velocity anisotropy is caused mainly by the foliation structure of alternating layers of clear and bubbly ice. When foliation is strong, velocity anisotropy from this cause predominates over velocity anisotropy due to crystallographic fabric. Crystallographic fabrics are seldom strong enough to cause significant velocity anisotropy.

The greatest depth of ice in the central arm of the glacier, which is 3000 m wide, and in the combined glacier, which is 5000 m wide, is about 1000 m. The north arm is somewhat less deep. The base of the ice is lower than the glacier terminus, 40 km downglacier, but no bedrock depression was found at the confluence. Both glacier arms are roughly parabolic in cross section. There is no break in the slope of the valley wall where the glacier surface meets it. The valleys of the two arms merge at approximately the same juncture at which the surface movements of the two glaciers merge into a uniform flow.

The acoustic impedances of the rocks found in the vicinity of the confluence were determined and the reflection coefficients at interfaces between ice and these rocks were calculated. Impedances of the rocks were too close to one another for subglacial contacts to be delineated.

It is concluded that only under especially favorable circumstances can seismic measurements be used practically in the study of crystallographic fabrics in glacier ice. Strongly foliated ice consisting of clear and bubbly layers, however, is potentially a good subject for such investigation.

Introduction

This investigation was undertaken in order to determine some of the physical properties of glacier ice and the nature of the subglacial topography at the confluence of two large temperate valley glaciers. The factors influencing the velocity of seismic waves are of particular interest. The problem of the sources of seismic noise in a glacier is also treated.

The major parts of the research program, in order of treatment, are as follows:

(1) Studies of seismic noise sources in the glacier and its surroundings with a continuously recording seismograph station
(2) Seismic refraction and wide-angle reflection measurements
(3) Investigation of the relationship of seismic wave velocity to ice crystal orientation, foliation, and fracture, and the velocity distribution near the upper surface of the glacier
(4) Seismic reflection survey, including the problems presented by glacier movement

These problems are interrelated. Seismic noise affects the collection of data for all the other investigations. The wide-angle reflection observations provide mean velocity values necessary for the interpretations of vertical reflection survey data. The validity of assumptions of homogeneity and isotropy that are made in the reflection survey is examined under topic (3). The primary interest in topic (3), however, is the use of seismological methods in petrological and structural studies.

Equipment and Operations

Station seismograph. A set of continuously recording station seismographs was operated on the Kaskawulsh Glacier during the 1965 field season. Its primary purpose was to register noise generated in and near the glacier. The instrumentation consisted of two horizontal-motion torsion seismometers (T_o = 1.0 sec) mounted at right

*This report is a modified version of *Report No. 27,* Institute of Polar Studies (1968), and is reprinted here with permission.

†Institute of Polar Studies, The Ohio State University, Columbus

angles to each other, a vertical motion seismometer-galvanometer combination (T_o = 0.5 sec; T_g = 0.3 sec), and a horizontal "strong-motion" seismometer (T_o = 1.0 sec). These instruments were arranged on a common base and recorded optically on separate strips of 35 mm film.

The seismograph station was established on the medial moraine near Kaskawulsh Camp. A tent covered by several layers of tarpaulin ensured lightproof conditions during film changing. Tilting due to differential ablation of the ice under the moraine was a serious problem. No suitable bedrock site adjacent to the glacier was found.

Drilling and explosives. Shot holes, usually 3 m deep, were hand drilled with a SIPRE 3-inch (7.6-cm) diameter auger. All operations were executed at elevations lower than the firn limit so that the holes were drilled directly into solid ice, covered only by a layer of residual snow at the start of the season.

High-velocity, high-density, gelatinized nitroglycerin was used as an explosive charge. A high-velocity explosion has a shattering effect on a brittle substance like ice. Number 8 no-lag electric blasting caps fired by a condenser discharge blasting machine were used as detonators. The shot holes were usually stemmed by 2–3 m of water.

Since it is necessary to know the shear wave velocities of a medium to determine fully its elastic properties, various methods of producing these waves were tried. Normally, vertically polarized shear waves are produced by internal reflection at a free surface and horizontally polarized shear waves are produced by propagation of vertical fractures near the shot point (Knopoff and Gilbert, 1960; Kisslinger, Mateker, and McEvilly, 1961). The generation of shear waves at short distances by asymmetric-energy radiation was attempted; a blasting cap, with or without a small charge, was detonated next to a plank or sheet of metal buried in the ground. In another attempt, an embedded plank, in contact with a geophone to provide a time break, was struck with a sledge hammer. For greater asymmetric-energy production, experiments were made using the principle of the Munroe effect (Lawrence, 1947; Poulter, 1950). This effect is illustrated in Figure 1. None of the above methods was entirely satisfactory.

Field operations. The seismic spreads were usually lined up by sighting and by compass; on spreads which were parallel to a cross-glacier profile the man laying out the cable would walk toward the stake that marked the next surveyed point on that profile. The perpendicular spreads were oriented with a Brunton compass. Where greater precision was sought, as in short refraction profiles, a theodolite was used for locating points.

The 1964 season lasted from late June until mid-August. The early part of this period was spent in trials of the effectiveness of various combinations of shot-hole depths, charge size and shape, and seismograph settings, in obtaining seismic reflections. This work was performed at points on the central arm of the glacier near the medial moraine (Fig. 2). During the latter half of the season reflection shooting was carried out on the upper line of the central arm of the glacier. The rest of the reflection profiles, the wide-angle reflection profile, and the short refraction investigations were carried out in 1965 from mid-May until late August.

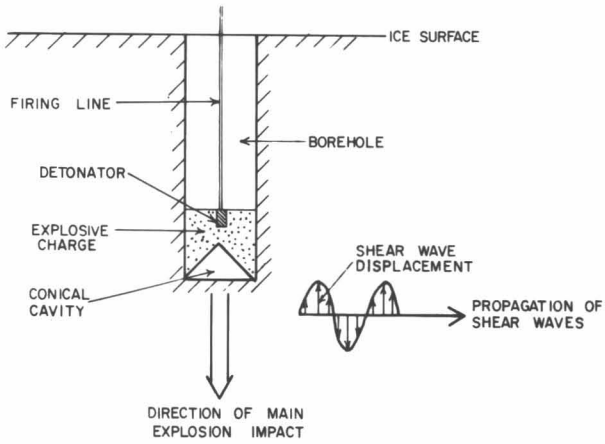

Fig. 1. Principle of the Munroe effect (shaped charge). The conical cavity in the base of the charge causes most of the explosion energy to be directed downward. The asymmetry of energy flux results in enriched production of shear waves.

Most of the shots of the exploration program were made at points marked by bamboo poles, which also served as markers for the determination of the movement of the glacier surface (Anderton, 1967). These points were arranged along three profiles which cross the glacier at an angle perpendicular to the direction of ice flow. The "upper line" is about 1.5 km above the confluence and is divided by the nunatak into two segments, the upper central-arm line and the upper north-arm line. The "strain line," whose points are surrounded by quadrilaterals measured for the calculation of strain rate, is about 200 m below the confluence and extends across the combined glacier. The "lower line" is about 1.5 km downstream from the strain line and also extends across the whole glacier. The strain and lower lines are each divided by the medial moraine.

The numbering of the points is shown in Figure 2. On the upper and lower lines right angle L spreads were used, with the cross spreads generally upglacier from the upper line and downglacier from the lower line. Double split-spreads at right angles to each other were used on the strain line where feasible.

Seismic Noise Sources and Related Topics

Introduction. An effort was made to obtain a record of the seismic background noise prevalent in the glacier area. For this purpose the continuously recording seismograph station was operated intermittently between June 9 and August 6, 1965. The noise considered here is natural ground oscillation as distinguished from noise produced by the investigative process itself, such as surface waves and air waves from seismic shots (Olhovich, 1964).

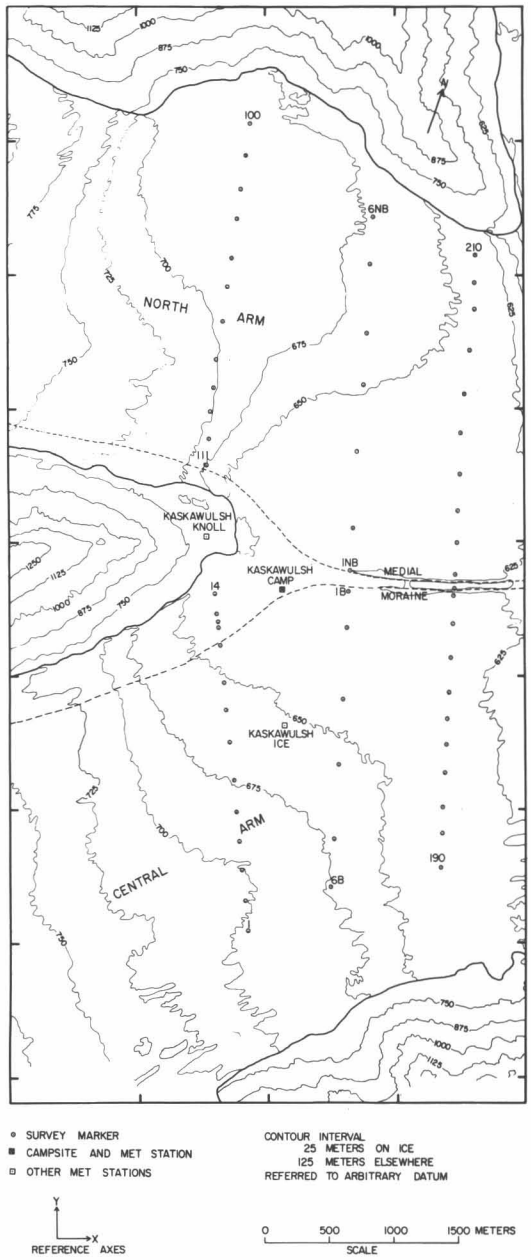

Fig. 2. Study area at confluence of north and central arms, Kaskawulsh Glacier. The base map used here was compiled by the Department of Geodetic Science of the Ohio State University from aerial photographs taken by the Royal Canadian Air Force in 1951. Ground observations in 1964 and 1965 indicated that the major features of the glacier surface had not changed significantly since the photos were taken.

The seismograph records exhibited four types of background noise:

(1) Continuous oscillations, varying in amplitude from barely perceptible to full-scale deflection of the traces; on the sensitive seismograph components, these deflections were 0.05 and 17 microns, respectively. Frequencies were 3–5 cps.
(2) Pulses of 1–3 cycles, lasting 0.8–1.0 sec (frequency 2–3 cps)
(3) Earthquake-like shock waves, separable into primary, secondary, and sometimes long-period phases. These were of variable duration and frequency, but always more prolonged than (2) and usually of lower frequency (1–2 cps).
(4) Extended disturbances (duration, 0.5–2 min), distinguished from (1) by greater amplitude and lower frequency (1–2 cps). These disturbances are not separable into definite phases. They frequently have a sudden commencement, but invariably fade away gradually.

Continuous noise. Experience showed that when the wind speed rose to more than 15 mph (6.7 m/sec) it was very difficult to obtain good shot records because of the high noise level. Diurnal temperature and wind-velocity variations have very similar patterns but the few calm days were reasonably quiet seismically regardless of temperature variations. Wind was a serious problem; at Kaskawulsh Camp in 1965 velocities greater than 6.7 m/sec were recorded during 140 of the 470 three-hour periods (29.8%) of the weather record (May 28–July 25); strong winds were recorded during an even greater percentage of the time in periods of good visibility.

On the days with the most complete records continuous noise was measured in the following manner: the peak-to-trough amplitudes of the ten oscillations of greatest amplitude during the 20-minute period from 10 minutes before the hour until 10 minutes after the hour were averaged arithmetically and the mean value was called the amplitude for that hour. The average amplitude for the quietest hour of record was arbitrarily used as the unit amplitude. A day of normal noisiness registered average values of about 5 units, and a very noisy day, on which it was difficult to obtain good exploration records, registered 10 or more. When the noise amplitude reached 7 or 8 the traces overlapped and the true amplitudes became hard to measure. At values over 15 units the noise became unreadable.

The value of 1 on the scale corresponded to approximately 0.1 mm of trace deflection. Magnification of the strong-motion horizontal-seismometer was about 500 and magnification of the seismometer-galvanometer systems was about 2000. Accordingly, deflection of 1 unit on the strong-motion horizontal record corresponded to ground motion of approximately 0.2-micron amplitude; on the more sensitive horizontal and vertical records, deflection of 1 corresponded to about 0.05 micron of ground motion. In the following discussion, units of deflection will refer to the more sensitive instruments unless otherwise stated.

The 3-hourly noise amplitude record for July 23, 1965 is shown in Figure 3. This day was chosen because the wind and temperature variations do not correlate as closely as they do on most days on which good records were obtained; hence, if either wind or temperature has a dominant effect on noise, it can be distinguished. The times of the amplitude readings were chosen to coincide with the times of the meteorological observations. Wind velocity and temperature values are also plotted in Figure 3; the close correspondence between noise amplitude and wind velocity is apparent.

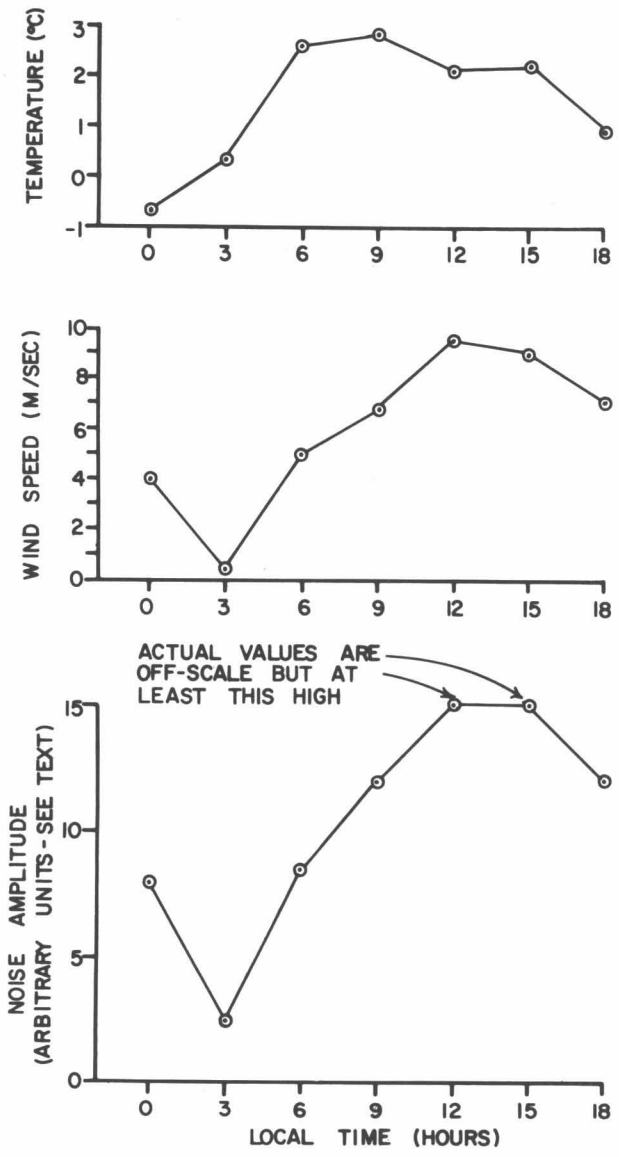

Fig. 3. Background noise, wind speed, and temperature at Kaskawulsh Camp at 3-hourly intervals, July 23, 1965.

The correlation between seismic-noise amplitude and rate of change of temperature is much closer for impulsive energy than for continuous noise (Fig. 4). Impulsive seismic noise will be discussed in the next section.

Running water produces continuous noise in the low-frequency range (1–50 cps). Noise of this type is unavoidable in the ablation zone of a glacier during the melt season, since innumerable streams cross the glacier, ranging in size from trickles to torrents with discharges of several cubic meters per second. Most of the streams drain into nearly vertical shafts—moulins or "glacier mills"—which enable them to reach great depth rapidly. Some of the kinetic energy acquired in this manner is converted into acoustic noise when the water strikes the sides or the bottom of the shaft. Exploration of several moulins revealed a series of steps that produce waterfalls

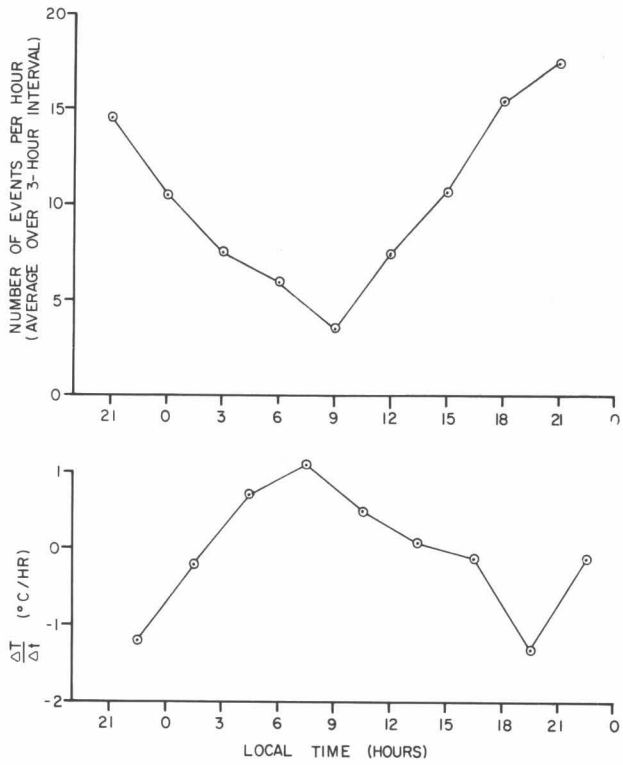

Fig. 4. Number of impulsive noise events and time rate of change of temperature at Kaskawulsh Camp at 3-hourly intervals.

in the streams (Dewart, 1966). The moulins received tributary tunnels and became larger in diameter with depth. A schematic section of a moulin is presented in Figure 5. The moulins contained corkscrew-shaped passages, plunge pools, and other evidence of highly turbulent flow and large changes of momentum in the water mass. Ground vibrations from moulins that were receiving large quantities of water were perceptible to the observer for distances as great as 50 m from the orifice.

If we assume that acoustic energy radiation is proportional to the kinetic energy, $1/2\ mv^2$, acquired by the water at the depth where it ends its fall, $X = v^2/2g$, and that the energy received from a source per unit area decreases as the square of the distance from the source, the relationship obtained is such that:

$$\frac{\text{energy return}}{\text{energy produced}} \propto \frac{1}{X}$$

Although more energy is released by a high waterfall, less is recorded at the surface than from a lower one of the same volume. The moulins which were investigated all had plunge pools near the surface. If this is generally true, then most of the moulin noise comes from near the surface. If the shafts unite at depth into a few large waterfalls, however, these may produce large local noise sources deep within the glacier.

Impulsive noise. Individual pulses were counted on seven days of relatively quiet continuous noise in order

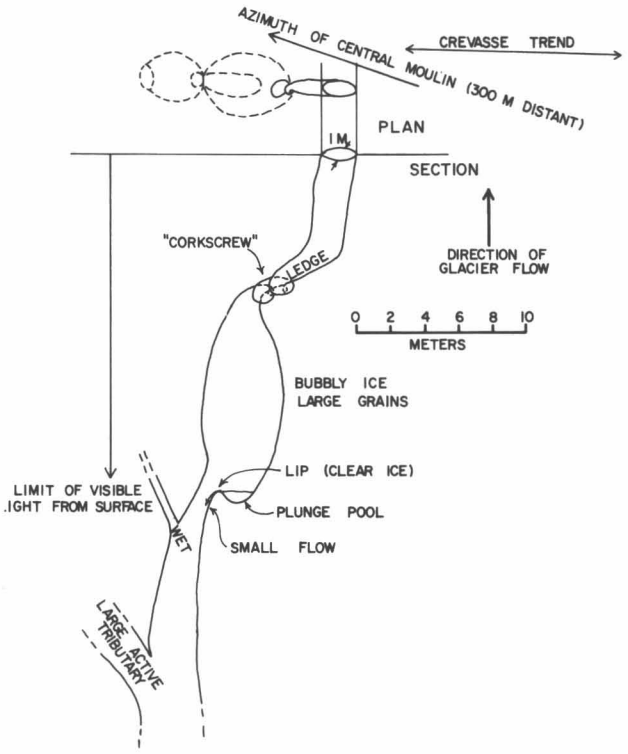

Fig. 5. Section of a moulin. The section lies parallel to the planes of the nearby crevasses. The "central moulin" was a large one receiving runoff from several square kilometers of glacier surface.

to avoid masking. The minimum amplitude of a countable impulse was 5 on the noise amplitude scale described in the last section. This amplitude was enough for an impulse to be distinguished from the background noise during the noisiest periods of the days of observation.

By this qualified definition of a countable impulse, a mean of 16.1 shocks per hour was registered. The scatter was large, ranging from a minimum of 1 to a maximum of 62 per hour. The percentage distribution with respect to amplitude range is shown in Figure 6. The frequency of events falls off rapidly with increasing amplitude; the curve approximates an inverse square relationship. Since the energy is proportional to the square of the amplitude, however, the few high energy shocks contribute a share of the total recorded energy comparable to that of the many low energy shocks (Fig. 7, 8). This suggests that the sources were not evenly distributed nor of equal energy, for if they were, the larger shocks would have a smaller proportion of the total energy, if low attenuation is assumed.

The durations of 100 shocks recorded successively on two days were measured. The distribution of pulse lengths is plotted in Figure 9; the mean length is 0.85 sec. If this value is representative of the whole period of seven days, then impulsive shocks occupied an average of only 13.7 seconds per hour.

In Figure 4 the rate of impulse occurrence is plotted against time on a 24-hour basis. The values are 3-day averages of the mean number of impulses per hour for 3-hour periods centered about the times of meteorological observations. The three days chosen were good record days for which complete meteorological observations were available. Figure 10 shows the 3-hourly temperatures averaged for the same three days. Data are given for the three weather shelters in the confluence area: Kaskawulsh Camp, about one hundred meters from the seismograph station, and Kaskawulsh Ice and Knoll (Fig. 2). From the data for Kaskawulsh Camp, the mean rates of change of temperature during the periods between observations were calculated and are plotted in Figure 4.

The maximum impulse rate occurred in the early evening, close to the time of greatest rate of temperature decrease, and lagged six hours behind the temperature and wind velocity peaks. This suggests a close relation to thermal contraction, as mentioned in the preceding section. The impulse rate, however, was moderately high when the temperature change was slight, so other factors were obviously involved. The minimum impulse rate occurred near the time of temperature minimum.

The data also show that the impulsive noise reached its maximum several hours after the continuous noise started to recede from its maximum. In fact, this was one of the best times for seismic exploration in midsummer; the wind had abated and light was still adequate.

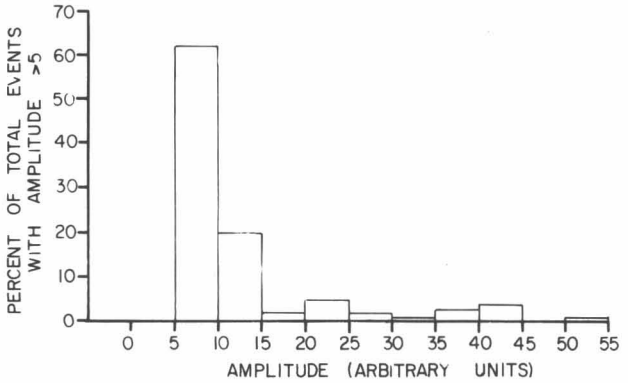

Fig. 6. Amplitude distribution of impulsive events for impulses with amplitudes greater than 5 units.

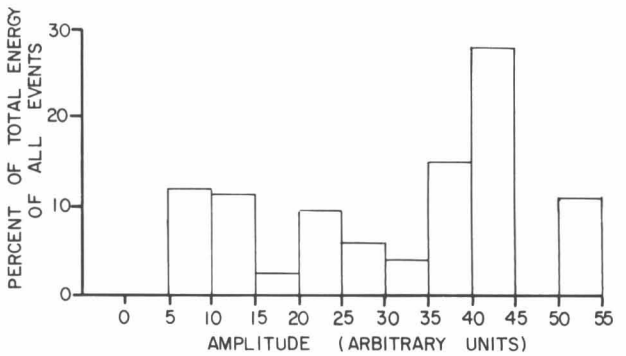

Fig. 7. The proportion of total impulsive energy as a function of amplitude level. This graph is based on the data of Figure 6.

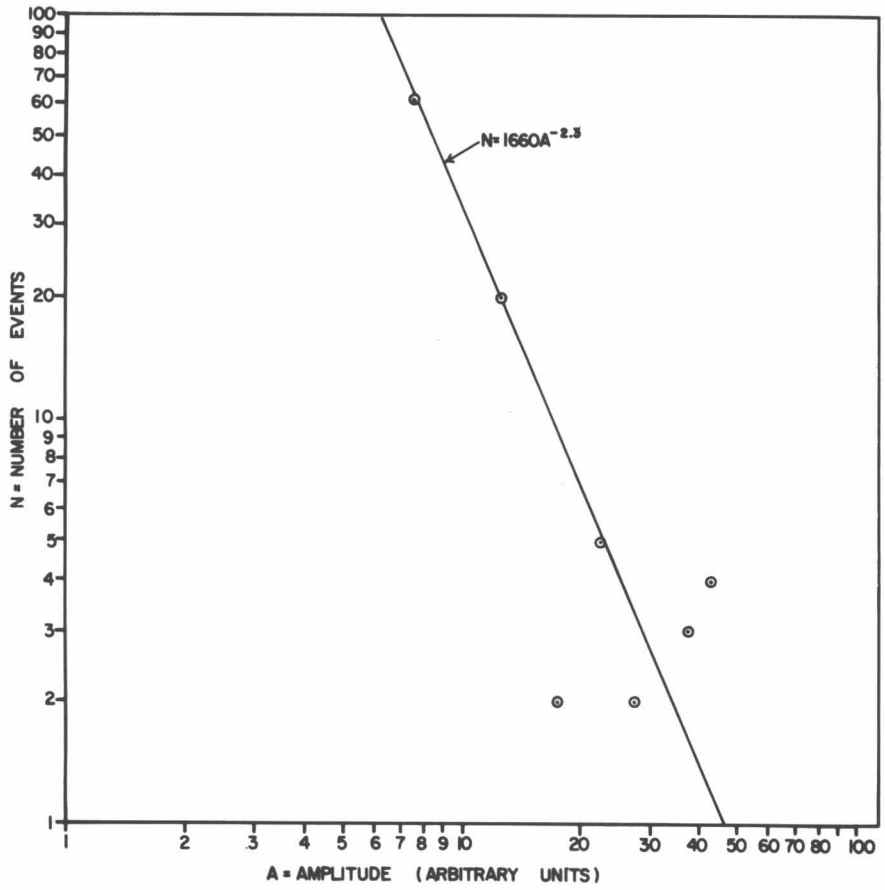

Fig. 8. Power law relationship between number and amplitude of impulsive events. The exponent -2.3 gives the best fit.

Mechanical sources. Investigations have shown that eigenimpulses are produced during the creep process in ice and are to be expected from a mass of ice under stress (Dewart, 1968). Following rupture the propagation of cracks produces elastic waves in the compressional and shear modes whose radiation patterns are determined by the velocity of crack propagation (Knopoff and Gilbert, 1960).

There is field evidence (Anderton, 1967) that the Kaskawulsh Glacier seismograph station was located in a region of tensile stress in which cracks were actively propagating. The station was surrounded by a zone of transverse crevasses of small size—less than 0.5 m wide—and several tens of meters long. Several of these crevasses were observed to enlarge during the summer of 1965. One small crevasse appeared under the moraine near the camp after several days of loud crackling sounds. Presumably the sounds are related to the deformation but it is not known whether the audible signals represent the same type of disturbance as the recorded eigenimpulses. Nor is it known whether the initial opening of crevasses and their widening and lengthening take place at such a rate as to produce elastic waves in the same frequency range as those recorded. There are not sufficient data to determine whether regions with high rates of crevasse formation have higher eigenimpulse rates than more stable regions. The mechanisms of crevasse formation and enlarging, however, are put forward as plausible contributors to eigenimpulse production.

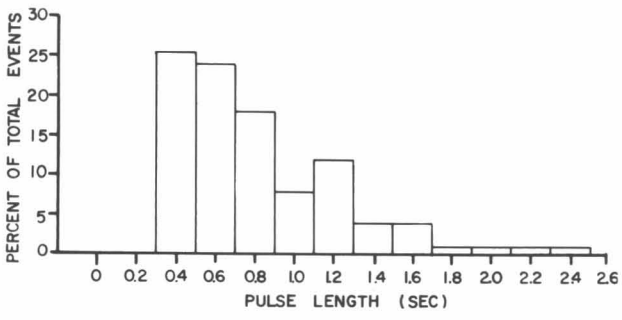

Fig. 9. Percentage distribution of impulsive events according to pulse length, at intervals of 0.2 sec.

The deformation process leading up to the formation of crevasses may also play a part in causing eigenimpulses. The following factors suggest that they are related:

(1) Crevasses exist, and appear to form, in the vicinity of the seismograph station.
(2) Crevasses represent ruptures that have occurred within the ice body.
(3) Prior to the rupture that produced the crevasse the ice in the immediate vicinity of the future crevasse must have experienced rapidly accelerating strain; that is, it must have gone through the process of tertiary creep.

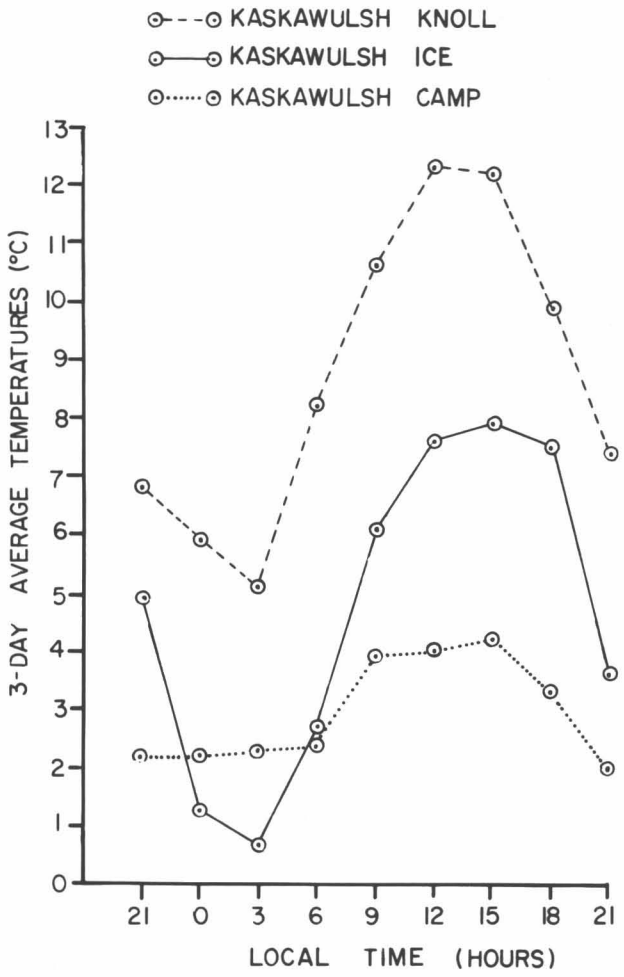

Fig. 10. Temperatures at 3-hourly intervals averaged for August 5, 6, and 12, 1965 at Kaskawulsh weather stations.

(4) Gold (1960) found that tertiary creep in ice is accompanied by microfracturing and the production of eigenimpulses. Gold's experiments involved compressive stress, whereas the crevasses in question are apparently caused by tensile stress. Gold's microfractures, however, were also genetically tensile; they developed perpendicularly to the directions of principal tensile stress.

Studies of eigenimpulses were originally made by Obert and Duvall (1945, 1957, 1961) in mines threatened by slumping and rockbursts. They found that regions of high stress could be delineated by measurements of the rate and amplitude of small shocks, which they called "microseismims." The rate of shock occurrence was found to be proportional to the rate of change of pressure in the rock. This was true whether the change was positive or negative, though the proportionality function was greater for increases in pressure. Although shocks were strongly generated both immediately before and concurrently with the occurrence of visible cracking, shocks were also produced by ground movement without visible cracking. The rate was found to vary widely with the physical properties of the rock, being highest for coarse-grained rock and lowest for fine-grained metamorphic rock containing lubricating constituents, for example, mica and talc.

A situation comparable to that found in deep mines may exist in glaciers. Though crevasses in glaciers are limited to the upper layers where tensile stresses can exist (Nye, 1951), moulins go considerably deeper. The greatest moulin depth measured on the Kaskawulsh Glacier was 65 m, and this may have been only the first plunge step. In hard rock mines where the rocks have ultimate compressive strengths of the order of 100 kg/cm^2 rockbursts occur at depths where one-fifth or more of that stress is attained. Relatively pure ice has an unconfined compressive strength of 35–60 kg/cm^2 and the value for glacier ice, with its imperfections and inclusions, is probably lower. At 65-m depth the hydrostatic pressure is about 6 kg/cm^2. It is conceivable that stress concentrations in the ice tunnels may exceed the breaking strengths of the ice locally and produce "icebursts."

Earthquakes. Several earthquakes were recorded by the station seismograph. Their proportion of the total recording time was very small, however. The largest was determined by the time lapse between P and S waves to have occurred at an epicentral distance of about 350 km. The azimuth was not determined but the distance is approximately that to Prince William Sound, and the earthquake may have been one of the long train of aftershocks of the great earthquake of March 28, 1964 (Hansen, *et al.*, 1966; Wood, 1966).

The smallest $S-P$ time observed was 2.4 sec. If we assume velocities in rock of 5.57 km/sec for compressional waves and 3.34 km/sec for shear waves in the upper layer of the earth's crust (Jeffreys and Bullen, 1948), we obtain a focal distance of 5.3 km for an all-rock path. Assuming values of V_p = 3.70 km/sec and V_s = 1.90 km/sec for ice, the distance to the focus of the shock would be only 4.8 km for an all-ice path. A shock at this distance from the seismograph could have occurred within the part of the glacier under investigation.

Avalanches. As might be expected from the physiographic description, the steep gulleys in the walls of the Kaskawulsh Glacier are the scene of frequent rock slides. Collisions between boulders can be detected by ear across the glacier. The hanging glaciers above the gulleys dislodge masses of ice and snow continually. Sometimes crevasse blocks as large as houses fall hundreds of meters. The times of observed large avalanches were checked against the seismograph record and found to coincide with extended disturbances—background noise Type 4. Avalanche noise may begin impulsively but as secondary slides are started and the fragments gradually roll to a stop the vibration passes into a prolonged dull rumble of incoherent noise. An average of two large disturbances of this nature, with duration of more than one minute, were recorded per twelve hours of seismograph operation.

Summary. Seismic noise types from several different sources and with differing characteristics were identified on the Kaskawulsh Glacier. The most important from

the standpoint of disturbance on the exploration seismic-records was continuous noise with frequencies of 30–200 cps. This high-frequency noise on the exploration seismograph records was most troublesome during periods when relatively low-frequency (0.5–20 cps) continuous noise was at maximum amplitude on the station seismograph records. It was concluded that these simultaneous disturbances on the exploration and station records represented parts of the spectrum of the same general type of noise. The major part of this noise appeared to be caused by wind. Other sources of continuous noise that may have been significant were running water and the explosive release of air pressure from bubbles in the ice. Seiches and distant microseismic activity probably were unimportant.

Impulsive noise (eigenimpulse) was less of a disturbance in the exploration seismological work. It appeared to be associated with thermal contraction during periods of rapid cooling. Other sources of impulsive noise may be the creation and expansion of cracks due to stress conditions within the ice or at the ice–rock interface. Impulse noise may be related to crevasse and moulin formation, but no direct evidence exists for this.

Seismic waves from earthquakes and avalanches were recorded, but their frequency of occurrence was insignificant compared with that of eigenimpulses. Avalanche signals were longer in duration than any of the others and were found characteristically to build rapidly to maximum amplitude, then gradually to die away.

In general, it may be said that seismic noise on the glacier was predominantly caused by climatic factors–wind and temperature changes. Noise related to movement of the glacier appeared to be of secondary importance. The extent to which the glacier was a "noisy" place seismically was chiefly determined by the climatic nature of the region. Running water was not an important source of noise but in the course of the investigations it was discovered that the drainage of water from the surface of the glacier involved an extensive system of shafts and tunnels deep within the glacier.

Practically speaking, the quietest part of the day for seismic investigation during the summer was the period from 1500 to 2400 hours, local time.

Wide-Angle Reflection Survey

Introduction. The determination of the average velocity of seismic waves through the body of the glacier is essential for the calculation of the depth and configuration of the average elastic properties of glacier ice. Serious problems in this determination arise because of the inhomogeneity of the ice and the variability of the subglacial terrain. In the first place, there is no guarantee that the average velocity of waves traveling between the top and bottom of the glacier, in a region where such velocity can be easily measured, is the same as in other regions where this velocity must be assumed in order to obtain the ice thickness and the orientation of the glacier bed. Secondly, the more valid the velocity determination is to be, the greater must be the areal extent of subglacial topography that serves as a reflecting or refracting interface.

With these considerations in view, the location of a site for the measurement of average velocity was delayed until some idea of the subsurface had been obtained from a reflection survey, for which an assumed value of average velocity was used. The survey indicated that beneath the central arm, slightly downslope from the confluence, the glacier bed was relatively smooth and its slope constant.

The wide-angle reflection profile was laid out from stations 1D, next to Kaskawulsh Camp, to 1B (Fig. 2), a distance of 583.4 m, and in a straight line beyond for a total length of 944.9 m. The profile crossed the direction of flow of the surface ice and the foliation bands at varying angles. The slope from 1D to 1B is about 2%. Beyond 1B the surface is nearly horizontal, so there is a slight concavity in the profile, and the direct waves are slightly diffracted.

This is one of the few extensive regions of the glacier in which there are no crevasses. The nearest ones are on the medial moraine, 50–100 m away. Snow was entirely gone from the surface by the time work began on the profile. A pond which collected meltwater from the surrounding glacier surface had covered part of the profile during the early summer. There is apparently an intricate subsurface drainage system in this part of the glacier, such as was described in a preceding section.

The cable was laid out in overlapping spreads along the profile. Shot points were established at both ends of the line. The forward profile–1D to the downglacier end–was completely covered. Most of the profile was also shot in the reverse direction. The reverse profile was extended two geophone separations (30.48 m) beyond 1D so that the total reverse profile length was 975.4 m. Spreads 183 m long perpendicular to the profile were shot at 1D, 1B, and the end.

The shot holes were bored to 4.5 m to contain the charges–as much as 12.5 lb (5.7 kg)–necessary for the most distant spreads. The larger shots (3.4–5.7 kg) shattered the sides of the holes after three or four shots and, at each end of the profile, holes had to be redrilled.

Most of the geophones were oriented to register the vertical component of reflected compressional wave motion. In order to distinguish direct and reflected shear waves, at least one geophone in each spread was oriented for transverse horizontal-components and one for longitudinal horizontal-components, relative to the profile.

The time–distance plot of the definitely observed phases for the forward and reverse profiles is presented in Figure 11. The phases plotted are the direct compressional, direct shear, surface, and first reflected compressional phases, which are designated *P, S, L,* and *PP,* respectively. Vertically and horizontally polarized shear waves will be called *SV* and *SH,* respectively.

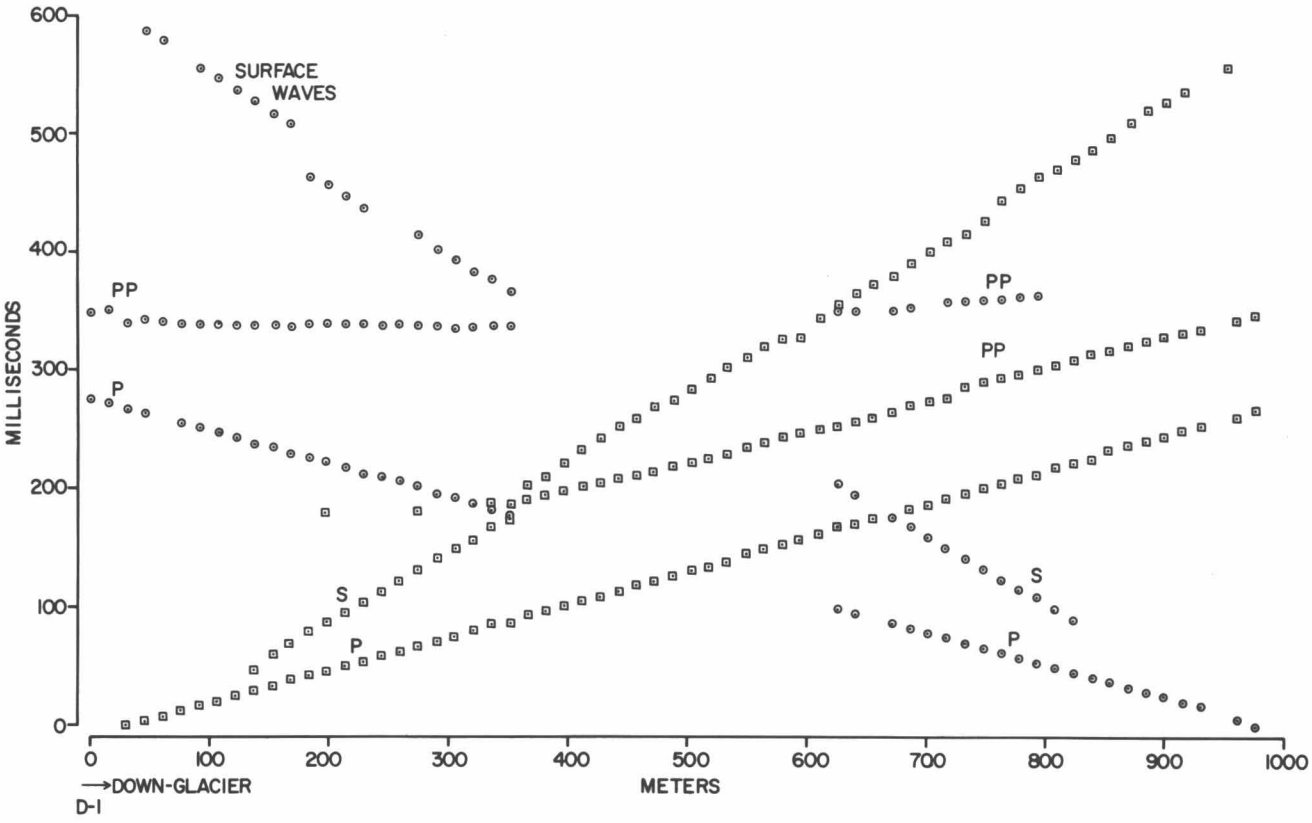

Fig. 11. Time–distance plots of the wide-angle reflection profile.

Direct P *waves.* The P phase was recorded strongly on both the forward and reverse profiles out to about 800 m. Beyond that range its amplitude became small and the first breaks became less distinct. The P phase consisted of a train of 3–4 cycles, strongly represented at low frequencies (20–50 cps). The train spread only slightly with increasing distance from the source. The first breaks as a rule showed up strongly for all three mutually perpendicular orientations of the geophones. By recording at various frequency ranges an approximate spectral analysis was obtained which showed an amplitude peak at 30–35 cps. Very distinct, almost perfectly sinusoidal, waves with amplitude equal to about half of the value at 30–35 cps occurred with frequencies between 70 and 100 cps.

The mean velocity of the P wave along the profile, computed as the least squares slope of the time–distance plot of the first arrivals, is

$$\overline{V}_p = 3.586 \pm 0.040 \text{ km/sec.}$$

The error is the standard deviation due to scatter about the regression line. The error due to time (read to 0.1 msec) and distance (read to 0.1 m) measurement is about 0.002 km/sec.

Aside from the situation very near the surface, which will be described in the next section, the plot shows little evidence of increase in velocity with depth. The plot is divided into segments which show the same general slope; least-squares velocities for these segments are given in Table 1.

TABLE 1. Mean Cross-Spread Velocities (V_p) of Direct Compressional Waves in Glacier Ice

Distance from shot point (m)	Mean V_p (km/sec)
15.2 - 182.9	3.60 ± 0.02
198.1 - 335.3	3.55 ± 0.03
350.5 - 533.4	3.58 ± 0.04
548.6 - 670.6	3.56 ± 0.03
585.8 - 807.7	3.60 ± 0.04
823.0 - 944.9	3.63 ± 0.04

Note: The seismic profile segments were distributed along a line 945 m long. Shots were fired at each end.

Direct S *waves.* Direct shear waves are often difficult to distinguish from surface waves. It is sometimes necessary to examine the orbital motion at detector sites where all three components of ground motion were recorded. The vertically polarized shear waves, SV, are often prominent. They commonly consist of 3 or 4 waves with frequency 30–50 cps and amplitude comparable to that of the direct P waves. They are invariably followed by motion approximating the elliptical retrograde motion of

TABLE 2. Seismic Wave Velocities and Isotropic Elastic Constants in the Ablation Zones of Temperate Glaciers of Europe and Asia

Glacier	Range	Investigator	ρ	V_p	V_s	σ	Y	μ
Kesselwand	Alps	Förtsch, Scheider, Vidal (1955)		3600				
Hintereis	Alps	Förtsch and Vidal (1956)		3600	1730	0.36		
Gurgler	Alps	Förtsch and Vidal (1958)		3510	1630	0.36		
Tuyuksu:	Tien Shan	Berzon, Bokanenko, Isaev (1959)						
Seismic								
(1)			0.90	3810	1905	0.334	8.93	3.34
(2)			0.90	3700	1830	0.338	8.22	3.08
Ultrasonic								
(1)			0.895	3530	1700	0.350	7.25	2.69
(2)			0.895	3840	1770	0.365	7.79	2.88
Elbrus:	Caucasus	Bokanenko and Isaev (1960)						
Seismic								
(3)			0.90	3650	1780	0.343	7.87	2.92
(4)			0.90	3540	1820	0.324	8.06	3.04
Ultrasonic								
(3)			0.87	3420	1760	0.320	7.34	2.74

Notes: (1) Lower profile, near terminus of glacier
(2) Upper profile, near firn line
(3) Near terminus
(4) Near terminus, higher than (3)
Frequencies of ultrasonic waves used:
Tuyuksu Glacier, 35 kHz.; Elbrus Glacier, 100-150 kHz
Ice temperature in each case was approximately 0°C

Symbols:
ρ = density (g/cm^3)
V_p = compressional wave velocity (m/sec)
V_s = shear wave velocity (m/sec)
σ = Poisson's ratio
Y = Young's modulus (10^{11} dynes/cm^2)
μ = rigidity (10^{11} dynes/cm^2)

Rayleigh waves. The commencement of the latter is usually indistinct. *SH* was not definitely identified. The *S*-wave arrivals are first separable from the noise following the first breaks at a distance of 106.7 m. They can be followed fairly clearly out to a separation between shot point and detector of 731.5 m. Within this range the least-squares mean velocity is

$$\overline{V}_s = 1.722 \pm 0.019 \text{ km/sec.}$$

Surface waves. Beyond 731.5 m the second direct phase that appears has a velocity of only 1.63 km/sec. It probably is a Rayleigh wave, since the shear wave is too weak to be detected at these distances. The velocity of the few coherent Rayleigh-wave crests at shorter distances is 1.625 ± 0.025 km/sec. On the reverse profile, weak arrivals with "cross-spread velocity" (determined from first breaks across the spread) of about 1.74 km/sec are registered between 807.7 m and 944.9 m.

Elastic constants. The isotropic elastic constants can be determined from the observed velocities by using Nicholls's (1961) formulas:

$$Y = \frac{\rho V_s^2 [3(V_p/V_s)^2 - 4}{(V_p/V_s)^2 - 1} = 7.284 \times 10^{10} \text{ dyne/cm}^2 \quad (1)$$

$$\mu = \rho V_s^2 = 2.698 \times 10^{10} \text{ dyne/cm}^2 \quad (2)$$

$$\lambda = \rho V_s^2 \left[\left(\frac{V_p}{V_s} \right)^2 - 2 \right] = 6.300 \times 10^{10} \text{ dyne/cm}^2 \quad (3)$$

$$K = \rho V_s^2 \left[\left(\frac{V_p}{V_s} \right)^2 - \frac{4}{3} \right] = 8.099 \times 10^{10} \text{ dyne/cm}^2 \quad (4)$$

where

ρ = density (0.91 g/cm^3)
Y = Young's modulus
μ = rigidity (shear modulus)
λ = Lamé's constant
K = bulk modulus (incompressibility)

Poisson's ratio, $\sigma = 0.350$, is somewhat lower than the values obtained by the early workers in the Alps, but higher than those given for "seismic" frequencies (Table 2) by Berzon, Bokanenko, and Isaev (1959), who suggest that the high European values might be due to mistaking the Rayleigh waves for shear waves. Our data, however, indicate that rather high values of σ are possible on temperate glaciers.

The reason for the differences in σ is not known, but they may be related to variations in elastic properties near the melting point of ice, at which temperature the rigidity decreases rapidly while the incompressibility remains large. From equations 2 and 4 it can be seen that V_s depends on the rigidity while V_p depends on both rigidity and incompressibility. It follows from previous studies (Knopoff, 1952) that near the melting point σ will increase, approaching the value 0.5 as a limit for $\mu = 0$. On the Kaskawulsh Glacier there was a good deal of interstitial water present near the surface, so one would expect the rigidity to be lower, and Poisson's ratio higher than for the case of drier, colder ice.

Reflected waves. Strong reflected compressional waves (*PP*) were obtained on both the direct and reversed profiles, but they did not appear strongly on the direct profile within a distance of 240 m from 1D, or on the reversed profile at all, within 183 m from the shot point. Second *P*-wave reflections or *P* waves converted to *S* waves (*PS*), or vice versa, at the ice–rock interface were not definitely recorded. The *PP* reflections usually had sharp first breaks followed by several coherent cycles of ground motion. They were recorded best in the 90–215 cps band-pass filter range. The strongest reflections had a frequency of 130–170 cps and their amplitude was only slightly less than that of the direct *P* waves. A sharp peak occurred in the amplitude of *PP* at distances 700–750 m from 1D. This phenomenon will be discussed later in connection with reflection coefficients at the ice–rock interface.

Amplitude of reflected waves. The fractions of incident elastic wave energy that are reflected or refracted from an interface between two different materials are called the reflection and refraction coefficients of the waves at the interface. Expressions for these coefficients at the boundary between two solids with greatly differing elastic wave velocities were developed by Nafe (1957). From Nafe's relations, Röthlisberger (1964) computed graphs of reflection and refraction coefficients at boundaries between ice and thirty different rock models with physical properties approximating those of common varieties of rocks and frozen ground. Röthlisberger considered shear and compressional plane waves incident at angles from 0° to 90° upon a plane interface. In seismic reflection studies the portion of the real, more or less spherical, wave surface that is considered is usually small enough so that it approximates a plane. All the materials were defined as isotropic and homogeneous. Ice was assumed to have compressional wave velocity 3.60 km/sec, shear wave velocity 1.80 km/sec, Poisson's ratio 0.333, and density 0.9 g/cm^3. These values are not very different from the values obtained from refraction data of this study. That is, $V_p = 3.63$ km/sec, $V_s = 1.72$ km/sec, $\sigma = 0.35$. Actually, the mean vertical compressional wave velocity, $\overline{V}_p = 3.70$ km/sec, would be more applicable in this discussion. For $\sigma = 0.35$, V_s would then be 1.78 km/sec. In either case, the difference from Röthlisberger's model is slight.

The properties of the rock underlying the glacier in the region of the wide-angle profile were not known. Densities and compressional wave velocities were determined, however, from samples collected from bedrock outcrops near the point of confluence, 200–300 m from the west end of the profile. Typical of the samples was a greenstone with $V_p = 5.77$ km/sec and $\rho = 2.95$ g/cm^3. Poisson's ratio is usually about 0.25 for igneous and metamorphic rocks (Jakosky, 1961). These properties are closely approximated by Röthlisberger's rock model Number 29, in which $V_p = 6.00$ km/sec, $\rho = 3.00$ g/cm^3, and $\sigma = 0.25$. The *PP* reflection from this model has a sharp peak in wave amplitude, reaching 90% of incident wave amplitude at angles of incidence between 30° and 40°.

According to the reflection survey, discussed below, the reflecting surface under the wide-angle profile has a downglacier dip of approximately 36° and depth of 485 m below the glacier surface at point 1B. A ray from shot point 1D with angle of incidence of 30°–40° on this reflecting surface, corresponding to the theoretical reflection amplitude peak, will have a *PP* reflection that emerges at the glacier surface between 700 and 750 m from 1D. This is in agreement with the observation given in the preceding section. The width of the observed peak, about 100 m at the glacier surface, corresponds to the angular width of the theoretical curve, about 3°–5° in angle of incidence. Furthermore, comparison of the observed amplitudes of *PP* waves and direct *P* waves that have traversed equal lengths of path from equivalent explosive sources reveals that the peak *PP* amplitude is 80–90% that of the unreflected *P* wave. This observation is also in fair agreement with Röthlisberger's theoretical value.

Theoretically, there should also be a peak in the amplitude of the *PS* reflection at a distance of about 800 m from 1D. This would not be as strong or sharp as the *PP* peak. Unfortunately, the travel time for the *PS* arrival at this distance—540 msec—is such that the *PS* phase falls among high amplitude surface waves and cannot be positively identified.

Röthlisberger's curves also show total reflection of incident *S* waves for angles of incidence corresponding to the distant half of the profile from 1D. *SS* reflections, however, were not observed. This lack may be attributed to deficient production of shear waves at the shot point and to the much higher attenuation that is commonly observed for shear waves, in comparison with compressional waves. The positioning of the shot in a shallow borehole in ice, a relatively homogeneous medium, is not conducive to large shear wave production (White and Sengbush, 1963).

Conclusions. From observed data, 3.70 km/sec appears to be the best obtainable value for the average velocity. The error in distance measurement over the whole profile was probably less than ± 10 cm, or 1 part in 10,000. The seismogram reading error is estimated at about 1% of travel time, which gives a velocity error of about ±0.04 km/sec. Twice this amount seems to be a more realistic

estimate of the probable error, however, in view of the variations in dip and surface slope that enter into the geometry upon which the calculations are based. The true mean vertical velocity seems unlikely to be less than 3.63 km/sec, the velocity apparently reached at a depth of 60–70 m. Ice thickness along the profile is 200–650 m, and velocity would be expected to increase as pressure increases at depths greater than 70 m. Near the bottom of the glacier, however, there may be a decrease in *P*-wave velocity due to pressure-melting.

There are no reliable data on reflected shear waves, so that Poisson's ratio at depth is unknown. It is probably lower than the value $\sigma = 0.350$ found for the near-surface zone, however, if that zone contains much ice at the melting point. As mentioned above, near the melting point rigidity and shear-wave velocity decrease greatly while compressibility and compressional wave velocity do not decrease as much proportionally, so Poisson's ratio becomes smaller.

Meier, *et. al.*, (1957), Holdsworth (1965), and others have demonstrated that fractures close at depth in a glacier. Fracture closing under pressure apparently increases compressional wave velocity in rocks (Simmons and Brace, 1965) but the effects on shear wave velocity and on Poisson's ratio have not been determined. Birch (1961) found that at very high pressures (4–10 kb) Poisson's ratio in rocks increased gradually with increasing pressure, but near atmospheric pressure the results were erratic.

The values of the isotropic elastic constants of ice, other than σ, obtained on the Kaskawulsh Glacier agree reasonably well with results for Eurasian glaciers obtained recently by Russian investigators (Table 2).

The glacier bed along the wide-angle reflection profile was found to have an apparent dip downglacier of approximately 30°.

Anisotropy of Seismic Wave Propagation

Introduction. A glacier consists predominantly of ice crystals but it also includes air bubbles, meltwater, dissolved salts, and particles of water-insoluble rocks and minerals. This section will be concerned chiefly with the effects of ice-crystal orientation and air-bubble distribution on the velocities of seismic waves. The other factors mentioned may be important locally, as in the case of meltwater at the surface, discussed above, and rock fragments near the base of the glacier (Robinson, 1964). Crystal orientation and the heterogeneous distribution of air bubbles, however, are of particular interest because of their pervasive character and their apparent connection with glacier mechanics (Shumskii, 1964; Anderton, 1967). For the purposes of the present discussion, the glacier will be considered to consist of an aggregate of ice crystals containing air bubbles. It is assumed that the crystals have hexagonal symmetry and that their axes, of six-fold symmetry (optic axes), may have almost any degree of preferred orientation.

Crystal orientation. If the elastic constants are known, the velocity of a wave whose normal has a given angular relationship to the symmetry axes of a crystal can be determined precisely from the Christoffel equations (Christoffel, 1877; Hearmon, 1956; Bechmann and Ayers, 1957). For media of transversely isotropic (that is, hexagonal) symmetry, Postma (1955) gives a graphic method for determining V_1 and V_2. V_3, the velocity of the wave whose particle motion is perpendicular to a plane through the axis of ∞-fold symmetry (meridonal plane), can be determined from a simple relationship between C_{44} and C_{66}, the two shear constants of a transversely isotropic medium

$$\rho V_3^2 = C_{66} \cos^2\theta + C_{44} \sin^2\theta \qquad (5)$$

According to the experimental results of Bass, Rossberg and Ziegler (1957), the elastic moduli of the single ice crystal are:

$$C_{11} = 13.3 \times 10^{10} \text{ dynes/cm}^2$$
$$C_{12} = 6.3 \times 10^{10} \text{ dynes/cm}^2$$
$$C_{13} = 4.6 \times 10^{10} \text{ dynes/cm}^2$$
$$C_{33} = 14.2 \times 10^{10} \text{ dynes/cm}^2$$
$$C_{44} = 3.06 \times 10^{10} \text{ dynes/cm}^2$$
$$(C_{66} = 3.50 \times 10^{10} \text{ dynes/cm}^2)$$

Using these values and $\rho = 0.91$ g/cm^2, the maximum variation in V_1 is found to be 4%, which occurs between $\theta = \pi/2$ and $\theta = 0$. The maximum variation in V_2 is 3%, which occurs between $\theta = 0$ or $\pi/2$ and $\theta = \pi/4$; and the maximum variation for V_3 is 5% between $\theta = 0$ and $\theta = \pi/2$.

Now consider the case of the *c*-axis fabric-pattern in Figure 12. The simplifying assumption is made that each of the four concentrations of *c*-axis poles is reduced to a single point located at the center of the concentration. Then, with respect to the axis c' perpendicular to the pattern and passing through its center, 30% of the crystals are inclined at 25° and 30% are inclined at 42.5°. The other 40% of crystals can be considered randomly oriented, that is, they act in the aggregate like an isotropic medium. If the crystals are assumed to be equidimensional, a wave whose normal, N, is parallel to the axis c', covers 30% of its path at the velocity dictated by the angle of 25° to the c axis, 30% at the 42.5° velocity and 40% at the isotropic velocity. The velocities at the given angular relationship can be calculated by Postma's method using the data of Bass, Rossberg and Ziegler (1957), and the mean velocity over the total path can be found.

The procedure outlined above was repeated for various angles between N and c', and the pattern of velocity variations for V_1, V_2, and V_3 was sampled. The maximum and minimum values occurred at the axis c' and at approximately 90° to the axis, respectively. Since the pattern is not axially symmetric, there are small variations with

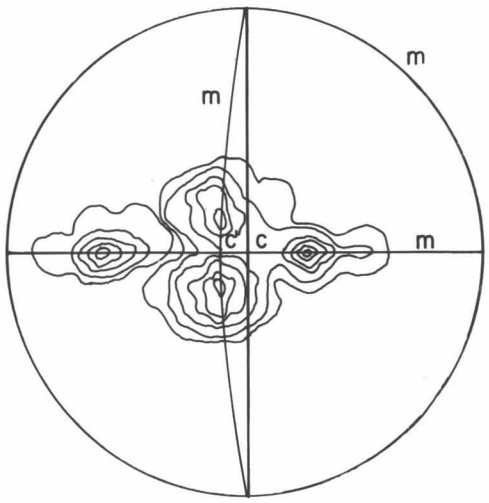

Fig. 12. Equal-area contour diagram of 4-maxima optic-axis fabric. The contours represent the percentage of points lying within one percent of the total area; contour values are 1, 3, 6, 9, 12, 15, and 18 percent. C' is the axis of symmetry of the fabric and c is the axis of symmetry of the foliation. The m's are symmetry planes of the optic-axis fabric. This fabric is typical of the region near point 1B (see Fig. 2).

longitude (Fig. 12). This result was similar to the case of the single crystal given above, with c' representing the c axis. The magnitude of the maximum variations of V_1, V_2, and V_3, however, were considerably less than for the case of the single crystal. For the simplified fabric, $\Delta V_1 = 2\%$; $\Delta V_2 = 2\%$; $\Delta V_3 = 3\%$.

The usual scatter in velocity measurements from readings of first breaks across the spread ("cross-spread velocity") was about ±1%. Hence it was clear that great care would have to be taken to detect velocity variations by field measurements.

Field experiment. A field test of seismic wave velocity versus ice-crystal c-axis orientation was made at point 1B. This point lies in a region of strong preferred orientation, relatively free of fractures. Geophone spreads were laid out at angles of $0, \pi/4$, and $\pi/2$ to the symmetry direction defined by the axis c' in Figure 12.

The geophones were closely spaced in order to detect any vertical refraction. Spacing between geophones was 2 m out to 24 m from the shot point, 4 m from 24 to 48 m away, 6 m from 48 to 72 m away, 8 m from 72 to 96 m away, and 15.24 m from 96 to 182.9 m away. The geometry is shown in Figure 13.

Detonators alone were sufficient for the shorter spreads. Detonators and small quantities of explosive (30–50 g) were used for the 96-m and 182.9-m spreads. The shots were fired at the surface in holes cut to the dimensions of the charges.

Geophones implanted with their axes parallel to the spreads recorded the compressional (longitudinal) wave displacement best, although vertical geophones also record this well. Since the plane of the spreads is also a meridional plane of the medium, vertical geophones, which are perpendicular to this plane, are best oriented to pick up the ground motion of the wave with velocity V_3. Geophones which are horizontal or perpendicular to the spreads respond principally to the V_2 movement and thereby differentiate it from the V_3 movement. Since V_2 (minimum) = V_3 (minimum) on the "axial" spread ($\theta = \pi/2$) while V_3 = maximum and V_2 = minimum on the "basal" spread ($\theta = 0$), the vertical geophones alone serve to record the maximum and minimum values of V_2 and V_3. On each spread, however, at least one geophone was oriented in each of the mutually perpendicular directions for a check.

The time–distance plots of the first breaks indicated an increase of velocity with depth, so numerical Herglotz-Wiechert integrations were made of the time–distance curves to obtain the velocity–depth relationship (Slichter, 1932).

$$h_d = \frac{1}{\pi} \int_0^{X_d} \cosh^{-1} \frac{V_d}{V_x} dx \approx \frac{\Delta X}{\pi} \sum_{x=0}^{X_d} \cosh^{-1} \frac{V_d}{V_x} \tag{6}$$

where h_d = depth at which velocity V_d is reached = depth of greatest penetration of the ray from the origin to X_d

X_d = distance at which ray of maximum velocity V_d is recorded at the surface

V_x = reciprocal of the slope of the t vs x curve at distance X, determined by obtaining the least-squares slope of a segment of length ΔX

V_d = reciprocal of the slope of the t vs x curve at distance X_d

This relationship assumes that the velocity increases continuously with depth and that the velocity gradient is perpendicular to the surface and does not vary horizontally.

The velocity–depth curves for V_1 when $\phi = 0$ and $\phi = 90°$ are shown in Figure 14. A low-velocity zone near the surface is apparent; this zone was also found in all direct P-wave velocities examined from other shot points. It is also clear that, down to a depth of 8 m, V_1 ($\phi = \pi/2$) > V_1 ($\phi = 0$). The direction of this inequality is the reverse of what would be expected on the basis of the known ice-crystal anisotropy. The observed anisotropy was also considerably greater in magnitude than values estimated from crystal orientation data.

The V_2 and V_3 data were insufficient for the construction of complete velocity–depth curves, but the velocity gradients were found to be similar in general form to those for V_1. At a distance of 30 m from shot point to detector the velocities are:

V_3 (maximum) = 1.71 km/sec ($\phi = 0$)
V_3 (minimum) = 1.67 km/sec ($\phi = \pi/2$)
V_2 (maximum) = 1.70 km/sec ($\phi = \pi/4$)
V_2 (minimum) = 1.67 km/sec ($\phi = 0$)

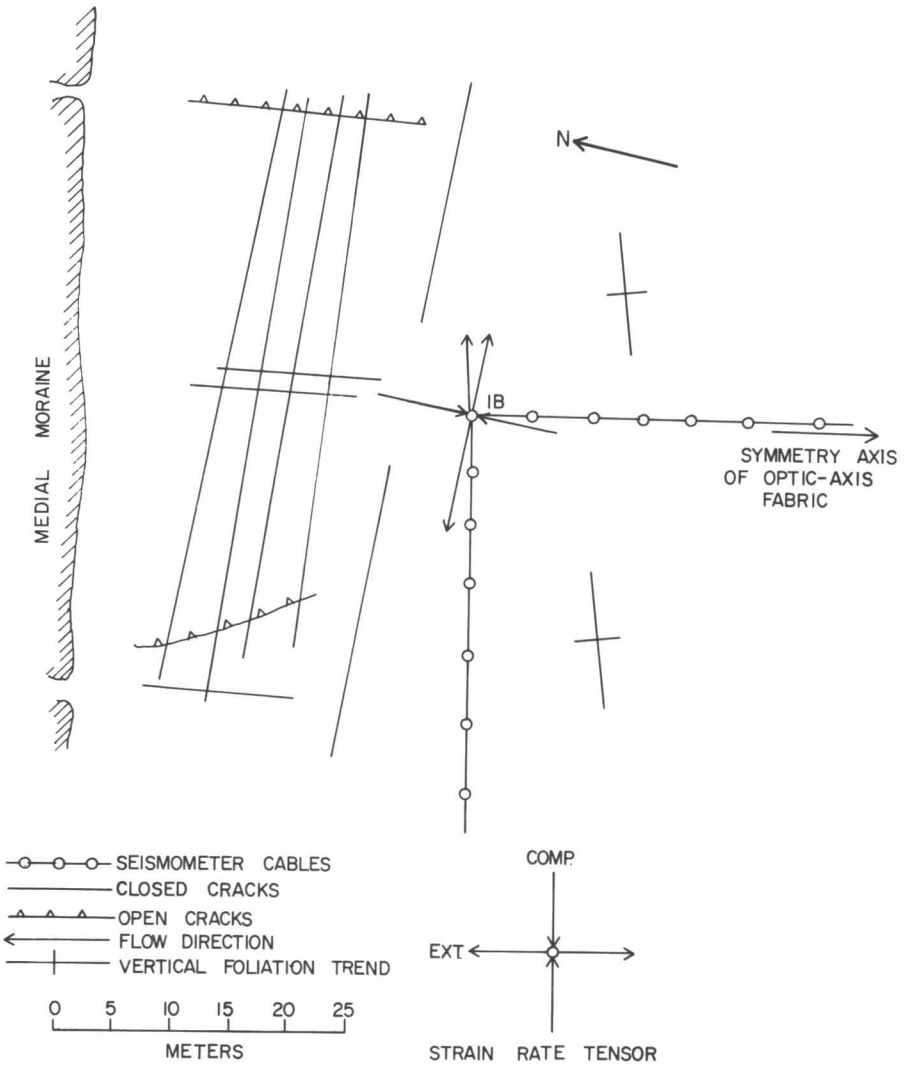

Fig. 13. Spread geometry at point 1B, showing crystallographic fabric, foliation, flow, and strain rate in the vicinity.

In these instances, the inequalities are in the directions predicted: $V_3\ (\phi = 0) > V_3\ (\phi = \pi/2)$; $V_2\ (\phi = \pi/4) > V_2\ (\phi = 0)$. The anisotropy factor—the ratio of $V_3\ (\phi = 0)$ to $V_3\ (\phi = \pi/2)$—is: $A_3 = 1.024$.

Foliation. A reason for the anomalous result obtained above has been sought in terms of the effects of foliation on elastic wave velocity. A medium consisting of periodically layered isotropic materials of different density and elastic moduli approximates a homogeneous, transversely isotropic medium for the propagation of elastic waves if the wavelengths are large compared with the thickness of the layers. A "large" wavelength is one for which the difference in ground displacement from one layer to the adjacent one is an insignificant fraction of the total displacement in the vicinity of those layers. A wavelength one hundred or more times the thickness of the thickest layer may be considered to fulfill this condition (Riznichenko, 1949; Thomson, 1950; Anderson, 1961). Such a homogeneous, transversely isotropic medium is called the "long-wave equivalent" of the periodically layered isotropic medium (Backus, 1962). The axis of ∞-fold symmetry in the long-wave equivalent medium is perpendicular to the faces of the layers in the periodically layered isotropic medium.

Various layered structures occur in the Kaskawulsh Glacier. The most prominent is foliation consisting of alternating layers of relatively bubbly and bubble-free ice (Anderton, 1967). This type of structure appeared to approximate the periodically layered medium discussed above because a bubbly layer would have different elastic constants and density from a bubble-free layer. Consequently, an investigation was made into the effects of this type of layering on elastic wave velocities.

Any planar metamorphic structure is generally referred to as foliation. In the context of this discussion, however, foliation consisting of clear and bubbly layers of ice will be the only type considered.

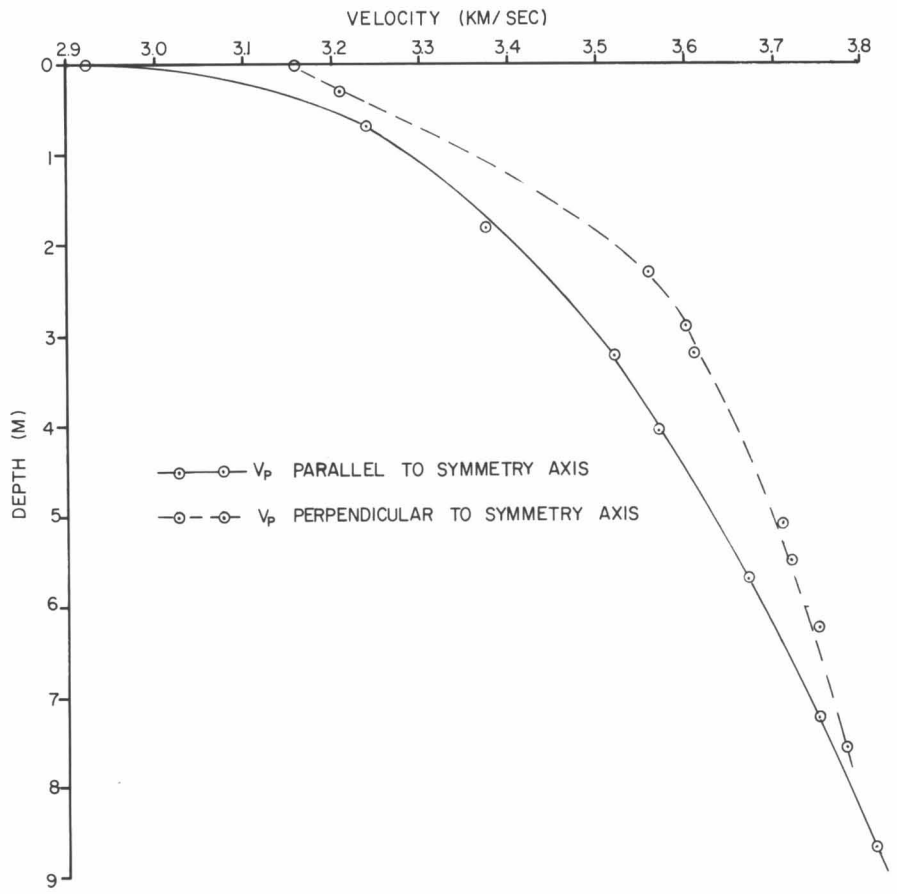

Fig. 14. Velocity–depth curves at point 1B for *P* waves.

On the Kaskawulsh Glacier strong preferred orientation of ice-crystal *c* axes generally coincides with pronounced foliation (Anderton, 1967). The only exception appears to be that in a zone under the medial moraine there is strong single-maximum preferred orientation, but very weak foliation. Even here, however, there are bubbles present (1–3 mm in diameter) which are somewhat flattened, with the short axis perpendicular to the foliation surfaces of adjacent foliated parts of the glacier.

Estimates were made of porosity by measurements on photographs of core cross sections (Fig. 15). Porosities ranged from 0.7% in the bubbly bands of weak foliation to 6.2% for the finely bubbled layers.

The layers ranged in thickness from 5 to 30 cm. The shortest wavelength with which this investigation was concerned was about 10 m, corresponding to a frequency of about 300 cps. Since the shortest wavelength is more than one hundred times the thickness of the layers, the layer-thickness condition for the long-wave equivalent medium is met.

In the vicinity of point 1B, the dip of the foliation was nearly vertical and the strike was about N 70° E. The foliation made a solid angle of about 20° to the "basal" plane of the crystallographic fabric (Fig. 13). The clear and bubbly layers were of approximately the same width, 5–20 cm, averaging about 10 cm. The porosity was about 2.8%.

The elastic behavior of a solid is altered by the presence of pores. If the pore concentration is small enough so that each pore can be considered as an isolated cavity in an infinite medium, and if the pores are assumed to be spherical, the relationships between the elastic constants are as follows (Walsh and Brace, 1966):

$$\frac{1}{K_p} - \frac{1}{K} = \frac{1}{K}\,\frac{1-\sigma}{1-2\sigma}\,\frac{2\pi a^3}{\overline{V}} \tag{7}$$

$$\frac{1}{Y_p} - \frac{1}{Y} = \frac{1}{Y}\,\frac{(1-\sigma)(9+5\sigma)}{(7-5\sigma)}\,\frac{2\pi a^3}{\overline{V}} \tag{8}$$

$$\sigma_p - \sigma = \sigma\,\frac{(1-\sigma)^2(5\sigma-1)}{(7-5\sigma)}\,\frac{2\pi a^3}{\overline{V}} \tag{9}$$

Here the subscript p refers to the constant for the porous medium; K = compressibility; Y = Young's modulus;

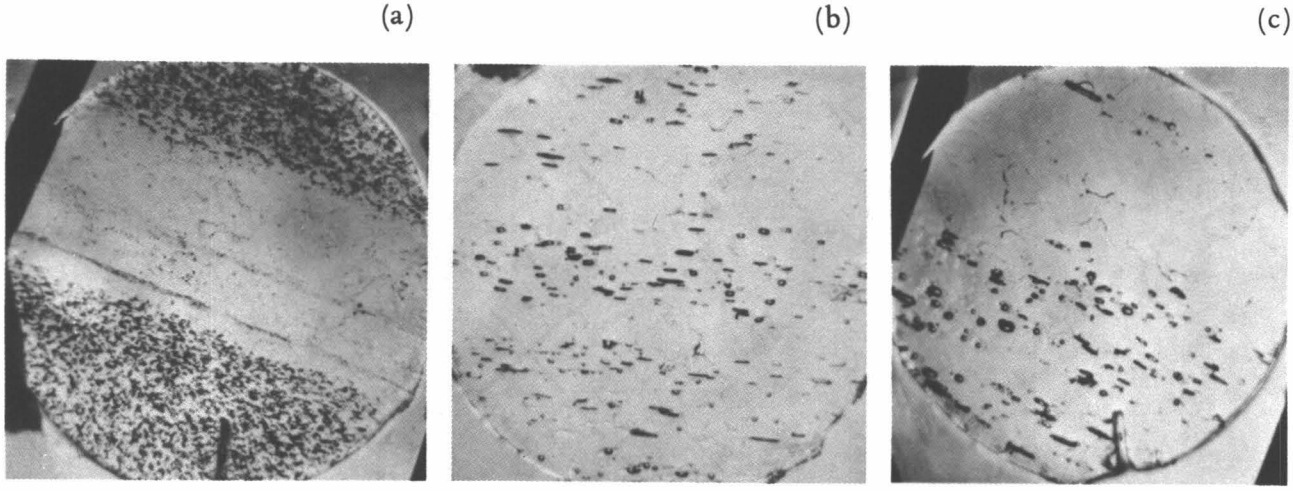

Fig. 15. Illustration of types of bubbly ice: (a) fine bubbles, cut by clean band, porosity 6 percent; (b) coarse bubbles, porosity 2 percent; (c) irregular boundary between clear band and ice with coarse bubbles.

σ = Poisson's ratio; a = average pore diameter; $\overline{V}$ = the volume of the body divided by the number of pores.

The isotropic elastic moduli for the porous medium can be found from the standard formulas:

$$\mu = \frac{Y}{2(1+\sigma)} \tag{10}$$

$$\lambda = K - \frac{2\mu}{3} \tag{11}$$

If it is assumed that a layered structure of alternating porous and nonporous isotropic sheets exists, a long-wave equivalent, transversely isotropic model can be constructed whose elastic moduli are determined by the elastic constants of the nonporous medium and the elastic constants of the porous medium. The latter are determined by equations 7 through 11.

For a layered structure comprising two media of thicknesses and moduli d_1, μ_1, λ_1, and d_2, μ_2, λ_2, the long-wave equivalent, transversely isotropic, elastic moduli are given by the following formulas (Postma, 1955):

$$C_{11}' = \frac{\{(d_1+d_2)^2(\lambda_1+2\mu_1)(\lambda_2+2\mu_2) + 4d_1d_2(\mu_1-\mu_2)[(\lambda_1+\mu_1)-(\lambda_2+\mu_2)]\}}{(d_1+d_2)[d_1(\lambda_2+2\mu_2)+d_2(\lambda_1+2\mu_1)]} \tag{12a}$$

$$C_{12}' = \frac{(d_1+d_2)^2\lambda_1\lambda_2 + 2(\lambda_1 d_1+\lambda_2 d_2)(\mu_2 d_1+\mu_1 d_2)}{(d_1+d_2)d_1(\lambda_2+2\mu_2)+d_2(\lambda_1+2\mu_1)} \tag{12b}$$

$$C_{13}' = \frac{(d_1+d_2)[\lambda_1 d_1(\lambda_2+2\mu_2)+\lambda_2 d_2(\lambda_1+2\mu_1)]}{(d_1+d_2)[d_1(\lambda_2+2\mu_2)+d_2(\lambda_1+2\mu_1)]} \tag{12c}$$

$$C_{33}' = \frac{(d_1+d_2)^2(\lambda_1+2\mu_1)(\lambda_2+2\mu_2)}{(d_1+d_2)[d_1(\lambda_2+2\mu_2)+d_2(\lambda_1+2\mu_1)]} \tag{12d}$$

$$C_{44}' = \frac{(d_1+d_2)\mu_1\mu_2}{d_1\mu_2+d_2\mu_1} \tag{12e}$$

$$C_{66}' = \frac{\mu_1 d_1+\mu_2 d_2}{d_1+d_2} \tag{12f}$$

TABLE 3. Transversely Isotropic Elastic Constants Computed by Using Equations 12a–12f

Porosity (%)	ρ (g/cm^3)	λ_2	μ_2	C_{11}'	C_{12}'	C_{13}'	C_{33}'	C_{44}'	C_{66}'
0.7	0.91	5.19	2.43	10.85	5.72	5.70	10.81	2.56	2.57
2.8	0.90	3.40	1.84	9.17	4.63	4.49	8.82	2.19	2.27
6.2	0.88	2.17	1.36	7.78	3.72	3.88	6.90	1.81	2.03

Notes

(1) Porosity 0.7% = weak foliation
Porosity 2.8% = strong foliation
Porosity 6.2% = foliation containing fine, densely distributed bubbles

(2) In all cases layer thickness d = 10 cm,
$\lambda = 6.30 \times 10^{10}$ dyne/cm^2,
$\mu = 2.698 \times 10^{10}$ dyne/cm^2.

Symbols

ρ = average density of bubbly and clear layers
μ_2 = Lamé's constant for bubbly layers
λ_2 = rigidity of bubbly layers
C_{ij} = elastic constant in units of dyne/cm$^2 \times 10^{10}$

The assumption is made that isotropic elastic constants λ and μ are applicable to the nonporous layers in the foliation (see Dewart, 1968, Chapter 4). The isotropic elastic constants for the bubbly layers are obtained from the constants of the nonporous layers by using equations 10 and 11 for measured values of porosity. These constants are called λ_2 and μ_2. The elastic constants for the clear and bubbly layers are combined according to equation 12 and the six transversely isotropic elastic moduli for the long-wave equivalent medium representing the foliation are computed. Table 3 gives these moduli for three different values of porosity of the bubbly layers.

Note that in Table 3 $C_{11}' > C_{33}'$, while $C_{66}' > C_{44}'$. These results are in agreement with inequalities obtained experimentally. They are the reverse of the inequalities cited previously for unfoliated ice in which the ice crystals have strong preferred orientation.

The values of the velocities V_1' and V_3' corresponding to the elastic moduli of Table 3 are given in Table 4. The velocity for each mode is given for ray paths perpendicular to or parallel to the plane of the foliation, and the corresponding anisotropy factor is given.

It can be seen that weak foliation has a negligible effect in producing velocity anisotropy. Strong foliation has an effect that is of the same order of magnitude, and in the same sense, as that observed at point 1B. The effect is strongest for foliation involving finely bubbled layers of ice.

Because $A_1 > 1$ for foliation, while $A_1 < 1$ for crystal preferred-orientation, a decrease in intensity of foliation with depth should be accompanied by a decrease in the anisotropy factor for V_1. In a region of strong crystallographic fabric in which the normal to the foliation layering is nearly parallel to the maximum c-axis concentration, as at site 1B, A_1 should change with depth, decreasing from a value equal to or greater than unity to a value less than unity. $A_3 > 1$ for both types of anisotropy, so while it will decrease in magnitude, it will remain greater than unity. These are the observed effects.

Fractures. Jones (1952) found significant anisotropy in the velocity of ultrasonic waves in concrete in which parallel cracks were preformed by casting, or created by the application of stress. Because fractures and crevasses are characteristic of much of the glacier surface, it appeared likely that they might cause significant anisotropy with certain orientations. The effects of density of spacing and orientation of fractures were investigated on the Kaskawulsh Glacier, in areas where the fracture patterns were distinct and relatively simple, by comparing the

TABLE 4. Computed Velocities, V_1' and V_3' Based on Elastic Moduli Given in Table 3

Porosity (%)	ϕ (radians)	V_1' (km/sec)	A_1	V_3' (km/sec)	A_3
0.7	0	3.453	1.002	1.679	1.002
	$\pi/2$	3.447		1.676	
2.8	0	3.228	1.019	1.606	1.043
	$\pi/2$	3.165		1.540	
6.2	0	3.015	1.062	1.540	1.060
	$\pi/2$	2.839		1.453	

Symbols:
V_1' = velocity in direction parallel to foliation planes
V_3' = velocity in direction perpendicular to foliation planes
A_1, A_3 = anisotropy factors
ϕ = angle between foliation planes and direction of propagation

highest direct *P*-wave cross-spread velocities in perpendicular directions. A map of surface fractures, taken from aerial photographs, is shown in Figure 16. The results of the velocity measurements are given in Table 5.

It can be seen that where fractures cut across a spread at a large angle, the velocity along that spread is less than the velocity along the perpendicular spread. If the region is intensely fractured, velocities along both spreads are less than they are in relatively unfractured regions. Intense fracturing can have an effect on seismic-wave velocity comparable in magnitude to the effect of strong foliation.

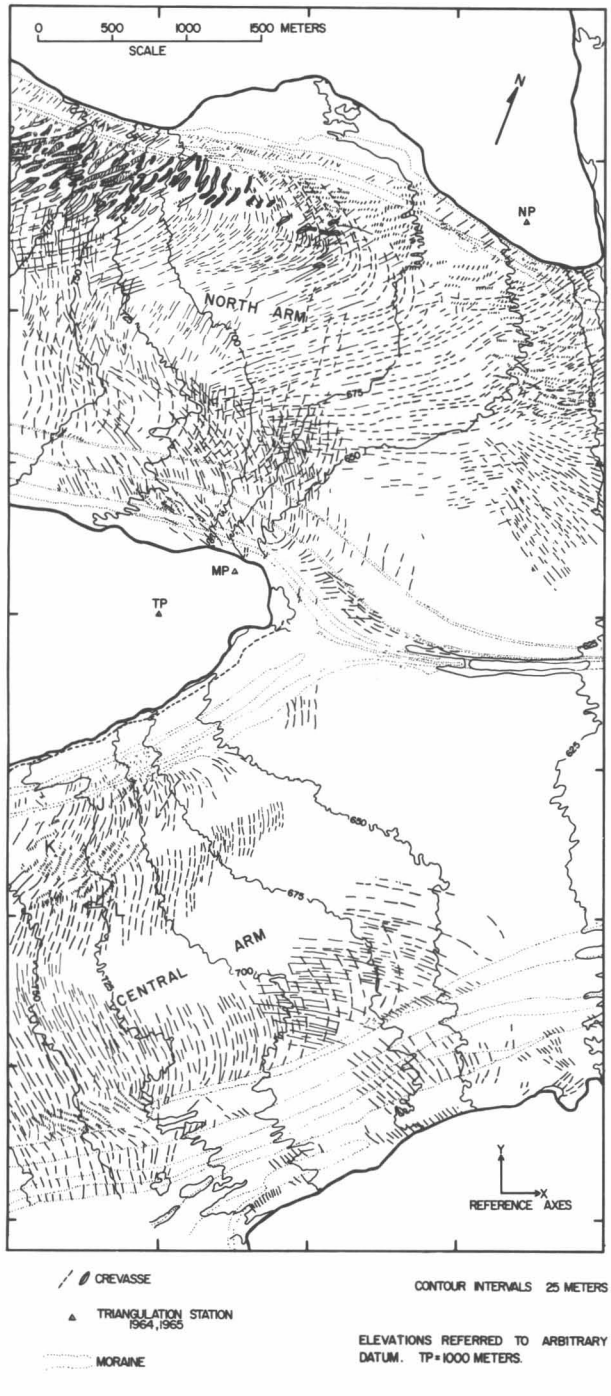

Fig. 16. Crevasse patterns at the confluence of the north and central arms of the Kaskawulsh Glacier.

Conclusions. To sum up, seismic-wave velocities in the ice of the Kaskawulsh Glacier were found to be affected by crystallographic fabric, foliation, and fractures. Ice near the surface of the glacier was heterogeneous with respect to porosity and elastic properties. Anisotropy due to foliation and anisotropy due to crystal orientation were superposed near the margins of the glacier and below the confluence in zones flanking the medial moraine. A low-velocity zone several meters thick was found at the upper surface of the glacier; *P*-wave velocity measured at the surface was as much as 25% less than it was 10 m below. Low velocity in this zone may be due to melting, fracturing, and high porosity of the ice. The zone appeared to contain a considerable amount of meltwater.

Even when the effects of foliation and fracturing are disregarded, the low symmetry of most of the ice petrofabrics observed near the surface of the Kaskawulsh Glacier results in complex relationships between seismic-wave velocity and the direction of wave propagation. The velocity anisotropy of the aggregates of ice crystals with the strongest preferred orientation in the glacier is much smaller than the anisotropy observed for a single crystal. Anisotropy due to the preferred orientation of ice crystals does not appear to be substantial enough to

TABLE 5. Velocity of Compressional Waves at Locations on the Surface of the Kaskawulsh Glacier Compared with Orientation and Estimated Intensity of Local Fractures

Station	Maximum *P*-wave velocity (km/sec)	A_f	Intensity		Ψ (degrees)
			Fracture	Foliation	
190	3.73	1.02	weak	strong	25
195	3.70	1.02	weak	weak	20
199	3.69	1.05	weak	weak	0
201	3.70	0.98	weak	strong	90
204	3.40	1.07	strong	weak	25
205	3.59	1.12	strong	weak	30
5B	3.74	1.02	weak	weak	5
6B	3.72	1.05	weak	strong	90
2NB	3.64	0.99	strong	strong	90
4NB	3.47	0.97	strong	strong	90
8	3.65	1.03	none	strong	0
10	3.68	1.00	weak	strong	45
107	3.43	1.05	strong	none	10
105	3.64	1.04	weak	none	25
103	3.71	0.98	weak	none	80

Symbols: A_f = anisotropy factor for P waves
Ψ = angle between trend of primary fracture and the normal to the reflection survey profile

affect significantly seismic reflection measurements in the glacier.

Because fracturing and foliation affect seismic velocities so strongly, the use of the seismic method to study ice-crystal fabrics appears to be severely limited. There are some regions in the Kaskawulsh Glacier, however, in which foliation and fracturing are virtually absent—for example, under the medial moraine; similar situations can undoubtedly be found in other glaciers. The use of more precise apparatus for measuring seismic-wave velocity than was available in this study might permit the investigation of small unfractured and unfoliated domains. Where the study of foliation itself is sought, the relatively strong anisotropic effect of some types of layering involving clear and bubbly ice suggests that the seismic method might be applicable.

Reflection Survey

Introduction. A seismic reflection survey was carried out to determine the ice thickness and shape of the glacier bed in the region of the confluence of the north and central arms of the Kaskawulsh Glacier. The distance to the bed of the glacier, converted to vertical depth, and the strike and dip of the bed were determined at 40 points, most of them on the three transglacier profiles of Figure 2.

In accordance with the results of the investigations reported in preceding sections, the ice has been assumed to be isotropic and homogeneous with respect to seismic-wave propagation. In interpreting the reflection data, it has been assumed that the glacier surface in the vicinity of each shot point, and the subglacial interface from which the seismic waves from that shot point are reflected, are planes; hence, the seismic rays are straight lines and their lengths are directly proportional to their travel times.

The reflection data have been corrected for the displacement and rotation of stations resulting from variations in strain rate along the profiles, because appreciable surface movement took place while the investigation was in progress. Corrections also have been applied for the slope of the glacier surface, and the change in ice thickness due to ablation of the surface during the field season.

The results of the reflection survey are presented in Table 6. Figure 17 is a contour map of the subglacial surface, constructed from the data of this table. Cross sections of the glacier along the survey profiles are plotted in Figure 18.

Interpretation of seismic reflection data. The results of the reflection survey are based entirely upon reflected *P* waves. The frequency of most of the good reflections was about 100 cps. The records are notable for the lack of *SS* or *PS* reflections or multiple *P* reflections. The large dips of the glacier floor probably prevented multiple reflections from being recorded on the relatively short spreads that were used.

As was noted previously, the normal method of reflection shooting in shallow holes and the high attenuation of shear waves militate against the production and propagation of shear waves; these factors may account for the lack of *SS* reflections. For the high angles of incidence involved in the reflection survey, the reflection coefficients for *PS* are small (Röthlisberger, 1964).

Sometimes more than one reflection appears on a record. When the differences in arrival times of separate

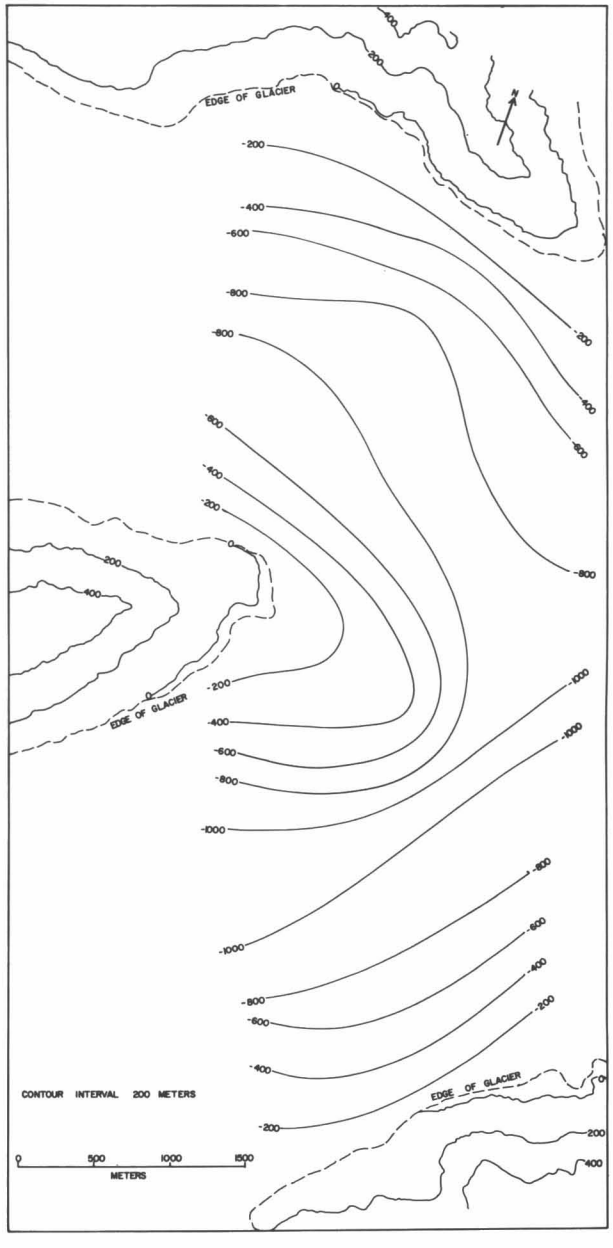

Fig. 17. Contour map of the subglacial topography at the confluence of the north and central arms of the Kaskawulsh Glacier. The contour interval is 200 m. The zero contour is taken as a contour on the valley wall that approximately coincides with the edge of the glacier. Its elevation is 675 m referred to the datum of Figure 2, and approximately 1800 m above sea level.

TABLE 6. Vertical Ice Thickness and Strike and Dip of the Ice–Rock Interface at Points on the Kaskawulsh Glacier

Profile	Glacier Arm	Shot Point No.	Shot Point Location		Surface Point Location(1)		Depth	Dip of interface	Azimuth of dip	Strike of interface
			x	y	x	y				
Upper Line	Central	5	10,766	7,986			(2) 790			
		6	10,744	8,230			(2) 1,010			
		8	10,805	8,831	10,689	9,039	532	24.0	151.0	61.0
		9	10,764	9,023	10,624	9,224	368	34.8	145.2	55.2
		10	10,686	9,276	10,556	9,409	250	36.6	135.9	45.9
		11	10,619	9,363	10,493	9,490	207	41.0	135.2	45.2
	North	109 a	10,740	10,900	10,675	10,898	457	12.5	49.0	139.0
		b			10,742	11,102	612	12.0	180.8	90.8
		108	10,783	11,081	10,686	10,826	415	33.2	20.9	110.9
		107	10,829	11,301	10,579	11,205	675	21.8	68.9	158.9
		106	10,881	11,591	10,654	11,289	714	28.0	36.2	126.2
		105	10,917	11,874	11,009	12,037	778	13.5	209.6	119.6
		104 a	10,946	12,078	11,007	12,394	618	27.5	190.9	100.9
		b			11,096	12,275	651	20.8	227.2	137.2
		c			10,655	12,076	728	21.7	89.6	179.6
		103	10,980	12,378	11,011	12,696	464	35.0	185.5	95.5
		102	10,968	12,608	11,031	12,733	343	22.0	203.2	113.2
Strain Network Line	Central	6B	11,584	7,476	11,714	7,307	457	25.2	322.2	52.2
		5B	11,618	7,842	11,562	7,654	737	14.9	16.9	106.9
		4B	11,645	8,413	11,738	8,348	964	6.7	304.9	34.9
		3B a	11,688	8,893	11,495	9,114	473	42.4	138.9	48.9
		b			11,500	9,212	408	16.9	149.6	59.6
		c			11,622	8,596	1,040	6.7	12.5	102.5
		2B	11,720	9,373	11,628	9,607	570	23.8	158.4	68.4
		1B	11,711	9,628	11,440	9,778	427	36.3	119.0	29.0
	North	2NB a	11,761	10,025	11,518	9,893	482	29.8	61.5	151.5
		b			11,506	9,819	449	36.2	51.0	141.0
		3NB	11,839	10,560	11,701	10,436	774	13.5	48.2	138.2
		34NB	11,886	11,044	11,699	10,924	843	14.6	57.4	147.4
		4NB a	11,910	11,418	12,157	11,593	643	25.1	234.7	144.7
		b			11,631	11,314	892	28.8	69.5	159.5
		5NB	12,051	12,107	12,094	12,309	368	28.8	191.9	101.9
Lower Line	Central	190	12,479	7,691			(2) 485			
		191	12,483	7,825	12,480	7,415	386	46.7	0.5	90.5
		193	12,525	8,647			(2) 832			
		194	12,528	8,478			(2) 925	(3) 9.3	(3) 93.0	3.0
		195	12,539	8,642	12,652	8,285	860	25.7	344.0	74.0
		196	12,549	8,879			(2) 1,006	(3) 8.5	(3) 3.0	93.0
		197	12,564	9,139			(2) 1,005	(3) 4.0	(3) 92.0	2.0
		198	12,574	9,385	12,548	9,482	925	6.2	165.0	75.0
		199 a	12,583	9,588	12,467	9,758	905	12.8	145.7	55.7
		b			12,633	9,752	915	10.6	196.7	6.7
	North	201	12,587	9,732	12,528	9,784	916	4.9	131.0	41.0
		202	12,613	9,953	12,756	10,226	871	17.5	211.4	121.4
		204	12,649	10,438	12,619	10,486	773	4.2	148.0	58.0
		205	12,678	10,750	12,737	10,997	744	18.9	193.7	103.7
		206	12,695	11,043	12,751	11,235	658	16.9	196.5	106.5
	Central	XI	11,607	9,285	11,375	9,350	480	25.6	106.3	16.3

Units

Locations:
meters measured geographically east (x) and north (y) of an arbitrary origin of a rectangular coordinate system

Depth:
meters measured vertically (with exceptions noted)

Dip of interface:
degrees

Azimuth of dip:
degrees measured clockwise from geographical north (0°–360°)

Strike of interface:
degrees measured clockwise from geographical north (0°–180°)

Notes

(1) The shot point does not, in general, coincide with the point at which depth is measured. The latter is designated "Surface point." One shot point may have more than one surface point, corresponding to different reflecting horizons. For some shot points only apparent dip and slant depth to the interface could be determined, and for these the surface point is indeterminate. All data have been corrected for the effects of ice movement and terrain, hence the location of a point is for the day on which the shot was made there.

(2) Slant depth.

(3) Apparent dip.

reflections on the same record are correlated, the reflections usually are from different parts of the glacier bed, suitably oriented for return of waves to the spreads. For example, the reflections indicated in Figure 19 are interpreted as due to reflecting horizons disposed as in Figure 20.

At stations 195, NB3, 104, and 106, however, low amplitude phases follow the first reflected phases after a few milliseconds (Fig. 21). They appear to be "sub-bottom" reflections. The two phases may represent reflection from the top and bottom of a layer of moraine or sediment at the bottom of the glacier. These cases all

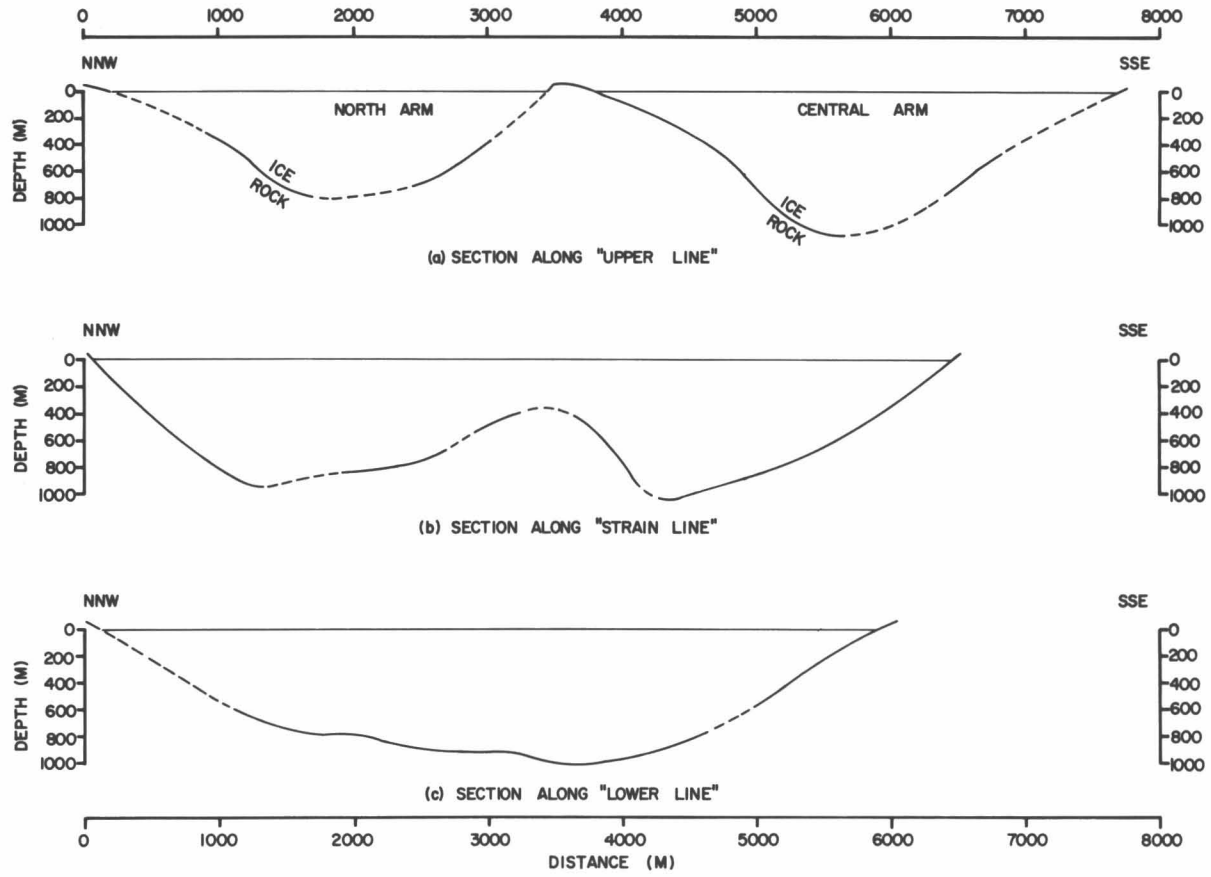

Fig. 18. Transverse sections across the Kaskawulsh Glacier along the lines of survey markers (see Fig. 2). The directions are approximate; the vertical and horizontal scales are equal.

occur near the centers of the valleys. The thickness of the layer can only be guessed at in the absence of velocity data. If the velocity is between 4 and 6 km/sec, the layer is 40–120 m thick.

Stations at which no reflections at all were recorded were rare, but at some stations there were no readable reflections in one of the perpendicular spread directions so only slant depth and apparent dip are known. Reasonable interpolations can be made, however, when more complete data are available at adjacent stations.

Poor recording of reflections may be due to roughness or convexity of the interface or the presence in the ice of debris that scatter the seismic waves. If there is water at the base of the glacier only weak reflections will be returned from the ice–water interface, but there may be strong reflections from the underlying water–rock interface. At each boundary that is encountered by the seismic waves, energy is lost by refraction or reflection downward, and the signal that ultimately returns to the glacier surface is correspondingly weakened.

Laboratory studies. The reflection coefficient of a plane elastic wave, that is, the fraction of incident energy that is reflected from a plane interface, depends upon the angle of incidence of the wave and the acoustic impedances of the media. In a preceding section there was a discussion of the results of Röthlisberger (1964) for the reflection and transmission coefficients at an ice–solid interface for solids of various densities, *P*- and *S*-wave velocities, and angles of incidence. For small angles of incidence, such as were involved in this survey, the reflected to incident signal amplitude ratio is, approximately,

$$R = \frac{A_r}{A_i} = \frac{(Z_2/Z_1) - 1}{(Z_2/Z_1) + 1} \qquad (13)$$

where A_r = amplitude of reflected *P* wave

A_i = amplitude of incident *P* wave

$Z_1 = P_1 V_{p_1}$ = acoustic impedance of upper medium

$Z_2 = P_2 V_{p_2}$ = acoustic impedance of lower medium

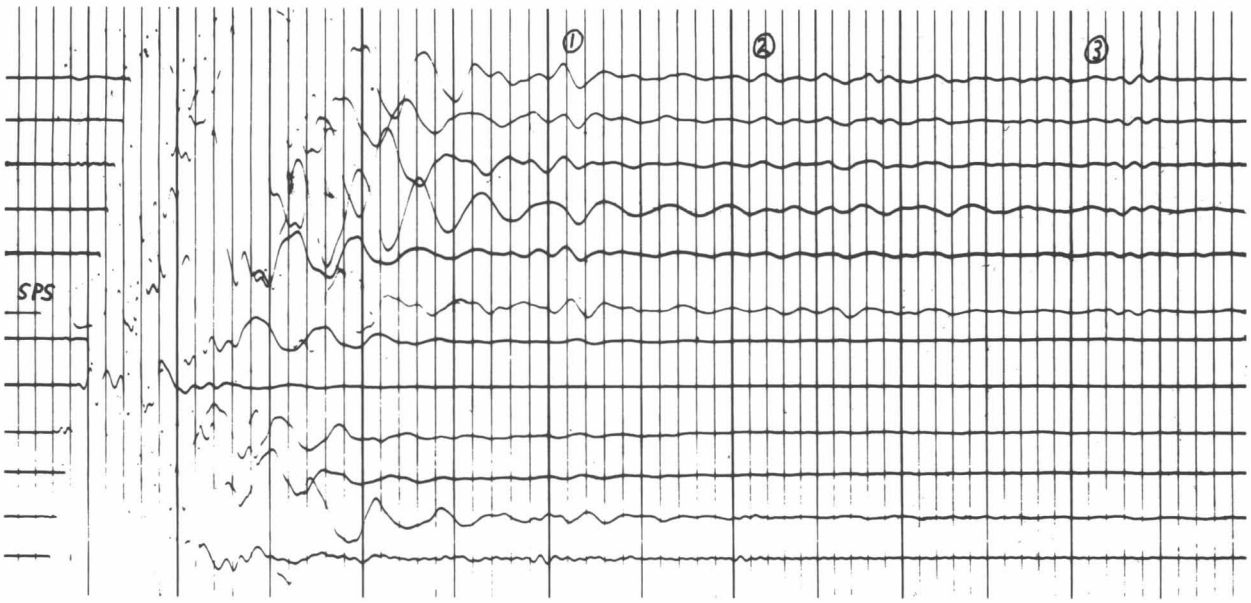

Fig. 19. Seismogram taken at point 3B. Reflections are designated 1, 2, and 3. This was a 0.5 lb (227 g) shot at 2.5-m depth, with filter passband 30–160 Hz. The heavy vertical lines represent 0.1 sec.

It proved impracticable to measure the seismic velocities of the valley wall rock *in situ,* so samples were brought back for laboratory study.

The densities of specimens of rock were determined to about 1 part in 300 with a Jolly balance. Compressional-wave velocities were calculated from the travel times of ultrasonic waves through cut specimens with measured dimensions.

The impedance and reflection data for the specimens are given in Table 7. The ratios of the amplitudes of reflected signal to incident signal calculated here are high compared with those encountered in most seismic-reflection work, where the reflecting horizon is an interface between different kinds of rock of low velocity-contrast. If the rock–ice boundary in the present case is a distinct interface, these data lead one to expect strong seismic reflections. The amplitude ratios for the different rock types, however, are so similar that there appears to be little chance of locating contacts between the different types of rock in the valley floor by comparing amplitudes of reflected waves.

The calculated amplitude ratios can be compared with field data. Strong *PP* reflections were obtained at shot points 10 and 11, which had ray paths of approximately 500 and 400 m. These shot points were near the point of confluence, where the bedrock is apparently composed chiefly of greenstone and graywacke which have reflected signal to incident signal amplitude ratios of approximately 2:3 (Table 7). The observed amplitude ratios were about 1:2. The disagreement is small but apparently significant. It is probably caused by a less than ideal ice–rock interface, but velocity dispersion and a greater attenuation constant at depth may also be factors.

Conclusions. Consideration of the results of the reflection survey leads to the following conclusions:

(1) The great thickness of the glacier—a maximum of approximately 1000 m—requires that the bed of the glacier at the confluence (about 750 m) be somewhat lower than the elevation of the terminus 40 km downglacier (800–850 m) where the ice is resting on outwash.
(2) In the immediate vicinity of the confluence, the mean longitudinal slope of the valley floor is approximately equal to the slope of the glacier surface. The trend of

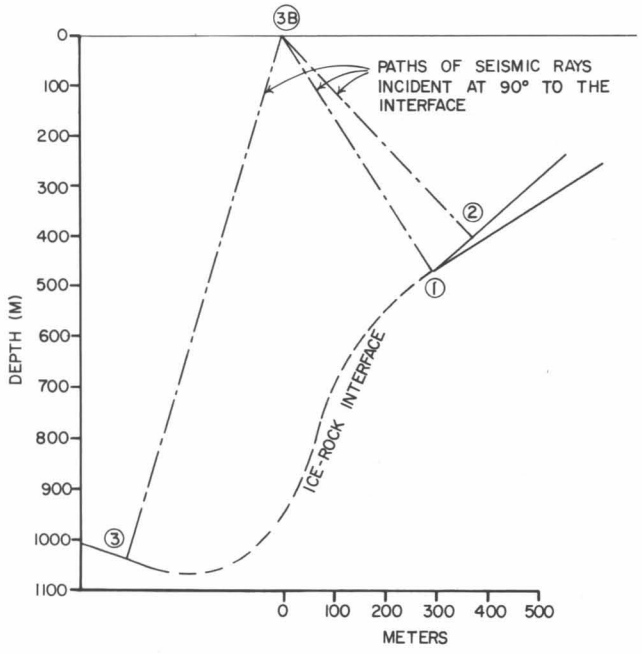

Fig. 20. Interpretation of seismogram at point 3B (Figure 19).

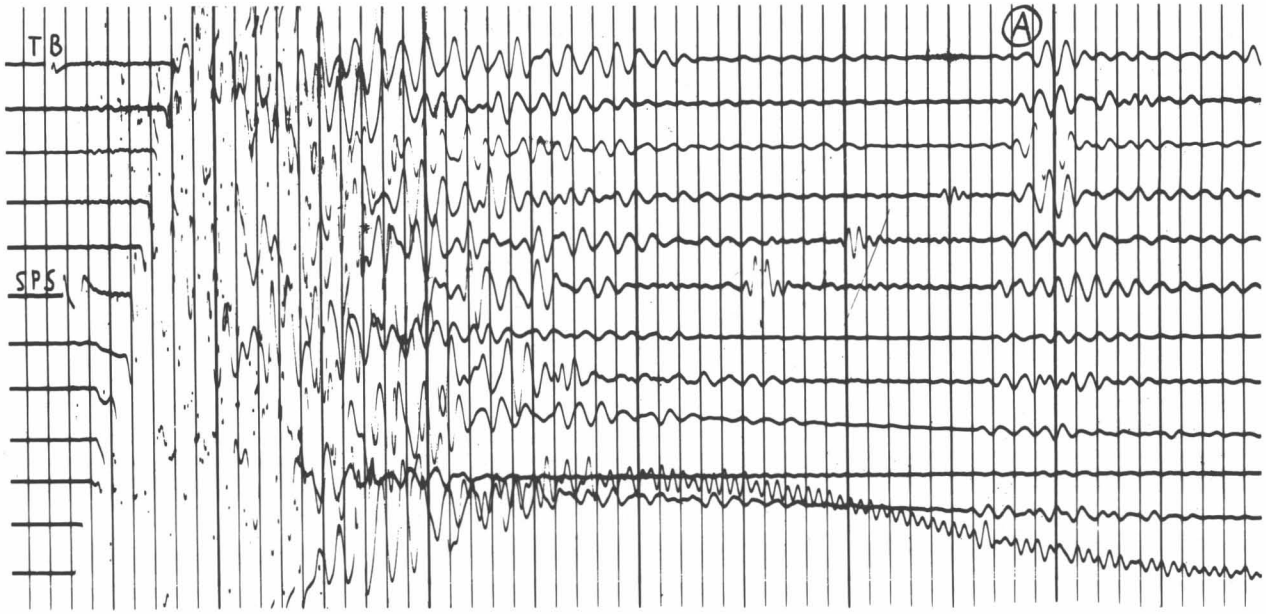

Fig. 21. Seismogram taken at point 106. A reflection occurs at A. This was a 1.25 lb (567 g) shot at 3-m depth, with filter pass-band 90–160 Hz.

TABLE 7. Acoustic Impedances and Reflected-Signal Amplitude Ratios for Ice and Rocks Found in the Kaskawulsh Glacier Confluence Area

Rock type	Collection site	ρ	V_p	Z	Z_r/Z_i	R_o
Ice		0.91	3.70	3.36		
Quartzite	North side of north arm	2.76	4.78	13.19	3.91	0.59
Granodiorite	South side of south arm	2.78	5.20	14.46	4.29	0.62
Limestone	Medial moraine	2.70	5.83	15.74	4.67	0.65
Greywacke	Dividing ridge at point of confluence	2.95	5.50	16.23	4.82	0.66
Greenstone	Dividing ridge at point of confluence	2.95	5.77	17.02	5.05	0.67

Symbols: ρ = density: g/cm^3
V_p = compressional wave velocity: km/sec
Z = acoustic impedance: g km/cm^3 sec
Z_r = acoustic impedance of rock
Z_i = acoustic impedance of ice
R_o = ratio of amplitude of P waves reflected back into the ice to P waves incident on the ice–rock interface, for 0° angle of incidence

Notes: (1) A plane compressional wave from the ice is considered to be incident upon a plane interface between the ice and rock.
(2) The wave normal is perpendicular to the interface.
(3) The rock names are descriptive, not necessarily definitive, and are taken from Wheeler (1963).

stepout times along the seismic spreads often indicates a slight concavity in the reflecting surface, rather than the planarity assumed. This concavity results in focusing of the reflected waves and should enhance the signals. The effect of concavity does not appear to be strong enough to cause spurious reflections from buried foci. The assumption that the bottom is locally nearly planar does not seem to lead to any large errors. There is a large increase in dip from Station 7 to Station 11, but in the vicinity of each station the change is not large. At Station 10 the dip, azimuth, and depth computed on the basis of the westward and northward spreads and again for the westward and southward spreads are nearly identical.

(3) The valleys of the two arms and the valley of the combined glacier have fairly symmetrical transverse sections. The valleys of the arms are roughly parabolic in section. The combined glacier is twice as wide as either of the arms but all have approximately the same depth; the floor of the combined glacier is merely wider and flatter than the floor of either of the arms.

(4) The rate of change of slope of the valley walls above and below the surface of the glacier is essentially constant. There is no evidence that glacial erosion has caused a break in slope.
(5) The floors of the two valleys merge only 2 km below the point of confluence. This is approximately where the ice flow of the two arms becomes merged into a uniform pattern of flow.
(6) The north arm, which has greater surface slope and surface velocity than the central arm (Anderton, 1967), also has a steeper valley floor and thinner ice.
(7) Features of significant relief on the valley floor, such as the irregularity illustrated in Figure 20, may not be reflected in any obvious way at the surface of the glacier. Presumably the feature illustrated presents no transverse obstruction to glacier flow. A transverse obstruction of similar magnitude would probably have greater surface expression (Nye, 1959).

Conclusions

Continuous seismograph recording on the Kaskawulsh Glacier established that it a source of seismic energy. Some of the energy is released in discrete events resembling minute earthquakes. These may be related to discontinuous movement of the ice mass.

Despite the large difference in acoustic impedance between ice and the surrounding rock demonstrated by laboratory studies of rock samples, the reflection of seismic energy from the bottom of the glacier was often poor. These nonreflecting areas may be characterized by the presence of morainal material in the lower layers of ice, melting in these layers, or unsuitable configuration of the ice–rock interface for the reflection of coherent energy.

No significant inhomogeneities were found within the glacier. Velocities of compressional and shear waves do not vary appreciably except near the surface. There a layer several meters thick possessed a positive velocity gradient apparently related to decreasing amount of porosity, melting, and open fracturing with depth.

The porosity of foliated ice was measured and porosity in bubbly layers was found to reach a maximum of 6%. The effect of foliation on seismic wave velocity anisotropy was calculated. Both foliation and preferred orientation of ice-crystal symmetry axes were found to produce small but measurable anisotropy in seismic wave propagation.

With respect to the symmetry axis of the fabric, the anisotropy factor is greater than unity for foliation and less than unity for crystallographic fabric. In regions of high strain rate, the S planes of both fabrics tend to be subparallel and the two anisotropy effects are opposed. Where porosity differences between foliation layers diminish with depth, the resultant anisotropy factor becomes less than unity at depth.

The gross structure of the confluence of the north and central arms of the Kaskawulsh Glacier was revealed by seismic reflection investigations. The valleys were found to be roughly parabolic and symmetrical in profile. Maximum ice thickness measured was slightly over 1000 m in the center of the central arm. The slope of the valley walls is continuous from above to below the surface of the glacier. The ridge separating the two arms of the glacier ends at the same juncture at which the two arms achieve unity of flow. The central-arm ice is thicker than the faster flowing north-arm ice. There is no basin and sill structure in the immediate confluence area.

Acknowledgments

The author would like to acknowledge the assistance of the following organizations: Arctic Institute of North America, Explorers' Club of New York, Institute of Polar Studies and Departments of Geodetic Science, Geology, and Welding Engineering of the Ohio State University, National Science Foundation, and Seismological Laboratory of the California Institute of Technology. Several individuals were especially helpful: Dr. Peter W. Anderton, Dr. Colin Bull, Dr. Albert P. Crary, Fred Erdmann, Matthew Golis, Francis Lehner, Phillip Muehrcke, Peter Simoni.

References

Anderson, D. L. (1961) Elastic wave propagation in layered anisotropic media, *J. Geophys. Res.*, 66, 2953–2963.
*Anderton, P. W. (1967) Structural glaciology of a glacier confluence, Kaskawulsh Glacier, Yukon Territory, Canada, Ph. D. dissertation, Ohio State Univ., Columbus.
Backus, G. E. (1962) Long-wave elastic anistropy produced by horizontal layering, *J. Geophys. Res.*, 67, 4427–4440.
Bass, R., Rossberg, D., and Ziegler, G. (1957) Die elastischen Konstanten des Eises, *Z. Physik*, 149, 199–203.
Bechmann, R., and Ayers, S. (1957) Thickness modes of plates excited piezoelectrically, in *Piezoelectricity*, British G.P.O. Res. Sta. Engin. Rept., pp. 33–41.
Berzon, I. S., Bokanenko, L. I., and Isaev, V. S. (1959) Seismic studies on the Tuyuksu Glacier, *LX and XII Sect. IGY Prog. (Glaciol. Seismol.) Akad. Nauk SSSR*, Moscow, 68 pp.
Birch, F. (1961) The velocity of compressional waves in rocks to 10 kilobars, Pt. 2, *J. Geophys. Res.*, 66, 2199–2224.
Bokanenko, L. I., and Isaev, V. S. (1960) Preliminary results of seismic determination of the thickness of ice on Mt. El'brus, *Info. Coll. IGY Prog. No. 5*, edited by G. V. Tushinsky, pp. 10–58, El'brus Exped. Moscow State Univ., Inst. Appl. Geophys. Acad. Sci. USSR, Moscow University.
Christoffel, E. B. (1877) Über die Fortpflanzung von Stössen durch elastische feste Körper, *Annali Matematica Pura Applicata*, Ser. II, Tomo 8, pp. 193–243.
†Dewart, G. (1966) Moulins on Kaskawulsh Glacier, Yukon Territory, *J. Glaciol.*, 6, 320–321.
Dewart, G. (1968) Seismic investigation of ice properties and bedrock topography at the confluence of two glaciers, Kaskawulsh Glacier, Yukon Territory, Canada, *Rept. No. 27*, Inst. Polar Studies, The Ohio State Univ., Columbus, 207 pp.
Förtsch, O., Schneider, H. J., and Vidal, H. (1955) Seismische Messungen auf dem Gepatsch- und Kesselwandferner in den Ötztaler Alpen, *Gerlands Beitr. Geophys*, 64, 233–261.
Förtsch, O., and Vidal, H. (1956) Die Ergebnisse der seismischen Messungen auf dem Hintereisferner in den Ötztaler Alpen, 1954, *Gerlands Beitr. Geophys.*, 65, 131–156.
Förtsch, O., and Vidal, H. (1958) Die seismische Vermessung des Grossen Gurgler Ferners in den Ötztaler Alpen in Spätsommer, 1956, *Gerlands Beitr. Geophys.*, 67, 1–30.
Gold, L. W. (1960) The cracking activity in ice during creep, *Can. J. Phys.*, 38, 1137–1148.

Hansen, W. R., Eckel, E. B., Schaem, W. E., Lyle, R. E., George, W., and Chance, G. (1966) The Alaska earthquake, March 27, 1964: Field investigations and reconstruction effort, *Prof. Paper 541,* U. S. Geol. Surv., 111 pp.

Hearmon, R. F. S. (1956) The elastic constants of anisotropic materials, II, *Advan. Phys.,* 5, 323–382.

‡Holdsworth, G. (1965) An examination and analysis of the formation of transverse crevasses, Kaskawulsh Glacier, Yukon Territory, Canada, *Rept. No. 16,* Inst. Polar Studies, The Ohio State Univ., Columbus, 91 pp.

Jakosky, J. J. (1961) *Exploration Geophysics,* Trija, Newport Beach, 1195 pp.

Jeffreys, H., and Bullen, K. E. (1948) Seismological tables, Brit. Assoc. Advance. Sci., Gray-Milne Trust, 50 pp.

Jones, R. (1952) A method of studying the formation of cracks in a material subjected to stress, *Brit. J. Appl. Phys.,* 3, 229–232.

Kisslinger, C., Mateker, E. J., Jr., and McEvilly, T. V. (1961) SH motion from explosions in soil, *J. Geophys. Res.,* 66, 3487–3496.

Knopoff, L. (1952) On Rayleigh wave velocities, *Bull. Seismol. Soc. Am.,* 42, 307–308.

Knopoff, L., and Gilbert, F. (1960) First motions from seismic sources, *Bull. Seismol. Soc. Am.,* 50, 117–134.

Lawrence, R. W. (1947) A scientific approach to the industrial application of shaped charges, *Explosives Engin.,* 25, 171–183.

Marcus, M. G. (1965) Icefield Ranges climatology program, St. Elias Mountains, 1964, Pt. I: data presentation, *Res. Paper No. 31-A,* Arctic Inst. North Am., 109 pp.

Marcus, M. G., Rens, F., and Taylor, B. E. (1966) Icefield Ranges climatology program, 1965 data presentation and programming analysis, *Res. Paper No. 33,* Arctic Inst. North Am., 111 pp.

Meier, M. F., Conel, J. E., Hoerni, J. A., Melbourne, W. G., Pings, C. J., Jr., and Walker, P. T. (1957) Preliminary study of crevasse formation, *Res. Rept. 38,* U. S. Army Snow, Ice, Permafrost Res. Establish., 80 pp.

Nafe, J. E. (1957) Reflection and transmission coefficients at a solid-solid interface of high velocity contrast, *Bull. Seismol. Soc. Am.,* 47, 205–219.

Nicholls, H. R. (1961) *In situ* determination of the dynamic elastic constants of rock, *U. S. Bur. Mines, Rept. Investig. 5888,* 13 pp.

Nye, J. F. (1951) The flow of glaciers and ice sheets as a problem in plasticity, *Proc. Roy. Soc. London,* A, 207, 554–572.

Nye, J. F. (1959) The motion of ice sheets and glaciers, *J. Glaciol.,* 3, 493–507.

Obert, L., and Duvall, W. I. (1945) The microseismic method of predicting rock failure in underground mining, *U. S. Bur. Mines, Rept. Investig. 3803,* 14 pp.

Obert, L., and Duvall, W. I. (1957) Microseismic method of determining the stability of underground openings, *U. S. Bur. Mines, Bull. 573,* 18 pp.

Obert, L., and Duvall, W. I. (1961) Seismic methods of detecting and delineating subsurface subsidence, *U. S. Bur. Mines, Rept. Investig. 5882,* 28 pp.

Olhovich, V. A. (1964) The causes of noise in seismic reflection and refraction work, *Geophysics,* 29, 1015–1030.

Postma, G. W. (1955) Wave propagation in a stratified medium, *Geophysics,* 20, 780–806.

Poulter, T. C. (1950) The Poulter seismic method of geophysical exploration, *Geophysics,* 15, 181–207.

Riznichenko, Yu V. (1949) About the seismic quasi-anisotropy, *Izvestiya Akad. Nauk SSSR, Ser. Geograf. Geofiz.,* 13, 518–544 (in Russian).

Robinson, E. S. (1964) Some aspects of subglacial geology and glacial mechanism between the South Pole and the Horlick Mountains, *Res. Rept. 64–7,* Univ. Wisconsin Geophys. Polar Res. Center, 86 pp.

Röthlisberger, H. (1964) Reflection and transmission coefficients at the interface ice-solid, *Res. Rept. 110,* U. S. Army Cold Regions Res. Engin. Lab., 17 pp.

Shumskii, P. A. (1954) *Principles of Structural Glaciology,* Dover, New York, 497 pp. (tr. by David Kraus).

Simmons, G., and Brace, W. F. (1965) Comparison of static and dynamic measurements of compressibility of rocks, *J. Geophys. Res.,* 70, 5649–5656.

Slichter, L. B. (1932) The theory of the interpretation of seismic travel-time curves in horizontal structures, *Physics,* 3, 273–295.

Thomson, W. T. (1950) Transmission of elastic waves through a stratified solid medium, *J. Appl. Phys.,* 21, 89–93.

Walsh, J. B., and Brace, W. F. (1966) Elasticity of rock, a review of some recent theoretical studies, *Rock Mechanics Engin. Geol.,* 4, 283–297.

Wheeler, J. O. (1963) Kaskawulsh map-area, Yukon Territory, *Geol. Surv. Canada, Map 1134A.*

White, J. E., and Sengbush, R. L. (1963) Shear waves from explosive sources, *Geophysics,* 28, 1001–1019.

Wood, F. J. (1966) editor, The Prince William Sound, Alaska, earthquake of 1964 and aftershocks, Vol. 1, *U. S. Coast Geod. Surv. Publ. 10–3,* 263 pp.

---

*Modified versions of these reports appear in the present volume.
†This article was reprinted in Icefield Ranges Research Project, Scientific Results, Volume 1.
‡A modified version of this report appeared in Icefield Ranges Research Project, Scientific Results, Volume 1.

APPENDIX

LIST OF SYMBOLS USED IN TEXT

A	amplitude
$A_{1,3,f}$	anisotropy factors
a	average pore diameter
c	crystallographic axis
C_{ij}	elastic modulus (stiffness)
d	thickness or diameter
θ	dip
g	acceleration of gravity
h	depth
K	compressibility
K_p	compressibility for porous medium
L	long period surface wave
λ	Lamé's constant
m	mass
μ	rigidity (shear modulus)
N	normal
P wave	compressional (longitudinal) elastic wave
PP	P wave reflected as a P wave

PS	P wave reflected as an S wave
R	ratio of amplitude of S waves reflected back into the ice to amplitude of P waves incident on the ice–rock interface
ρ	density
SH	horizontally polarized S wave
SV	vertically polarized S wave
SS	S wave reflected as an S wave
σ	Poisson's ratio
T_o	natural period of seismometer pendulum
T_g	natural period of galvanometer
t	time (used with various subscripts)
ϕ	angle between basal plane of crystal and wave normal
v	velocity (general)
V	volume
V_x	reciprocal of the slope of the time–distance curve of refracted rays at distance x
V_d	reciprocal of the slope of the time–distance curve for maximum distance
V_s	S-wave velocity
V_p	P-wave velocity
$V_{1, 2, 3}$	velocities of anisotropic wave modes
X	distance
Y	Young's modulus
Y_p	Young's modulus for porous medium
x, y, z	Cartesian coordinates
Z	acoustic impedance

The Collapse of Solifluction Lobes as a Factor in Vegetating Blockfields*

Larry W. Price†

ABSTRACT: The development of soil and vegetation in blockfields through normal processes is very slow. It is surprising, therefore, to find in the Ruby Range of southwest Yukon Territory, tongues and islands of vegetation occurring amidst certain blockfields. The collapse of solifluction lobes from upslope is suggested as the mechanism responsible. The lobes pass from the more gentle solifluction slope of the alb onto the steeper slope of the blockfields, and eventually become unable to maintain themselves because of steeper slope, change in composition of vegetation, and deeper active layer. Once the lobes do collapse, they flow downslope carrying with them clumps of vegetation which may become established somewhere along the mudflow channel or levee. In this way, small outposts of vegetation are created and speed up a process which would otherwise take indeterminately longer.

For anyone who has spent time beyond tree line in alpine or Arctic areas, felsenmeer or blockfields are a fairly common sight. They are slopes consisting of large and small angular blocks arrayed in chaotic fashion, usually believed to be the result of rapid mechanical weathering *in situ* of bedrock. They also occur in the Arctic on more nearly level areas, and they may include glacially transported materials as well (Bird 1967, pp. 168–171). The origin of these features is not of particular concern here except to point out that, where they occur in present periglacial climates, they are usually still active owing to frost activity. The more unstable areas are easily identified by the relative absence of lichens on surface rocks and, conversely, areas heavily lichen-covered are usually more stable. One quickly learns to take advantage of this fact when climbing on these rocky slopes.

As might be expected, even within the Arctic or alpine context, blockfields are inhospitable environments. Several factors contribute to this condition including the lack of fines (and therefore the almost complete absence of soil), the lack of water near the surface, and the great diurnal extremes in temperature during the summer due to high conductivity of the bare rocks. Thus, it is surprising to find scattered strips of soil and vegetation occurring amidst this sea of rocks. The origin of these "islands" of vegetation is of considerable interest since they can be considered as forerunners in the process of vegetating the slope, a process which would otherwise take indeterminately longer. It is suggested that the collapse of solifluction lobes from upslope is in some areas responsible for the early development of a plant cover on these slopes. The purpose of this paper is to describe this phenomenon and discuss the processes involved.

The study area is in the Ruby Range of southwestern Yukon Territory, Canada, approximately 150 miles (241 km) northwest of Whitehorse and about 35 miles (56 km) north of mile 1050 on the Alaska Highway (Fig. 1). The specific study site is near the head of an east-west valley of recent glacial origin with paternoster lakes occupying the valley floor. The south side of the valley (north-facing) consists of a steep rock wall with a number of talus cones emerging onto the valley floor. There is little vegetation on this slope and the rocks are largely lichen-free suggesting considerable weathering activity and mass movement. The south-facing slope is not quite as high as the north-facing slope and consists mainly of felsenmeer or blockfields. The rocks are lichen-covered, and occasionally interspersing the blockfields are tongues of soil and vegetation (Fig. 2).

The slope on which the blockfields are formed has an angle of 25° to 29°. Immediately above is an abrupt break in slope, marking the beginning of the alb of the glacial trough. The alb has a slope of 14° to 17°, and supports a relatively complete cover of tundra vegetation. There is no comparable alb on the north-facing slope where there is a very steep rock wall. The reason for this initial asymmetry is probably direction of ice movement and therefore more severe erosion on the south side of the valley (Gilbert 1904, pp. 579–588). Snow and ice patches still remain through the summer on this steep north-facing rock wall, and contemporary nivation along the rock wall has maintained its steepness, as well as contributing to the material of the talus cones below, which have formed since the valley was glaciated.

The entire area has been glaciated except for occasional peaks which remained as nunataks during glaciation, and

*This report has previously appeared in *Arctic*, Vol. 22, pp. 395–402 (1969), and is reprinted here with permission.
†Department of Geography, Portland State University, Portland, Oregon

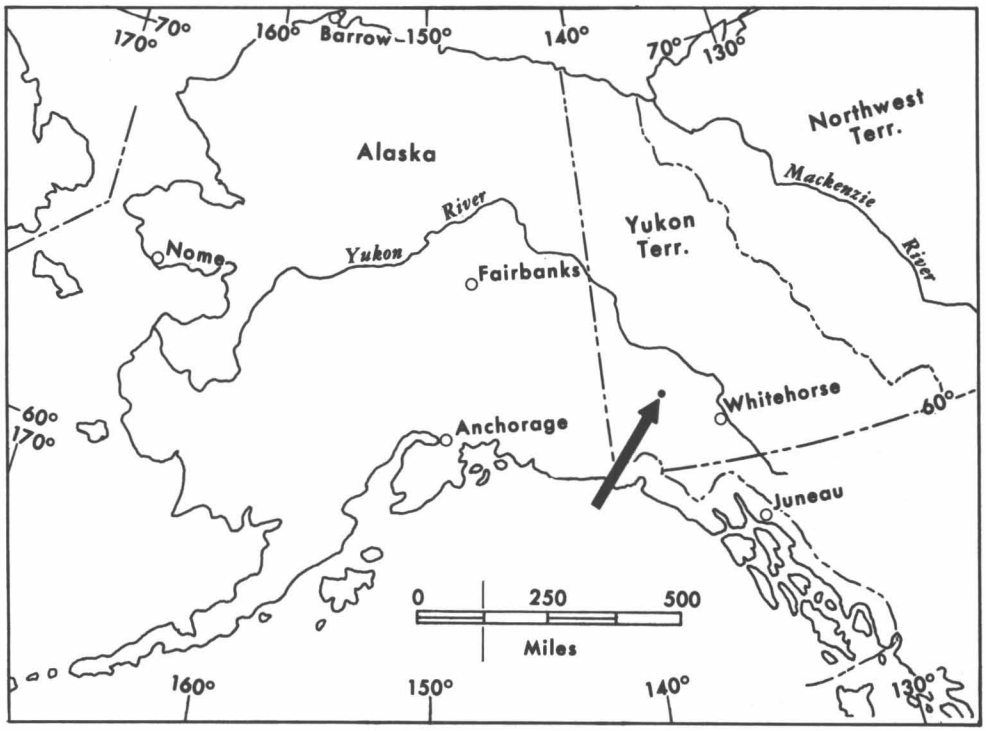

Fig. 1. Location of study area.

it is probable that the upper slope was free of ice while the lower part of the valley was still occupied by valley glaciers (Muller 1967, pp. 9–16). Therefore, the upper slope has had more time for the accumulation of fines (through frost comminution), and the development of a soil and plant cover. This slope has also had more time to undergo mass wasting due to solifluction and frost creep.

Solifluction gives rise to several features, one of the most striking being solifluction lobes or terraces which are also known as soil runs, turf-banked terraces and detritus benches among other names (Taber 1943, p. 1461). These features are best developed where there is ample soil moisture (usually from late snow melt or from ground ice) and a good vegetation cover to act as a retarding agent to form the initial bulge which becomes the front of the lobe (Wilson 1952, pp. 251–252). Both of the above conditions are present in the study area and the lobes are well developed. They vary in height at the front from 1 to 6 feet (.3-1.8 m), and occur as a series of scattered lobate tongues moving in the direction of greatest slope. Measurements made by the author at a nearby site (the results of which will be published separately) indicate a downslope surface movement on the order of ½ to 1 inch (1.3 to 2.5 cm) per year. The lobes continue to retain their characteristic shape for several years even after passing over the abrupt break in slope between the alb and the lower valley slope. Eventually, however, they collapse and spill their contents downslope.

During the summer of 1967, four freshly collapsed lobes were observed to occur in less than 1,000 feet (305 m) along the study slope (Fig. 3). Arcuate-like tension cracks immediately upslope from the basins testify to the "stretching" that has taken place in the surface layer after the collapse of the lobe fronts. Small streamlets from late snow melt and ground ice keep these crevasses water-filled until the middle of July and the area above the basins is quite unstable.

The largest collapsed basin (No. 1, Fig. 3) is the least active, as indicated by moss and lichens growing on the sides of the basin. The two smaller collapsed areas, Nos. 3 and 4, have fresh signs of movement including recently

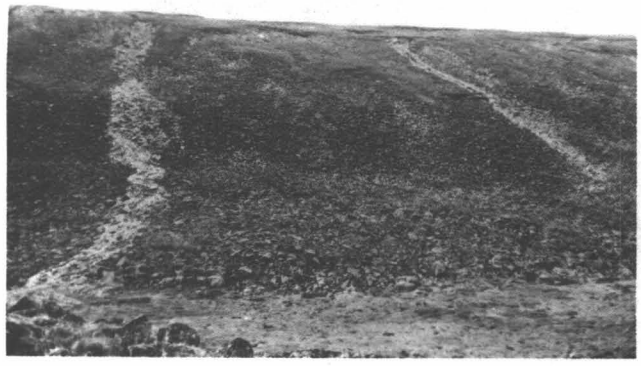

Fig. 2. South-facing slope showing two collapsed lobes which have moved downslope as mudflows (light areas). The one on the left (No. 1) completely reaches the valley floor while the one on the right (No. 2) terminates ¾ the way down the slope. Solifluction lobes can been seen on the crest of the ridge as they pass onto the steeper blockfield below. Note the occasional tongues of soil and vegetation penetrating the blockfield.

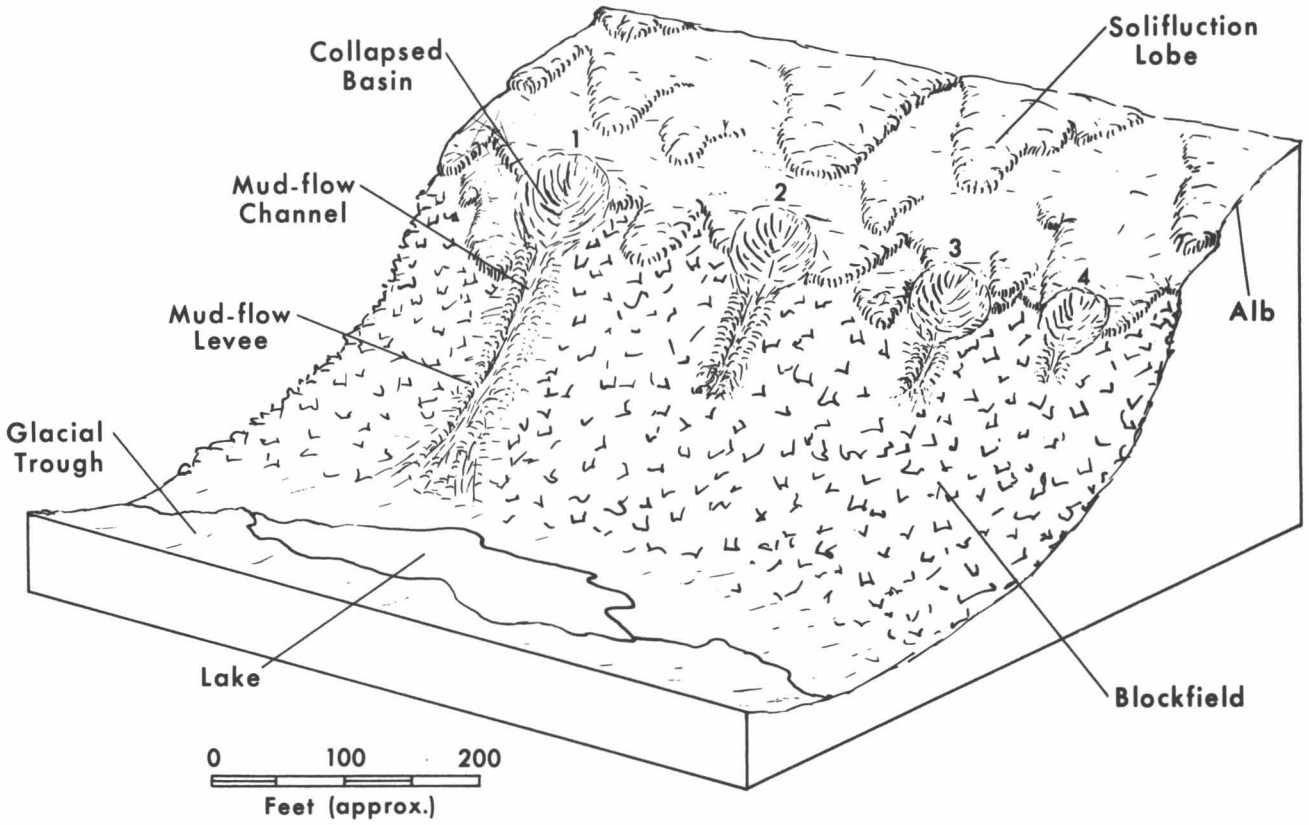

Fig. 3. Idealized block diagram of south-facing slope showing recently collapsed solifluction lobes and mud flows.

displaced mud, rocks, and clumps of vegetation. It is probable that these two sites will experience mudflows in the near future, although not more than 1 or 2 feet (30 to 61 cm) of material from the sides collapsed during 1967 and 1968. The most active of the four collapsed basins is No. 2. The collapsed area of the lobe was 65 feet (19.8 m) wide and 95 feet (29 m) long in the summer of 1967, but when we arrived for the 1968 field season, considerable collapse had taken place that spring and the basin was 73 feet (22 m) across and 99 feet (30 m) long. After a period of heavy rains in early August, the basin collapsed an additional 2 feet (61 cm) headward and 4 feet 6 inches (1.4 m) on the sides.

The most obvious reason why the lobes collapse after having passed the edge of the alb, is that the slope is 10° to 12° steeper. More specifically, it appears that once the lobes have passed the crest of the ridge onto the steeper part of the slope, collapse may be aided by a change which occurs in composition of the vegetation. This is supported by the fact that cotton-grass tussocks grow on the upper surfaces of the lobes occurring above the break in slope, but not on the lobes below the alb.

The tussocks are ball-like masses of plants and soil standing a few inches to 1 or 2 feet (30 to 61 cm) above the poorly drained surface. Principal species include *Salix pseudopolaris, Carex microchaeta, Salix reticulata,* and *Eriophorum angustifolium.* Mosses accumulate to a depth of 10 inches (25 cm) or more around the rhizomes and adventitious roots of these plants, and provide excellent insulation helping to maintain the permafrost (tjaele) near the surface through the summer (Bliss 1956, p. 329). Reciprocally, the frozen layer maintains a high moisture content at the surface, which is necessary for the existence of the tussocks. The roots of tussocks are very intricate and well-developed, and several excavations showed live roots extending to a depth of 36 inches (91 cm). Average depth, however, is about 20 inches (41 cm). This well-developed root system acts as a binding agent and is largely responsible for maintaining the fronts of the solifluction lobes as virtual scarps up to 6 feet (1.8 m) in height on the gentle upper slopes above the blockfields.

Once the crest of the slope is passed, however, the angle of incidence of solar radiation changes substantially (Fig. 4). The surface temperature increases and the active layer becomes deeper [measurements made nearby indicate that the surface of the risers of the lobes are on the average 20°F (11°C) warmer than the treads]. With the retreat of permafrost there is less surface moisture. The higher surface temperature also increases the rate of evaporation. The tussocks are therefore slowly replaced by other species, especially *Dryas octopetala, Festuca altaica, Polygonum viviparum,* and *Cassiope tetragona.* The root systems of these species are not so well-developed and there are very few associated mosses, so the vegetation is less able to maintain the surface material of the lobe.

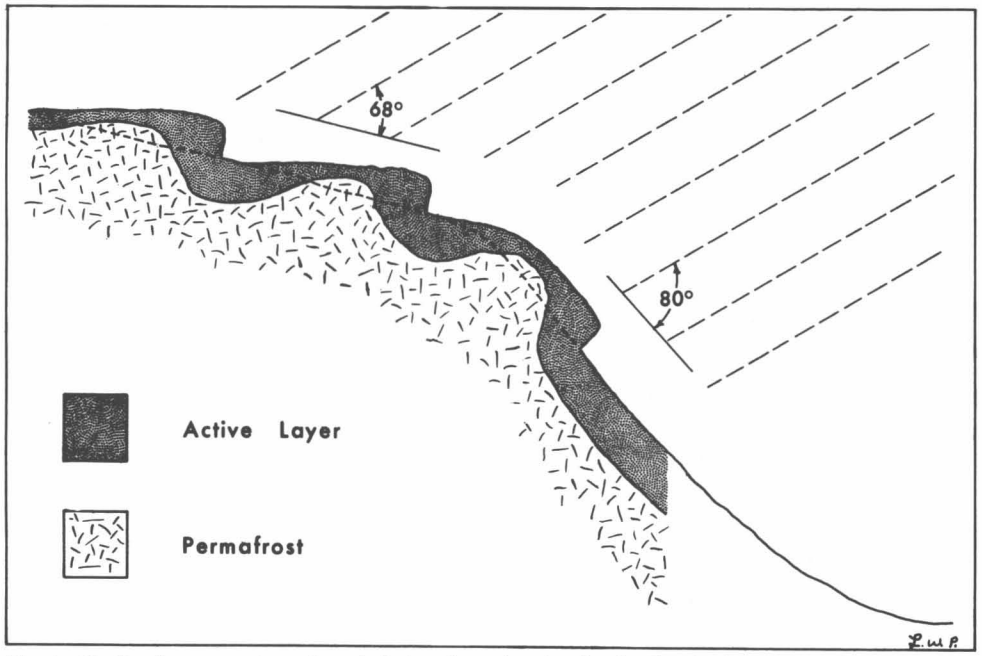

Fig. 4. Idealized cross section of south-facing slope showing depth of active layer on study slope. Variations in depths are largely in response to the insulating qualities of vegetation and the angle of incidence as discussed in text. Note the major difference in angle of incidence between the upper and lower slopes. These angles are calculated for slopes of 16° and 28°, respectively, at noon on summer solstice at 61°30′ North Latitude.

In addition to the changes which take place in the composition of the vegetation, there is a corollary development in the level of permafrost as a result of varying vegetation and slope. The data for permafrost depths were gained by augering at 5-foot (1.5-m) intervals in transects up the slope. A generalized picture of what occurs is shown in Fig. 4. As can be seen, on the upper slope the active layer is deeper near the front of the solifluction lobes. This is due to the greater angle of incidence of solar radiation and a vegetation cover having poor insulating qualities. The active layer becomes shallower both above and below the front because of tussock vegetation containing quantities of moss which is good insulation material. The lobes are apparently able to maintain themselves indefinitely under these conditions.

On the steeper slope, as shown in Fig. 4, the active layer below the last lobe does not arch upward as it did on the gentler slope because the insulating vegetation has disappeared for the reasons stated above. The entire area, then, is subject to movement due to gravity with no retardation to movement by the upward swell of permafrost below the lobe as exists on the gentler slope. The combination of factors: (1) shallower root systems, (2) deeper active layer below the lobe, and (3) steeper slopes, all contribute to the collapse of the lobes.

In spring when melt occurs and the land is a well-saturated morass, the surface of the lobe moves slowly downhill due to solifluction. Permafrost is still relatively near the surface on the upper part of the lobe and is parallel to its outer surface. Movement takes place in the saturated zone above permafrost and pressure is built up against the vegetation retaining the front of the lobe. Eventually the front is not able to retain itself and collapses. The above conditions would be especially enhanced after two or three days of steady rain (Sharpe 1938, p. 55). This additional water adds a great deal of weight to the active layer above the permafrost, and exerts even more pressure in the downslope component. In addition, it acts as a lubricant and reduces the shear strength of the soil (Williams 1957, p. 52; Taber 1943, p. 1458).

All of the major movements (i.e., slumping and mudflow), that we observed during the summers of 1967-68, occurred during or soon after heavy rains. This, of course, is in addition to the movement to be expected during break-up and freeze-up in spring and fall. During a three-day period in late July, 1967, 2.86 inches (7.26 cm) of rain fell, and on the third night we were awakened by the rumble of falling rocks and debris caused by part of a slope giving way near our camp. In the local area, there were several scars on the landscape as a result of that particular rainfall. Although these disturbed areas were not all solifluction lobes, they nevertheless illustrate conditions under which collapse might be expected to take place. During the summer of 1968, 2 heavy rain periods occurred—one in early July with 1.70 inches (4.3 cm) in 2 days, and the other in early August with 3.97 inches (10.1 cm) in 7 days. Considerable fresh movement was observed on several of the disturbed areas after each rainfall, including that which took place on collapsed lobe No. 2, as previously mentioned.

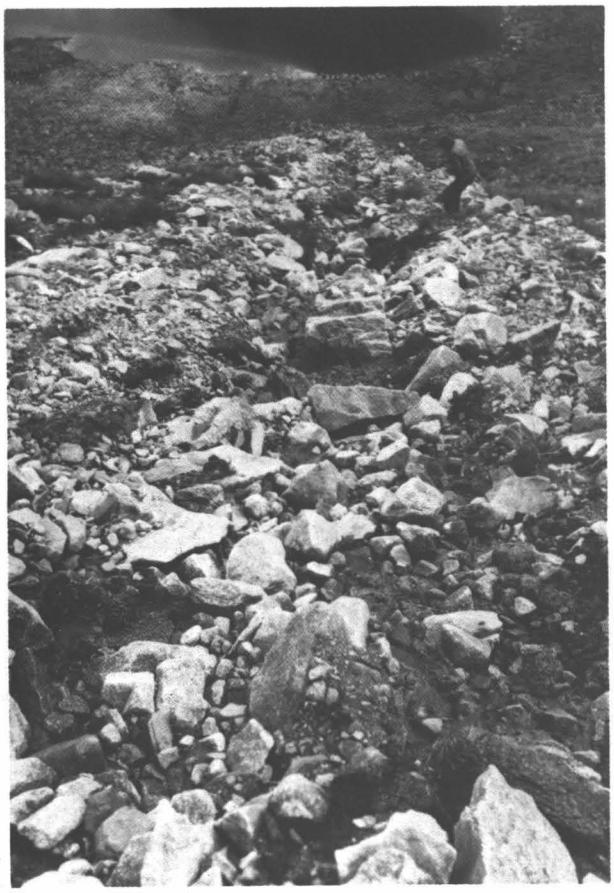

Fig. 5. Looking downslope at mudflow channel immediately below collapsed basin of solifluction lobe. Note clumps of vegetation at the level where man is standing. Lake on valley floor is at top of photo. Even though this mudflow channel is at least 9 years old, it still appears surprisingly fresh.

When the lobes do collapse, the movement appears to be fairly rapid, as suggested by the mudflow channels and levees immediately downslope. These are of the same type as described by Sharp (1942, pp. 222–227), although his observations deal mainly with alluvial slopes. Basically, it is the downhill flowing of rocky detritus, including boulders two or three feet in diameter, in a saturated mass of mud. The material tends to move in spurts, the snout of the flow wedging its way along the leading edge, windrowing the material in snow-plow fashion on either side, giving rise to features similar to natural levees on a stream. Clumps of vegetation, broken loose from the upper surface of the lobe, are also carried down the mudflow channel and they are deposited helter-skelter on the levees (Fig. 5).

It is not surprising that these dislocated plants survive in their new habitat. Tundra vegetation in general exists because of its ability to live in an environment of constant flux. The particular adaptation with survival value in this case would be the ability to reproduce vegetatively. Nevertheless, if the plants are successful in becoming established before the fine material is carried away by erosion, a small island of vegetation is established. The amphitheater-like collapsed area of the lobe eventually becomes vegetated and the slope again appears to maintain some semblance of stability until another lobe from above moves downslope and collapses, and the process is repeated.

The foregoing is not meant to suggest that this process of developing a plant cover on blockfields is rapid. On the contrary, although the collapsed lobes appear very recent, they are present on airphotos taken by the Canadian Air Force in 1959. Collapsed basin No. 1 (see Fig. 3) is the oldest of those mentioned, and revegetation has partially begun. Its mudflow channel has completely reached the valley floor and a similar prospect seems to be in store for the other collapsed lobe sites if current rates of movement continue. Evidence of former collapsed basins, and mudflow channels and levees, are present on the slope as well, and some may be several hundreds of years old. So, succession is very slow, but the process is directional and there is enough evidence on the slope representing different stages in its development, to suggest the central hypothesis of this paper: that the collapse of solifluction lobes is one way in which certain Arctic and alpine slopes are vegetated more quickly than they would be otherwise.

Acknowledgments

Financial assistance for this research was provided by the Arctic Institute of North America and is gratefully acknowledged. Excellent field support was provided by the Icefield Ranges Research Project, and I would like to thank Dr. J. Peter Johnson, Mr. Richard Ragle, Mr. Phil Upton, Dr. Walter Wood, and Dr. Melvin Marcus for their help. My wife, Nancy, Mr. Jim Sij, and Mr. Charles Volk were field assistants. Plant species were identified by Dr. James A. Neilson and Dr. David F. Murray. The manuscript was critically read by Dr. C. S. Alexander and Dr. L. C. Bliss. All of the above persons are due my sincere thanks.

References

Bird, J. B. (1967) *Physiography of Arctic Canada,* Johns Hopkins Press, Baltimore, 336 pp.

Bliss, L. C. (1956) A comparison of plant development in microenvironments of arctic and alpine tundras, *Ecol. Monogr.,* 26, 303–337.

Gilbert, G. K. (1904) Systematic asymmetry of crest lines in the High Sierra of California, *J. Geol.,* 12, 579–588.

Muller, J. E. (1967) Kluane Lake map area, Yukon Territory, *Geol. Soc. Can. Mem.,* 340, 135 pp.

Sharp, R. P. (1942) Mudflow levees, *J. Geomorphol.,* 5, 222–227.

Sharpe, C. F. S. (1938) *Landslides and Related Phenomena,* Columbia Univ. Press, New York, 137 pp.

Taber, S. (1943) Perennially frozen ground in Alaska, *Bull. Geol. Soc. Am.,* 54, 1433–1548.

Williams, P. J. (1957) Some investigations into solifluction features in Norway, *Geogr. J.,* 72, 42–58.

Wilson, W. J. (1952) Vegetation patterns associated with soil movement on Jan Mayen Island, *J. Ecol.,* 40, 249–264.

PAPERS IN THE BIOLOGICAL SCIENCES

Notes on Mammals in Alpine Areas of the Northern St. Elias Mountains, Yukon Territory and Alaska*

Barbara M. Murray and David F. Murray†

Introduction

The St. Elias Mountains reach their northern extent at the White River of Alaska (cf. Wahrhaftig, 1965, Plate 1). These spectacular mountains have the most extensive glacierization in continental North America. Extensive areas of alpine vegetation are found adjacent to the glaciers, and limited tundra is found on nunataks in the icefield. Incidental to botanical studies during the summers of 1965-68, observations were made on mammals in the vicinity of the Kaskawulsh, Steele, and Russell Glaciers which are among those flowing eastward from the icefield on the continental slope of the range (Fig. 1).

Three study areas are along the Kaskawulsh Glacier and the Slims River: (1) Kaskawulsh Nunatak. At the edge of the icefield an extensive bedrock ridge protrudes through the ice and divides the upper Kaskawulsh Glacier into north and central arms. At the extreme down-glacier end of the nunatak is a low, vegetated knoll (Fig. 2). The knoll is about 20 miles upglacier from the glacier terminus and lies a few miles below the firn limit. It is separated by a mile of ice on each side from adjacent mountains. The relatively stable and vegetated surface is at 6000 feet, about 200 feet above the central arm, but somewhat less above the north arm. The vegetated surface is less than ¼ mile in its longest dimension. (2) Observation Mountain. Just upglacier from the terminus and on the north side of the Kaskawulsh Glacier is a saddle at 5000-5500 feet between two ridges that reach 7000 feet (Fig 3). The saddle drops abruptly to the glacier on one side and into the canyon of Canada Creek on the other. (3) Between Sheep and Bullion creeks in the mountains north of the Slims River is a large expanse of rolling tundra at 5000 feet, with ridge crests to 6000 feet. Muller (1967, p. 124, Plate 2) gives an aerial view of this locality.

Two study areas are in the vicinity of the Steele Glacier: (4) on the south wall at the big bend in the glacier at 5800-7000 feet (Wood, 1942, p. 46, Fig. 8 is an aerial view), and (5) on the north side of the valley at 6000-7000 feet (Wood, 1942, p. 46, Fig. 7 is a photograph of this area).

Three study areas at 4000-6000 feet are in the mountains flanking the upper White River on the south side: (6) near the Guerin Glacier, (7) near the Sheep Glacier, and (8) near the terminus of the Russell Glacier.

The Icefield Ranges Research Project, under whose auspices the botanical studies were begun, has maintained camps in the icefield; one of these is the Seward Nunatak (9) at 6000 feet on the upper Seward Glacier on the coastal slope of the range (Wood, 1948, p. 110 is a photograph of this site). This is a small, sparsely vegetated nunatak. It is the most isolated of all the sites and is miles from extensive vegetation.

Little information is available concerning the mammals in the St. Elias Mountains, especially in remote interior areas. Banfield (1960) presented an annotated list of the mammals of the Kluane Game Sanctuary, of which two thirds is in the St. Elias Mountains, and he cited previous work in the area. This paper presents our notes and reports by other participants in the Icefield Ranges Research Project.

Annotated List of Mammals

GRIZZLY BEAR. *Ursus arctos.* We observed bears or sign at areas 1–8. At Observation Mountain, where the greatest variety of wildlife was seen, two Grizzly Bears (one brown and one blonde) were seen periodically throughout July 1966. The bears preferred cool, moist, north- and east-facing slopes where lush herb mats of the snow-flush areas provided food. One such site was near our camp, and we were able to observe a bear on 9 July as it alternately fed and rested for nine hours. The bear was sighted at 0930 hr; it grazed until 1200 hr when it lay on its side and rested for an hour. It fed again until 1430 hr, then rested until 1600 hr. After grazing until 1800 hr it was alerted to our presence by the noise of radio contact with the project plane overhead. The bear went high onto talus and lay down and looked in the

---

*This report has previously appeared in *The Canadian Field-Naturalist,* Vol. 83, pp. 331–338 (1969), and is reproduced here with permission.

†Department of Biology, Memorial University of Newfoundland, St. John's, at the time of writing; present address, Department of Biological Sciences, University of Alaska, College

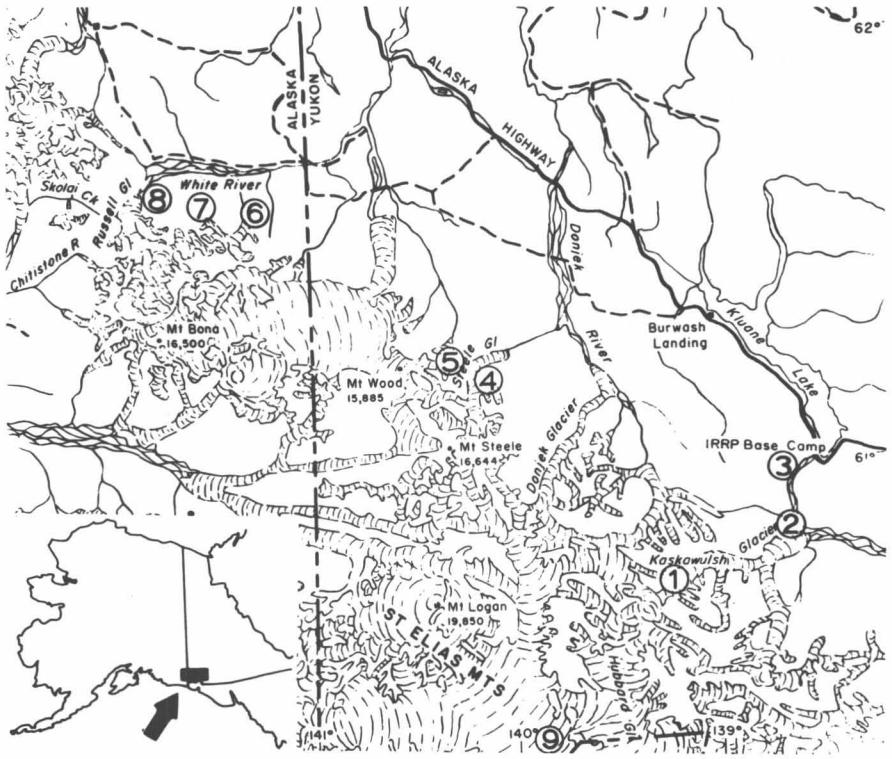

Fig. 1. Study areas.

direction of our camp for 30 minutes before disappearing over the mountain at 1900 hr.

On 22 July a Grizzly Bear gave chase to 10 adult Mountain Goats and 6 kids up a very steep slope. The speed and duration of the sprint was impressive, but the goats easily reached the safety of the ridge crest and disappeared. Another bear was seen running back and forth between ground squirrel burrows, presumably in an attempt to trap ground squirrels that had strayed too far from their burrows. Otherwise the bears spent their time seeking vegetable food. Studies on Grizzly Bear ecology are being conducted in Kluane Game Sanctuary by A. M. Pearson, Canadian Wildlife Service.

TIMBER WOLF. *Canis lupus.* Little Timber Wolf sign was observed along the Kaskawulsh and Steele drainages, and only one was glimpsed in the forest on the north side of the Slims River. At the upper White River in Alaska, sign was more common where tracks of wolves, caribou, and grizzly dotted many gravel bars.

COYOTE. *Canis latrans.* Tracks were seen frequently along the Slims River floodplain and up into the tundra, and yapping was heard on several occasions when we camped near site 3.

RED FOX. *Vulpes vulpes.* Red Foxes were seen at Observation Mountain, the north side of the Steele valley, and along the upper White River. One afternoon we observed a Red Fox barking at and advancing toward a Wolverine. The Wolverine was backing away and was in no apparent hurry to break off the encounter.

WEASEL. *Mustela* sp. A weasel (probably *M. erminea)* was sighted on two occasions in the first week of August 1964, at the Seward Nunatak. It was believed to be feeding on bird remains at the base of a cliff (Ray Lougeay, personal communication). This is just one of several remarkable cases of mammals having traveled long distances over glaciers. Pruitt (1957) reported a weasel at 15,000 feet on Mt. McKinley, Alaska, and concluded that it had "traveled some two vertical miles above timberline . . . before dying, presumably of starvation."

WOLVERINE. *Gulo gulo.* Reported by Banfield (1960) as common. A Wolverine was seen five times in July (twice on the 8th at 0900 hr and 1600 hr, at 0400 hr on the 9th, and at 0200 hr on the 12th, in addition to the fox incident on the 17th) at Observation Mountain. Its curiosity was not dampened by being chased twice by our dog, when it again exhibited no signs of aggressiveness.

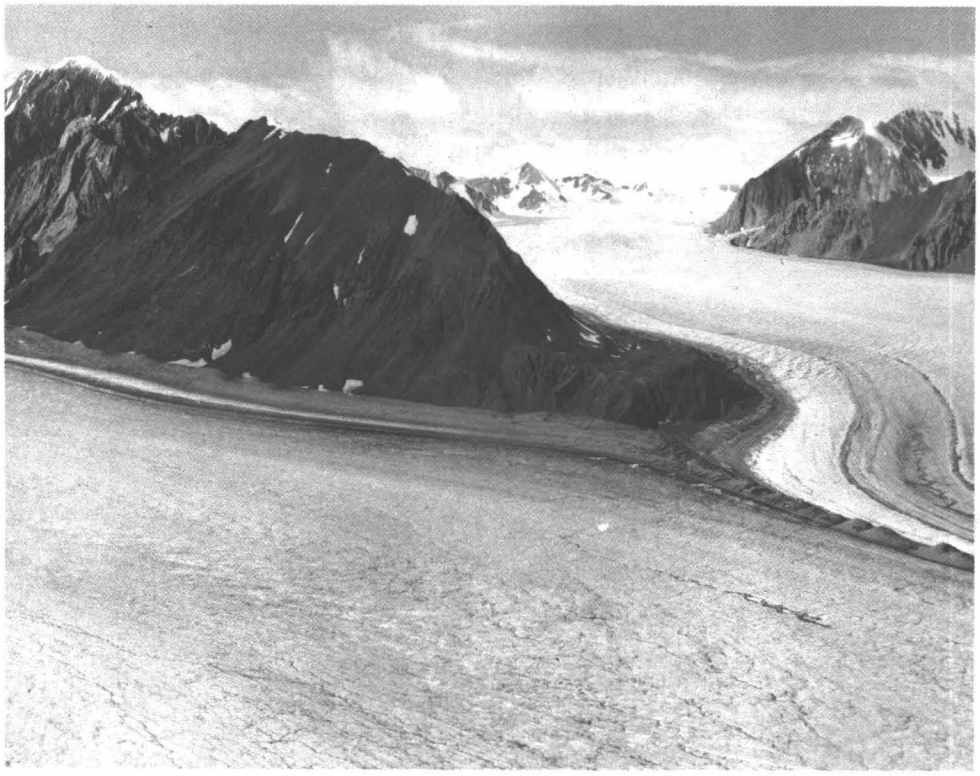

Fig. 2. Kaskawulsh Nunatak.

Other Wolverines were seen on the south side of the Steele Glacier (Walter A. Wood, personal communication) and at 7000 feet on a small glacier near the Steele Glacier (Michael Hebb, personal communication) in August 1967.

COUGAR. *Felis concolor.* The nearest reliable (published) records of Cougar are from northern British Columbia (Rand, 1944) and from west of Watson Lake, Y.T. (Youngman, 1968). However, during 1964-1966 residents along the Alaska Highway between Haines Junction and Burwash Landing and some Icefield Ranges Research Project personnel reported sighting a Cougar along the Alaska Highway and the environs of the south end of the Kluane Lake. Neither these sightings nor the reference in Wood (1967) have been verified. Nevertheless, it is significant that people from the area and familiar with the wildlife caught glimpses of an animal they could not immediately identify.

LYNX. *Lynx canadensis.* We saw no live Lynx but found an entire Lynx skeleton in a snow accumulation area on the Kaskawulsh Nunatak in 1965. They have been seen well into the icefield near the base of Mt. Bering and on the Lowell Glacier (M. E. Alford, 1966, personal communication).

HOARY MARMOT. *Marmota caligata.* Marmots were not observed by Banfield (1960) but were reported by Cameron (1952). We saw only two marmots at Observation Mountain in July 1966.

ARCTIC GROUND SQUIRREL. *Spermophilus undulatus.* Arctic Ground Squirrels are common from meadows and flats at Kluane Lake (2600 feet) to the alpine areas, where they are found on tundra and on sparsely vegetated moraines up to 6500-7000 feet. The most detailed observations were made between 1 July and 1 August 1965 on the Kaskawulsh Nunatak, where there were at least 13 adults, 7 with young. The ground squirrel population more than doubled in 1965; at least 23 young were born in litters of one to four.

The limited habitat restricts the size of the population, and once maximum numbers are attained, dispersal of the annual increment becomes a necessity. Even before the emergence of the young, all suitable habitat on the knoll was utilized by the adult population. In July 1967 we noted no further development of burrow systems, which indicates that the carrying capacity of the terrain had been reached.

In addition to dispersal, the origin of the population is a problem, since the nunatak is separated from adjacent mountains by a mile of ice. Two routes are possible for migration to or emigration from the nunatak. The stock for the population may have originated from the areas of tundra at the glacier terminus for which the medial moraine could have served as a route to the nunatak. However, this is unlikely, since it would require a 15 to 20 mile trek over rough, essentially vegetation-free terrain. A more likely source is from known ground squirrel

Fig. 3. Observation Mountain, saddle.

populations in mountains directly across the ice from the nunatak, where tundra vegetation is present, but discontinuous (Peter Anderton and Gil Dewart, personal communication). In this case the medial moraine could serve to direct ground squirrels crossing the glacier from either side, downglacier from the nunatak.

The nunatak could have been visited first during Hypsithermal time when its surface was ice-free, and the glacier terminus had begun its retreat. Maximum retreat is documented to within about 10 miles of the nunatak (Denton and Stuiver, 1966) and is postulated to a few miles upglacier of the nunatak (Borns and Goldthwait, 1966), which would place the nunatak in contact with the valley floor.

Due to their impact on the vegetation, it is unlikely that an Arctic Ground Squirrel population could persist for a long period of time on the nunatak. Burrowing activity obliterates or buries vegetation. This and geomorphic processes promote soil instability, thus revegetation is slow.

Young were first seen on the nunatak on 11 July around a burrow system which had been snow covered until the end of the first week in July. The mother grazed at a considerable distance from the young, and even remained in the burrow for up to 20 minutes while the young grazed and dozed near the burrow entrance. Two weeks after emergence the young were ranging far out of the territory of their natal burrow and were digging and "hay collecting." The ground squirrels did not appear to be wary, and no predation was observed during July 1965, probably because of our presence. However, grizzly and canid scats and the Lynx skeleton indicate that these predators visit the area. Any large predator could drastically reduce population size in a short time. An Arctic Ground Squirrel carcass was found decomposed intact indicating that predators do not necessarily reach the nunatak each year. No raptors were seen, but skeletal remains of one were found.

Ground squirrel territories were well defined and covered most of the vegetated surface. Boundary squabbles occurred every morning, and the antagonism between ground squirrels seemed to be of greater intensity and frequency than on the tundra above the Slims River where extensive habitat was available. Late in July there were signs of antagonism between mothers and young. One young ground squirrel was seen on the moraine 200 feet below the nunatak in early August.

Greatest population pressure occurs in the fall when the young of the year require hibernacula, and probably most emigration attempts would be made then. However, glacier conditions would be most hazardous for ground squirrels at this time. Since the nunatak lies below the firn limit, the cover of snow melts by late July. Consequently crevasses are no longer bridged, and the

ice surface is crisscrossed by meltwater streams, some of which are swift and deep. Early spring conditions would present far less difficulty, but then one would expect the necessity to seek new territories to be less severe.

A behavior study with a tagging and recapture program on the nunatak and flanking mountains could yield information as to the dynamics of an Arctic Ground Squirrel population in a restricted and isolated area, and whether or not they do, in fact, repeatedly attempt movement across the glacier, and if so, at what season, and with what success. Since a weasel was seen on the Seward Nunatak and pikas or pika sign have been found there and on the Kaskawulsh Nunatak, it is apparent that these small mammals are also capable of crossing large expanses of ice. A. H. Tinker (personal communication) confirmed by trapping without success in 1966 our impression that mice and voles are not on the Kaskawulsh Nunatak.

SINGING VOLE. *Microtus gregalis (M. miurus).* We did no trapping, but the distinctive haypiles (consisting here of *Salix arctica* and *S. barrattiana)* and their "singing" identified a population of *M. gregalis* on the tundra between Sheep and Bullion creeks in 1966. There was more sign in 1967, and the population was obviously high. We noted at least 25 burrow entrances in an area 5 by 8 feet. By June 1968 the population had crashed; no animals were seen and much of the old haypiles remained, although on the north side of the Steele valley *M. gregalis* were plentiful. During 1967 when the mouse population was high between Sheep and Bullion creeks, numbers of this species were low at nearby Kluane Lake (A. H. Tinker, personal communication).

COLLARED PIKA. *Ochotona collaris.* Pikas were observed in areas of blocky talus at Observation Mountain and in the vicinity of Steele Glacier among moraine boulders and in talus. Pikas or sign have also been noted well into the icefield. According to Walter A. Wood (1948, and personal communication) pikas were found on Seward Nunatak and other nunataks in the vicinity in 1945 and 1948 but were not seen in 1951. We found old pika scats and the remains of a haypile in the talus of a snow accumulation area on the Kaskawulsh Nunatak. No pikas were heard or observed there in July 1965, 1966, or 1967.

PORCUPINE. *Erethizon dorsatum.* A Porcupine was seen on 4 July 1968 at 5500 feet on the tundra between Sheep and Bullion creeks.

MOOSE. *Alces alces.* Banfield (1960) mentioned evidence of feeding and tracks on the tundra. We saw Moose tracks along an old mining road in the tundra above the Slims River. The road was heavily used since it is a convenient route through the shrub zone between the forest and tundra. Tracks and scats of bear, moose, fox, and coyote were common.

Three Moose were seen together on two occasions a week apart on the tundra at Observation Mountain in 1966. They spent 18 hours there on 15 July and 12 hours there on 23 July and climbed on talus to 6000 feet and rested high on the slope for several hours not far from a band of White Sheep.

CARIBOU. *Rangifer tarandus.* Caribou were observed on the Burwash Uplands west of Kluane Lake and in the White River valley, on the floodplain and on the tundra. Several sets of small antlers, presumably from females, were found on high, exposed tundra slopes near Sheep Glacier indicating that this may be an area of calving.

WHITE SHEEP. *Ovis dalli.* Banfield (1960) presented a distribution map for White Sheep in the Kluane Game Sanctuary. They are common throughout the St. Elias Mountains; we saw them at locations 2-8. We camped at Observation Mountain from 6 July to 2 August 1966. Bands of 5 to 20 adults were seen daily. Small bands of lambs and ewes appeared for the first time that season on 25 July and were often seen after that date. Undoubtedly they had been hidden in more precipitous areas. As the summer progressed, the bands of sheep stayed higher on the mountain, perhaps to remain near the retreating edge of snowbanks to feed on the new vegetation.

MOUNTAIN GOAT. *Oreamnos americanus.* Banfield (1960) stated that local reports placed goats in the Alsek River valley alone. We observed goats at Observation Mountain and in the mountains flanking Bullion Creek, and in 1914 Auer (1916; cf. Rand, 1945) hunted and photographed them in the Slims River-Canada (Kennedy?) Creek area.

Mountain Goats have been seen on the Kaskawulsh Nunatak in 1964 (Peter Anderton, personal communication), and many "beds" and scats were found there. A recent sighting near the mouth of Steele Creek (Cliff Armstrong, personal communication) places goats further north along the range. It is possible that Mountain Goats are now extending their range east and north in the St. Elias Mountains.

At Observation Mountain one, two, and three males were seen from time to time until 21 July when does and kids appeared. The males often rested and grazed near and even mixed with bands of White Sheep. The nursery bands ranged in size from 2 to 10 adults with up to 6 kids.

Acknowledgments

These notes were made possible through support from grants awarded to the second author by: Arctic Institute of North America 95, 1965; National Science Foundation GB-5008, 1966, 1967; and National Research Council of Canada A-4467, 1968. We wish to thank Walter A. Wood, Director, for his encouragement and aid and other participants in the Icefield Ranges Research Project. We are grateful to William O. Pruitt, Jr., Memorial University of Newfoundland, for reading the manuscript.

References

Auer, H. A. (1916) *Camp Fires in the Yukon,* Stewart & Kidd, Cincinnati, 204 pp.

Banfield, A. W. F. (1960) Notes on the mammals of the Kluane Game Sanctuary, Yukon Territory, *Nat. Mus. Can., Bull. 172, Biol. Ser. 65, Contrib. Zool.,* 1959, 128–135.

*Borns, H. W., and Goldthwait, R. P. (1966) Late-Pleistocene fluctuations of Kaskawulsh Glacier, southwestern Yukon Territory, Canada, *Am. J. Sci.,* 264, 600–619.

Cameron, A. W. (1952) Notes on mammals of Yukon, *Nat. Mus. Can., Bull. 126 (Ann. Rept., 1950–1951),* 176–184.

*Denton, G. H., and Stuiver, M. (1966) Neoglacial chronology, northeastern St. Elias Mountains, Canada, *Am. J. Sci.,* 264, 577–599.

Muller, J. E. (1967) Kluane Lake map-area, Yukon Territory, *Geol. Surv. Can., Mem. 340,* 137 pp.

Pruitt, W. O., Jr. (1957) A high altitude weasel, *Murrelet,* 38, 36.

Rand, A. L. (1944) The southern half of the Alaska Highway and its mammals, *Nat. Mus. Can., Bull. 98, Biol. Ser. 27,* 1–50.

Rand, A. L. (1945) Mammals of Yukon, Canada, *Nat. Mus. Can., Bull. 100, Biol. Ser. 29,* 1–93.

Wahrhaftig, C. (1965) Physiographic divisions of Alaska, *U. S. Geol. Surv., Prof. Paper 482,* 52 pp.

Wood, W. A. (1942) The parachuting of expedition supplies, *Geogr. Rev.,* 32, 36–55.

Wood, W. A. (1948) Project "Snow Cornice," *Arctic,* 1, 107–112.

Wood, W. A. (1967) A history of mountaineering in the Saint Elias Mountains, *Yukon Alpine Cent. Exped.,* 45 pp.

Youngman, P. M. (1968) Notes on mammals of southeastern Yukon Territory and adjacent Mackenzie District, *Nat. Mus. Can., Bull. 223, Contrib. Zool.,* 4, 70–86.

---

*These articles were reprinted in Icefield Ranges Research Project, Scientific Results, Volume 1.

Nesting of the Long-Tailed Jaeger in Southwest Yukon Territory — An Extension of the Known Breeding Grounds*

Larry W. Price†

An extension of the known breeding grounds of the Long-tailed Jaeger *(Stercorarius longicaudus)* was discovered during summer 1967 and noted again in 1968 while carrying out geomorphological field work in the Ruby Range of southwest Yukon Territory, Canada. The exact locality is Gladstone Lakes, about 30 miles due north of Mile 1045 Alaska Highway, 61°23′ N 138°12′ W. Location of the site, with respect to the presently known breeding grounds, is shown in Figure 1.

The general environment of this breeding ground extension is that of alpine tundra at an elevation of 6,300 feet on a southeast facing 14° slope. Tree line is at 3,800 feet, about three miles distant. Well-developed solifluction lobes occur on the slope and they present, in cross section, a series of treads and risers, as in a stairway. Favorable microhabitats for both flora and fauna are provided, particularly at the fronts (risers) of the lobes, where there is late snow lie to serve as insulation, water availability through the summer from melting permafrost, and a higher temperature because of the greater angle of incidence of solar radiation.

A pair of jaegers was observed to be nesting both summers, 1967 and 1968, in almost exactly the same spot. The nest was on the top (tread) of a solifluction lobe in wet and mossy cotton-grass tussocks. Dominant species include *Eriophorum angustifolium, Carex microchaeta, Salix pseudopolaris, Salix reticulata,* and mosses and lichens. As far as we could tell, there were no special preparations for the nest – it was simply in a small depression between two tussocks.

One offspring was born each year, apparently late in June. The picture (Figure 2) was taken on July 2, 1968, of the young jaeger. It was perhaps a week old at the time because it could stagger around a little, but not very successfully. Life processes are very compressed and accelerated in the short tundra summer and it was interesting to note the young bird's progress. On July 16, we observed one of the parents flying over the young, diving and screeching at it. This continued incessantly until July 22, when we first saw the young bird flying.

The jaeger has remarkable eyesight and we found them to be excellent watchdogs. Nothing happened on the slope but what they knew about it. Indeed, their presence affected the ecology of the slope in important ways. For example, any eagle which came closer than two or three miles, was promptly chased away. Occasionally we would hear the jaegers begin their high shrill calls and look in the direction they were flying to see an eagle – just a speck in the sky. The same treatment was given to other unwelcome creatures such as wolf, fox, wolverine, bear, and ermine. The elimination of these carnivores from the slope during the summer was somewhat counterbalanced by the jaegers themselves, because they essentially filled the predator niche in the food chain. They harvested many of the small rodents which occurred in abundance on the slope, i.e., shrews, lemmings, voles, and mice of various kinds. For the larger burrowing mammals, however, such as ground squirrels, pika, marmot, as well as the ptarmigan, it made for a rather trouble-free existence. The jaegers' presence may, in part, be responsible for maintaining the particularly high population of these animals on this slope.

There were other Long-tailed Jaegers in the vicinity, and they occasionally visited our slope. Generally only one other jaeger would be seen and the most we ever saw at one time was five (including the two adults and one young from our slope). The jaegers from our slope seemed

---

*This report has previously appeared in *The Canadian Field-Naturalist,* Vol. 83, pp. 138–141 (1969), and is reprinted here with permission.

†Department of Geography, University of Illinois, at time of writing; present address, Department of Geography, Portland State University, Portland, Oregon

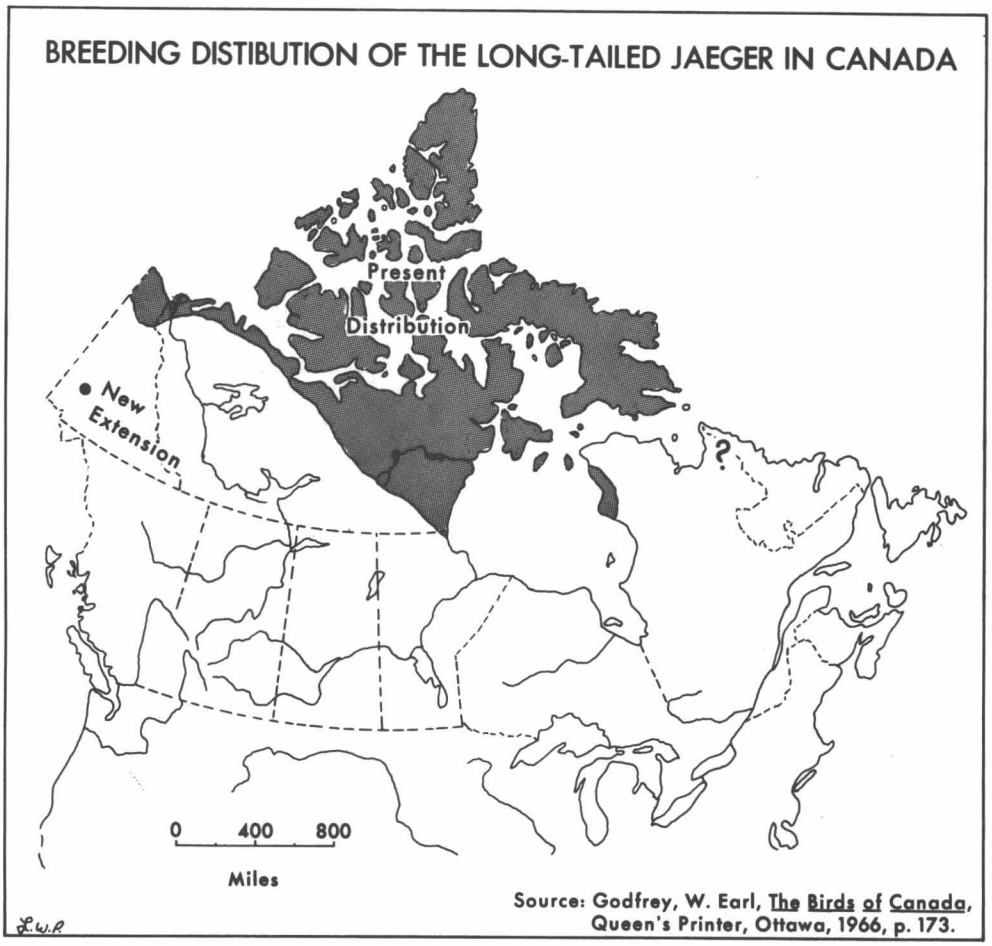

Fig. 1. Breeding distribution of the Long-tailed Jaeger in Canada.

Fig. 2. Photo of baby Jaeger taken on July 2, 1968. He is about 6 inches tall, and is assumed to be about one week old.

to resent these visitors, however, and when they came, a great deal of screaming and chasing about the sky resulted.

The time of arrival of the jaegers in the spring is not known. They were there both years when we arrived on June 18, and as mentioned, the young was born probably in the last week of June. According to Godfrey (1966), the incubation period is 23 days, so from inference, they may have arrived late in May. As to their departure in the fall, they were still on the slope in 1967 when we left on August 24. In 1968, however, they left the slope on August 10.

Acknowledgments

The author wishes to thank Miss Virginia Vincent and W. Earl Godfrey for their help in the formulative stages of this paper. Field support was provided by the Icefield Ranges Research Project of the Arctic Institute of North America.

Reference

Godfrey, W. E. (1966) The birds of Canada, *Nat. Mus. Can. Bull. No. 203,* Queen's Printer, Ottawa, 1966, 428 pp.

Interesting Fungi of the St. Elias Mountains, Yukon Territory, and Adjacent Alaska*

Orson K. Miller, Jr.†

ABSTRACT. Nine species of agarics and agaric allies are described from the tundra and boreal forests of the Yukon and Alaska. All 9 species are previously unreported from the St. Elias Mts. and adjacent Alaska. Several species are previously unreported from Canada or from North America. Descriptions and ecological data are given for all species, accompanied by drawings of the salient morphological features and photographs of 4 species.

With the aid of the Arctic Institute of North America I collected fungi in the Yukon Territory and adjacent Alaska during June, July, and early August, 1967. My field laboratory was at the base camp of the Institute's Icefield Ranges Research Project near Kluane Lake at Mile 1054 on the Alcan Highway.

I collected in forests of white spruce [*Picea glauca* (Moench) Voss], and aspen stands (*Populus tremuloides* Michx. and *P. balsamifera* L.) at low elevations, among dense willow shrubs at low and middle elevations and in tundra at high elevations. The elevation at Kluane Lake is 2,563 ft, and the limits of vegetation are from 6,000 to 7,000 ft elevation, depending on the amount of slope, aspect, proximity to glaciers and other local conditions. The yearly rainfall at Kluane Lake over the past 6 seasons has averaged 17 inches per year, with 23 inches the highest recorded. Exposed lower south slopes near the Lake have few trees and contain species of *Artemisia* and other plants adapted to very dry sites. Other lower slopes have dense tree cover (mostly *Picea glauca*) and are more moist with a well developed duff layer. The occurrence and distribution of the fungi also vary. Typical desert, forest, and tundra fungi may occur within a few hundred yards of each other.

The line drawings were made with the aid of a camera lucida. Ridgway (1912) colors are indicated in quotation marks, e.g., "verona brown." Munsell equivalents are from Hamly (1949). The collections are in the herbarium designated following the collection number, e.g., O. K. Miller 5638 (BFDL).

MARASMIUS EPIDRYAS Kühn. Ann. Soc. Lyon 79: 115–117. 1936. Figs. 1-4, 26

Pileus 5–10 mm broad, glabrous faintly striate on margin when moist, dark reddish brown, reviving when moistened. Lamellae subdistant, adnate, light yellow-brown. Stipe 25–40 x 1.5–2 mm, deep blackish brown, densely pubescent, tapering noticeably downward, inserted in substrate at base.

Spores (6.0–) 8.0–11.0 x (4.5–) 5.0–6.0 μ, elliptical in face view, almond-shaped in profile, thin-walled, hyaline in KOH and Melzer's solution, often with a large grayish oil globule. Basidia 35–45 x 7.5–8.0 μ, narrowly clavate, thin-walled, 4-spored, hyaline in KOH, yellow in Melzer's solution. Pleurocystidia and cheilocystidia 45–50 x 4.2–6.0 μ, tibiiform to narrowly fusiform, thin-walled, protruding 1/3 from hymenium, hyaline in KOH and Melzer's solution. Stipe cuticle clothed with voluminous caulocystidia 50–100 x 4–8 μ, usually cylindric to somewhat bent and irregular; thick-walled (1–2 μ thick, yellow-brown in KOH and arising from a cutis which is cellular, of thick-walled elements, and yellow-brown in KOH; pith of interwoven, thin-walled, hyaline hyphae 4–8 μ diam.

Cuticle a hymeniform palisade of pyriform cells 17–20 (–35) x 8.5–10.0 μ wide, often clamped, with slightly thickened walls, hyaline or intermixed with some which are deep yellow in KOH or Melzer's solution. Trama of pileus of interwoven hyphae 4.2–7.6 μ diam, thin-walled, hyaline in KOH, light yellowish to hyaline in Melzer's solution, with clamps. Trama of lamellae of interwoven hyphae as in pileus.

Habit, habitat, and distribution. Gregarious on dead plants of *Dryas alaskanus* A. E. Porsild which grow in open willow and alder associations usually on sand and gravel near Kluane Lake, at 2,200–2,600 ft elev. Fruiting in July following heavy rains.

Material examined. Canada; Yukon Terr.; O. K. Miller 5638 (BFDL) (K), 5809 (BFDL).

Observations. It is distinguished by its minutely pubescent stipe which characteristically tapers toward the base. The well-developed caulocystidia and pileocystidia indicate a close relationship to the genus *Xeromphalina*. Thick-walled caulocystidia illustrated by Miller (1968) in Section *Xeromphalina* subsections *Mutabile* and *Cornuae* are more

---

*This report has previously appeared in *Mycologia*, Vol. 60, pp. 1190–1203 (1968), and is reprinted here with permission.
†United States Forest Service, United States Department of Agriculture, Laurel, Maryland

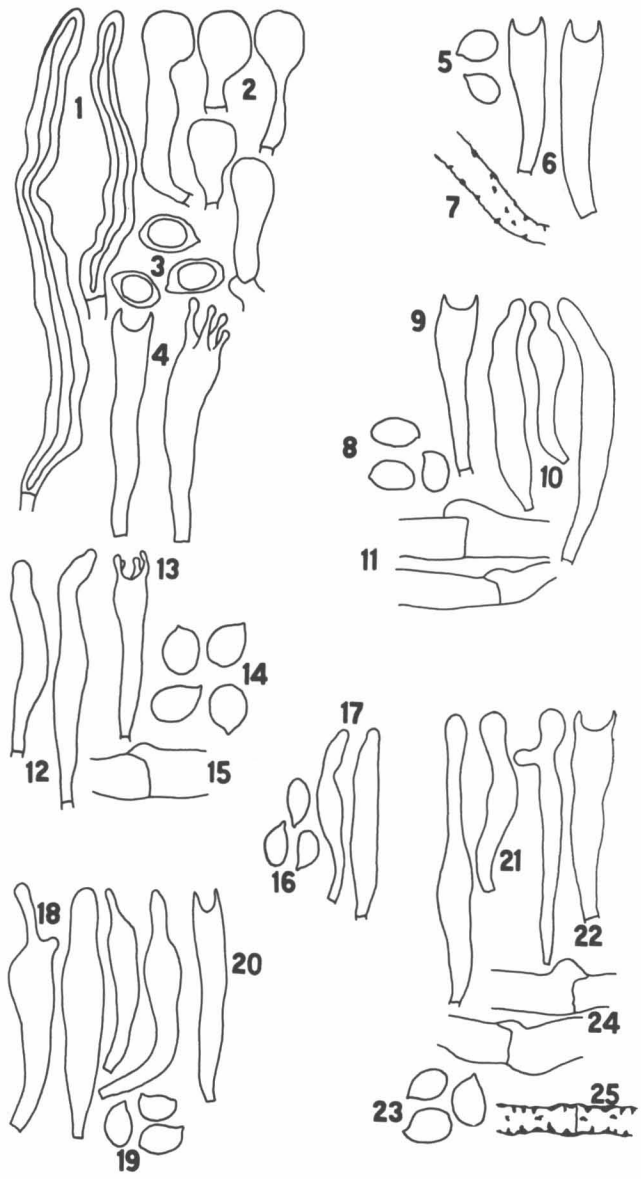

Figs. 1–4. *Marasmius epidryas.* 1. Caulocystidia. 2. Cuticular cells of pileus. 3. Basidiospores. 4. Basidia. Figs. 5–7. *Arrhenia auriscalpium.* 5. Basidiospores. 6. Basidia. 7. Incrusted cuticular hypha. Figs. 8–11. *Leptoglossum lobatum* (Amer.). 8. Basidiospores. 9. Basidium. 10. Cheilocystidia. 11. Clamped hyphae of pileus trama. Figs. 12–15. *L. lobatum* (Eu.). 12. Cheilocystidia. 13. Basidium. 14. Basidiospores. 15. Clamped hypha of pileus trama. Figs. 16–17. *Leptoglossum muscigenus.* 16. Basidiospores. 17. Cheilocystidia. Figs. 18–20. *Omphalia luteovitellina.* 18. Cheilocystidia. 19. Basidiospores. 20. Basidium. Figs. 21–25. *Omphalina pyxidata.* 21. Cheilocystidia. 22. Basidium. 23. Basidiospores. 24. Clamped hyphae of pileus trama. 25. Incrusted cuticular hypha. (All x 900).

contorted but resemble those of *M. epidryas.* The spores of the latter are not amyloid, and therefore it must be retained in *Marasmius.* Favre (1960) reported this species in Switzerland from 2,550 m down to 1,100 m following the distribution of species of *Dryas.* Lange (1955) has described *M. epidryas* from Greenland on *Vaccinium uliginosum* L. as well as on *Dryas.* To the author's knowledge this is the first report of this fungus in North America.

ARRHENIA AURISCALPIUM (Fr.) Fr. Summa Veg. Scand. p. 213. 1849. Figs. 5–7, 28

Cantharellus auriscalpium Fr. El. p. 54. 1828.

Pileus 3–9 mm high x 3–5 mm wide, spathulate, fan-shaped, sometimes nearly inverted, glabrous, moist, not viscid, brown ("bone brown" to "natal brown") fading somewhat on drying, margin somewhat scalloped. Lamellae reduced to shallow veins, often anastomosing, distinct, usually 5–7, reasonably broad in some caps, brown, "verona brown" with light brown interstices, clearly delineated from the stipe by a sterile rim. Stipe 2.5–7 mm long, 0.5–1.5 mm wide, nearly equal enlarging somewhat at base, concolorous with pileus near apex, lower 3/4 covered with a minute soft white mycelium, eccentric, never centrally attached.

Spores 6.5–8.7 x (4.5–) 5.0–6.0 μ, elliptical, thin-walled, hyaline in KOH to deep yellow in Melzer's solution. Basidia 26–39 x (7.0–) 7.5–8.5 μ, clavate, thin-walled, 4-spored, hyaline in KOH and Melzer's solution. Cystidia infrequent, fusiform, fusiform-capitate, thin-walled with hyaline or light yellowish contents in KOH or Melzer's solution.

Cuticle of upright, thin-walled hyphae 3.5–9.5 μ diam, dingy red-brown in Melzer's solution in mass, individual cells hyaline, smooth to encrusted (Fig. 7), with clamps, hyphae of subcutis interwoven. Trama of pileus of interwoven hyphae 2.5–8.5 μ diameter, with clamps, thin-walled, hyaline to yellowish in KOH or Melzer's solution. Trama of lamellae of interwoven hyphae 5–8 μ wide, thin-walled, hyaline to yellowish in KOH and Melzer's solution, clamped.

Habit, habitat, and distribution. Gregarious on hard ground in tundra composed of low prostrate mosses, fruiting in late July at 5,000 ft, Skolai Pass, Alaska. Barbara Murray and O. K. Miller OKM-5685 (BFDL) (K) (MICH).

Observations. The sterile rim which separates the hymenium from the stipe is evident on all sporophores. The stipe arises just below the hymenium, and is present on all sporophores. Extensive areas of tundra were examined but only one collection was made.

LEPTOGLOSSUM LOBATUM (Pers. ex Fr.) Ricken. Blatterpilz I. p. 6. 1915. Figs. 8–15, 27

Omphalia lobatus Pers. Syn. Meth. Fung. p. 450. 1801.
Cantharellus lobatus Fr. Syst. Mycol. p. 323. 1821.
Cantharellus lobatus Fr. Epicrisis p. 369. 1838.

Pileus 5–25 mm broad, single or several joined, crenulate, flabelliform, even, glabrous, moist, eccentric, and curved downward at maturity, brown ("verona brown," "bone brown" to "natal brown") fading in age and when

dry. Hymenium of shallow, widely separated, anastomosing veins slightly darker brown ("verona brown") than the smooth interspaces. Stipe absent or short and rudimentary, concolorous with the pileus and covered with fine, downy, white mycelium where it joins the moss stems.

Spores 6.5–9.0 (–10.0) x 4.2–5.5 (–6.6) μ, elliptical, thin-walled, with a small apiculus, hyaline in KOH and Melzer's solution. Basidia 25–39 x 6.0–7.6 μ, clavate, thin-walled, 4-spored, hyaline in KOH, dingy yellowish in Melzer's solution. Cheilocystidia and pleurocystidia 29–52 x 5.0–7.6 μ, fusiform, sometimes capitate, thin-walled, hyaline in KOH, protruding 1/3 above hymenium or sometimes not at all, infrequent, usually on the veins.

Hyphae of cuticle erect, 2.5–13 (–15) μ diam, thin-walled, with frequent clamps, hyaline or with dingy yellow-brown incrusted walls in KOH, reddish brown in Melzer's solution, often aggregated into loose fascicles. Trama of pileus a narrow layer of interwoven hyphae 5–13 μ in diam, thin-walled, with frequent clamps, hyaline to yellowish in KOH, light reddish brown in Melzer's solution. Trama of lamellae of interwoven hyphae 3.5–12 μ diam, as in pileus trama but with a dingy yellow brown sub-hymenium containing portions of incrusted hyphal walls in KOH or Melzer's solution.

Habit, habitat, and distribution. Single or gregarious on the tops of moss plants, standing erect, or commonly curved downward, joining with the living erect stems in a mass of white mycelium at the point of attachment. Fruiting in late July in tundra at 5,500 ft, on the Kaskawulsh Nunatak isolated by the Kaskawulsh Glacier in the St. Elias Mts., Yukon Terr., and on high tundra sites at 5,500–6,000 ft in the Skolai Pass at the headwaters of the White River in Alaska.

Material examined. Alaska; O. K. Miller 5686 (BFDL), 5687 (BFDL) (K), 5688 (BFDL) (BPI), 5689 (BFDL) (MICH), 5690 (BFDL) (MICH), 5691 (BFDL), 5692 (BFDL), 5693 (BFDL), 5717 (BFDL) (MASS). Yukon; David and Barbara Murray and O. K. Miller 5872 (BFDL), 5873 (BFDL). Germany; H. and P. Sydow 1419 (BPI).

Observations. The location on moss, shallowly veined lamellae, lack of stipe, and the lobed to flabelliform habit are distinctive. More than 150 spores were measured. They are elliptical (Figs. 8, 14) compared with the lachrymiform spores (Fig. 16) of *L. muscigenus.* Corner (1966) describes the spores of *L. muscigenus* as elliptical and those of *L. lobatum* as "more or less lachrymiform" but I find the reverse to be true. Clamp connections were found in all the collections of *L. lobatum* (Figs. 11, 14) and were absent in *L. muscigenus.* Cystidia are not reported by Corner (1966) in the genus *Leptoglossum,* but I found them in *L. lobatum* from the Yukon (Fig. 11) and in European material (Fig. 12). European material of *L. muscigenus* [L. Romell. Sept. 30, 1889 (BPI), H. Zimmerman Nr. 643 (BPI), P. Sydow 8.9 1905 (BPI)] also had cystidia (Fig. 17) which were identical to those in *L. lobatum.* They are most frequently found on the edges of the blunt lamellae and often protrude above the basidia. I agree with Möller (1945) that these are sterile cells, not immature basidia.

The similarities between the cystidia, spores, clavate basidia, and tramal hyphae of *Arrhenia, Leptoglossum* and *Omphalina* indicate a closer relationship to the Tricholomataceae than to the cantharelloid fungi. Figs. 27–29 show a transition from the veined to the sub-lamellate and lamellate hymenium. The tundra and arctic-alpine distribution of *Arrhenia* and *Leptoglossum* also parallels that of many species of *Omphalina.*

OMPHALIA LUTEOVITELLIAN Pilat & Nannf. Friesia 5: 22–25. 1955. Figs. 18–20

Pileus 10–18 broad, convex to convex-depressed in age, glabrous, even, moist, obscurely translucent striate at margin, yellow, ("apricot yellow," "deep chrome," to "pale yellow-orange"). Lamellae subdistant, decurrent, pale yellow, ("mustard yellow" to "apricot yellow"). Stipe 12–16 mm long 2–4 mm broad, equal or tapering somewhat toward the base, "light buff," minutely pruinose at apex to fine white tomentose below.

Spores 7.0–9.5 x 4.0–5.0 μ, elliptical, thin-walled, yellowish to hyaline in KOH and Melzer's solution, spore print buff. Basidia 34–40 x 6.0–7.6 μ, clavate, thin-walled, 4-spored, with long narrow sterigmata (± 6.0 μ long), hyaline with granular contents in KOH or Melzer's solution, projecting only slightly above basidia or not at all, infrequent but found in all the collections studied.

Cuticle a thin layer of hyphae 3.5–9.5 μ diam, thin-walled, decumbent or somewhat interwoven, hyaline in KOH or Melzer's solutions. Trama of pileus of hyphae 3.5–15 μ diam, thin-walled, cylindric to somewhat inflated, without clamps, hyaline in KOH, light reddish brown in Melzer's solution in mass. Trama of lamellae of interwoven hyphae 3.5–10 μ diam, same as pileus trama.

Habit, habitat, and distribution. Solitary in high elevation tundra (4,000–5,500 ft) where it grows in constant association (see Kallio, 1966) with the small foliose lichen, *Coriscium viride* (Ach.) Vain, on the Skolai Pass near the Russell Glacier in southeastern Alaska. Fruiting occurred following a period of cool wet weather in late July.

Material examined. Alaska; O. K. Miller, 5670 (BFDL) (K), 5677 (BFDL), 5678 (BPI).

Observations. Bigelow's (1959) report of this species from West Dawson, Yukon Terr., is the only previous report from western North America. Bigelow and Barr (1960) discuss the close relationship between *Clitocybe hudsonianus* (Jenn) Bigelow and the above fungus. Favre (1955) reports it from the Swiss Alps and Lange (1955) discusses its distribution in Greenland and the mountains of Norway. He reports that he has never found it below timber line or in Denmark and observes that "it seems to

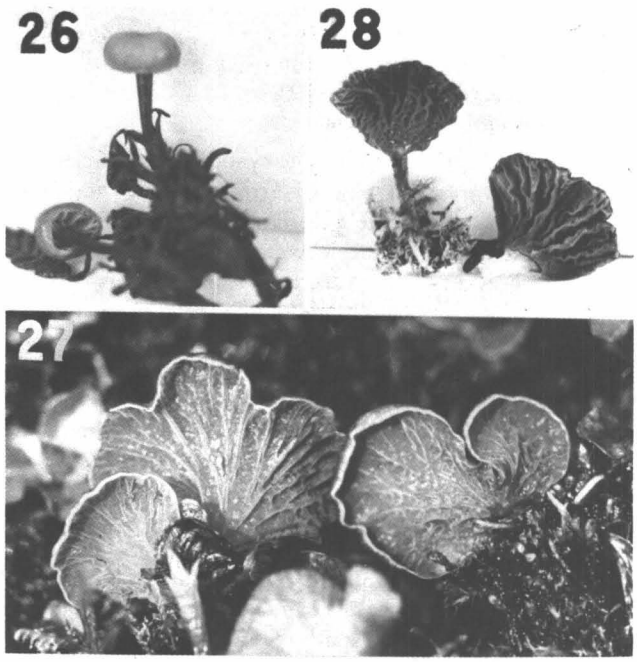

Fig. 26. *Marasmius epidryas,* x 2 (OKM 5809). Fig. 27. *Leptoglossum lobatum,* x 2.5 (OKM 5689). Fig. 28. *Arrhenia auriscalpium,* x 2.5 (OKM 5685).

be one of the few species restricted to arcto-alpine regions." The occurrence of *O. luteovitellina* in North America supports this hypothesis. I will retain this species in *Omphalia* until a comparative study of the omphaloid fungi is completed, with emphasis on: the presence or absence of cystidia, spore size and color, and descriptions of fresh specimens. A viscid species, *Hygrophorus vitellinus* Fr., sensu Möller, without cystidia was reported from Arctic Alaska by Kobayasi et al. (1967) and it seems to resemble *O. luteovitellina.* The waxy appearance of the lamellae is a character which must be checked in all fresh collections which are referred to *Hygrophorus.* Favre (1955) described *O. luteolilacina* Favre, which is also associated with the lichen, *Coriscium viride.* It has no clamps, an apricot tinted pileus, and a stipe which is tinted lilac.

OMPHALINA PYXIDATA (Bull. ex Fr.) Kumm. Fuhrer. Pilzkunde p. 107. 1871. Figs. 21–25, 29

Agaricus pyxidatus Fr. Syst. Mycol. p. 164. 1821.

Pileus 7–17 mm broad, convex, convex depressed in age, even, glabrous with translucent marginal striations, brown ("verona brown" to "warm sepia"), lamellae decurrent, subdistant, "pinkish buff," often forking. Stipe 14–22 mm long, 1–3 mm wide, dry, glabrous, even "pinkish cinnamon" darkening to "orange cinnamon" near the apex.

Spores 7.5–9.5 x 5.0–6.0 μ, short elliptical, thin-walled, smooth, hyaline in KOH, yellowish in Melzer's solution. Basidia 30–40 x 7–8 μ, clavate, thin-walled, 4-spored, hyaline in KOH and Melzer's solution. Cheilocystidia 32–50 x 6.0–8.0 μ, narrowly fusiform, thin-walled, protruding about 1/3 of total length, hyaline in KOH or Melzer's solution. Pleurocystidia infrequent, usually near gill edge, resembling cheilocystidia.

Cuticle a thick layer of erect to loosely interwoven hyaline hyphae 3.5–15 (–17) μ, interspersed with hyphae covered with dingy yellow-brown incrustations (Fig. 25), often clamped, combined with a few deeply pigmented yellow-brown oleiferous hyphae as seen in KOH or Melzer's solution. Trama of pileus of interwoven hyphae 3.5–13 μ diam, simply branched, often clamped, largely hyaline with an occasional oleiferous hypha or very lightly incrusted wall in KOH resulting in a very light yellow-brown cast to the tissue. Trama of lamellae of loosely parallel hyphae 2.5–11 μ diam, thin-walled, mostly hyaline, often clamped, also containing scattered deep yellow-brown hyphae.

Habit, habitat, and distribution. Single to gregarious usually in moss on tundra near the Russell Glacier and in the Skolai Pass at 4,000-5,000 ft, southeastern Alaska.

Material examined. Alaska; O. K. Miller 5679 (MICH), 5680 (BPI), 5681 (BFDL), 5682 (K), 5683 (BFDL), 5684 (MASS), 5816 (BFDL); Sweden; Lundell & Nanfeldt 1756 (BPI), 1757 (BPI).

Observations. The description of *O. pyxidata* given by Favre (1955) agrees with the characters recorded for this small *Omphalina* found commonly in the tundra of the Yukon and Alaska. The microscopic characters of (Nos. 1756 & 1757) in the Fungi Exsiccati Suecici at The National Fungus Collections agree with those of the Yukon and Alaskan collections.

PANELLUS PATELLARIS (Fr.) Konr. & Maubl. Icon. sel. fung. VI, p. 379. 1924. Figs. 30–31

Panus patellaris Fr. Epicr. p. 400. 1838.

Pileus 8–15 mm broad, eccentric, convex, viscid to glutinous at first, soon becoming fibrillose to villose and

Fig. 29. *Omphalina pyxidata,* x 3.0 (OKM 5679).

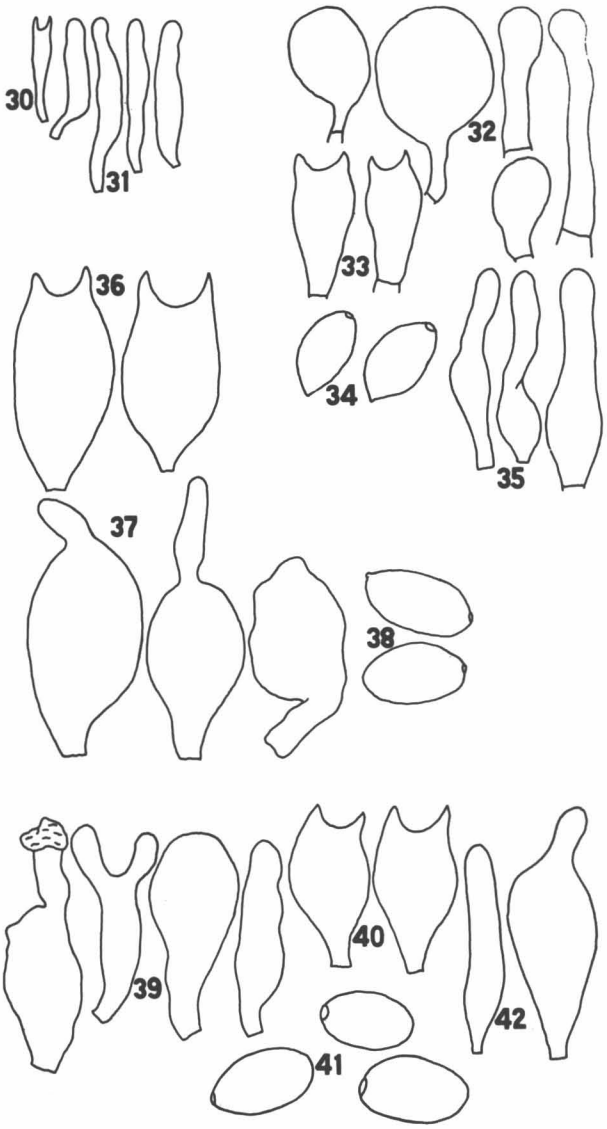

Figs. 30–31. *Panellus patellaris.* 30. Basidium. 31. Cheilocystidia. Figs. 32–35. *Panaeolus campanulatus.* 32. Five cuticular cells of pileus. 33. Basidia. 34. Basidiospores. 35. Three cheilocystidia. Figs. 36–38. *P. solidipes.* 36. Basidia. 37. Cheilocystidia. 38. Basidiospores. Figs. 39–42. *P. semiovatus.* 39. Cheilocystidia. 40 Basidia. 41. Basidiospores. 42. Cuticular cell of pileus (All x 900.)

moist to dry, brown, "snuff brown." Lamellae subdistant, narrow, "cinnamon-buff," covered at first by a thin membranous, dry "pinkish buff" veil which soon disappears leaving no trace of its presence at maturity. Stipe 1–3 mm long x 0.5–1.5 mm wide, equal, dry, usually somewhat curved or sometimes nearly absent. Context a narrow water-soaked brown, "sayal brown" layer just beneath the glutinous cuticle, remainder of context of pileus and stipe of firm pale cinnamon tissue, "pale pinkish cinnamon."

Spores 4.5–5.5 x 0.5–1.5 μ, allantoid, thin-walled, amyloid (light blue) in Melzer's solution, to hyaline or very light yellowish in KOH, spore print white; test for amyloidity carried out using masses of spores. Basidia 17–28 x 3.5–4.2 μ, narrowly clavate, thin-walled, 4-spored, hyaline in KOH and Melzer's solution. Cheilocystidia 22–35 x 3.5–5.0 μ, clavate to fusiform, thin-walled, hyaline with some yellowish contents in KOH and Melzer's solution, protruding 1/3 to 1/2 of total length. Pleurocystidia—none seen.

Cuticle of pileus a thick-gelatinous layer of interwoven hyphae 1.5–3.5 μ diam, thin-walled, clamps frequent, hyaline except for a thin pigmented zone near the surface; trama of pileus of interwoven hyphae 2.5–3.5 μ in diam, thin-walled, clamps frequent, dingy yellow brown near cuticle, otherwise yellowish to hyaline in KOH or Melzer's solution. Trama of lamellae of interwoven hyphae 2.5–4.5 μ diam, thin- and thick-walled (1.5 μ diam), hyaline in KOH, hyaline or occasionally yellow contents in Melzer's solution.

Habit, habitat, and distribution. On alder and willow sticks in white spruce near Mile 1,058 Alcan Highway, Yukon Terr., Can., fruiting at about 2,300 ft in mid-July.

Material examined. Canada: Yukon Terr.; O. K. Miller 5547 (BFDL), 5639 (BFDL); U. S. A.: New York; *Panus operculatus,* 1884 (NY).

Observations. Fresh spore prints on paper and on agar were examined in Melzer's solution. The blue color was obvious at once. The spores are typical of other species of *Panellus.* In addition, a cross section of the veil (operculum) shows it to be, at least in part, nothing more than the inrolled margin of the pileus complete with rudimentary lamellae. I would retain this species in *Panellus* until a study of the development of closely related species can be completed. The viscid to glutinous cuticle in young caps is mentioned by Fries (1863) and Konrad and Maublanc (1948), but not by Singer (1962) or Kuhner and Romagnesi (1953). In addition, a collection of *Panus operculatus* Berk. & Curt (NY) was found to have cell walls which were thicker than the above fungus from the Yukon, but in other aspects it is quite similar.

PANAEOLUS CAMPANULATUS (Fr.) Quel. Fl. Mycol. p. 54, 1888. Figs. 32–35

Agaricus campanulatus Fr. Syst. Mycol. p. 295. 1821.

The pileus is brown to dark-brown over the disc with an indefinite gray over the margin. The white appendiculate veil has a tooth-like appearance on the margin in young caps. The microscopic characters agree with those given by Smith (1949) with spores 16–18.5 x 8.5–10 μ, broadly elliptical in profile, lemon-shaped in face view. Cheilocystidia are 25–42 x 6.5–11.0 μ, thin-walled, laginiform to nearly cylindric with a basal swelling. The cuticle is composed of a hymeniform palisade of pyriform to globose elements 20–45 x 10–24 μ with scattered elongate nearly cylindric pileocystidia 28–61 x 6–8 μ. Fruiting on horse dung during rainy weather, Cultis Bay, Kluane Lake. (OKM 5593 BFDL).

P. sphinctrinus Fr. is closely related but has grayish green to olivaceous colors in the pileus and the pileus margin is appressed to the stipe in young caps like a narrow

collar according to Kuhner and Romagnesi (1953, Fig. 457). *P. retirugis* has a reticulate veined disc and somewhat shorter spores.

PANAEOLUS SOLIDIPES Pk. Ann. Rep. N.Y. St. Mus. 23: 101. 1872. Figs. 36–38

The single large specimen has a pileus 6 cm broad, moist, obtusely campanulate and "vinaceous-buff" with scattered "avellaneous" appressed squamules. The 18 cm long exannulate stipe was ridged over the upper 2/3 with fine lines. The spores are large, 20–22 x 11–12.5 μ, elliptical with an apical pore. Pleurocystidia and cheilocystidia 25–52 x 8–23 μ, ventricose-rostrate, ventricose to sphaeropedunculate, thin-walled, hyaline or with fine yellow-brown granular content; intermixed with chrysocystidia. The pileus cuticle is a hymeniform palisade of large clavate to broadly fusiform cells 40–70 x 10–22 μ, which break down in early maturity leaving a subcutis of interwoven hyphae. Fruiting on horse dung during rainy weather, Cultis Bay, Kluane Lake, (OKM 5593 BFDL).

This fungus is separated from other species of *Panaeolus* by its large size, distinctive chrysocystidia (Fig. 37), large spores (Fig. 38), and basidia (Fig. 36), lack of an annulus and the fine lines near the upper part of the stipe.

PANAEOLUS SEMIOVATUS (Fr.) Lund. Fung. Exsic. Suec. Fasc. XI–XII p. 14. 1938[1]. Figs. 39–42

Agaricus semiovatus Fr. Syst. Mycol. p. 300. 1821.
Panaeolus separatus Fr. Epicr. p. 234. 1838.

The Yukon material does not differ from specimens collected and examined by the author in other places in North America. The abundant, characteristic clavate-rostrate to flexuous cheilocystidia, 29–45 x 6.5–21 μ, are a distinctive feature of this species and separate it microscopically from the younger sporophores of *P. solidipes* Pk. The persistent annulus and viscid pileus separate it from all other species of *Panaeolus*. The cuticle is a hymeniform palisade of clavate, fusiform or clavate-rostrate cells 40–70 x 8–18 μ, but they collapse or partially disintegrate in early maturity. This species has been placed in a separate genus, *Anellaria*, by Karsten and accepted by Singer (1962). The veil which adheres to the stipe when the cap expands and the viscid pileus are used as generic characters.

Herds of horses are maintained by guides at low elevations in the vicinity of Kluane Lake, where unrestricted grazing is permitted. In these areas this species was frequently encountered on horse dung during July. O. K. Miller 5543 (BPI), 5549 (BFDL), 5585 (BFDL), 5775 (BPI).

[1] Lundell explains the nomenclatural problem.

Acknowledgments

I would like to thank Robert Faylor, Philip Upton, and Richard Ragle of the Arctic Institute of North America for their support which made this expedition possible. I also wish to express my appreciation to Hope Miller, Dr. and Mrs. David Murray, A. H. Tinker, Virginia Vincent, and the others who collected fungi in remote locations in the Yukon and greatly aided in making the 1967 season a success. Dr. Alexander H. Smith and Dr. John G. Palmer gave valuable assistance and criticism in the preparation of the paper. John A. Lindsay assisted in the preparation of material for study and the preparation of plates. The curators of the following herbaria very kindly loaned material for the study: The National Fungus Collections, Kew, and the University of Michigan Herbarium.

References

Bigelow, H. E. (1959) Notes on fungi from northern Canada, IV, Tricholomataceae *Can. J. Bot.*, 37, 771.
Bigelow, H. E., and Barr, M. E. (1960) Contribution to the fungus flora of northeastern North America, *Rhodora*, 62, 189–190.
Corner, E. J. H. (1966) *A Monograph of Cantharelloid Fungi*, Oxford Univ. Press, London, 255 pp.
Favre, J. (1955) Les champignons supérieurs de la zone alpine du Parc National Suisse, Ergeb. Wiss. Untersuch. Schweiz, *National Parks*, 5, 43–44.
Favre, J. (1960) Catalogue descriptif des champignons supérieurs de la zone subalpine du Parc National Suisse, Ergeb. Wiss. Untersuch. Schweiz, *National Parks*, 6, 323–610.
Fries, E. (1863) *Monogr. Hymen. Sueciae, Vol. 2.*
Hamly, D. H. (1949) The Ridgway color standards with a Munsell notation key., *J. Opt. Soc. Am.*, 39, 592–599.
Kallio, Paavo (1966) Observations on the lichens of Labrador and Ungava, *Ann. Univ. Turku*, 36, 85–100.
Kobayasi, Y., and others (1967) Mycological studies of the Alaskan Arctic, *Ann. Rept.*, Inst. Ferment., Osaka, No. 3, 138 pp.
Konrad, P., and Maublanc, A. (1948) *Les Agaricales*, Lachevalier, Paris, 469 pp.
Kuhner, R., and Romagnesi, H. (1953) *Flore Analytique des Champignons Supérieurs*, Masson, Paris, 556 pp.
Lange, M. (1955) II Greenland Agaricales, *Medd. Grønland*, 147, 1–69.
Miller, O. K. (1968) A revision of the genus *Xeromphalina*, *Mycologia*, 60, 156–188.
Möller, F. H. (1945) *Fungi of the Faroes*, Einor Munksgaard, Copenhagen, 294 pp.
Ridgway, R. (1912) *Color Standards and Color Nomenclature*, The Author, Washington, 44 pp.
Singer, R. (1962) *The Agaricales in Modern Taxonomy*, 2 ed., J. Cramer, Weinham, 915 pp.
Smith, A. H. (1949) *Mushrooms in Their Natural Habitats*, Sawyer's, Portland, Ore., 626 pp.

Notes on Gastromycetes of the Yukon Territory and Adjacent Alaska*

Orson K. Miller, Jr.†

ABSTRACT. *Cyathus* in the Nidulariales and seven species in five genera of Lycoperdales including *Battarrea, Calbovista, Calvatia, Lycoperdon,* and *Tulostoma* are reported from the Yukon Territory and adjacent Alaska. Descriptions and notes of each species are given and accompanied by photomicrographs of the salient microscopic characters. Macrophotographs of four species are included.

Introduction

The species reported were collected in the summer of 1967 in the St. Elias Mts. and near Kluane Lake, the Skolai Pass in the Alaskan Range, and the vicinity of Juneau, Alaska. The author worked in cooperation with the Arctic Institute of North America as a member of the Icefield Ranges Research Project. Logistical support and facilities of the Arctic Institute's base camp at Kluane Lake enabled the author to reach remote areas to study and collect fungi.

Ridgway (1912) colors are indicated in quotations marks, e.g., "ferruginous". Each collection is deposited in the herbarium designated after the collection number, e.g., O. K. Miller 6233 (BFDL).

Battarrea phalloides (Dicks.) Pers. Persoon Syn. Fung. 129. 1801. Fig. 1.

Sporophore 3.5 cm wide, 3 cm high, ovoid, usually with a smooth, membranous, light brown, peridium but only the lower recurved pallid peridium remained in my specimens; the top had dehisced circumscissilally and was gone, revealing a brown gleba ("ferruginous", "cinnamon-rufous", to "kaiser brown"). Stipe 22 cm long, 6–10 mm wide, woody with thin, fibrillose, fine scales, light brown, thickening somewhat in center and tapering toward the apex. Volva missing in my specimens, usually ovoid, whitish, and fragile (Long 1943) often with inner membranous leaflets. However, Long (1943) stated that the volva often rots and is lost at an early age.

Spores 5.5–8.5 x 4.4–6.6 μ, subglobose to short elliptical with thick, blunt warts, dingy brown in KOH, appearing nearly echinulate in H_2O. Capillitium of elaters 27–46 (–75) x 5–6 μ in diameter, hyaline contents with distinct yellow-brown bands, usually not spiraled (Fig. 1), scattered throughout the gleba but not abundant.

Habitat and distribution. On the ground of a rock glacier, at about 3500 ft elevation, on Sheep Mt. near Kluane Lake, collected by Peter Johnson, O. K. Miller 6233 (BFDL). Fruiting in August in a very dry habitat occupied by *Artemisia* species and other plants characteristically found on dry sites.

Observations. No volva was obtained with the collection so the key characters as described for *B. laciniata* Underwood by White (1901) could not be examined. However, *B. laciniata* is a stocky, robust fungus as described by Long (1943), and does not agree with the description of *B. phalloides.* I have not been able to find any record of a *Battarrea* this far north. However, the Arctic Institute has recorded an annual average rainfall of only 17 in. in this general area over the past 6 years at the Institute's base camp at nearby Kluane Lake (personal communication, Richard Ragle). Desert-like conditions prevail on the south-facing slopes of Sheep Mt. from about 2200 to 4000 ft elevation. Arid conditions in this local area could easily account for the unusual northern distribution of the desert fungus, *B. phalloides.*

Calbovista subsculpta Morse. Mycologia, 27: 96–101. 1935. Figs. 2–4.

Sporophore 7.5 cm broad, 7.5 cm high, globose, tapering somewhat just at base; exoperidium dull white, composed of low warts with a central fascicle of hairs, dingy brown to vinaceous tinged at the apex, lower sides and base are smooth; endoperidium a thin layer which is dull to shiny whitish and often very indistinct. Gleba white at first then yellow to red-brown, finally dark brown ("snuff brown" to "bister") at maturity. Subgleba well developed, dull white.

Spores (3–) 4–5 μ, globose, thin-walled, some appear to have minute pores in the wall, usually uniguttulate, light yellowish in KOH with a minute, thin apiculus. Capillitium of fascicles of antler-like hyphae 4–9 μ in diameter, walls thin to thickened, bluntly pointed, light yellow-brown in KOH and Melzer's solution; irregularly inflated or

---

*This report has previously appeared in the *Canadian Journal of Botany,* Vol. 47, pp. 247–250 (1969), and is reprinted here with the permission of the National Research Council of Canada.

†United States Forest Service, United States Department of Agriculture, Laurel, Maryland

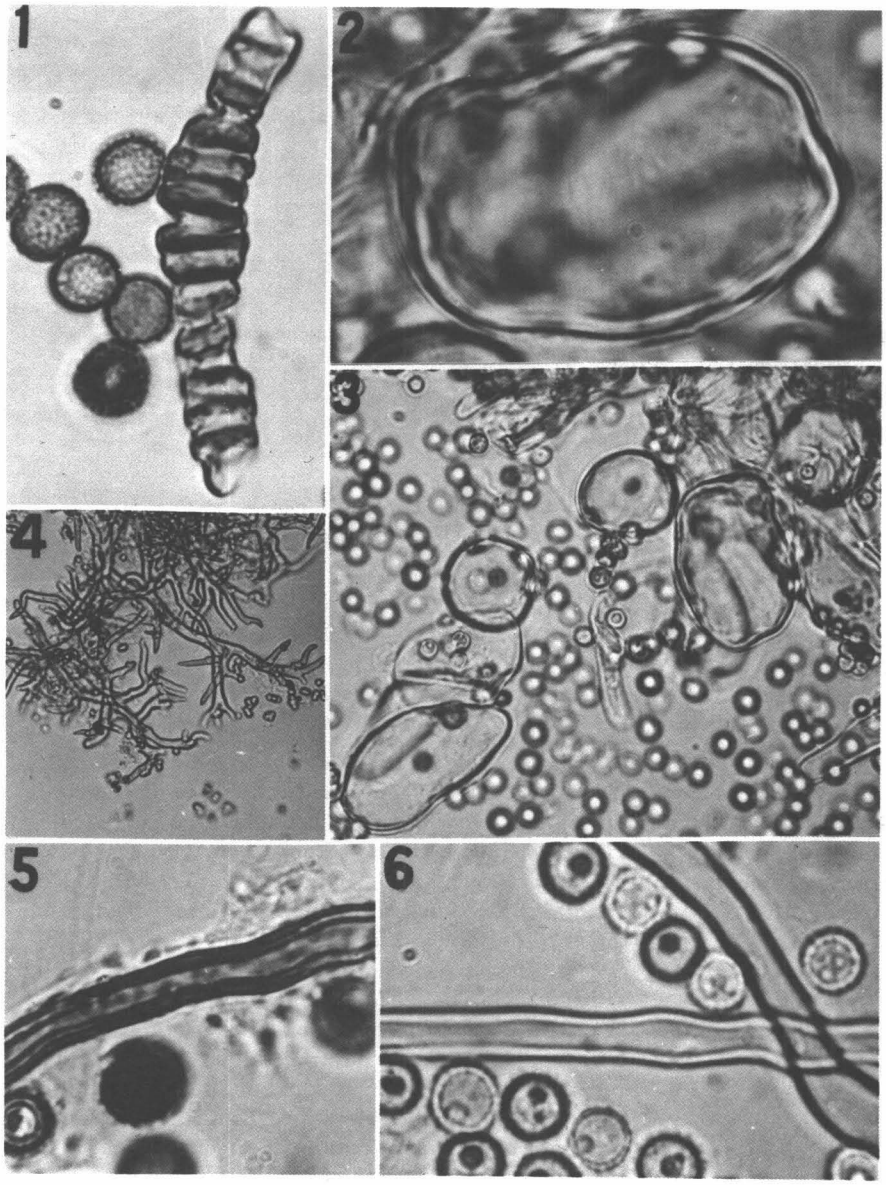

Fig. 1. *Battarrea phalloides.* Spores and elater (x 1800). Figs. 2–4. *Calbovista subsculpta.* Fig. 2. Inflated thick-walled cell of capillitium (x 1800). Fig. 3. Inflated cells of capillitium and spores (x 800). Fig. 4. Antler-like capillitial elements (x 200). Fig. 5. *Calvatia cretacea.* Incrusted thick-walled capillitial element (x 1800). Fig. 6. *Calvatia artica.* Smooth, thick-walled capillitial elements and spores with echinulations or minute warts (x 1800).

swollen cells up to 36 μ long with thickened walls (± 1.5 μ thick) scattered throughout (Figs. 2, 3), often infrequent but always present, hyaline in KOH and Melzer's solution.

Habitat and distribution. Growing on hard ground near white spruce *(Picea glauca* [Moench] Voss.) in July, Mile 82, Haines Highway, Yukon Terr., Canada.

Material examined. CANADA: Yukon; O. K. Miller 5772 (BFDL). U.S.A.: California; E. E. Morse, Soda Springs, May 9, 1934 (TYPE) (BPI); E. E. Morse, Yosemite Valley, May 9, 1935 (BPI). Idaho; O. K. Miller 4031 (BFDL).

Observations. The obscurely duplex peridium and the distinctive fascicles of antler-like capillitial elements (Fig. 4), illustrated by Morse (1935), pl. 15B), distinguish this genus from other genera. The spines found on the capillitial elements of *Mycenastrum* (Morse 1935, pl. 15A) separate the genus *Mycenastrum* from *Calbovista. Calvatia* may have attenuated terminal elements but they are seldom short-branched and never antler-like. However, the irregularly inflated to swollen cells of *C. subsculpta* shown in Figs. 2 and 4 have not been previously described. A number of specimens from different areas were studied to determine the extent and distribution of these cells. It was also deemed desirable, therefore, to include a complete description of the species. Inflated cells were found in the type and in all the collections studied to date (cited above). Cells of this type have not been seen by the author in *Calvatia* or *Mycenastrum.* To the author's knowledge this is the first report of *C. subsculpta* in the Yukon or in Canada.

Calvatia cretacea (Berk.) Lloyd. Mycol. Notes, No. 46, pp. 650–651. 1917. Fig. 5.

This species was found in tundra above the Slims River at ± 5000 ft elevation, fruiting in early July. The spores

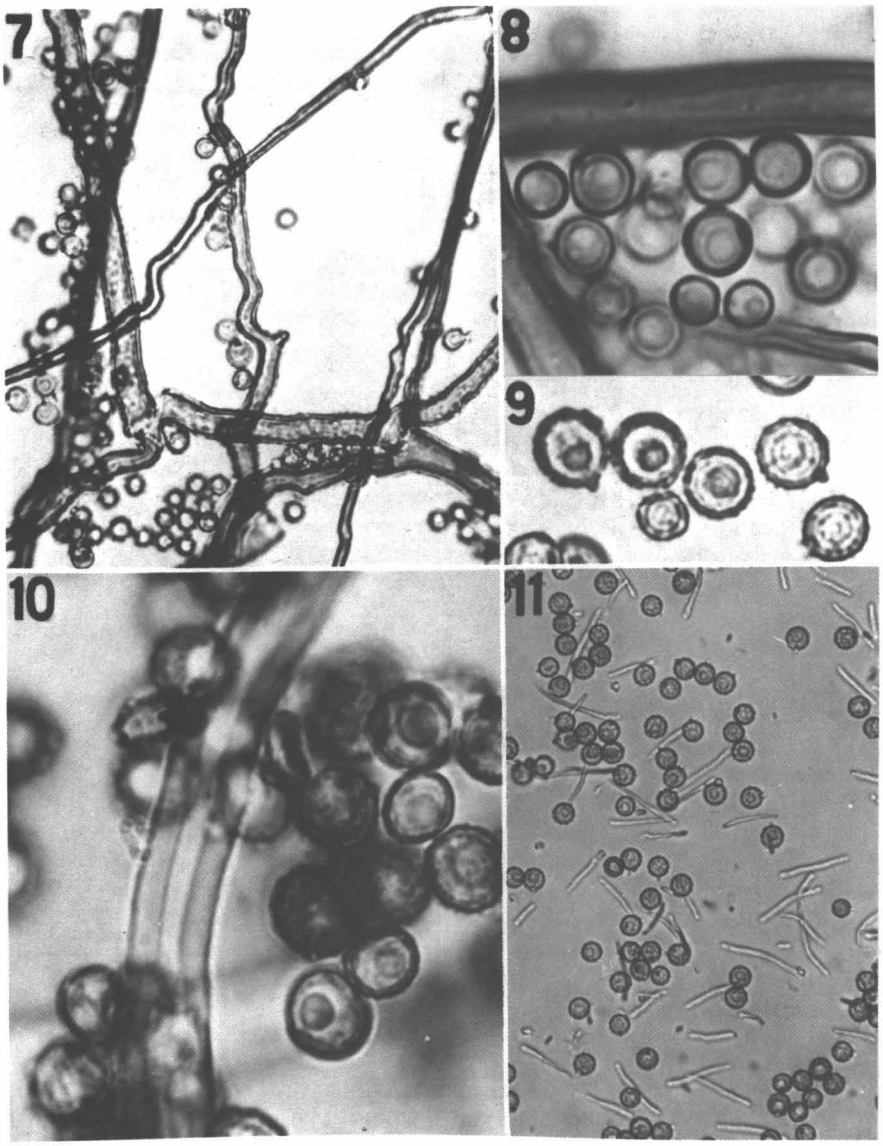

Figs. 7–8. *Lycoperdon pusillum.* Fig. 7. Crooked capillitial elements (x 800). Fig. 8. Nearly smooth spores with an eccentric oil drop (x 1800). Figs. 9 and 11. *Lycoperdon umbrinum.* Fig. 9. Spores with low blunt warts (x 1800). Fig. 11. Spores with pedicles broken off and floating in the medium (x 800). Fig. 10. *Tulostoma simulans.* Spores with warts and thick-walled capillitial element (x 1800).

are globose, 5.0–6.0 μ, with blunt, dark brown warts and walls in 3% KOH and have a short, hyaline pedicle. The capillitium consists of hyphae 3.5–6.0 μ wide, occasionally branched, thick-walled (walls 1.0–2.0 μ thick) with rounded pits, frequently incrusted (Fig. 5) and yellowish to light yellow-brown in KOH. Zeller and Smith (1964) emphasized these characters in the separation of this species from *C. arctica* and *C. polygonia.*

Dearness (1923) reported *C. cretacea* from Herschel Island, Yukon Terr., and the Mackenzie River delta, Yukon Terr. Bowerman and Groves (1962) reported it from Keno, Yukon Terr.

In tundra near the Slims River at Kluane Lake, Yukon Terr. O. K. Miller 5523 (BFDL).

Calvatia arctica Ferd. & Winge. Medd. om Grønl. XLIII, pp. 142–145. 1910. Figs. 6, 12.

Sporophore 3–5 cm broad, 5–7 cm high, ovoid to somewhat pyriform, dull white, low warts over the top but not on the sterile base, white rhizomorphs proliferating from base. Gleba white at first, then yellowish, finally dull brown. Subgleba of minute chambers (three to five per millimeter), white, occupying the lower one-fourth of the base.

Spores 4.0–6.0 μ, globose, echinulate or with minute warts, hyaline with light yellowish walls, and a short, hyaline pedicle. Numerous indistinct warts or echinulations up to ± 0.5 μ high. Capillitium of occasionally branched hyphae 3.5–7.0 μ, thickened walls (±0.5 μ thick) with rounded pits, not incrusted (Fig. 6), hyaline or faintly yellowish in 3% KOH.

Habitat and distribution. Found only in tundra at 4500-5000 ft elevation in the Yukon and in the Skolai Pass, Alaska. Fruiting occurs in late July.

Material examined. CANADA: Yukon Terr.; O. K. Miller 6258 (BFDL). U.S.A.: Alaska; O. K. Miller 5699 (BFDL).

Observations. The light yellow capillitium without incrustations and the pale yellowish, small warts on the spores as described by Zeller and Smith (1964) separate this fungus from *C. cretacea,* which it closely resembles. The latter species has been reported from the Arctic and Subarctic in North America by Dearness (1923) and Kobayasi *et al.,* (1967). Bowerman and Groves (1962) discussed the presence of *C. arctica* in Canada and concluded that it is synonymous with *C. cretacea.* However, Lange (1948) and Zeller and Smith (1964) retained it as a separate species. I have, therefore, included a complete description of my material and a photograph of it. Further study of fresh material seems essential before a decision can be reached concerning the validity of this species. A specimen labelled *C. arctica* in the Lloyd Herbarium (BPI) No. 34254 has a smooth peridium, heavily incrusted capillitial threads, and spores with dull, blunt, dingy brown warts. It is badly crushed so any positive identification is impossible but the characters stated above would rule out *C. arctica.*

Lycoperdon pusillum Pers. Persoon Syn. Fung. 138. 1801. Figs. 7–8, 14.

The single sporophore found measured 12 mm high and 11 mm wide with no sign of a subgleba. The globose, minutely echinulate spores, with an eccentric oil drop (Fig. 8); contorted to crooked capillitium (Fig. 7) with many pores and the general life form (Fig. 14) of this small puffball are the characters which make it a distinctive species. Smith (1951) indicated that it is on "thin soil" and on "waste land." Lange and Hora (1963) described it under the name *L. ericetorum* Pers. and indicated that it is found in heaths in central Europe. Bowerman (1961) reported it from a number of localities in eastern Canada. Lange (1948) found it only once in Greenland and regarded it as a rare species there.

A single sporophore was found in tundra on the Kaskawulsh Nunatak on July 26, 1967, by David and Barbara Murray (O. K. Miller 5900 BFDL).

Lycoperdon umbrinum Pers. var. *umbrinum.* Persoon Syn. Fung. p. 147. 1801. Figs. 9, 11, 15.

This species was solitary to gregarious on the ground in low elevation forested areas, 2000-3000 ft elevation, often under aspen. It has been reported from northern Alaska by Kobayasi *et al.,* (1967) and from the Canadian Arctic by Dearness (1923) and Bowerman and Groves (1962). It is reported by Lange (1948) and others from widely separated areas of the European Arctic and by Favre (1960) in the Swiss Alps.

The pyriform fruiting bodies with dense woolly tufts of hyphae over the upper part of the sporophore are shown in Fig. 15, which also well illustrates the conspicuously chambered subgleba. The spores are globose 3.5–5.5 μ and verucose (Fig. 9) with low, blunt, truncate warts. The pedicles, which are 6–10 μ long, are usually broken off and floating in the medium as illustrated in Fig. 11.

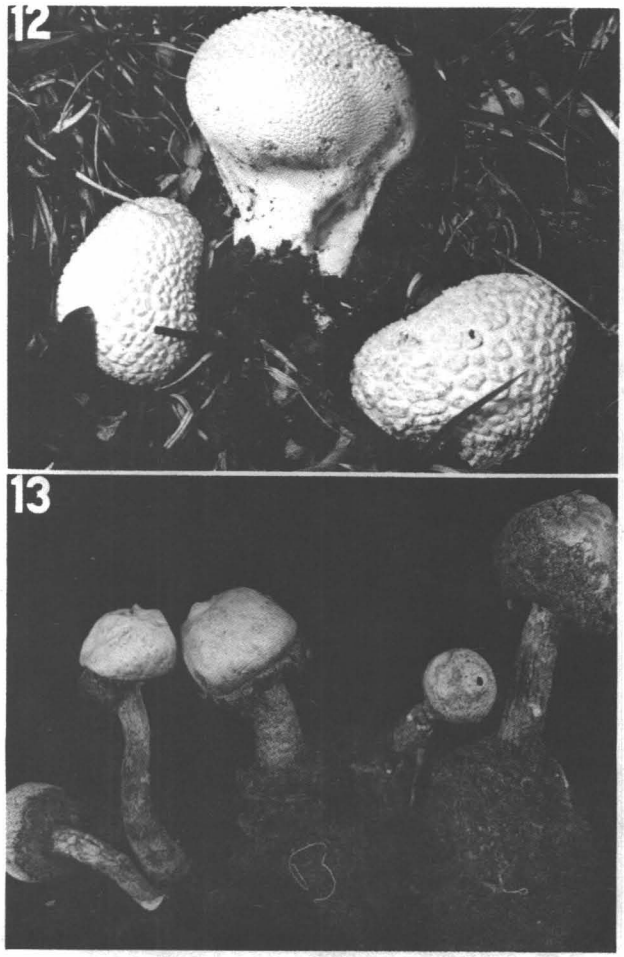

Fig. 12. *Calvatia arctica* OKM 5699 (x¾). Fig. 13. *Tulostoma simulans* OKM 5499 (x 2).

Material examined. CANADA: Yukon Terr.; O. K. Miller 5785 (BPI), 5789 (BFDL), 5790 (BFDL), 5840 (BFDL). U.S.A.: Alaska; O. K. Miller 5970 (BFDL), 5997 (BPI).

Tulostoma simulans Lloyd. Mycol. Writ. 2: 18. 1906. Figs. 10, 13.

Sporophore with an oval spore case 4–10 mm high x 5–13 mm wide; peridium smooth, dull whitish in age, membranous, covered at first with particles of sand and possessing a round slightly raised, apical pore. Gleba reddish brown, exposed in age at base surrounding the inserted stalk which is 10–20 mm long x 1.5–3 mm wide, nearly equal, appressed fibrillose to somewhat lacerate, dull brown, longitudinally ridged in some when dry; the base consists of a loose ball of mycelium and sand. Context of stalk pallid, firm, with a hollow center containing silky threads.

Spores 5.0–7.5 x 5.0–6.0 μ, subglobose to globose, with warts up to 0.9 μ high, yellow-brown in H_2O, KOH, and Melzer's solution, often appearing somewhat echinulate in KOH and seemingly surrounded by a thin mucilaginous sheath in H_2O. Capillitium of hyphae 2.0–6.0 μ

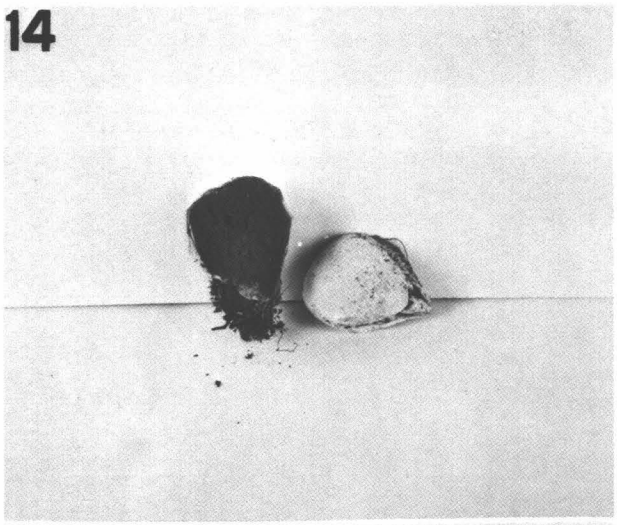

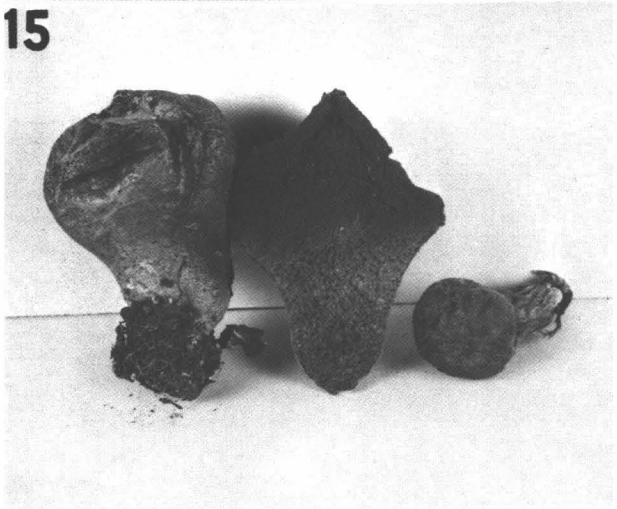

Fig. 14. *Lycoperdon pusillum* OKM 5900 (x1¼). Fig. 15. *Lycoperdon umbrinum* OKM 5970 (x1).

wide, intermixed thin- and thick-walled (±1.5 μ thick), nearly equal or with swellings at the septa, simple branching, hyaline to light yellowish in KOH and Melzer's solution.

Habitat and distribution. Buried in sand along an intermittent stream near the Donjek River, Mile 1130 Alcan Highway, Fruiting in early July after heavy June rains.

Material examined. CANADA; O. K. Miller 5499 (BFDL).

Observations. Tulostoma brumale Pers. has smaller, largely globose spores 3.5–4.4 (– 5.0 μ) with minute warts and echinulations and a nearly naked peridium in youth. However, in all other respects *T. simulans* Lloyd is similar and closely related to *T. brumale.* It is interesting to note that the capillitium of both species has thick-walled hyphae (Fig. 10) which are identical but not described or compared by most authors.

Cyathus striatus Pers. Persoon Syn. Fung. 237. 1801.

The shaggy tangled fibrils over the epiphragm and the rest of the sporophore, the shiny striate drab to gray-brown inner surface, along with the typical pad of cinnamon-brown mycelium at the base of the sporophore, are distinctive characters of this common species. It was found on hardwood sticks between willow shrubs, near Kluane Lake, A. H. Tinker and O. K. Miller 6253 (BFDL).

Acknowledgments

I greatly appreciate the help and support of Robert Faylor, Richard Ragle, and Philip Upton of the Arctic Institute of North America. I thank Hope Miller, Dr. and Mrs. David Murray, A. H. Tinker, and the others who collected valuable specimens during the 1967 season. Dr. Kent McKnight of the National Fungus Collections and Dr. Harold Burdsall of the Beltsville Forest Disease Laboratory made valuable comments and suggestions during the preparation of this paper. The curator of the National Fungus Collections very kindly loaned material for the study.

References

Bowerman, C. A. (1961) Lycoperdon in eastern Canada with special reference to the Ottawa District, *Can. J. Bot.,* 39, 353–383.

Bowerman, C. A., and Groves, J. W. (1962) Notes on fungi from northern Canada, V, Gastromycetes, *Can. J. Bot.,* 40, 239–254.

Dearness, J. (1923) Fungi, *Rept. Can. Arctic Exped.,* 1913–1918, Vol. 4, Bot., Pt. C, King's Printer, Ottawa, 24 pp.

Favre, J. (1960) Catalogue descriptif des champignons supérieurs de la zone subalpine du Parc National Suisse, Ergeb. Wiss. Untersuch. Schweiz, *National Parks,* 6, 323–610.

Kobayasi, Y., and others (1967) Mycological studies of the Alaskan Arctic, *Ann. Rept.,* Inst. Ferment., Osaka, No. 3, 138 pp.

Lange, M. (1948) Macromycetes I, the Gastromycetes of Greenland, *Medd. Grønland,* 147, 1–23.

Lange, J., and Hora, F. B. (1963) *A Guide to Mushrooms and Toadstools,* E. P. Dutton, New York, 257 pp.

Long, W. H. (1943) Studies in the Gastromycetes VIII, *Battarrea Laciniata, Mycologia,* 35, 546–556.

Morse, E. (1935) A new puffball, *Mycologia,* 27, 96–101.

Ridgway, R. (1912) *Color Standards and Color Nomenclature,* The Author, Washington, 44 pp.

Smith, A. H. (1951) *Puffballs and their Allies in Michigan,* Univ. of Michigan Press, Ann Arbor, 131 pp.

White, V. S. (1901) The Tylostomaceae of North America, *Bull. Torrey Bot. Club,* 28, 421–444.

Zeller, S. M., and Smith, A. H. (1964) the genus *"Calvatia"* in North America, *Lloydia,* 27, 148–186.

Notes on Homobasidiomycetes from Northern Canada and Alaska*

Orson K. Miller, Jr.† and Robert L. Gilbertson‡

Since 1962 we have collected fungi in Alaska and in the Yukon and Northwest Territories in Canada. Reports of some of the fungi (Miller, 1968, 1969) have been published, but the Polyporaceae, Hydnaceae, and Thelephoraceae are included here for the first time. Baranyay (1968) reported 11 of the fungi from the N. W. Territories which we also report here, but he did not collect in the Yukon Territory.

Polyporaceae

Daedalea unicolor Bull. ex Fr., RLG 3383 (ARIZ) on *Betula papyrifera,* Brabant Island, Wrigley Harbor, MacKenzie River, N.W.T., Can,; RLG 3435 on *Populus tremuloides,* Enterprise Junction, N.W.T., Can.

Fomes cajanderi Karst., RLG 3303 (ARIZ) on *Pinus banksiana,* Enterprise Junction, N.W.T., Can.

Fomes fomentarius (L. ex Fr.) Kickx., OKM 5738 common on *Betula papyrifera* logs, Northway, Alaska.

Fomes nigrolimitatus (Rom.) Egeland, OKM 5449, 5633 on *Picea glauca* logs, Mile 1056, Alcan Highway, Y.T., Can.

Fomes pini (Thore ex Fr.) Lloyd, RLG 3392 (ARIZ) on *Picea mariana,* Brabant Island, MacKenzie River, N.W.T., Can.

Fomes pinicola (Swartz ex Fr.) Cooke, OKM 5622, 5488 frequent on *Picea glauca* logs, near Kluane Lake, Y.T., Can.

Ganoderma applanatum (Pers. ex Wallr.) Pat., OKM 5465 (BPI) on *Populus balsamifera* log, south of Haines Jun. near Klukshu River, Y.T., Can.

Lenzites saepiaria (Wulf. ex Fr.) Fr., RLG 3426 (ARIZ) on *Pinus banksiana,* Enterprise Junction, N.W.T., Can.

Polyporus abietinus Dicks, ex Fr., OKM 5645 (BPI), frequent on *Picea glauca* logs, near Kluane Lake, Y.T., Can.; RLG 3391 on *Picea mariana,* Brabant Island, MacKenzie River, N.W.T., Can.

Polyporus adustus Willd. ex Fr., OKM 6240 (BPI), on *Picea glauca* twigs, near Kluane Lake, Y.T., Can.

Polyporus anceps Peck, RLG 3424 (ARIZ) on *Pinus banksiana* logs, Enterprise Junction, N.W.T., Can.

Polyporus betulinus Bull. ex Fr., OKM 6176 (BPI) on *Betula papyrifera* snag, near Tesslin, Y.T., Can.; RLG 3397A, on *Betula papyrifera,* Brabant Island, MacKenzie River, N.W.T., Can.

Polyporus biformis Fr., RLG 3382 (ARIZ), 3398 on *Betula papyrifera,* Brabant Island, MacKenzie River, N.W.T., Can.

Polyporus dichrous Fr., OKM 6000 (BPI), on *Alnus* stick, near Mendenhall Glacier, Tongass Nat. For., Alaska; RLG 3386 on *Betula papyrifera,* Brabant Island, MacKenzie River, N.W.T., Can.

Polyporus elegans Bull. ex Fr., OKM 5737, 6241, 6246 (BPI), very common on alder and willow, near Kluane Lake, Y.T., Can. and Alaska.

Polyporus lapponicus Rom., OKM 5657 (BFDL), on *Picea glauca* log, Sheep Creek, Mile 1061, Alcan Highway, Y.T., Can.

Polyporus melanopus Fr., OKM 5829, 6255 (BPI) common on willow, near Kluane Lake, Y.T., Can.

Polyporus nidulans Fr., RLG 3396 (ARIZ) on *Betula papyrifera* and 3395 on *Alnus,* Brabant Island, MacKenzie River, N.W.T., Can.

Polyporus pargamenus Fr., OKM 5607 (BFDL) on *Populus tremuloides* logs, Mile 1019 Alcan Highway, Y.T., Can.; RLG 3431 on *Populus tremuloides,* Enterprise Junction, N.W.T., Can.

Polyporus picipes Fr., RLG 3414 (ARIZ) on *Populus tremuloides,* Hay River, N.W.T., Can.

Polyporus planellus (Murr.) Overh., OKM 5448 (BFDL) on willow *(Salix)* stick, near Kluane Lake, Y.T., Can.

Polyporus radiatus Sow. ex Fr., OKM 6027 (BFDL) on decorticated aspen *(Populus tremuloides)* log, near Terance, B.C., Can.

Polyporus subcartilagineus Overh., RLG 3432 (ARIZ) on *Populus tremuloides,* Enterprise Junction, N.W.T., Can. Not generally found on angiosperms.

Polyporus tulipiferae (Schw.) Overh., RLG 3390, on *Betula papyrifera,* Brabant Island, MacKenzie River, N.W.T., Can.

Polyporus varius Fr., OKM 5482 (BFDL) on willow *(Salix)* stick, near Kluane Lake, Y.T., Can.; RLG 3388, on *Alnus,* Brabant Island, MacKenzie River, N.W.T., Can.

Polyporus versicolor L. ex Fr., OKM 5963 (BPI) on *Alnus,* Tongass Nat. For., Alaska.

Polyporus vulpinus Fr., RLG 3413 (ARIZ) on *Populus tremloides,* Hay River, N.W.T., Can.

Poria aneirina (Sommerf.) Cooke, RLG 3423 (ARIZ) on *Populus tremuloides* logs, Hay River, N.W.T., Can.

Poria crustulina Bres., OKM 5644 (BFDL), on *Picea glauca* log, near Kluane Lake, Y.T., Can.; RLG 3383A, on

*This report has previously appeared in *Mycologia,* Vol. 61, pp. 840–844 (1969), and is reprinted here with permission.
†United States Forest Service, United States Department of Agriculture, Laurel, Maryland
‡Department of Plant Pathology, University of Arizona, Tucson

Betula papyrifera log, Brabant Island, Wrigley Harbor, MacKenzie River, N.W.T., Can.

Poria ferrea (Pers.) Bourd. & Galz., RLG 3394 (ARIZ) on *Alnus* log, Brabant Island, Wrigley Harbor, MacKenzie River, N.W.T., Can.

Poria ferruginosa (Schrad. ex Fr.) Karst., RLG 3393 (ARIZ) on *Alnus* Log, Brabant Island, Wrigley Harbor, MacKenzie River, N.W.T., Can.; RLG 3412 on *Populus tremuloides,* Hay River, N.W.T., Can.

Poria obliqua (Pers. ex Fr.) Karst., RLG 3406 (ARIZ) on *Betula papyrifera,* Brabant Island, Wrigley Harbor, MacKenzie River, N.W.T., Can.

Poria pannocincta (Rom.) Lowe, RLG 3407 (ARIZ) on *Populus tremuloides,* Hay River, N.W.T., Can.

Poria salmonicolor (Berk. & Curt.) Cooke, RLG 3425 (ARIZ) on *Pinus banksiana,* Enterprise Junction, N.W.T., Can.

Trametes heteromorpha (Fries) Bres., OKM 5650, 5635, 5375 (BFDL), on *Picea glauca* logs, near Kluane Lake, Y.T., Can.

Trametes hispida Bagl., OKM 5608, 6256 (BFDL), on *Populus tremuloides* logs, near Kluane Lake, Y.T., Can.

Trametes odorata (Wulf, ex Fr.) Fr., OKM 5489 (BFDL) on *Picea glauca* log near Kluane Lake, Y.T., Can.

Trametes serialis Fr., RLG 3384 (ARIZ) on *Picea mariana,* Brabant Island, Wrigley Harbor, MacKenzie River, N.W.T., Can.

Hydnaceae

Hydnum auriscalpium Fr., RLG 3429 (ARIZ) on *P. banksiana,* Enterprise Junction, N.W.T., Can.

Hydnum imbricatum Fr., OKM 6254 (BFDL) on ground, near Kluane Lake, Y.T., Can.

Steccherinum setulosum (Berk. & Curt.) Miller, RLG 3421 (ARIZ) on *Populus tremuloides,* Hay River, N.W.T., Can.

Thelephoraceae

Corticium bombycinum (Sommerf.) Bres., RLG 3380, on *Populus tremuloides,* Brabant Island, MacKenzie River, N.W.T., Can.

Corticium confluens Fr., RLG 3381, on *Betula papyrifera,* Brabant Island, MacKenzie River, N.W.T., Can.

Cristella farinacea (Pers. ex Fr.) Donk, RLG 3402 (ARIZ) on *Betula papyrifera,* Brabant Island, MacKenzie River, N.W.T., Can.

Cytidia flocculenta (Fr.) Hoehn. & Litsch., OKM 5634 on *Salix glauca,* Mile 1059, near Kluane Lake, Y.T. Can.

Cytidia salicina (Fr.) Burt, OKM 5630 on *Salix alaxensis,* Mile 1059 near Kluane Lake, Y.T., Can.

Merulius molluscus Fr., RLG 3430 (ARIZ) on *Pinus banksiana,* Enterprise Junction, N.W.T., Can.

Peniophora aurantiaca (Bres.) v. Hoehn. & Litsch., RLG 3401, on *Alnus* sp., Brabant Island, MacKenzie River, N.W.T., Can.

Peniophora byssoides (Pers. ex Fr.) Bres., OKM 5458, on *Picea glauca* sticks, near Kluane Lake, Y.T., Can.

Peniophora media Bourd. & Galz., OKM 5572 (BFDL) on *Picea glauca* log, Mile 1058, Alcan Highway, Y.T., Can.

Peniophora polygonia (Pers. ex Fr.) Bourd. & Galz., RLG 3404, on *Alnus* sp., Brabant Island, MacKenzie River, N.W.T., Can.

Peniophora subserialis (Bourd. & Galz.) Slysh, RLG 3437, on *Pinus banksiana,* Enterprise Junction, N.W.T., Can.

Stereum abietinum Pers., OKM 5472 (BRDL) on conifer wood, near Jarvis Creek on Alcan Highway, Y.T., Can.

Trechispora brinkmannii (Bres.) J. Erikss., RLG 3397 (ARIZ) on old basidiocarp of *Polyporus betulinus,* Brabant Island, MacKenzie River, N.W.T., Can.

Trechispora raduloides (Karst.) Rogers, RLG 3379 (ARIZ) on *Populus tremuloides,* Brabant Island, MacKenzie River, N.W.T., Can.; RLG 3410 on *Populus tremuloides,* Hay River, N.W.T., Can.

Acknowledgments

The collections are located at BFDL unless otherwise indicated. Field work by Gilbertson in 1962 was supported by grant G24382 from the National Science Foundation. The kind assistance of Dr. R. J. Bouchier (then at the Forest Research Laboratory, Calgary, Alberta) in arranging and participating in the 1962 collecting trip is gratefully acknowledged. The authors would like to thank the members of the Icefield Ranges Research Project of the Arctic Institute of North America for their generous help and logistical support extended to the senior author during the summer of 1967.

References

Baranyay, J. A. (1968) Fungi collected during forest disease surveys in Northern Alberta and the District of MacKenzie, Northwest Territories, *Forestry Branch Dept. Publ. 1238,* Can. Dept. Forestry Rural Devel., 25 pp.

*Miller, O. K., Jr. (1968) Interesting fungi of the St. Elias Mountains, Yukon Territory, and adjacent Alaska, *Mycologia,* 60, 1190–1203.

*Miller, O. K., Jr. (1969) Notes on gastromycetes of the Yukon Territory and adjacent Alaska, *Can. J. Bot.,* 47, 247–250.

*These articles are reprinted in the present volume.

CONVERSION TABLES

LENGTH

Inches to millimeters
(1 in. = 25.4 mm)

in.	mm
0	0
2	50.8
4	101.6
6	152.4
8	203.2
10	254.0
12	304.8

Millimeters to inches
(1 mm=0.039370 in.)

mm	in.
0	0
10	0.39
20	0.79
30	1.18
40	1.57
50	1.97
60	2.36
70	2.76
80	3.15
90	3.54
100	3.94

Feet to meters
(1 ft = 0.3048 m)

ft	m
0	0
10	3.05
20	6.10
30	9.14
40	12.19
50	15.24
60	18.29
70	21.34
80	24.38
90	27.43
100	30.48

Meters to feet
(1 m = 3.28084 ft)

m	ft
0	0
10	32.81
20	65.62
30	98.43
40	131.23
50	164.04
60	196.85
70	229.66
80	262.47
90	295.28
100	328.08

Miles to kilometers
(1 mi = 1.609344 km)

mi	km
0	0
10	16.1
20	32.2
30	48.3
40	64.4
50	80.5
60	96.6
70	112.7
80	128.7
90	144.8
100	160.9

Kilometers to miles
(1 km = 0.621371 mi)

km	mi
0	0
10	6.2
20	12.4
30	18.6
40	24.9
50	31.1
60	37.3
70	43.5
80	49.7
90	55.9
100	62.1

VELOCITY

Knots to meters per second and miles per hour

kn (Int)	m/s	mi/h
1	0.51	1.15
2	1.03	2.30
3	1.54	3.45
4	2.06	4.60
5	2.57	5.75
6	3.09	6.90
7	3.60	8.05
8	4.12	9.20
9	4.63	10.36

Miles per hour to meters per second and knots

mi/h	m/s	kn (Int)
1	0.45	0.87
2	0.89	1.74
3	1.34	2.61
4	1.79	3.48
5	2.24	4.34
6	2.68	5.21
7	3.13	6.08
8	3.58	6.95
9	4.02	7.82

Meters per second to miles per hour and knots

m/s	mi/h	kn (Int)
1	2.24	1.94
2	4.47	3.89
3	6.71	5.83
4	8.95	7.77
5	11.18	9.72
6	13.42	11.66
7	15.66	13.61
8	17.90	15.55
9	20.13	17.49

TEMPERATURE

°F to °C

$$\left[°C = \frac{5}{9}(°F - 32)\right]$$

°F	°C
–50	–45.6
–45	–42.8
–40	–40.0
–35	–37.2
–30	–34.4
–25	–31.7
–20	–28.9
–15	–26.1
–10	–23.3
– 5	–20.6
0	–17.8
5	–15.0
10	–12.2
15	– 9.4
20	– 6.7
25	– 3.9
30	– 1.1
35	1.7
40	4.4
45	7.2
50	10.0
55	12.8
60	15.6
65	18.3
70	21.1
75	23.9
80	26.7

°C to °F

$$\left[°F = \frac{9}{5}°C + 32\right]$$

°C	°F
–45	–49.0
–40	–40.0
–35	–31.0
–30	–22.0
–25	–13.0
–20	– 4.0
–15	5.0
–10	14.0
– 5	23.0
0	32.0
5	41.0
10	50.0
15	59.0
20	68.0
25	77.0
30	86.0

ICEFIELD RANGES RESEARCH PROJECT STATIONS

Station No.	Name used in this volume	Names used previously by various authors	Used as: Camp	Used as: Scientific station	Type of Surface †
1	Base Station	Kluane, Kluane Camp, Base Camp	+	+	Gravel
2	Terminus Station	Moraine Camp, Terminus	+	+	Gravel (outwash)
3	Kaskawulsh Station A	Kask, Kaskawulsh Camp	+	+	Ice-cored moraine
4	Kaskawulsh Station B	Kask Ice		+	Ice (glacier)
5	Kaskawulsh Station C	Kask Knoll		+	Rock (knoll)
6	Crevasse Camp		+	+	Firn (glacier)
7	Divide Station A	Upper Camp, Glacier Central	+	+	Firn (glacier)
8	Divide Station B*	Divide, Meteorological Station	+	+	Firn (glacier)
9	Divide Station C	Divide Cache		+	Rock (nunatak)
10	Divide Station D	Cairn B		+	Snow-covered ridge
11	Seward Station A	Seward	+	+	Rock (nunatak)
12	Seward Station B	Seward Ice		+	Firn (glacier)
13	Lucania Camp		+	+	Firn (glacier)

*Divide Station B used by Havens and Saarela (pp. 17–22) was located ½ mile north of Divide Station B shown on Plates 1 and 2.

†Stations on glaciers move with the glacier at a rate varying from a few centimeters to as much as a meter per day. Therefore, locations of stations on glaciers are only approximate.

PLATE 1